ISTANBUL TECHNICAL UNIVERSITY ★ GRADUATE SCHOOL

DEVELOPMENT OF NOVEL THERMAL CONDUCTIVE POLYMER NANOCOMPOSITES

Ph.D. THESIS

Eliften SEMERCİ

Department of Chemistry

Chemistry Programme

NOVEMBER 2021

ISTANBUL TECHNICAL UNIVERSITY ★ GRADUATE SCHOOL

DEVELOPMENT OF NOVEL THERMAL CONDUCTIVE POLYMER NANOCOMPOSITES

Ph.D. THESIS

Eliften SEMERCİ
(509152004)

Department of Chemistry

Chemistry Programme

Thesis Advisor: Prof. Dr. Nilgün KIZILCAN
Thesis Co-Advisor: Assoc. Prof. Dr. Tuba ERDOĞAN BEDRİ

NOVEMBER 2021

İSTANBUL TEKNİK ÜNİVERSİTESİ ★ LİSANSÜSTÜ EĞİTİM ENSTİTÜSÜ

YENİ NESİL TERMAL İLETKEN POLİMER NANOKOMPOZİTLERİN GELİŞTİRİLMESİ

DOKTORA TEZİ

Eliften SEMERCİ
(509152004)

Kimya Anabilim Dalı

Kimya Programı

Tez Danışmanı: Prof. Dr. Nilgün KIZILCAN
Eş Danışman: Doç. Dr. Tuba ERDOĞAN BEDRİ

KASIM 2021

Eliften SEMERCİ, a Ph.D. student of ITU Graduate School student ID 509152004, successfully defended the thesis entitled “DEVELOPMENT OF NOVEL THERMAL CONDUCTIVE POLYMER NANOCOMPOSITES”, which she prepared after fulfilling the requirements specified in the associated legislations, before the jury whose signatures are below.

Thesis Advisor :	**Prof. Dr. Nilgün KIZILCAN** İstanbul Technical University	.....
Co-advisor :	**Assoc. Prof. Dr. Tuba ERDOĞAN BEDRİ** The Scientific and Technological Research Council of Turkey Marmara Research Center	.....
Jury Members :	**Prof. Dr. Belkıs USTAMEHMETOĞLU** Istanbul Technical University	.....
	Prof. Dr. Esma SEZER Istanbul Technical University	.....
	Prof. Dr. Ayben KİLİSLİOĞLU Istanbul University	.....
	Prof. Dr. Bahire Filiz ŞENKAL Istanbul Technical University	.....
	Assoc. Prof. Dr. Dolunay ŞAKAR DAŞDAN Yıldız Technical University	.....

Date of Submission : 29 September 2021
Date of Defense : 15 November 2021

To my family and Pamuk,

FOREWORD

I would like to express my sincere gratitude to my thesis supervisor, Prof. Dr. Nilgün KIZILCAN, for agreeing to work on this issue, accompanying me in conducting this research under the TUBITAK MAM institution and providing encouragement, support and guidance during this process.

I would also like to give special thanks to my co-advisor, Assoc. Prof. Dr. Tuba ERDOĞAN BEDRİ, for providing me to fully leverage the TUBITAK MAM infrastructure during my course of this thesis process, enabling this work to be accomplished, and encouraging me to develop my career vision during this process.

I would like to convey my profound gratitude to Dr. Serhat ODABAŞ for being there for me when i needed, for his guidance and support, and for his colleagues' assistance, especially during the characterization stages of my doctorate journey.

I am grateful to all the stuff of the Chemical Technology Instıtute of TUBITAK MAM for their invaluable supports.

I must also express my gratitude to my labmate and dear friend, Dr. Sümeyra BAYIR, for always being there for me and for experiencing all the ups and downs of the life with me by trusting and believing in me and for taking care of me with patience. She provided her support when i needed most and directly and indirectly, contributed the great to the completion of my PhD period.

Finally, I would like to dedicate this thesis to my family who have been giving their endless love, sacrifice and never complained about by never-ending education phases during my life. I am thankful to my mother, Hanife SEMERCİ and my father Aydın SEMERCİ. I would aslo like to extend special thanks to my aunt, Fatma ÖZEN for her financial and moral support throughout all stages in my life. And my special appreciations goes to my late grandmother, Nadire ÖZEN, for always believing and trusting in me even if she won't be unable to witness me graduated.

I would like to thank The Scientific and Technological Research Council of Turkey (TUBITAK) (Project No: 216M149) and Istanbul Technical University, Scientific Reseacrh Fund (Project No: TDK-2019-41841), for financial support.

November 2021

Eliften SEMERCİ
(Chemist)

TABLE OF CONTENTS

Page

ABBREVIATIONS

β-Si_3N_4	: Beta phase (hexagonal) silicon nitride
α- Si_3N_4	: Alfa phase (cubic) silicon nitride
SN	: Silicon Nitride nanoparticles
SNNS	: Silicon Nitride Nanosheet
NP	: Nanoparticle
PMMA	: Poly(methyl methacrylate)
PSU	: Polsulfone
PEEK	: Poly(ether ether ketone)
PC	: Polycarbonate
PPSF	: Polyphenylsulfone
PES	: Polyethersulfone
PAEK	: Poly(aryl ether ketone)
CuAAC	: Copper(I)-catalized azide-alkyne cycloaddition
ATRP	: Atom Transfer Radical Polymerization
SI-ATRP	: Surface Initiated Atom Transfer Radical Polymerization
SIP	: Surface Initiated Polymerization
FRP	: Free Radical Polymerization
C/LRP	: Controlled/Living Radical Polymerization
NAS	: Nucleophilic Aromatic Substitution
EAS	: Electrophilic Aromatic Substitution
Nu	: Nucleophile
2D, 3D	: Two-dimensional, three-dimensional
RAFT	: Reversible Addition-Fragmentation Chain Transfer Polymerization
NMP	: Nitroxide Mediated Radical Polymerization
RX	: Alkyl halides
LPE	: Liquid Phase Exfoliation
MW	: Molecular Weight
MWD	: Molecular Weight Distribution
PDI	: Polydispersity Index
$[M]_o$	: Initial molar concentration of the monomer
$[I]_o$	: Initial molar concentration of the initiator
$M_{n,theo}$	: Theoretical Molecular Weight
$M_{n,GPC}$	: Determined Molecular Weight by GPC
PDMS	: Poly(dimethyl siloxane)
FWHM	: Full width at half maximum
cps	: Counts Per Second
deg	: Angular degree
2-theta	: The Bragg angle
nm	: Nanometer
mm	: Milimeter

DPn : Degree of polymerization
$M_{w,M}$: Molecular weight of monomer
$M_{w,I}$: Molecular weight of initiator
BLT : Bond-Line Thickness of TIM
HFT : Heat flux Transducer
ASTM : American Society for Testing and Materials
CVD : Chemical Vapor Deposition
TBR : Thermal Boundary Resistance
TC : Thermal Conductivity
VR : Volume Resistivity
MMA : Methyl Methacrylate
APTES : (3-Aminopropyl) triethoxysilane
BIBB : 2-bromoisobutyryl bromide
NaN_3 : Sodium azide
DCDPS : 4,4′-Dichlorodiphenyl sulfone
BPA : Bispehol A (4,4′-Isopropylidenediphenol)
MeHQ : Methylhydroquinone
DFBP : 4,4'-difluorobenzophenone
CuBr : Copper (I) bromide
CuCl : Copper (I) chloride
DCM : Dichloromethane
EtOAc : Ethyl acetate
TEA, Et_3N : Trimethylamine
PMDETA : N, N, N′, N″, N″-Pentamethyldiethylenetriamine
MeOH : Methanol
EtOH : Ethanol
NMP : N-Methyl-2-pyrrolidone
DMAc : N,N-Dimethyl acetamide
CDCl3 : Deutarated chloroform
DMF : N,N-Dimethylformamide
DMAP : 4-(Dimethylamino) pyridine
DCC : N,N'-Dicyclohexylcarbodiimide
DCU : Dicyclohexylurea
TIM : Thermal Interface Material
XRD : X-ray diffractometry
^{1}H-NMR : Proton Nuclear Magnetic Resonance Spectroscopy
FT-IR : Fourier transform infrared spectrometer
GPC : Gel Permeation Chromatography
DSC : Differential scanning calorimeter
TGA : Thermogravimetric analyzer
SEM : Scanning electron microscopy
DTC : Thermal conductivity analysis
DMA : Dynamic mechanical analysis

SYMBOLS

R_{TIM}	: Effective thermal resistance
R_{Bulk}	: Bulk resistance at interface
k_{TIM}	: Thermal conductivity of TIM
R_c, R_{c1}, R_{c2}	: Contact resistances of TIM
$Wm^{-1}K^{-1}$	: Thermal conductivity unit
m^2KW^{-1}	: Thermal resistivity unit
Ω.cm	: Electrical (volume) resistivity unit
MPa	: Megapascal, pressure unit
Hz	: Hertz, frequency unit
λ	: Thermal conductivity of solid substances
v	: Average phonon velocity
l	: Mean free path of the phonon
Cp	: Specific heat capacity per unit volume
α	: Thermal diffusivity
d	: Density of a material
c	: Specific heat capacity
A	: Area
q	: Rate of heat transfer through a cross-section of area A
L	: Thickness of a material
ΔT	: Temperature difference that exists over thickness L
I	: Initiator
M	: Monomer
k_{act}	: Pseudo-first-order activation rate constant
k_{deact}	: Pseudo-first-order deactivation rate constant
k_p	: Rate constant of propagation
k_t	: Rate constant of termination
P_n^*	: Active radicals
P-X	: Dormant species
K_{ATRP}	: Catalyst activity
K_{eq}	: ATRP equilibrium constant
T_g	: Glass transition temperature
M_n	: The number average molecular weight
M_w	: The weight average molecular weight
M_w/M_n	: The molecular weight distribution
wt%	: The weight percentage
D	: The crystallite size
K	: A dimensionless shape factor
λ	: The X-ray wavelength
β	: The line broadening at half the maximum intensity
θ	: The Bragg angle

d	: The distance between layers
n	The reflection order
Đ	: Polydispersity
Y_c	: Char yield
$T_5\%$	: The temperature for which the weight loss is 5%.
$T_{10}\%$	: The temperature for which the weight loss is 10%.
E'	: Storage modulus
E"	: Loss modulus
Tan δ	: Damping factor

LIST OF TABLES

Page

LIST OF FIGURES

Page

DEVELOPMENT OF NOVEL THERMAL CONDUCTIVE POLYMER NANOCOMPOSITES

SUMMARY

Developments in semiconductor industry have revealed thermal management problems causing shrinkage of the components and increased power densities. This tendency in technology has rendered the development of materials, for thermal management, having excellent thermal conductivity, high electrical resistance and low density important. Especially, materials that are light, cost-effective, easily handled and suitable component design with desired thermal and electrical properties, namely polymeric matrix nanocomposites, are regarded as new generation materials for electronic/microelectronic technology components.

Among many nano-filling materials used to prepare thermally conductive polymeric nanocomposites, the dielectric ceramic particle, β-phase (hexagonal) silicon nitride (β-Si_3N_4) (SN), has high thermal conductivity as well as high mechanical strength and high electrical insulating properties where carbon nanotube and graphene cannot provide. Therefore, it attracts attention as a strategic material for electric/electronic applications. In the literature, SN-containing polymeric composite/nanocomposite preparation includes many methods, as SN is added into a commercial thermoplastic polymeric matrix or into thermoset pre-polymer cured lated and shaped by operations such as extrusion or injection molding. Although there are improvements in the thermal conductivity of the material with current methods, especially SN-containing polymeric composites have limitations and problems in their practical applications. One of them is that the advanced handling of the polymer nanocomposite, caused by thermoset matrix and strong filling-filling interactions. The other is the low interaction between filling material and polymeric matrix and low performance caused by the interface. Therefore, for electronic/microelectronic technology, effective surface modification methods and new composite preparing trends providing improvements in electrical, thermal and mechanical properties of the nanocomposite and determination of the microelectronic component performance are important.

In the design of thermal conductive nanocomposite, the SN, which was prepared in the nanosheet morphology, was not added as a polymer matrix additive, the covalent bond between the modified SNnanosheet and the end-functional polymer matrices were formed and the problems preventing the further processing of the material such as filling-filling interaction in nanocomposite production were eliminated. The other unique value of the silicon nitride filled thermal conductive polymer nanocomposites is that they were produced by a synthetic approach that provides structure-property control in the material. In other words, the molecular weight, molecular weight distribution, end-group functionality of the polymer structure to be grown onto the surface of SNNSs can be controlled.

In the synthetic approach proposed in this work, in order to increase the interphase interactions between the polymer and the nanoparticle and to provide a homogeneous

distribution of the nanofiller in the matrix, the *"grafting to"* method was implemented. Click chemistry was used as an essential tool to form covalent bond between the filler and matrix. A new polymer nanocomposites consisting of silicon nitride (Si_3N_4) nanoparticle as a conductive filler and poly(methyl methacrylate) (PMMA), polysulfone (PSU) and poly(ether ether ketone) (PEEK) as a polymer matrices were fabricated using *"click"* chemistry. The synthesis of these three nanocomposites is a five-step procedure including (i) the preparation of silicon nitride nanosheet (SNNS) by mechanical exfoliation, (ii) the modification of SNNS with successive chemical modification processes, (iii) the synthesizing of polymer matrices with end-funtionality, iv) the modification of these end-groups to compatible with click reaction, v) the performing Copper Catalyzed Azide-Alkyne Click reaction (CuAAC) between alkyne functionalized polymer matrices (PMMA-Alkyne, PSU-Alkyne and PEEK-Alkyne) and azide functional SNNS (SNNS-N_3). Characterization results confirmed the functionalization of SNNS surface and the successful *"grafting to"* method using click reaction. The average crystallite sizes of β-Si_3N_4 and SNNSs obtained from mechanical exfoliation process were calculated using the X-ray diffractometry analysis (XRD) results according to the Debye Scherrer equation. The particle size distribution of SN and SNNSs was investigated by photon correlation spectroscopy (PCS) using Zetasizer. The main-chain structures and end-functionalities of polymer matrices were confirmed by proton nuclear magnetic resonance spectroscopy (^{1}H-NMR). The chemical structres of all nanocomposites, also their precursors and the success of click chemistry were verified by Fourier transform infrared spectroscopy (FT-IR). The molecular weights and polydispersities of polymer matrices were calculated using gel permeation chromatography (GPC). The glass-transition temperatures (T_g's) of polymers and nanocomposites were determined by differential scanning calorimetry (DSC). Thermal stabilities and char yield values of nanocomposites and their precursors were performed on thermogravimetric analyzer (TGA). The surface morphologies and crystal structures of pristine SN and ball-milled SN (SNNS) and the dispersion of SNNSs within the polymer matrices were investigated by scanning electron microscopy (SEM). Electrical resistivities (volume resistivities) of nanocomposites were measured using electrometer. Viscoelastic behaviours of polymer matrices and nanocomposites were analysed by a dynamic mechanic analyzer (DMA).

The novel thermal conductive polymer nanocomposites were formulated as a thermal interface material (TIM) and their performance as a TIM material was investigated by Thermal Conductivity Analysis (DTC). It has been found that the thermal conductivity of the chemically modified nanocomposites (PMMA-SNNS, PSU-SNNS and PEEK-SNNS) based TIM is considerably higher than that of TIM prepared with physically blended nanocomposites (PMMA+SNNS, PSU+SNNS and PEEK+SNNS) having the same composition.

YENİ NESİL TERMAL İLETKEN POLİMER NANOKOMPOZİTLERİN GELİŞTİRİLMESİ

ÖZET

Bilgisayar ve elektronik endüstrisindeki minyatürizasyon eğilimi aşırı ısınmayı en önemli problem haline getirmiştir. Aşırı ısınma sebebiyle sistemlerin performansının, gücünün ve güvenilirliğinin arttırılması ve daha küçük hacimlerde sistem tasarlamak zorlaşmaktadır. Elektronik sistemlerde artan ısı yükleri, bilgi teknolojileri, iletişim, enerji dağıtım, depolama ve aydınlatma sistemlerinde etkin elektronik soğumanın daha kritik bir konu olmasına sebep olmaktadır. Teknolojideki bu eğilim, mükemmel termal iletkenliğe, yüksek elektriksel dirence ve düşük yoğunluğa sahip çok fonksiyonlu malzemelerin geliştirilmesini önemli hale getirmiştir.

Elektronik sistemlerin tek parçalı olmaması, metal, polimer, seramik ve yarıiletken gibi malzemelerden oluşuyor olması, termal arayüz malzemesi kullanımını kaçınılmaz kılmıştır. Yüksek ısı atan elemanlarla bu elemanları soğutan yapılar arasındaki temas alanı mikro düzeydeki düzlemsellik farklarından dolayı %3'e kadar düşebilmektedir. Termal arayüz malzemesi kullanılarak bu temas yüzey alanının arttırılarak termal kontakt direncinin azaltılması ve böylece arayüzden ısı transferinin artması beklenmektedir. Doğru termal arayüz malzemesinin seçimi, elektronik cihazın veriminin belirlenmesinde önem kazanmaktadır.

Termal arayüz malzemesinin geliştirilmesine yönelik çalışmalar ile karmaşık soğutma teknolojilerinin araştırılmasına alternatif çözümler bulunabilmesinin mümkün olduğu değerlendirilmektedir. En uygun termal arayüz malzemesinin seçimiyle sistemin toplam maliyeti, sıvı soğutma sistemlerine duyulan gereksinim, soğutma sistemine ait enerji ihtiyacı azalmakta ve ürünün ömrü uzayabilmektedir.

Kompozit malzemeler geleneksel olarak yapısal malzeme kullanımına göre tasarlanmaktadır. Elektronik endüstrisinin hızlı gelişimi, kompozit malzemelerin elektronik uygulamalarda daha fazla yer bulmasını sağlamıştır. Yapısal ve elektronik kompozitlerin özellik gereksinimleri arasındaki fark çok büyük olduğundan, bu iki kompozit grubu arasındaki tasarım kıstasları farklıdır. Yapısal kompozitlerde yüksek dayanım ve yüksek modül önemli olurken, elektronik kompozitlerde ise belirli elektronik uygulamalara bağlı olarak yüksek termal iletkenlik, düşük termal uzama, düşük dielektrik sabiti, düşük/yüksek elektrik iletkenliği, düşük/yüksek elektromanyetik girişim kalkanlama (EMI shielding) etkinliği önemli olmaktadır. Yapısal kompozitlerin panel gibi büyük parçalara işlenebilirliği önemli olurken, elektronik kompozitlerin tek başına film ve kaplama gibi küçük parçalara işlenebilirliği ön plana çıkmaktadır. Polimer matris kompozitlerin elektronik/mikrolektronikteki uygulamaları genel olarak; baskı devre kartları, devre altlıkları, elektronik ambalaj, elektronik kapsül, ısı havuzu, elektrik kontak ve termal ara yüzey malzemelerini içermektedir.

Termal kontak direnç, birbiriyle temas eden iki yüzeyde ısının bir yüzeyden diğerine olan iletiminin ne kadar iyi olduğunun göstergesidir. İşlemci ile işlemciye temas eden

soğutucu plaka arasındaki termal kontak direnç, işlemci üst yüzey sıcaklığı ile soğutucu taban sıcaklığı arasındaki farkın toplam ısı akısına olan oranı olarak tanımlanmaktadır.

Termal kontak direncin azaltılması için başlıca iki metot önerilmiştir. Yüzeyler arasındaki basıncın artırılması veya yüzeylerin pürüzlülüğünün düşürülmesiyle temas alanının arttırılması veya termal arayüz malzemesi kullanılması. Ancak elektronik komponentler üzerindeki temas basıncının arttırılması bu komponentlere zarar verebileceği için ve düşük pürüzlülükte malzeme üretiminin çok pahalı olması sebebiyle temas alanının bu şekilde arttırılması tercih edilen bir yöntem olmamıştır. Bu sebeple iki yüzey arasını doldurabilen ve termal iletkenliği havanın termal iletkenliğinden yüksek olan malzeme kullanımının kontak direnci düşürme açısından daha uygun bir yöntem olacağı değerlendirilmektedir.

Bu çalışmada ideal termal arayüz malzemesinin sahip olması gereken özellikler şu şekilde sıralanmıştır; yüksek termal iletkenlik, düşük basınç altında kolayca deforme olarak iki temas yüzeyinin de pürüzlü bölgelerini doldurabilme ve kontak direnci minimize etme, minimum kalınlık, arayüzden dışarı akma yapmaması, uzun ömürlü olması, toksin içermemesi, kolay uygulanabilir ve sökülebilir olması.

Termal iletken nanokompozit tasarımında, nano tabaka morfolojisinde hazırlanan silikon nitrür (SN), bir polimer matris katkısı olarak eklenmemiş, modifiye edilmiş silikon nitrür nantabaka (SNNS-R) ve uç-işlevsel polimer matrisler arasında kovalent bağ oluşturulmuş, ve nanokompozit üretiminde dolgu-dolgu etkileşimi gibi, malzemenin daha sonraki işlenebilirliğini olumsuz etkileyebilecek problemlerin de önüne geçilmiş oldu. Silikon nitrür dolgulu termal iletken polimer nanokompozitlerin bir diğer benzersiz özelliği, malzemede yapı-özellik kontrolü sağlayan sentetik bir yaklaşımla üretilmiş olmalarıdır. Başka bir deyişle, silikon nitrür nano tabaka yüzeyinden bağlanan polimer yapısının moleküler ağırlığı, moleküler ağırlık dağılımı ve uç grup işlevselliği kontrol edilebilir özelliktedir.

Bu çalışmada önerilen sentetik yaklaşımda, polimer ve nanoparçacık arasındaki ara-yüzey etkileşimini artırmak ve nanodolgu maddesinin matris içinde homojen dağılımını sağlamak için *"grafting to"* yöntemi uygulanmıştır. Dolgu ve matris arasında kovalent bağ oluşumunu sağlamak için modüler bir sentetik yaklaşım olan Klik Kimyası kullanılmıştır.

İletken dolgu maddesi olarak silikon nitrür (Si_3N_4) nanoparçacık içeren nanokompozitler, üç farklı termoplastik matris kullanılarak üretilmiştir. Bunlardan ilki bir mühendislik polimeri olan, amorf poli(metilmetakrilat) (PMMA), diğer ikisi de yüksek performans polimerlerinden amorf polisülfon (PSU) ve yarı-kristalin poli(eter eter keton) (PEEK)dur. Nanokompozitlerdeki silicon nitrür oranı, termal iletkenlikler ve boyutsal kararlılıklar göz önünde bulundurularak, her polimer matrisi için yapılan formulasyon çalışmaları sonucunda belirlenmiştir. Bu üç nanokompozitin sentezi, beş aşamalı bir prosedürü kapsamaktadır. Bu prosedür; (i) mekanik eksfoliasyon yoluyla silikon nitrür nano tabakaların hazırlanması (SNNS), (ii) SNNS'nin ardışık kimyasal fonksiyonlandırma prosesleriyle modifikasyonu, (iii) uç fonksiyonel polimer matrislerin sentezi, iv) bu uç grupların klik reaksiyonu ile uyumlu olacak şekilde modifikasyonu, v) alkin uç-fonksiyonel polimer matrisler (PMMA-Alkin, PSU-Alkin ve PEEK-Alkin) ile azid fonksiyonel SNNS (SNNS-N_3) arasında Bakır Katalizli Azid-Alkin Click reaksiyonu (CuAAC) gerçekleştirilmesi aşamalarını içermektedir.

Bu kapsamda tezin ilk aşamasında, polimer ve nanoparçacıklar arasındaki yüzeyler arası etkileşimleri arttırmak, polimer matris içinde nanoparçacıkların homojen

dağılımını sağlamak ve yüzey fonksiyonelliğini kolaylaştırmak için silikon nitrür nanoparçacıkları nano tabaka morfolojisinde modifiye edilmiştir. Kimyasal modifikasyon işlemini kolaylaştırmak için, mekanik eksfoliyasyon yöntemi ile partikül boyutu küçültülmüş ve katmanlı formda silikon nitrür nano tabakalar (SNNSs) elde edilmiştir. Belirlenen koşullar altında gerçekleştirilen eksfoliyasyon işlemleri sonucunda izole edilen örneklerin kristalit boyutundaki değişim x-ray kristolografi (XRD) ile takip edilmiştir. Ham silikon nitrür (SN) ve mekanik eksfoliasyon ile nano tabaka haline getirilmiş SN'lerin (SNNSs) yüzey morfolojileri ve kristal yapıları, Taramalı Elektron Mikroskobu (SEM) ile araştırılmıştır. SN ve SNNS'lerin partikül büyüklüğü dağılımı Zetasizer kullanarak, foton korelasyon spektroskopisi (*ing. Photon correlation spectroscopy*) (PCS) ile araştırılmıştır.

Tezin ikinci aşamasında, eksfoliye edilmiş silikon nitrür nano tabakalar (SNNS), nanodolgu yüzeyinde, klik reaksiyonu sırasında yüzeyler arası etkileşimi arttırmada etkili olan, aktif başlatıcı bölgeler oluşturmak için kimyasal modifikasyon işlemlerine tabii tutulmuştur. Bu işlemler sırasıyla, aminasyon, bromo-amidasyon ve azidasyon reaksiyonlarıdır.

Tezin üçüncü aşamasında ise, SNNS ile üç farklı polimer matrisin kimyasal bağlanmaa yoluyla nanokompozit üretimi gerçekleştirilmiştir. Poli(metil metakrilat) (PMMA), polisülfon (PSU) ve poli(eter eter keton) (PEEK) gibi polimer fazları ile termal iletken dolgu maddesi olarak silikon nitrür nano tabakalarını içeren polimer nanokompozitler tez kapsamında sentezlenmiş ve fonksiyonel hale getirilmiş, farklı morfolojileri ve yapıları aydınlatılmıştır. Her bir polimer matris için, klik kimyası ve fiziksel harmanlama olmak üzere iki farklı nanokompozit hazırlama yöntemi kullanılmış ve her bir nanokompozit ürünün yapısal analizi karşılaştırılmıştır. Bu nedenle nanokompozitlerin karakterizasyon sonuçları bu iki yöntemin karşılaştırmalarını içermektedir. Bu iki teknik arasındaki farklar, kimyasal etkileşim yaklaşımıyla termal iletken polimer nanokompozit üretiminin üstünlüğünü göstermek için her bölümde ayrıntılı olarak rapor edilmiştir.

Poli(metil metakrilat) (PMMA) matrisleri ile termal iletken nanokompozitlerin (PMMA//SNNS ve PMMS-SNNS)'in hazırlanmasında iki sentetik yaklaşım kullanılmıştır: İlk yaklaşımda, yüzey başlatmalı atom transfer radikal polimerizasyon (*ing. Surface initiated atom transfer radical polymerization, SI-ATRP*) kullanılmıştır. Bu yöntemde, metil metakrilatın (MMA) kontrollü polimerizasyonu için, bir ATRP başlatıcısı olarak davranabilen, SNNS'nin kimyasal modifikasyonu ile elde edilen brom sonlu silikon nitrür (SNNS-Br) kullanılmıştır. Bu sayede, PMMA zincirleri, direk SNNS yüzeyinden büyütülmüştür. İkinci yaklaşımda, metil metakrilatın (MMA)'ın ATRP ile kontrollü polimerizasyonunda, alkin fonksiyonel başlatıcı kullanılmış ve polimer matris direk alkin uç-fonksiyonel olarak (PMMA-Alkin) elde edilebilmiştir. Sonrasında, klik reaksiyon ajanı olarak kullanılabilen, SNNS'nin kimyasal modifikasyon prosesler sonucu elde edilen azid sonlu silikon nitrür (SNNS-N_3), PMMA-Alkin ile klik reaskiyonuna tabii tutulmuştur.

Polisülfon matrisli nanokompozitleri (PSU-SNNS) hazırlamak için iki aşamalı polisülfon sentez prosedürü gerçekleştirilmiştir. Sentez prosedürünün ilk aşaması, yoğunlaştırma polimerizasyonu ile üç farklı moleküler ağırlığına sahip hidroksil uç-fonksiyonel polisülfon sentezini (PSU-OH), ardından bu uç grupların klik reaksiyonunda kullanılmak üzere, esterifikasyon reaksiyonu ile (Steglich Esterifikasyonu) alkin fonksiyonuna (PSU-Alkin) dönüştürülmesini içerir. Nanokompozit hazırlama aşamasında PSU matris olarak, en iyi termal davranışı veren

9,000 g/mol molekül ağırlıklı PSU-OH (PSU-OH-9000) kullanılmıştır. Nanokompozit hazırlama metodu ve polimer matrisin moleküler ağırlığının nanokompozitin termal davranışı üzerindeki etkisi, karakterizasyon çalışmaları ile incelenmiştir.

Poli(eter eter keton) matrisli nanokompozitleri (PEEK-SNNS) hazırlamak için iki aşamalı poli(eter eter keton) sentez prosedürü gerçekleştirilmiştir. Sentez prosedürünün ilk aşaması, yoğunlaştırma polimerizasyonu ile hidroksil uç-fonksiyonel poli(eter eter keton) sentezini (PEEK-OH), ardından bu uç grupların klik reaksiyonunda kullanılmak üzere, esterifikasyon reaksiyonu ile (Steglich Esterifikasyonu) alkin fonksiyonuna (PEEK-Alkin) dönüştürülmesini içerir. Nanokompozit hazırlama metodu ve polimer matrisin moleküler ağırlığının nanokompozitin termal davranışı üzerindeki etkisi, karakterizasyon çalışmaları ile incelenmiştir.

Polimer matrislerin ana zincir yapıları ve uç grup fonksiyonaliteleri, proton nükleer manyetik rezonans spektroskopisi (^{1}H-NMR) ile doğrulandı. Tüm nanokompozitlerin kimyasal yapıları, nanokompozit bileşenleri ve klik kimyasının başarısı, Fourier transform kızılötesi spektroskopisi (FT-IR) ile doğrulandı. Polimer matrislerin molekül ağırlıkları ve molekül ağırlık dağılımları jel geçirgenlik kromatografisi (GPC) kullanılarak hesaplandı. Polimer matrislerin ve nanokompozitlerin camsı geçiş sıcaklıkları (T_g) diferansiyel taramalı kalorimetre (DSC) ile belirlendi. Nanokompozitlerin ve öncüllerinin termal kararlılıkları ve kömür verim değerleri, termogravimetrik analiz (TGA) ile gerçekleştirilmiştir. Ham SN ve mekanik eksfoliasyona tabii tutulmuş SN'nin (SNNS) yüzey morfolojileri ve kristal yapıları, ve SNNS'lerin polimer matrisleri içindeki dağılımı, taramalı elektron mikroskobu (SEM) ile araştırıldı. Nanokompozitlerin elektriksel dirençleri (hacim dirençleri), elektrometre kullanılarak ölçüldü. Polimer matrislerin ve nanokompozitlerin viskoelastik davranışları dinamik mekanik analiz (DMA) ile analiz edildi.

Yeni termal iletken polimer nanokompozitler, bir termal arayüz malzemesi (TIM) olarak formüle edildi ve bir TIM malzemesi olarak performansları, Termal İletkenlik Analizi (DTC) ile araştırıldı. Kimyasal olarak modifiye edilmiş nanokompozit (PMMA-SNNS, PSU-SNNS ve PEEK-SNNS) bazlı TIM'lerin termal iletkenliğinin, fiziksel olarak harmanlanmış aynı bileşime sahip nanokompozitler (PMMA+SNNS, PSU+SNNS ve PEEK+SNNS) ile hazırlanan TIM'lerden oldukça yüksek olduğu bulunmuştur.

1. INTRODUCTION

Thermal conductive polymer composites for their excellent thermal properties, easily forming, flexibility and low density features have a wide range of application areas such as electronic packaging, printed circuit boards, phase change materials, and thermal interface materials (TIM) [1]. TIMs are extensively used as thermal conductive material to remove excess heat generated by computer processors from the system by heat dissipation [2]. Therefore, the material to be used as TIM must have high thermal conductivity as well as low electrical conductivity [3].

Thermal conductivity of nanocomposites depends on the numerous factors. For example, enhancing the thermal conductivity of polymer nanocomposites is directly associated with the heat transfer at interface between the filler and matrix. One of the essential parameter affecting the heat transfer is the thermal interface resistance [4] caused by defects and impurities in the lattice, boundary scattering or phonon-phonon scattering [5]. In order to enhance the thermal conductivity, these phonon scatterings derived from the flaws in the filler-matrix interface must be reduced [6]. It is therefore, to overcome this problem and ensure better compatibility at interface, the interaction type between the filler and matrix should be considered [7, 8].

Many interphase properties depend on the interaction type of interaction between filler and matrix and so optimizing the filler-matrix interface is an important strategy in tailoring nanocomposite properties. Establishing chemical bonds between filler and matrix reduces the thermal interfacial resistance and minimizes flaws such as voids. This phenomenon suppresses phonon scattering and improves effective heat dissipation [9, 10]. By means of functionalizing the filler, the chemical bond formation between filler and matrix can be realized; thereby the higher interface compatibility between the two can be achieved [11, 12].

Another critical parameter governing the thermal conductivity of nanocomposites is the dispersion of the filler in polymer matrix. Since, the uniform and homogeneous dispersion of nanoparticles in polymer matrix is one of the major problem encountered

in polymer nanocomposite fabrication. In order to achieve nanocomposites with enhanced properties, nano-sized particles should be dispersed in matrix material properly, otherwise there will be agglomeration of the particles and the properties of nanocomposites will deteriorate. There are several fabrication methods to control the dispersion of nanofillers in the polymer matrix. One of them is mechanic exfoliation via ball milling that enables the increase in surface area of nanofillers, as well as offering a uniform dispersion in polymer matrices [4, 13, 14]. This method also leads to alteration of the nanofiller morphology allowing the nanofiller to be compatible with the polymer matrix. Therefore, SNs were exposed to mechanic exfoliation process as the first stage of the process to serve easy way for chemical surface functionalization steps.

As it mentioned before that the thermal interface resistance generally arises from the incompatibility between filler and matrix caused by imperfect interfacial adhesion [15, 16]. It is therefore strong C-C covalent bonds should be involved between filler and matrix by means of chemical surface modifications of nano-filler [12, 17, 18]. This covalent interaction leads the enhanced interfacial adhesion suppresses the phonon scattering and increase the heat conduction through interfaces of substances [11]. Silane coupling agents are being extensively used to modify the ceramic filler surfaces [7, 15]. They act as a linkage between the inorganic filler and the polymer matrix through their bifunctional structure [19]. One end reacts with the hydroxyl groups on filler surface, forms covalent bond; the other end yields another covalent bond with the end-functional polymer matrix [18].

In this study, beta phase silicon nitride nanoparticles were converted to nanosheet morphology via mechanical exfoliation technique and their surfaces were modified through chemical processes. SNNS modified with three distinct polymer matrices reported in the thesis proposal, thermal conductive polymer nanocomposites were synthesized by establishing covalent bonds by means of click chemistry, which is a modular synthetic approach. A thermal interface material (TIM) formulation study has been carried out using a series of polymer nanocomposites with optimized silicon nitride ratio, thermal conductivity and dimensional stability. The physical properties (thermal, electrical, mechanical) of polymer nanocomposites containing SNNS and the morphology of Polymer-SNNS nanocomposites, investigation of the physical properties of the material and the structure/morphology relationship have been studied.

2. THEORETICAL PART

2.1 Thermal Management and Electronic Packaging

Progresses in the area of microelectronics have ended up with the substantial escalation in density integration, clock rates and so the requirement of minimization of electronic components. As the necessities for the miniaturization of electronic components, low cost and high performance increase, electronic packaging industry will maintain its developments in the product technologies and the new generation of electronics [20]. It is therefore thermal management of microelectronics have become significant issue and it is highly critical for electronic industry.

The semiconductor industry has been making an effort for a long time to minimize the size of the devices. The growth in power density is expected to more increase in forthcoming years due to the diminishment in size of electronic components and the enhancement of power dissipation [21].

The reduction in size of electronic components causes the component density to increase, which requires more power the device to run. This increased power density generates greater heat, leading to hardware failures, graphical errors, chip malfunctions and even permanent damages on mainboard. To put it another way, the developments in this area is stringently depend on the novel solutions in the heat elimination [22]. The enhancements in heat elimination have been launched and will proceed with the design of changes requiring advanced technology in electronic packaging comprising innovative thermal management solutions.

Almost every circuit simulation systems depend on the temperature changes affecting the electrical parameters such as offset, leakage, gain, impedance, open circuit voltage and short circuit current etc. It can be calculated that the every 10 ˚C increase in temperature doubles the circuit leakage currents. Furthermore, the temperature might reach the values that exceed the manufacturer's specifications and might cause permanent damage if the heat elimination in the device is not performed properly [23].

Therefore, high performance components need to be used besides heat sinks in order to run the electronic devices below critical temperature values. Composite materials are the promising materials that can provide appropriate heat dissipation for entire packaging of the electronic system as well as electrical insulation, mechanical support, environmental protection and useful life for the electronic assembly [24].

2.1.1 Materials for thermal management

The need for the high thermal conductivity materials has been enhancing markedly due to the continuing increment in electronic packaging density. In many practice regarding compact systems like mobile phones and laptops require low mass-density materials. Moreover, low cost, mechanical durability, chemical resistivity and electrical insulation are also the key considerations for electronic packaging applications, since conventional materials cannot meet all of these necessities. Hence, novel multifunctional materials need to be developed for this field [25].

The high power density stemmed from high electronic packaging density ends up with the instant and quick heat generation. In these circumstances, conventional materials are insufficient to eliminate the heat from the system. For instance, metal-based heat sinks and heat spreaders have been utilized for a long time to dissipate the excess heat and preserve the device temperature within the limits [26]. Yet, these traditional materials such as copper and aluminum alloys do not have involve the properties like ease of manufacture, low weight and low electrical conductivity for electronic packaging [27].

In this sense, multifunctional materials with low weight, higher thermal conductivity than polymers, lower electrical conductivity than metals and comparable thermal expansion coefficient to metals, have been designed and fabricated for the concept of electronic packaging system. Furthermore, these materials might also be utilized to manufacture the whole packaging system as well as heat sinks. They provide mechanical durability, protection from environmental effects, enhanced heat dissipation besides contributing the reduced weight of electronic components. Therefore, a new generation material called thermal conductive filler filled polymer-matrix composites might be employed for designing the electronic packaging systems [28].

2.1.2 Thermal interface materials (TIMs)

Most electronic components like processors and transistors produce substantially heat during use. This heat must be eliminated from the system as it adversely affects the performance of the electronic components and the device. Heat sinks generally used to remove the heat from such components through heat dissipation. Due to the incompatibility of the surfaces of device and the heat sink, air gaps between these two surfaces can be retained. These gaps, even at the micro level, decrease the efficiency of the thermal conduction (Figure 2.1) [29]. To overcome this situation, a thermal conductive material which fills the surface defects must be used between the heat sink and the device to eliminate surface irregularities and leave no air gaps [2, 30, 31].

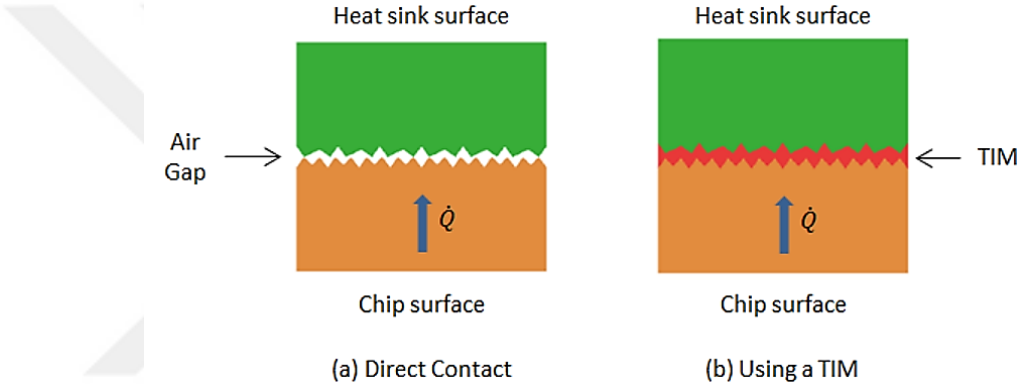

Figure 2.1 : The schematic illustration of the contact area between two solid surfaces.

Thermal interface materials (TIM) are used as thermal conductive material to remove excess heat generated by computer processors from the system by heat dissipation [2]. Therefore, the material to be used as TIM must have high thermal conductivity as well as low electrical conductivity [3]. They are commonly used with the object of ameliorate thermal conduction for enabling the heat transfer in electronic packaging. There are two types of TIMs; TIM1 is used between die and heat spreader, while TIM2 is used between heat spreader and heat sink (Figure 2.2). A TIM is generally applied in the form of grease, paste, gel or pad form to eliminate the surface irregularities that causes thermal impedance between two solid surfaces. The resilient nature of TIM provides the surface conformability that helps to reduce thermal boundary resistance (TBR) arising from air gaps residing between two solid surfaces [32].

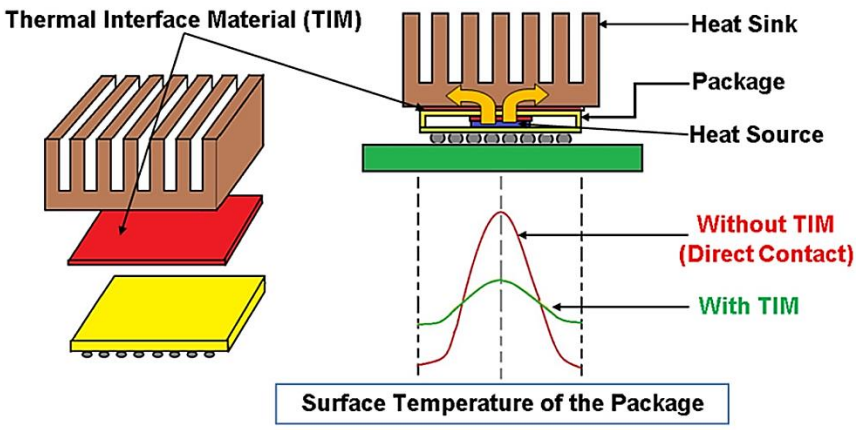

Figure 2.2 : The schematic depiction of a typical chip packaging design.

The thermal barrier between the surfaces is an essential obstacle that TIMs have to overcome to provide the heat dissipation properly. The effective thermal conductivity depends on the two main characteristic of TIMs, which are the interfacial heat transfer coefficient alongside the intrinsic bulk thermal conductivity.

Effective thermal resistance across the interface after the implementation of TIM between two solid surfaces is demonstrated in Figure 2.3 [32].

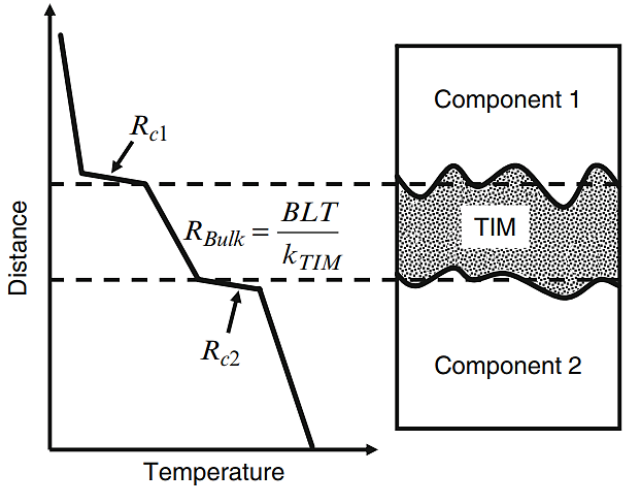

Figure 2.3 : Thermal resistance across the interface of a TIM.

Effective thermal resistance R_{TIM}, at the interface consist of the bulk resistance R_{Bulk}, of the TIM arising from its finite thermal conductivity, and the contact resistance R_c, between the TIM and two solid surfaces. Hence, thermal resistance calculation can be formulates as seen in equation (2.1).

$$R_{\mathrm{TIM}} = \frac{BLT}{k_{\mathrm{TIM}}} + R_{\mathrm{c1}} + R_{\mathrm{c2}}, \tag{2.1}$$

Where BLT is the bond-line thickness of TIM, k_{TIM} is the thermal conductivity of TIM, and R_{c1} and R_{c2} are the contact resistances of the TIM with the two solid surfaces [32].

2.1.3 Material design for thermal interface materials (TIMs)

Thermal conductivity has an essential role on the heat transfer of any material. The thermal conductivity of the interface material has a substantial effect on its thermal behavior. The higher the ability of thermal conduction of a material, the more effective way to heat elimination from the electronic system is achieved [32].

The design of TIMs requires consideration of many features such as mechanical, thermal, optical, electrical, surface properties, depending on applications besides the factors like economic efficiency, easy handling, tensile strength, flexibility etc. For example, TIMs should display good mechanical conformity and fill well the voids between two solid surfaces to enhance heat transportation. Furthermore, TIMs must have high electrical resistivity, high breakdown strength and low dielectric constant for some electronic applications. Breakdown electric field of a TIM is a significant factor for handling the design of a material. The electric field distortion stemms from the differences between the dielectric constants of filler and matrix. In order to obtain high breakdown strength, filler and matrix materials having closer electrical conductivities to each other must be chosen. In addition to them, thermal conductivity, material thickness and contact thermal resistance at the interface are the key factors to take into consideration for designing TIM. Therefore, thermal contact resistance must be reduced to enhance thermal conductivity. For this purpose, bond line thickness (BLT) which causes the thermal contact resistance might be minimized by lowering the material thickness [33].

The most important factor determines the thermal conductivity of a TIM is the heat transfer capacity of TIM itself, and so it is anticipated to be high. Generally, typical TIMs are made up of micro or nano-sized thermal conductive particles filled polymer matrices.

2.2 Materials Selected for Preparation of TIMs in This Thesis

2.2.1 Filler materials

In thermally conductive interface material applications, polymers are promising materials. However, their low thermal conductivity between 0.1 and 0.6 $Wm^{-1}K^{-1}$ [34] restricts their use in this area. In order to increase thermal conductivity of polymers, several thermal conductive fillers can be used with polymers matrix [35]. Metallic powders [36, 37], carbon based fillers [15, 38] and ceramic fillers are the most utilized conductive fillers in the preparation of polymer nanocomposites. Metallic powders and carbon based fillers have high thermal conductivity, but they do not show optimal performance as thermal interface materials due to their also high electrical conductivity [39]. Ceramic fillers have higher thermal conductivity than polymers at about between 1-300 $Wm^{-1}K^{-1}$ besides their electrical insulations [35]. Therefore, they can be used as fillers for the applications of thermal conductivity in electronic devices. Fillers like silicon carbide (SiC) [40, 41], silicon nitride (Si_3N_4) [42, 43], silicon dioxide (SiO_2) [44, 45], aluminum oxide (Al_2O_3) [11, 45], aluminum nitride (AlN) [7, 46] and boron nitride (BN) [47, 48] have been frequently utilized for a long time in the fabrication of polymer nanocomposites with high thermal conductivity.

In recent years, nitride ceramics have received much more attention in the field of electronics due to their high thermal conductivity, low thermal expansion coefficient and electrically insulating nature [49]. AlN has been frequently used as a ceramic filler in power devices due to its high thermal conductivity above 200 $W.m^{-1}K^{-1}$ [49, 50]. However, AlN suffers from poor mechanical properties (Figure 2.4) [51, 52]. Superior mechanical properties are essential for the high-power electronic devices.

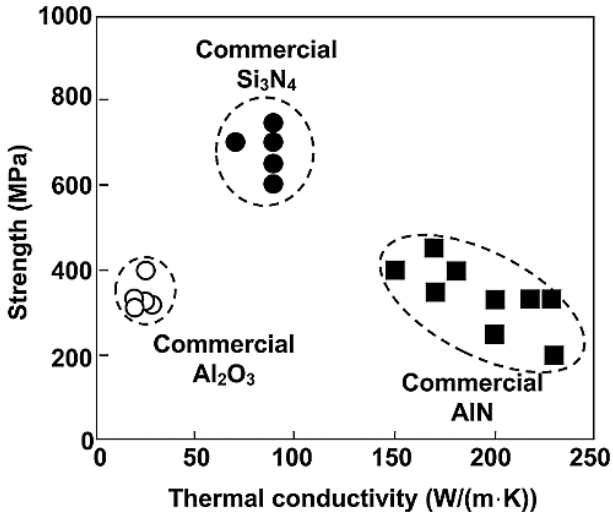

Figure 2.4 : Thermal conductivity comparisons of commercially available ceramic fillers based on their mechanical strength.

2.2.2 Silicon nitride as filler material (Si_3N_4) for TIMs

Silicon nitride is a non-oxide promising ceramic material for used as structural component in a wide range of applications. It is an inorganic and non-metallic compound. The first synthetic silicon nitride was developed by Deville and Wohler in 1859 after its first discovery in 1857. The first commercial application of silicon nitride was realized in 1950's [53].

Silicon nitride is principally found in two hexagonal polymorphs as α-Si_3N_4 and β-Si_3N_4 as shown in Figure 2.5, which are generally considered as low temperature and high temperature crystal forms, respectively [53, 54]. The *c* axis of α unit cell is just about twice that of the β unit cell [55, 56]. β-Si_3N_4 was used as a ceramic filler in this work due to its high thermal conductivity.

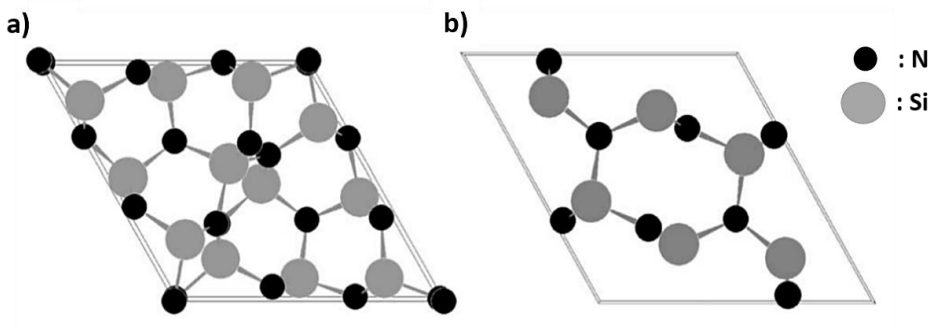

Figure 2.5 : Crystal structures of a) α-Si_3N_4 and b) β-Si_3N_4.

Recently, silicon nitride ceramics with thermal conductivity above 100 $W.m^{-1}K^{-1}$ have been investigated. Although having high thermal conductivity, its mechanical properties such as high strength, high durability, high wear resistance, as well as its chemical stability at room and high temperatures makes SN an interesting material for mechanical applications while its thermal applications remain less explored. With this thesis, it is aimed to extend the application area of silicon nitride in thermal applications alongside their very pronounced mechanical applications [54]. Silicon nitride (Si_3N_4) (SN) has high mechanical strength and high thermal conductivity with 100 $W.m^{-1}K^{-1}$ as well as high mechanical strength such as high fracture toughness (5-7 MPa $m^{1/2}$) and a high bending strength (600-1500 MPa) [54, 57]. When considered of all unique properties of silicon nitride, it has become the most qualified non-oxide ceramic with wide range of applications even under harsh conditions. Table 2.1 shows the properties of silicon nitride ceramics with different treatments [58].

Table 2.1 : Material properties of hot-pressed, pressureless sintered and reaction sintered Si_3N_4.

Item	Hot Pressed Si_3N_4	Pressureless Sintered Si_3N_4	Reaction Sintered Si_3N_4
Density (kg/m^3)	3.07-3.37	2.8-3.4	2.0-2.8
Thermal Conductivity (W/mK)	29.3	15.5	2.6-20
Specific Heat (J/kgK)	711.756	711.756	-
Flexural Strength (MPa)	(20 ˚C) 450-1200	(20 ˚C) 275-1000	(1400 ˚C) ~ 300
Compressive Strength (MPa)	4500	4000	-
Linear Thermal Expansion ($x10^{-6}$/˚C) at 20-1000 ˚C	3-3.9	~ 3.5	2.5-3.1
Young's Modulus (GPa) at 20 ˚C	250-320	195-315	100-220
Fracture Toughness (MPa $m^{1/2}$)	2.8-12	3.0-10	~ 3.6

2.2.3 Matrix materials

In electronic packages, operating and usage conditions can adversely affect the properties of TIM material and lead to performance deterioration. In order to avoid these problems, thermal, mechanical, compression and surface properties of matrix material and interface compatibility between filler and matrix need to be considered. Furthermore, the adhesion of TIM to solid electronic surfaces is another essential issue to consider in the concept of thermal performance of packages. Therefore, the materials that are easy to form and blend well with filler should be selected as matrix material of TIM [33].

Materials used for the thermal management applications have to display high service temperature. In this sense, thermoset polymers such as epoxies, polyesters, polyurethanes, silicones etc. might be the good option due to their low cost and their high thermal stability. However, the criterias like processability and recyclability should be taken into consideration to determine matrix materials. Therefore, engineering thermoplastics would be more suitable material selection for TIM application owing to their excellent thermal and mechanical properties besides their processability and recyclability [22].

Commonly used thermoplastic polymers matrixes are polycarbonate [59, 60], polyamide [61, 62], polyvinylchloride [63], polyethylene [64, 65] and polypropylene [66, 67]. However, considering thermal conductivity, processability, ease of modification, service temperature and compatibility with silicon nitride; poly (methyl methacrylate) (PMMA), polsulfone (PSU) and poly (ether ether ketone) (PEEK) were used as the matrix materials in this thesis.

2.2.3.1 Poly (methyl methacrylate) (PMMA) as matrix material for TIMs

PMMA is a thermoplastic polymer and has been extensively used in the engineering applications for a long while. It was first commercialized by German Company Rohm and Haas five years after its discovery in 1928 by W. Chalmers, O. Röhm and W. Bauer [68]. The first application of PMMA was aircraft windows and bubble canopies for gun enclosures during World War II [69]. PMMA is generally known as acrylic glass with the trade name Plexiglas or Lucite due to its high impact strength, lightweight and shatter-resistant nature. It exhibits outstanding properties like easy processing conditions, scratch and weather resistance [70].

The unique properties of PMMA lead several processing conditions and ease of implementation. Besides, large pendant groups of MMA unit prevent the chains from packing intimately in crystalline trend. Hence, this structural arrangement (Figure 2.6) leads MMA monomer to polymerize with amorphous morphology. As a result, PMMA is a brittle and rigid material with high glass transition temperature around 105 °C and low shrinkage in molding conditions [69, 70].

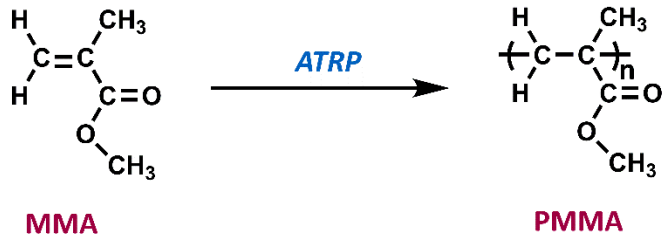

Figure 2.6 : Schematic representation for the synthesis of PMMA via ATRP.

PMMA can be synthesized with different methods such as solution polymerization, bulk polymerization, emulsion polymerization, anionic polymerization and free radical polymerization. Krzysztof Matyjaszewski discovered a new technique called Atom Transfer Radical Polymerization (ATRP), a kind of living polymerization technique, which enables [71] to synthesize PMMA with even higher molecular weight at almost 100,000 g/mol with over 80 % conversion and ~ 1.1 – 1.3 polydispersity range [72]. ATRP (Atom Transfer Radical Polymerization) is the most commonly utilized and effective technique with controlled functionalities and compositions providing well-defined polymers [73].

PMMA is a well-recognized and widely studied polymer having significant dielectric properties in electronic industry. The advantages of utilizing PMMA in electronic industry is its ease of processability, preparation and application alongside its stability [74, 75]. It is therefore the compatibility of nanoparticles with PMMA matrix results in substantial outcomes due to the rigid nature of PMMA comparing to other conventional polymers [73, 76]. It is a hard thermoplastic for instance with high modulus, high strength and low elongation at break together with its higher scratch resistance than other traditional polymers like polycarbonate (PC). Moreover, PMMA is an economical substitute of other polymers [69]. The outstanding characteristics of PMMA for a wide range of applications are listed in Table 2.2 [77].

PMMA was selected as one of the matrix material in this thesis owing to its low cost and ease of synthesis conditions besides having excellent thermal and mechanical properties for TIM application.

Table 2.2 : Main properties of PMMA.

Properties	Value
Density	1.18-1.20 g/cm3
Water Absorption	0.3-2 %
Transmission, Visible	~ 92 %
Young's Modulus	1.8-3.2 GPa
Tensile Strength	47-79 MPa
Compression Strength	70-120 MPa
Electrical Resistivity	~ 10^{15} Ω.cm
Thermal Conductivity	~ 0.2 W/mK
Glass Transition Temperature	~ 105 ˚C
Softening Point	~ 115 ˚C
Melting Point	~ 160 ˚C

2.2.3.2 Polysulfone (PSU) as matrix material for TIMs

Aromatic polysulfones are commercially available amorphous high-performance engineering thermoplastics including several superior characteristics such as its outstanding strength and flexibility even at higher temperatures, high glass transition temperature, chemical and thermal stability, high resistance to hydrolysis and chemicals, dimensional stability as well as good film forming properties [78]. In addition, polysulfone is the one of engineering thermoplastic with highest service temperature. The heat resistance capability leads PSU to be used as a flame retardant material even in the applications need high stiffness [79]. Therefore, polsulfones (PSU) haven been utilized for a long time in the fields of engineering applications, material sciences, polymer and biology sciences, medical equipments, automotive parts, food processing chains and electronic industry owing to these excellent properties [80].

The first synthesis of PSU was realized by Kreuchunas in 1958 [81]. Then, Johnson and coworkers discovered high molecular weight polysulfones. The various types of polysulfones like polysulfone (PSU), polyphenylsulfone (PPSF) and polyethersulfone (PES) have been commercialized with the trade names of UDEL® PSU, Radel® PPSF and Victrex® PES since 1965 (Table 2.3) [78].

Table 2.3 : Commercially available polysulfones.

Structure	Trade Name	Company	Year
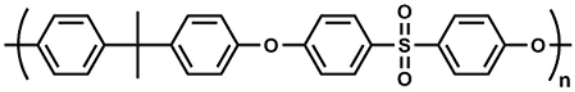	UDEL (PSU or PSF)	Union Carbide	1965
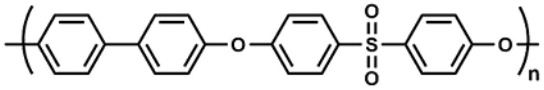	RADEL (PPSF)	Union Carbide	1976
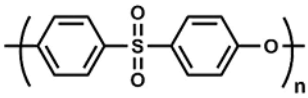	VICTREX (PES)	ICI America Inc.	1972

Polysulfone is known for having diphenylene sulfone repeating units in its structure. The inflexible and immobile -SO_2- groups give mechanical stability to PSU. Furthermore, the phenylene rings in repeating units generate dimensional stability, high rigidity and strength, creep resistance and high heat deflection temperature. The ether linkages provide to PSU resilient and stiff but strong structure. What is more, phenyl ether and phenyl sulfone groups allow PSU long-term availability and high temperature, oxidative and PH stability during use [80, 82]. Due to these structural characteristics (Table 2.4), PSUs are extensively applied in the wide range of industrial areas [83].

Table 2.4 : Main properties of PSU.

Properties	Value
Density	1.24 g/mL
Water Absorption at Equilibrium	0.5 %
Glass Transition Temperature	185 ˚C
Tensile Strength	70 MPa
Elongation at Break	50-100 %
Flexural Modulus	2.7 GPa
Impact Strength, notched, 23 ˚C	50-70 j/m
Processing Temperature	330-385 ˚C
Volume Resistivity	~ $5x10^{16}$ Ω.cm
Coefficient of Thermal Expansion	$56x10^{-6}$ K^{-1}
Thermal Conductivity	0.22-0.26 W/mK

Polysulfones have been employed extensively in numerous application areas such as composites [84, 85], thin film technology [86], fuel cells [87-89], coatings [90, 91], biomaterial [92] and microelectronic devices [93, 94] due to their excellent mechanical and thermal properties. Also, polysulfones are generally used as ion-exchange membranes in electrodialysis and polymer electrolyte membrane electrolysis [80, 95].

In the preparation of PMMA grafted silicon nitride (PMMA-SNNS) nanocomposite, synthesis of PMMA was achieved with alkyne-end functionality via ATRP in accordance with click reaction. The polymers synthesized by polycondensation reaction, need to be functionalized to be used in click reaction. Therefore, polysulfones with hydroxyl-end functionality synthesized via polyetherification route were subjected to alkynylation reaction of terminal groups in order to be utilized in click reaction. The modification of polysulfones can be performed also to obtain several properties desired like processability and reactionability, besides alkynylation of polysulfones to carry out click reaction. For this purpose, two different approaches can be applied to functionalize polysulfone, which are post-polymerization of polymers synthesized and direct copolymerization of already functionalized monomers. Post-polymerization technique was applied to functionalize polysulfone in this thesis.

PSU was selected as one of the matrix material in this thesis because of being amorphous engineering thermoplastic allowing ease of processing at low temperatures and having functionalized end groups to modify the structure to adapt click reaction besides having excellent thermal and mechanical properties for TIM application.

2.2.3.3 Poly (ether ether ketone) (PEEK) as matrix material for TIMs

Poly (ether ether ketone) (PEEK) is a semi-crystalline high-performance engineering thermoplastic having excellent thermomechanical properties [96, 97]. Amongst traditional engineering thermoplastics, PEEKs show outstanding characteristics (Table 2.5) like high working temperature and high glass transition temperature, outstanding thermal stability, superior mechanical strength and excellent resistance towards high boiling point organic solvents, making them unique candidate for the developing of structural components in leading industries like aerospace and automotive industry [98]. Furthermore, they are also utilized in medical applications such as implants and sterilizable surgical instruments due to its biocompatible nature [99, 100].

Table 2.5 : Main properties of PEEK.

Properties	Values
Density	1.3–1.35 g/mL
Continuous Working Temperature	250 ˚C
Dielectric Constant	3.1
Volume Resistivity	$>10^{16}$
Tensile Strength	95 MPa
Elongation	25 %
Compressive Strength	120 MPa
Tensile Strength	90-100 MPa
Elastic (Young's) Modulus	3.5-4.1 GPa
Flexural Modulus	3650 MPa
Toughness (Notched Izod Impact at RT)	80 – 94 J/m
Melting Point	334 ˚C
Glass Transition Temperature	143 ˚C
Thermal Conductivity	0.25–0.29 W/mK
Specific Heat Capacity (at 20 ˚C)	2100–2200 J/kgK

Poly (ether ether ketone) (PEEK) is a member of Poly (aryl ether ketone) (PAEK) family. It is a light weight, biocompatible thermoplastic with aesthetic appearance and good strength. It was first developed by the US aerospace industry in 1970 and first produced by Victrex PLC and later by Imperial Chemical Industries (ICI) in 1980. It was also started to be used for dental applications by 1992 [99]. Some commercially available PAEKs are seen in Table 2.6 [101, 102].

Table 2.6 : Commercially available poly (aryl ether ketone)s (PAEK)s.

Structure	Trade Name	Company
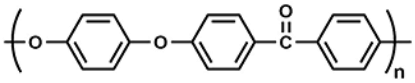	VICTREX (PEEK)	ICI
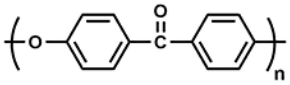	STILAN (PEK)	Raychem Corporation
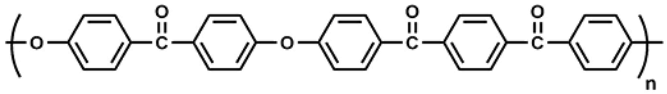	ULTRAPEK (PEKEKK)	BASF

The diphenylene ketone groups provide the high thermal stability to PEEK structures besides ensuring high strength and high resistance to oxidation, yet give rigidity to polymer. In addition, ether linkages procure flexibility alongside thermal stability. PAEKs preserve their high degree mechanical properties even at close to their melting temperature owing to semi-crystalline nature they have. Also, their creep resistance

and wear properties which can be maintained over a wide range of temperature degrees also excellent [100, 103].

As in the manner of preparing PSU matrix nanocomposite, by means of nucleophilic aromatic substitution (NAS) reaction, poly (ether ether ketone)s (PEEK)s with hydroxyl-end functionality were synthesized and then alkynylation of terminal groups was achieved successfully so as to obtain TIM through click reaction.

PEEK was selected as one of the matrix material in this thesis to demonstrate the effect of the differences between amorphous polymers and semi-crystalline polymers on thermal conductivity besides asserting excellent thermal and mechanical properties of PEEKs for TIM application.

2.3 Thermal Conductive Polymer Nanocomposites

The require for polymer composites with high thermal conductivity emanates from the demand for heat management and heat dissipation in electronic packaging as a result of miniaturization of electronic components [104]. Therefore, effective thermal management is crucial to control the performance and dependability of these components. In this sense, it is of great importance to produce and develop novel thermal conductive materials with effective characteristics in order to manage these problems [105].

2.3.1 Thermal conductivity theory

In thermal conductivity theory, thermal dissipation proceeds throughout several media by means of convection, conduction or radiation processes. Heat conduction refers to the transportation of vibrational energy of particles to the neighboring particles [106]. When two pieces having different temperatures contact with each other, heat energy conveys from the piece with high temperature to the one with low temperature. In other words, the heat conduction process signifies the energy transportation process in the same time, denoted as thermal conduction phenomenon [107]. Thereby, heat is an indicator of how much and how fast this energy transferred from which direction to which direction, while temperature is an indicator of how many particles are vibrating. Figure 2.7 illustrates the thermal conduction phenomenon in a solid matter [4].

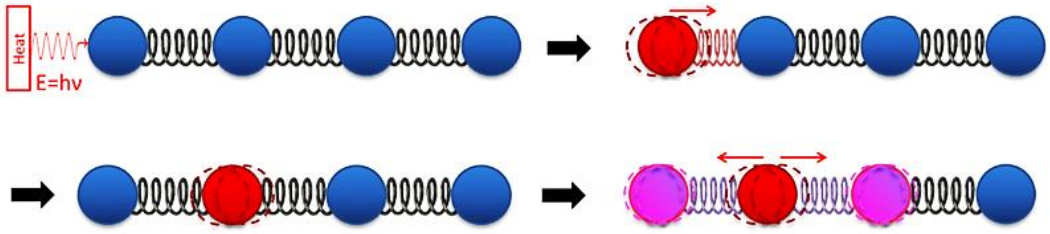

Figure 2.7 : The illustration of a thermal conduction in a matter via collision of particles.

In compliance with the thermal conductivity phenomenon, heat is transferred by free electrons, phonons (lattice vibration waves) or photons (electromagnetic radiation) in solids [108]. The thermal conduction mechanism of solids is a complex phenomenon hinges on several significant parameters such as morphology of materials, type, thickness and proportions [109]. For example, when evaluated in size and proportion aspect, a thicker material conveys the heat from one face to opposite face in a longer time according to thinner material [110]. Also, crystalline materials have invariably higher thermal conductivity in comparison with amorphous materials when assessed in the morphological aspect [111].

The thermal conductivity mechanism of perfect crystalline filler-based nanocomposites is easily predictable [112]. When the phonon transfer through a crystalline structure is evaluated in the vibrational and wavelike aspects, thermal conductivity can be appraised as follows with the Debye equation (2.2) [107, 113]:

$$\lambda = C_p \upsilon l / 3 \qquad (2.2)$$

Where λ is the thermal conductivity of solid, υ is the average phonon velocity, l is the mean free path of the phonon and C_p is the specific heat capacity per unit volume.

Another extensively employed parameter relevant to thermal conductivity is also thermal diffusivity. It can be evaluated as follows with this equation (2.3) [107]:

$$\alpha = \lambda / dc \qquad (2.3)$$

Where α is the value of thermal diffusivity, d is the density of a material, c is the specific heat capacity and λ is the thermal conductivity. Thermal diffusivity is related to the concept of transient heat conduction which is a process including heat transfer and so temperature change and indicates the temperature change rate [114, 115]. When temperature change through the entire body of sample is low, the thermal diffusivity will be great under equivalent heating and cooling conditions. Overall, the thermal

diffusivity substitutes for the speed of the heat transfer in a material, while thermal conductivity symbolizes the heat conducting capacity of a material. To put in a different way, thermal diffusivity can be considered as an indicator of the speed of heat transportation between two faces of a material [4, 116, 117]. Hence, in the processes of calculating the heat retention time of a material in heat treatments, thermal conductivity is always a significant parameter [107].

2.3.2 Thermal conductivity in polymer nanocomposites

Over the past two decades, thermal conductivity of polymers has become a critical parameter for numerous applications. Typically, the characteristic features of polymers like the high molecular vibrations, crystal structure, comparatively low atomic density and intrinsically weak chemical interactions and bonding, give rise to the polymers display poor thermal conductivity [105, 118]. The lower intrinsic thermal conductivities of polymers than metals and ceramic materials provide them become of a good candidate for the thermal insulation applications such as electronic packaging which includes chemical and moisture resistances, excellent processability, lightweight and electrical insulation as well [105, 119].

The intrinsic thermal conductivity of polymers is typically low approximately within the range of 0.1–0.5 W/mK due to the complexity of polymer chain morphology [120, 121]. Table 2.7 shows the thermal conductivity values of few important polymers.

The long-chain molecular nature of polymers ranges from highly ordered crystalline structures to random amorphous structures. Also, the imperfections of polymers such as voids, impurities, random orientation, chains entanglements and dangling chain ends, bring about to phonon scatterings and substantial diminishment in phonon's mean free path. These results contribute to thermal resistance in thermal conduction of polymers [105, 122].

The heat dissipation in polymers realizes by the phonon transfer that occurs because of the heat transportation generated by the collision of particles with each other and with subatomic particles throughout the polymer. Furthermore, the morphology of polymers has a great effect on the thermal conductivity of polymers. For example, amorphous polymers cannot oriented into single direction, therefore contribute to thermal resistance, and hence lead to decrease in thermal conduction [123-125]. On the other hand, the high degree crystalline polymers can transfer the heat quickly

throughout the structure. In other words, heat conduction is managed by the interconnected vibrations of well-oriented molecular chains in the crystalline regions [126].

Table 2.7 : Thermal conductivities of selected polymers.

Polymer	Thermal Conductivity ($Wm^{-1}K^{-1}$) at 25 ˚C
Polypropylene (PP)	0.11
High-density polyethylene (HDPE)	0.44
Low-density polyethylene (LDPE)	0.30
Polycarbonate (PC)	0.20
Polystyrene (PS)	0.14
Poly(butylene terephthalate) (PBT)	0.29
Poly(methyl methacrylate) (PMMA)	0.21
Poly(ethylene terephthalate) (PET)	0.15
Nylon-6 (PA6)	0.25
Nylon-6.6 (PA66)	0.26
Epoxy Resin	0.19
Poly(acrylonitrile-butadiene-styrene) (ABS)	0.33
Poly(dimethyl siloxane) (PDMS)	0.25
Poly(ether ether ketone) (PEEK)	0.25
Polyimide, Thermoplastic (PI)	0.11
Polyphenylene Sulfide (PPS)	0.30
Poly(ethylene vinyl acetate) (EVA)	0.34
Polysulfone (PSU)	0.22
Polytetrafluoroethylene (PTFE)	0.27
Polyvinylidene difluoride (PVDF)	0.19
Polyphenylsulfone (PPSU)	0.35

Promoting the thermal conductivity of polymers and polymer nanocomposites by making no concessions from many other desirable properties of polymers are of great interest. Hence, most of the studies devoted to enhance the thermal conductivity of polymers denotes the incorporation of nanofillers with thermal conductivity with polymers need to be realised. Some of the commonly used thermal conductive nanofiilers are tabulated in Table 2.8.

Table 2.8 : Thermal conductivities of mainly used fillers.

Filler	Thermal Conductivity (W/mK) at 25 ˚C
Aluminum (Al)	247
Copper (Cu)	398
Gold (Au)	315
Silver (Ag)	427
Graphene (GnP)	2000-6000
Graphite	100-400
Carbon nanotube (CNT)	3000
Silicon Carbide (SiC)	120
Hexagonal boron nitride (hBN)	300
Silicon nitride (Si_3N_4)	200
Aluminum nitride (AlN)	100-300
Beryllium oxide (BeO)	230-330

2.3.3 Factors affect the thermal conductivity of polymer nanocomposites

Thermal conductivity of the nanocomposites depends on the numerous factors. For example, enhancing the thermal conductivity of polymer nanocomposites is directly associated with the heat transfer at interface between the filler and matrix. In this sense, several parameters are unveiled to be indispensable to comprehend the heat transfer at interfaces. For instance, crystallinity is one of the main factor to effect the heat conduction relating to defects in structure leading to phonon scattering. Furthermore, due to the fact that the thermal conductivity is an anisotropic property, aspect ratio, length, size, diameter and surface area of the filler are considered as the key factors relating to thermal conductivity.

One of the essential parameter affecting the heat transfer is the thermal interface resistance caused by defects and impurities in the lattice, boundary scattering or phonon-phonon scattering [4]. Because, the heat transfer in nonmetallic substances is controlled by phonons or lattice vibrations [5]. In order to enhance the thermal conductivity, these phonon scatterings arise from the flaws in the filler-matrix interface must be reduced [6]. It is therefore to overcome this problem and ensure better compatibility at the interface, the interaction type between the filler and matrix should be considered [7, 8]. If the interface region has a good bond between matrix and filler material, the overall properties of the nanocomposite will be better.

Many interphase properties depend on the type of interaction between filler and matrix and so bound, and therefore optimizing the filler-matrix interface is an important strategy in tailoring the nanocomposite properties. Establishing chemical bonds

between filler and matrix reduces the thermal interfacial resistance and minimizes flaws such as voids. This phenomenon suppresses phonon scattering and improves effective heat dissipation. By means of functionalizing the filler, the chemical bond formation between filler and matrix can be realized, thereby the higher interface compatibility between the two can be achieved besides improving the mechanical and electrical properties[11, 12].

Another critical parameter governing the thermal conductivity of nanocomposite is the dispersion scheme of fillers in polymer matrix. Polymer matrix nanocomposites can be fabricated either by chemical or mechanical process. If reinforcing material in nanocomposite could dispersed on a molecular scale (nanometer level) and interacted with matrix by chemical bonding, then significant improvements in the mechanical properties of the material or unexpected new properties might be realized. Uniform and homogeneous dispersion of nanoparticles in the polymer matrix is one of the major problem encountered in polymer nanocomposite fabrication. In order to achieve nanocomposites with enhanced properties, nano-sized particles should be dispersed in matrix material properly, otherwise there will be agglomeration of the particles and the properties of nanocomposites will deteriorate. There are several fabrication methods to control the dispersion of nanofillers in the polymer matrix. One of them is mechanic exfoliation method realized via ball milling technique that enables an increase in the surface area of nanofillers, as well as offering a uniform dispersion in polymer matrices [4, 13, 14]. This method provides also an alteration of the nanofiller morphology, allowing the nanofiller to be compatible with the polymer matrix. Therefore, SNs were exposed to mechanic exfoliation as the first stage of the process to serve easy way for chemical surface functionalization steps.

2.3.4 Thermal conductivity measurement techniques

The measurement of thermal conductivity is one of the essential and effective way for comparing different materials. It is therefore a calculation known also as Fourier's Law, which provides the thermal conductivity measurement of a material, based on a heat transfer in single direction, has been proposed. The thermal conductivity calculation according to Fourier’s Law can be evaluated as follows with this equation (2.4):

$$k = -\frac{q/A}{\Delta T/L} \quad (2.4)$$

Where q is the rate of heat transfer through a cross-section of area A, and ΔT is the temperature difference that exists over thickness L of the material [127]. Several methods have been proposed for measurement of the thermal conductivity of polymer nanocomposites and some of which have been accepted as ASTM standards [119]. These methods can be divided into two main classes as steady-state methods and transition methods. The steady-state method is a standard technique used especially to determine the thermal conductivity of materials with low thermal conductivity. This method is based on the basic principle which is the rate of heat transfer is equal to the cooling rate at steady-state. In this sense, the thermal conductivity is calculated via measuring the heat flux throughout the specimen, the thickness of the specimen and the temperature difference at both ends of the specimen, consistent with the one-dimensional heat transfer model [34, 107, 128].

The steady-state method is classified into two group as a guarded hot plate method and a heat flow meter method. The accuracy of the guarded hot plate method is the highest, but the measurement processes take long time and intricate, whilst the procedure of heat flow meter method is faster, but its measurement range is limited [129]. On the other hand, the transient methods execute a measurement through heating up process. The advantage of transient methods is that the measurement process takes less time as there is no need to wait until steady state condition is reached. However, the complexity of the mathematical data analysis process is a disadvantage for this method. Also, transient methods are generally favored for diffusivity measurements and necessitate a constant power heat source so that to record the temperature changes of specimens over time. Thus, the values of thermal conductivity, heat capacity and thermal diffusivity can be obtained from the time dependent temperature changes of specimens [130]. The classification of thermal conductivity methods is seen in Table 2.9.

Table 2.9 : Classification of the thermal conductivity measurement methods.

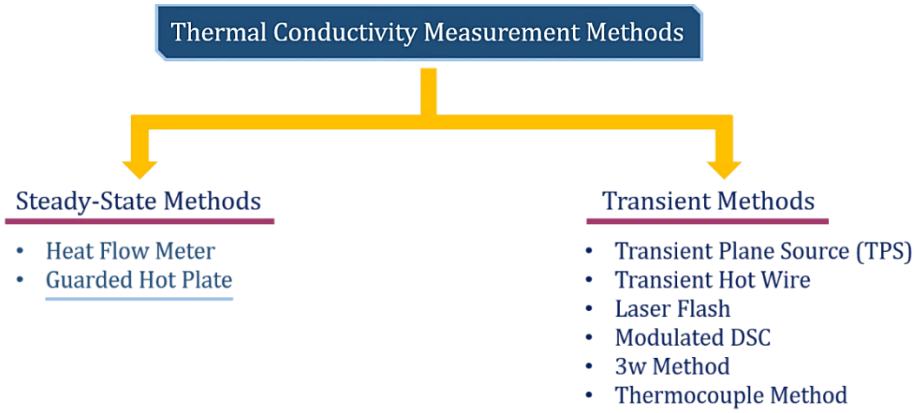

In this thesis, thermal conductivity measurements of thermal conductive polymer nanocomposites were realized via guarded heat flow meter technique complies with the ASTM E1530 standard. ASTM E1530 is one of the steady-state method for thermal conductivity measurement of thin conductive composites. The working principle of this method based on comparing the heat flow of samples with known thermal conductivities with that of unknown test specimens. In this technique, test specimens are sandwiched between two metal bars, bearing thermocouples to attain temperature gradients. In this system, there are heaters located in the upper and lower parts of the two metal rods to manage the heat flow. Besides, to measure the heat flux throughout the test specimen, a heat flux transducer (HFT) that generates voltage as a function of heat flux (q) has been placed in the system [131]. Three different steady-state measurement technique are shown in Figure 2.8 [127].

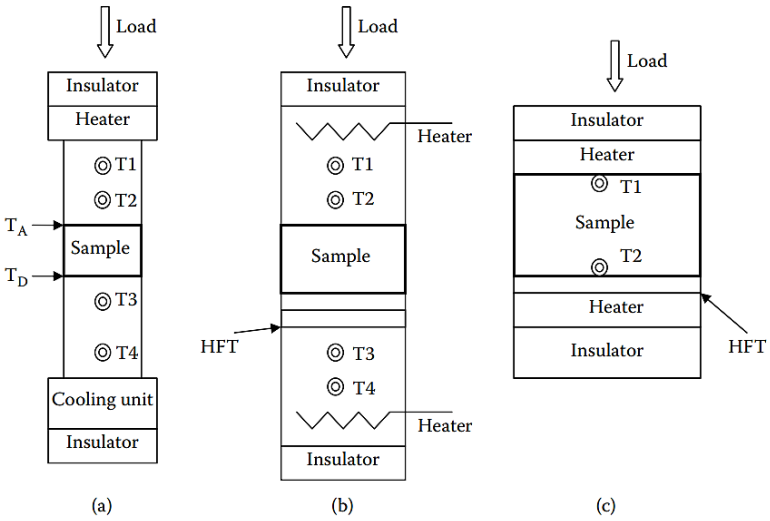

Figure 2.8 : Schematic depiction of steady-state measurement techniques; a) ASTM D5470, b) ASTM E1530, c) F433.

2.4 Nanocomposite Preparation Techniques

Thermal conductive polymer nanocomposites can be manufactured either by physical and chemical processes. Homogeneous and consistent distribution of nanofillers in polymer matrix is one of the critical issue in polymer nanocomposite manufacturing [132]. The uniform dispersion of nanofillers can be restricted by the inclination of nanofillers to agglomeration and to form clusters, which deteriorate the substantial characteristics of nanocomposites [133]. Researchers have developed many techniques such as mechanic mixing, chemical reactions or surface modifications of nanofillers to provide homogeneous distribution of nanofillers in polymer matrix [134].

The preference of the fabrication method is essential to obtain nanomaterials with desired characteristics. Techniques to prepare nanomaterials can be sorted in two ways as bottom-up and top-down approaches [135, 136]. The bottom-up approach is based on the assembly of precursors by chemical reactions. Chemical processes like chemical vapor deposition (CVD), spray pyrolysis, template synthesis or sol-gel methods can be given as the examples of most prevalent techniques for bottom-up methodology [137, 138]. Contrarily, the top-down approach is based on the breaking up of bulk material into smaller pieces by physical methods. It covers specifically the self-assembly principles, the surface chemistry and physicochemical interactions of adjacent atoms. Techniques such as intercalation, direct mixing, melt-mixing, solution mixing and ultrasonication can be given as the examples of widespread techniques for top-down methodology [139].

2.4.1 Physical methods

2.4.1.1 Mechanical intercalation

Intercalation method is based on the direct dispersion of nanofilllers in polymer matrix and it is one of the top-down methodology, which necessitates surface modification of nanofillers to improve the dispersion in polymer matrix basically. This method is principally based on the direct intercalation of polymer chains in co-solvent into swollen nanofiller layers in solvent and replacing of polymer chains with the solvent in which is swelled the nanofiller layers [134].

2.4.1.2 Direct mixing of polymer and nanoparticles

Another of the top-down approach is direct mixing of polymer matrix and nanofillers, which is based on the method of breaking up the aggregated nanofillers into small particles during mixing. This method consists of two accustomed ways of mixing the polymer and nanofillers, which are direct melt mixing and direct solution mixing [134].

2.4.1.3 Melt intercalation

This method enables principally the fabrication of composites made of polymers insoluble in any solvent and it is thereby used extensively in industrial processes such as extrusion and injection molding. Hence, this method necessitates no solvent and chemicals. Melt intercalation is conducted with the polymer matrix at molten state and involves the incorporation of nanofillers, generally clays, into the matrix under shear force [140]. However, the disadvantage of this method is that the blending of layered nanofillers with high molecular weight polymers can be challenging due to shear force [141].

2.4.2 Chemical methods

2.4.2.1 Sol-gel method

Sol-gel synthesis is one of the widespread method to fabricate the polymer matrix nanocomposites by chemical routes. This method comprises of two interrelated techniques as sol and gel. Sol is a colloidal solution of solid nanoparticles in a monomer solution and gel is a 3D interconnected network structure formed between the phases, followed by hydrolysis process [134]. The dispersed solid particles in a monomer solution produce the interconnecting network structure between the phases called gel through polymerization. The formed polymer chains behave as a nucleating agent and support the growth of layered particles to form nanocomposite structure [142].

2.4.2.2 Template synthesis

This technique allows the fabrication of exfoliated nanocomposites. In this process where the polymer is used as a template and behaves as a nucleating agent, the polymer promotes the growth of inorganic crystals and entraps these crystals between the cross-

layers [143]. Therefore, this method can be considered as one of the in-situ techniques. Moreover, the dispersion of nanofillers in polymer matrix takes place in a single step. However, template synthesis is not a technique generally preferred. It is rather utilized mainly in the field of inorganic porous material production instead of polymer nanocomposite fabrication [144].

2.4.2.3 In-situ polymerization

In-situ polymerization is one of the effective technique that enables the great distribution of nanofillers in polymer matrix. This system is consists of well-dispersed nanofillers in low molecular weight monomer or prepolymer, since low molecular weight monomers can emanate readily between the filler layers, results in swelling of nanofillers. This mixture is then polymerized by several agents like initiator, heat or radiation [143]. The adsorption of monomer/prepolymer molecules on the surface of well-dispersed nanofillers is obtainable with this technique. In other words, it is ensured that growing of these molecules from the surface of nanofiller and hence polymers are grafted onto the filler surface [145]. Another advantageous feature of this technique is that nanocomposites with both thermoset and thermoplastic matrix are attainable [146].

2.4.2.4 Chemical vapor deposition

This technique is preferred mainly to produce 2D nanomaterials. In this method, 2D nanosheets grow on the solid substrate by the reaction or decomposition of gas or vapor precursors at high temperatures in a vacuum chamber [147].

CVD method allows large-scale production of crystal products with high quality and high purity together with barely discernable defects on the solid substrate. However, the disadvantages of this method are that the removing of nanosheets from deposited substrates are challenging and the production costs are high [148].

2.4.2.5 Click chemistry

The basic problem in the production of polymer matrix nanocomposites is the challenging of uniform dispersion of nanofiller in the matrix due to the aggregation tendencies. Therefore, several methods have been proposed to facilitate the homogeneous dispersion of nanofiller in polymer matrix such as sol-gel method, in-situ polymerization, melt intercalation, ultrasonication, functionalization of the filler

surface and some grafting approaches. Nevertheless, these methods are not efficient with regard to form covalent interaction between the filler and matrix by reason of some drawbacks like reaction conditions, less control on the molecular weight of polymers, insufficient functionalization of nanofillers and low reaction yields [149, 150].

In this context, click chemistry has drawn much attention in the fields of polymer science and material engineering. It brings various advantageous like moderate reaction conditions, high reaction yields, stereospecific reaction types, tolerance to varied functional groups and easily obliterable byproducts [151]. Especially, the effective coupling of functionalized nanofiller and polymer matrix via click reaction results in a remarkable distribution of the nanofillers in polymer matrix [152, 153]. Therefore, click chemistry can be postulated as a versatile tool for the fabrication of polymer matrix nanocomposites owing to having high reactivity, reliability and selectivity [154]. Moreover, commonly utilized click reactions of copper(I)-catalyzed azide-alkyne cycloaddition (CuAAC) [153], nucleophilic or radicalic thiol-ene [155] and thiol-yne [156] reactions and Diels-Alder (DA) [157] reactions have been introduced into the literature as the essential click tools for the fabrication of polymer matrix nanocomposites.

2.5 Modifications Applied to Nanocomposite Precursors

The greatest challenge in the fabrication of the polymer matrix nanocomposites is tuning the interfacial compatibility between the matrix and nanofiller [136]. Otherwise, the essential properties of nanocomposites such as morphological, thermal and mechanical characteristics will be worse than the properties of the pristine parents of nanocomposite [134]. To overcome this situation, one should consider the homogenous and uniform dispersion of nanofillers in polymer matrix and also the procedures that aim the enhanced interfacial interaction between the filler and matrix should be performed [158, 159]. In other words, the interface border between filler and matrix has an effect on the end-property of a nanocomposite. Furthermore, the interaction characteristics, nanostructure and the composition at the interface diversify throughout the interface border and are unlike to both matrix and filler [160]. The interaction or bonding type at interface is so significant, since most of the interface properties depend on this interaction and therefore the entire characteristics of the

nanocomposite can be modified by optimizing the interfacial bond. Hence, some treatments and surface functionalization procedures for both nanofiller and polymer matrix should be carried out to tailor the interfacial interaction [161].

2.5.1 Modifications of inorganic fillers

In the fabrication of polymer matrix nanocomposites, the nanofillller dispersion in polymer matrix is a critical issue due to the tendency to agglomeration, which stems from nanoscale size and high aspect ratio of nanofillers [162]. However, the high aspect ratio of one-dimensional or two-dimensional nano-fillers creates easy contact of the layers with each other, leading to the formation of a thermal conductive path; yet this is an anisotropic conductivity [163, 164]. Therefore, the dispersion of nanofillers in polymer matrix is a critical issue for thermal performance. In other words, the poor contact area between the filler and matrix could contribute to interface resistance and extra scattering over heat carriers resulting in enhanced thermal boundary resistance (TBR) which deteriorate the thermal performance of the nanocomposite [165]. Accordingly, several techniques such as ultrasonication, mechanical treatments, surface functionalization with coupling agents and chemical functionalization etc. have been suggested and performed to obtain nanocomposites with fine dispersion [34].

2.5.1.1 Preparation of nanosheet structure

The adjacent plates of the inorganic filler are in the form of stuck tightly to each other due to the common sharing of the counter-ions and cause the filler to form a bulk structure. Therefore, they must be subjected to appropriate treatments before the nanocomposite preparation to make the filler plates suitable to interact properly with the polymer matrix as shown in Figure 2.9 [111, 166, 167].

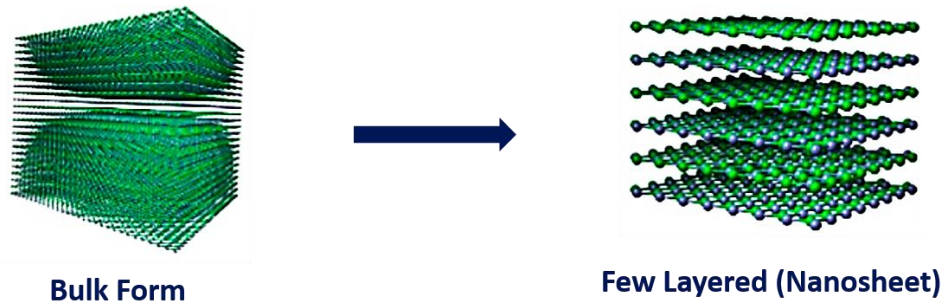

Figure 2.9 : The schematic illustration of nanosheet formation.

Apart from the situation mentioned above, the shape and size of the nanofiller have also a significant role on the thermal conductance performance of the nanocomposite [6, 168]. From a particular point of view, the fillers with smaller size have large surface area showing improved surface energy, while the fillers with larger size display the vice versa. In other words, the larger fillers give rise to less filler-matrix interface due to having smaller surface area, leading to thermal barrier formation and phonon scattering and hence their thermal conductivity show low values when compared to the thermal conductivity (TC) of nanocomposites having smaller particle size [169-171].

i. Liquid exfoliation

A number of methods have been proposed for the nanosheet formation such as surface passivation, oxidation, ion-exchange or ion intercalation [172]. However, there is one of the versatile, scalable and sustainable technique named liquid phase exfoliation (LPE) have been employed for a while to produce layered materials [173, 174]. The production of few-layered nanosheets are obtained by applying ultrasound or high shear to bulk form of layered inorganic crystals in predetermined stabilizing liquids using bath or tip sonicators [175]. Furthermore, this method enables the scalable production of 2D nanosheet-based nanocomposite materials [176].

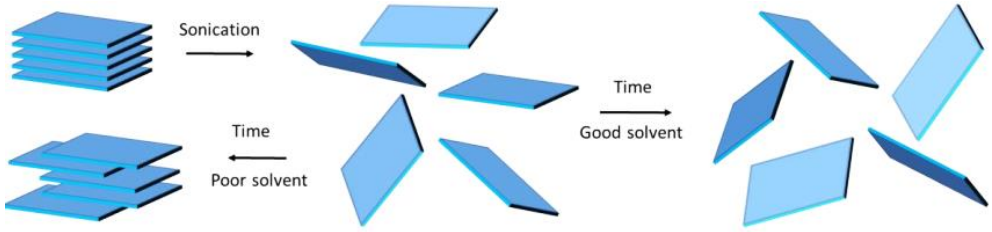

Figure 2.10 : Schematic description of sonication assisted liquid exfoliation.

The liquid phase exfoliation process (Figure 2.10) results in the formation of nanosheets having high aspect ratio and large surface area, which are suitable for the applications that necessitate surface performance [177]. Therefore, this technique can be utilized as a practical tool before subsequent chemical modification processes of nanosheets [177]. However, liquid exfoliation has some drawbacks, one of them is the variabilities in both longitudinal and lateral sizes ranging from nanometers to microns [177-179]. Another disadvantage of this technique is that only small-scale fabrication

is allowed. Hence, more effective techniques need to be performed to obtain 2D nanosheet formation [180].

ii. Mechanic exfoliation

Two-dimensional materials have been drawn much attention over the last few years due to their excellent structural, thermal and electronic properties. Yet, their significance was realized even more after the isolation of layers from their bulk crystals into individual monolayers [181]. In recent years, many methods have been proposed to prepare two-dimensional layered structure. However, mechanical ball milling one of the simple, cost effective and functional method has been practiced effectively for a while to produce monolayer flakes from layered bulk crystals [182]. Mechanical exfoliation method has been considered as the most convenient method to obtain single crystalline flakes with superior quality in accordance with a number of research areas [183, 184]. Moreover, mechanical ball milling enables the large scale fabrication of bulk nanofillers, so it might be considered as an ideal method to fulfill a high quality morphology in nanocomposites with reduced particle size and low cost [185].

Ball milling is a kind of mechanical process based on the energy and heat released during collision of balls with each other and with powder. The working principle of grinding process can be explained simply by the centrifugal force, inducing the grinding of a powder, with the help of the frictional force created by collision of balls to walls as mill rotates as shown in Figure 2.11a. There is also the reverse rotary motion of disk on the other hand, which implements an inverse centrifugal force to the mill. This movement causes the ball to migrate the opposite cell walls of the mill and create the strike effect. The size reduction of fillers with ball milling is realized mainly by this impact effect (Figure 2.11b) [186].

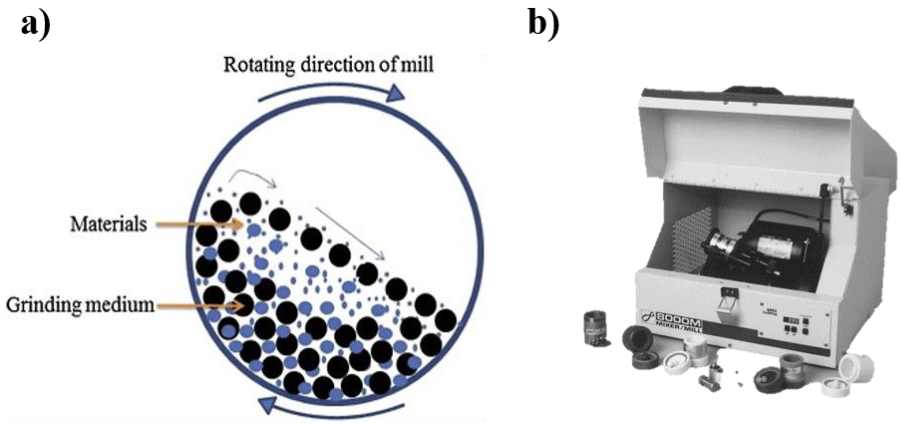

Figure 2.11 : a) The internal view of grinding cell and planetary movement, b) The internal and external view of the milling device.

Mechanical ball milling has been employed in a number of business and research fields on the purpose of size reduction for a while. In recent years, the production of nanomaterials with superior physical properties and novel microstructures has been achieved effectively by means of this high-energy ball milling processes [187]. Furthermore, the essential advantages such as scalability, cost-effectiveness and versatility provided the widespread application of high-energy ball milling techniques. Therefore, the mechanical exfoliation with high-energy ball milling is a better candidate according to other exfoliating techniques for the size reduction and the large-scale fabrication of nanofillers [14, 188].

Ball milling has two different impacts on layered materials, compression force and shear force (Figure 2.12). Therefore, layered materials can be cleaved into 2D nanosheet structure from both surfaces and edges through these forces [189, 190, 191].

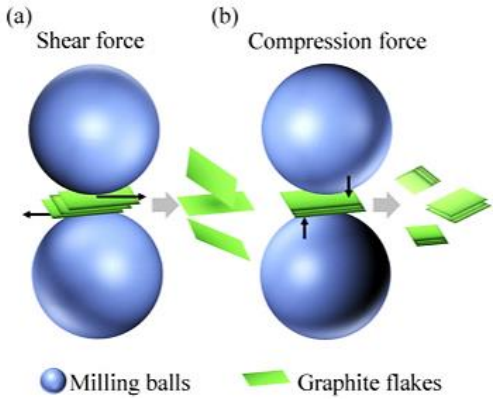

Figure 2.12 : The illustration for the effect of a) shear force and b) compression force on the layered materials.

The most advantageous characteristic of milling process is that it can be carried out in the absence of solid or liquid exfoliating agents, which enables to obtain 2D nanosheets without contaminants in comparison with the conventional methods (Figure 2.13). Hereby, the post-production treatments for removing contaminants in nanosheet manufacture can be thus eliminated by this way [192].

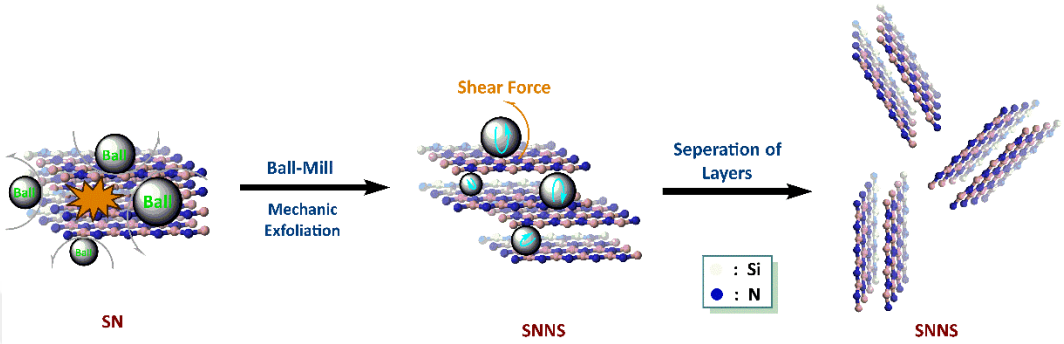

Figure 2.13 : The schematic illustration of the mechanic exfoliation process via ball milling.

The exfoliation trends of starting materials are effected by some milling parameters involving milling ball size, ball-to-powder ratio, milling speed and milling time [193]. Characteristically, the milling balls are made up of generally stainless steel. Similarly, the diameter of balls varies within the range of 1-25 mm. The ball-to-powder ratios are determined according to type of material will be grinded. For example, the ratio of 75:1 to 150:1 can be desirable for the rough powders, while the range between 5:1 to 10:1 will be sufficient for smoother materials [194]. Also, the milling time varies from less than 1 hour to more than 30 hours, in accordance with the particle size desired [195].

2.5.1.2 Surface functionalization of nanosheets

Studies on thermal conductivity improvement of polymer matrix nanocomposites are carried out by incorporating the inorganic fillers with high thermal conductivity into the polymer matrix. The differences in physical and chemical structure between the polymer matrix and inorganic filler and the weak chemical affinity between these two materials cause difficulties in tailoring and improving the performance of nanocomposites [169].

The surface functionalization processes of inorganic fillers have an essential role in the development of TIM performance. A considerable amount of investigations have

been carried out on thermal resistance, also known as Kapitza Resistance, which deteriorates the performance of nanocomposite as a result of inconsistent temperature distribution at the filler-matrix interface [33]. Therefore, the surface functionalization procedures of fillers offer an opportunity to achieve better compatibility between the filler and matrix, which leads to efficient heat transfer throughout the filler-matrix interface, reduced the thermal boundary resistance (TBR) and minimized flaws such as voids [196, 197].

Surface functionalization procedures can be separated into some routes such as forming covalent interaction, physical blending, air plasma and low oxide. Covalent modification of the filler surface is the most efficient way for the functionalization and based on a chemical reaction between the filler surface and the functional groups of modifying agent [198, 199]. Modifying agents are amphiphilic compounds, a kind of coupling agents, having functional groups that are compatible with both matrix and filler, which provide interface compatibility between the filler and the matrix. Accordingly, one can suggest that the chemical interaction between nanofiller and polymer matrix can reduce the thermal resistance at interface by means of this method [200, 201].

On the other hand, unmodified Si_3N_4 nanoparticles have an inclination to agglomerate due to the possession of high surface energy. Hence, providing the uniform distribution of nanofiller is one of the great challenge in fabrication of nanocomposites [202, 203]. Therefore, surface functionalization procedures have to be utilized in order to obtain homogenous distribution of nanofiller into polymer matrix. Thus far the materials used to modify the surface of Si_3N_4 can be listed as small molecular coupling agents [204, 205], macromolecular coupling agents [206, 207] and surface-grafting polymer chains [208].

Several studies affirms that the nanocomposites having modified nanofillers allows to obtain higher thermal conductivities compared to nanocomposites containing unmodified nanofillers [16, 209-211]. In this thesis, three-step modification procedure was applied to the mechanically exfoliated silicon nitride nanosheets; these are amination, bromo-amidation and azidation reactions, respectively.

i. Amination

The performing the surface functionalization of nanoparticles via chemical reactions is the most preferred route for the modification processes, since the chemical bonds provide strong interactions between the nanofiller and modifying agents [212]. This method is realized by silane coupling agents (Figure 2.14) as modifier or by grafting polymer chains onto surface of silicon nitride. Surface functionalization of nanoparticles is carried out by the chemical reaction between silanol groups on the nanoparticle surface and functional groups of silane reagents in appropriate conditions. The amination mechanism of nanofilers starts with the hydrolysis of alkoxy groups of coupling agents in first, then hydrogen bonds constructed between the silanol groups on the surface of nanofiller and coupling agent, end up with the formation of covalent bond in the end [108, 213-215].

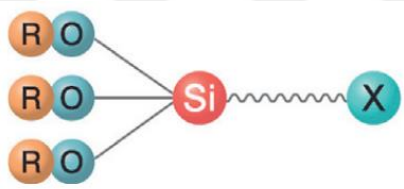

Figure 2.14 : General formula of silane coupling agents.

A large number of coupling agents known as functional silanes permit us to ameliorate the interaction between the nanofillers and polymer matrix, and as a result phonon scattering is minimized. The general formula of the coupling agents is $ROSiX_3$, where X- corresponds to the organofunctional end group and RO- refers to the hydrolysable groups like alkoxy or acetoxy silanes [216]. Some commercial coupling agents are listed in Table 2.10.

Table 2.10 : Types of commercial silane coupling agents.

Name and Abbreviation	Ref.
3-Aminopropyltriethoxysilane (APTES)	[217]
3-Glycidoxypropyltrimethoxysilane (GPS)	[218]
3-Aminopropyltrimethoxysilane(APTMS)	[219]
Aminopropyl methyldiethoxysilane (APMDES)	[220]
(3-Acryloxypropyl)methyldimethoxysilane (APMDMS)	[221]

The functionalization processes of filler surfaces with coupling agents are performed through the reaction of the hydroxyl groups on the surface of Si_3N_4 with the

hydrolysable RO- group of the coupling agents to attain hydrophobized Si_3N_4. Then, the another functional groups on coupling agents designated as X, generally amine groups for silane coupling agents, are reacted with the functional end-groups of polymer matrices to produce composite structure [222-224]. The whole bonding mechanism of silane coupling agents to inorganic surfaces is given schematically in Figure 2.15.

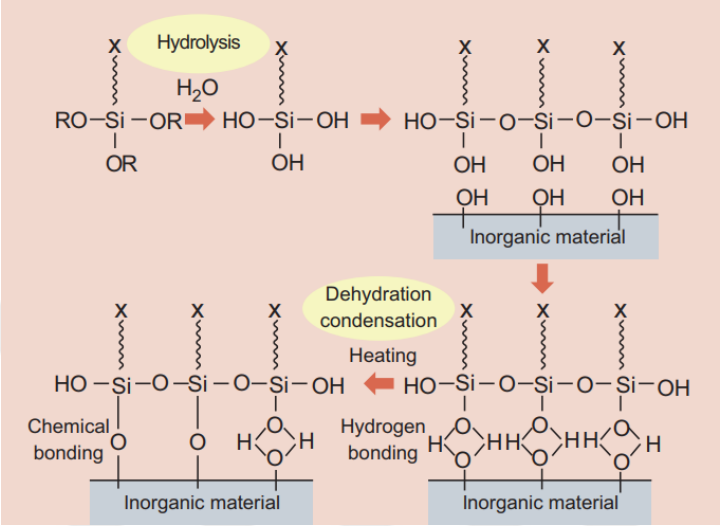

Figure 2.15 : The bonding mechanism of silane coupling agent to inorganic surface.

In this thesis, the first surface modification reaction was carried out with silane coupling agent, (3-Aminopropyl) triethoxysilane (APTES) which involve three ethoxy groups and terminal amine to obtain amine-end functional silicon nitride nanosheets ($SNNS\text{-}NH_2$). This process is depicted in Figure 2.16.

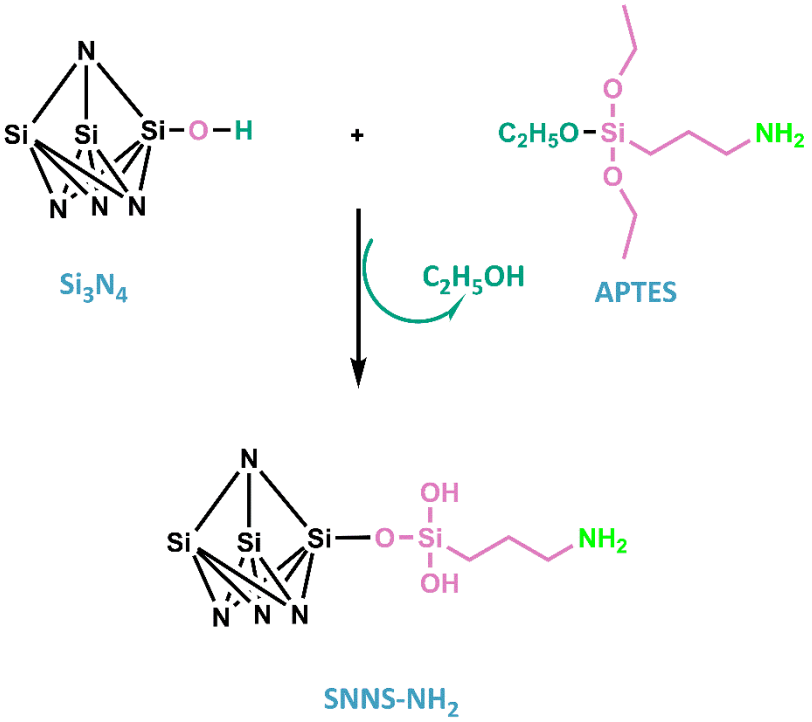

Figure 2.16 : The surface modification process of SNNS with APTES.

ii. Bromo-amidation

In this thesis, silicon nitride nanocomposites with PMMA matrix were fabricated by two different methods as SI-ATRP and click chemistry to compare the effect of different preparing routes on thermal conductivity. The second modification step is conducted by bromoamidation. Accordingly, bromination process (Figure 2.17) of amine end-functional silicon nitride nanosheet (SNNS-NH_2) was conducted with the use of α-bromoisobutyryl bromide (BIBB) as tertiary brominating agent in basic conditions. Eventually, the bromoamide end-functional SNNS (SNNS-Br) was used as ATRP initiator for SI-ATRP reaction, while it was also subjected to azidition process to obtain azide-end functional SNNS (SNNS-N_3) to be used in the click reaction.

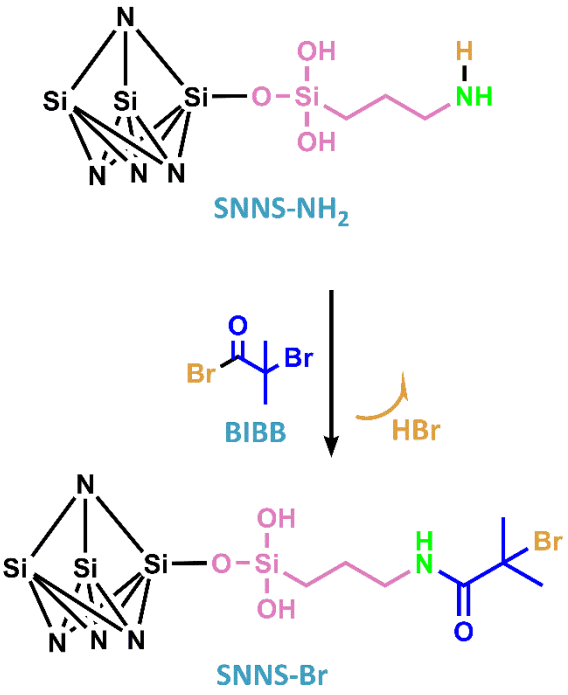

Figure 2.17 : The surface modification process of SNNS-NH_2 with BIBB.

iii. Azidation

Traditional modification procedures generally use Si-OH or Si-H bonds on the surface of nanoparticle for silanization [225] or halogenation [226]. One practicable reaction of amine function is the transformation to azide functionality after brominating process [227]. The azide moiety is a practical tool for click reactions especially in copper catalyzed azide-alkyne cycloaddition (CuAAC) [228] as well as in strain-promoted alkyne-azide cycloaddition (SPAAC) [229] and Staudinger ligation [230].

The click chemistry in this thesis based mainly on the Huisgen cycloaddition between alkyne-end moiety of polymer matrix and azide moiety on the surface of modified silicon nitride nanosheets, thus the last modification step is azidation of SNNS-Br. In this regard, the azide end-functional silicon nitride nanosheet (SNNS-N_3) was obtained through the substitution reaction of the bromide end-functionality of SNNS-Br with sodium azide (NaN_3) as can be seen in Figure 2.18. Then, click reaction was carried out between the SNNS-N_3 and alkyne-end functional polymers in presence of copper catalyst to yield thermal conductive polymer nanocomposites.

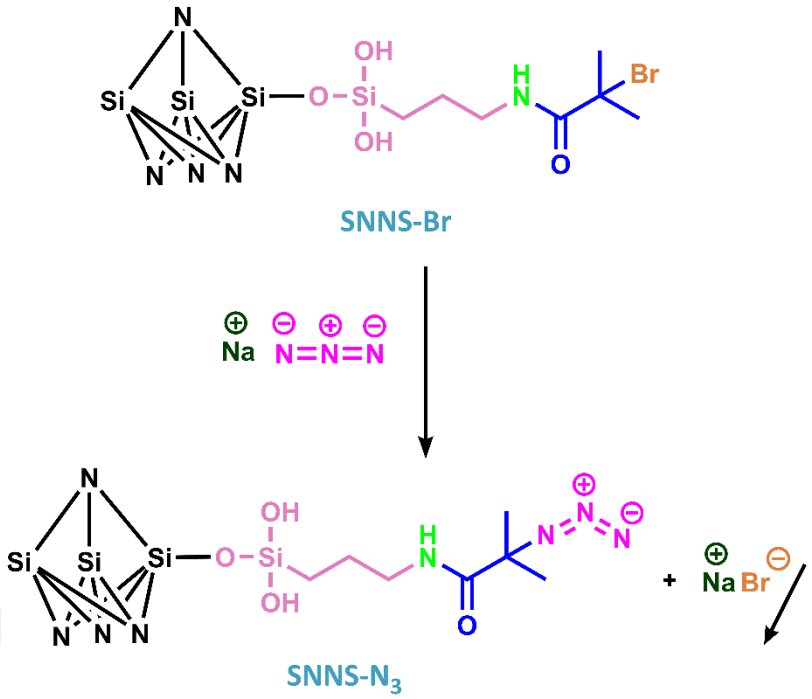

Figure 2.18 : The surface modification process of SNNS-Br with NaN_3.

2.6 Synthesis and Modifications of Polymer Matrices

The formation processes of synthetic polymers are mainly based on the creating chemical bonds between hundreds up to many thousands of monomers, at the end of the process, macromolecular structures are obtained. The chain formation process of polymerization reactions can be categorized in two main classes as chain-growth polymerization and step-growth polymerization [231, 232]. In chain-growth polymerization, an initiator is needed for the formation of active sites to initiate the polymerization, and then propagation step takes place by means of the consecutive addition of monomers to the active site. Free radical polymerizations and ionic polymerizations can be evaluated as examples of chain-growth polymerization. In step-growth polymerization, no initiator is needed and the chain formation occurs progressively through the sequential reactions of two monomers consisting reactive functional groups. To obtain linear polymers via step-growth polymerization, di-functional monomers are preferred instead of mono-functional monomers since the reaction of mono-functional monomers ends up with the species having two unreactive end groups.

2.6.1 Chain-growth polymerization

Chain-growth polymerizations, known as addition type polymerizations, can be defined briefly as the chain reactions of activated species called initiators [232]. The mechanism of chain reactions are based on the addition of new monomers to the growing polymer chain one after another trough active sites, double or triple bond, in the monomer [233]. Each addition of repeating unit to the growing chain recreates the active sites on the polymer chain and so polymerization progresses through the addition process of active sites [234]. The chain-growth polymerization proceeds through these three steps as also given in Figure 2.19 [233, 235]:

Chain Initiation: This step is generally conducted by means of external initiators capable of creating active sites such as radicals, anions, cations or organometallic complex.

Chain Propagation: This step involves the addition of repeating units to polymer chain by creating new active sites on growing chain to propagate the polymerization.

Chain Termination: In this step, chain propagation is ceased by the deactivating or neutralizing of the active sites by several routes to terminate the polymerization.

Comparing to step-growth polymerization (polycondensation), the high molecular weight polymers are obtainable even within a very short time from the beginning of the reaction in the chain-growth polymerization. Such that, it is observable that both the monomer and the large molecular weight polymer can be present together at any time of the reaction, although the concentration of the monomer decreases steadily in the reaction media [236].

Depending on the type of active center, chain-growth reactions can be mainly categorized into four main types as radicalic polymerization (free-radical polymerizations), anionic polymerization (monomers with electron withdrawing groups), cationic polymerization (monomers with electron donating groups) and transition-metal mediated polymerization (coordination polymerization with Ziegler-Natta catalysts) [232].

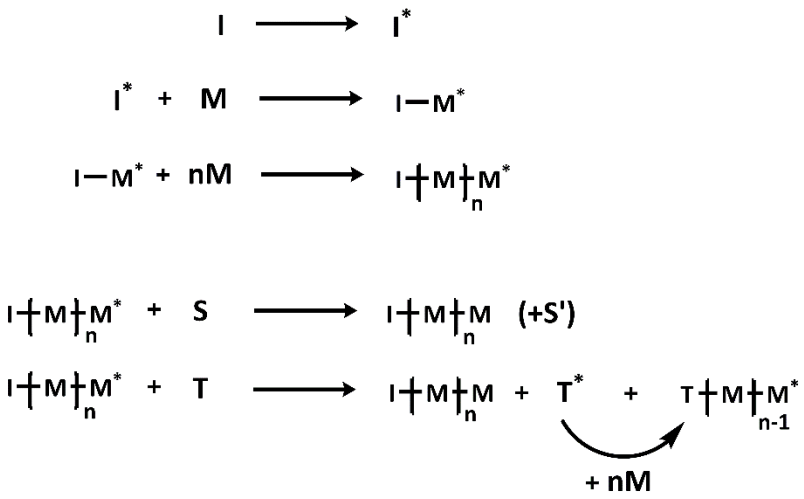

Figure 2.19 : Reaction steps of chain-growth polymerization.

2.6.1.1 Free radical polymerization (FRP)

In FRP, the first step of initiation process covers the homolytic bond scission of initiator to yield radical species. These species then attach to a monomer having multiple bonds to create new active sites capable of propagating the chain growing on the monomer units. After producing the chain with active site in initiation step, the chain then continue to grow by means of sequential addition of monomer to growing chain within the propagation step and proceed in the same trend till the termination step [231].

For a conventional free radical monomer, there are two potential routes to addition of a monomer to the growing chain (Figure 2.20). The most preponderant route denoted as head-to-tail addition is the one, which enables the minimum steric hindrance for the active species participating the propagating chain and generates the most stable radical. In other words, due to the steric hindrance of the groups in the growing chain encountered in the head-to-head addition and considering the fact that the stable radicals can only form through the head-to-tail addition, the propagating stage predominantly proceeds over the head-to-tail addition even if the head-to-head addition may still occur [231].

a) Head-to-Head Addition

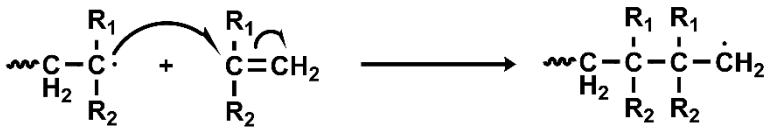

b) Head-to-Tail Addition

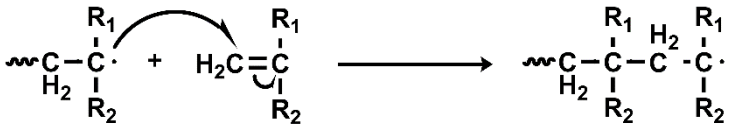

Figure 2.20 : Routes of a) Head-to-head addition and b) head-to-tail addition for propagation stage in free-radical mechanism.

Termination process of free radical polymerization can occur through two different mechanisms as can be seen in Figure 2.21. In the first mechanism, known as combination mechanism, two propagating chains bearing active radicals combine to transform into single chain containing no active sites able to continue polymerization. In the second mechanism, known as disproportionation mechanism, one of the propagating chain bearing active radical abstracts a proton from the other active chain to form two chains with different dead-end groups [231].

a) Termination with combination mechanism

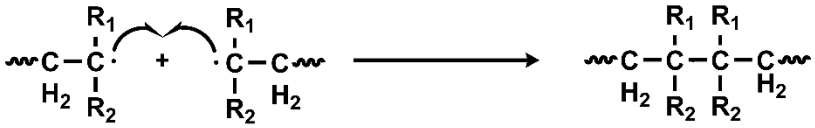

b) Termination with disproportionation mechanism

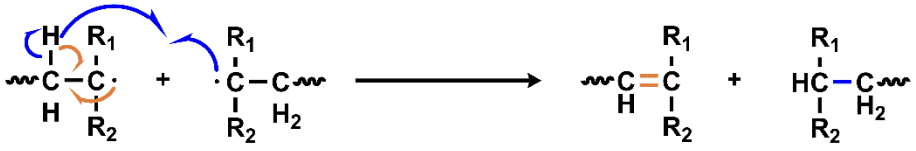

Figure 2.21 : Termination mechanisms of free radical polymerization.

2.6.1.2 Controlled/living radical polymerization (C/LRP)

Conventional free radical polymerization methods are used prevalently in industrial applications to manufacture high molecular weight polymers from several vinyl monomers. The FRP systems require an oxygen and moisture free environment; they can also be carried out under mild conditions and in such a wide temperature range like ranging from -80 to 250 °C.

The principal disadvantages of conventional free radical polymerization systems are generally associated with the uncontrollability of polymer structure. Although the high molecular weight polymers can be produced with conventional FRP, but their polydispersities will be high due to relatively slow initiation step, fast chain propagation and the irreversible termination process of monomers. Therefore, in order to overcome the disadvantages of FRP, it has been acknowledged that the free radical mechanism had to be conducted in conjunction with a living character. Live polymerization techniques can meet easily the requirements of radical polymerizations enabling to obtain well-defined polymers with various end functionalities through controlled synthesis procedures.

Live polymerization was first described by Szwarc in 1955 as a type of chain growth process without chain transfer and chain termination [237]. Well-defined polymers with molecular weight control, narrow molecular weight distribution, structural and compositional diversity can only be obtained by controlled/living radical polymerization (C/LRP) techniques.

Such a polymerization provides molecular weight (MW) control and molecular weight distribution (MWD) control as well as end-group control [238]. Some certain conditions to achieve these ultimate results involve the necessities such that the consumption of initiator should take place in the early stages of polymerization and the rate of propagation should be at least fast as the rate of initiation and the rate of substitution between active species [239, 240]. Controlled polymerization can be at issue as so long as these conditions are met [240]. Yet another affective way to proceed the polymerization in a controlled manner is reducing the active radical concentration, and so the undesirable side reactions, which allows to synthesis polymers with a predictable MW and also MW increasing over time while maintaining a narrow MWD [241].

Living polymerization techniques enable the synthesis of functional and multifunctional polymers, graft and block copolymers, macroinitiators and macromonomers. Hence, it can be concluded that the living polymerization is an indispensable technique to synthesize polymeric structures in a controlled manner [242, 243]. The most well known controlled/living polymerization techniques include reversible addition-fragmentation chain transfer polymerization (RAFT), nitroxide-mediated polymerization (NMP) and atom transfer radical polymerization (ATRP).

2.6.1.3 Atom transfer radical polymerization (ATRP)

Metal-catalyzed living/controlled radical polymerizations mediated by Fe, Ru, Ni and Cu metal complexes are one of the most effective techniques to synthesize polymers/copolymers with multifunctionality [244]. The most widely utilized one among the abovementioned methods is the atom transfer radical polymerization (ATRP) discovered by Professor Krzysztof Matyjaszewski from Carnegie Mellon University in 1995 [245]. This method performs through copper catalyzed LRP in the presence of an amine ligand and organic halide initiator. The very essential step of the ATRP is the atom transfer step responsible for the consistent growing of polymer chains [246].

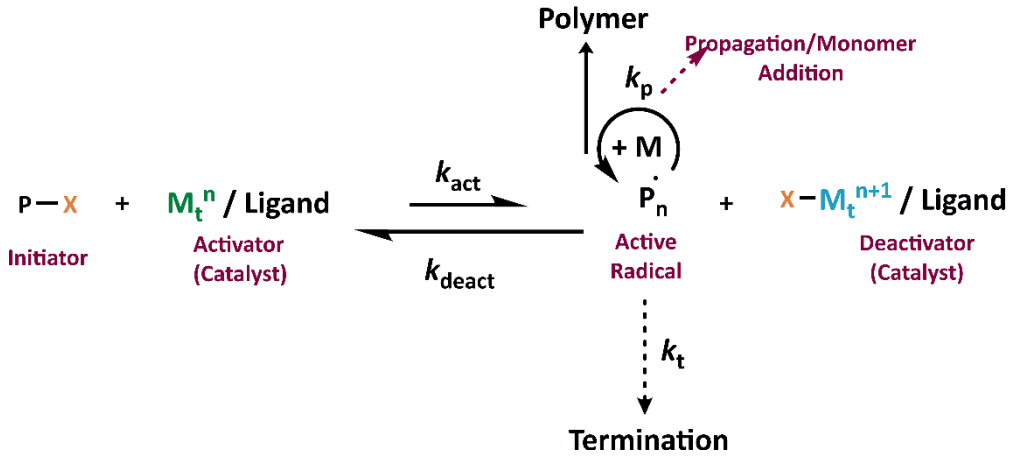

Figure 2.22 : The concise demonstration of ATRP mechanism.

Figure 2.22 shows the general mechanism of ATRP [247, 248]. This process is instantaneous and governed by an equilibrium between dormant species and propagating radicals and that equilibrium is constituted favors the dormant species (P-X). This kind of progress allows the propagating chains able to grow simultaneously and also ensures the suppressed the irreversible radical-radical termination reactions

by keeping the radical concentrations rather low [249]. Moreover, chain propagation step occurs through the rate constant of activation (k_{act}) and deactivation (k_{deact}), respectively. The rate of polymerization is defined through the first order reaction kinetic in regard to initiator (alkyl halide) and transition metal complex composed of catalyst and ligand [250, 251].

The mechanism of ATRP can be explained briefly as; a reversible redox reaction catalyzed by a transition metal complex, called as an activator (M_t^n / Ligand), produces propagating species (active radicals, P_n^*) through subjecting the transition metal to one electron oxidation together with by abstracting simultaneously a halogen atom (X) from the dormant species (P-X). The active radicals then react reversibly with the oxidized metal complexes called as deactivator (X-M_t^{n+1} / Ligand), to reproduce the activator and dormant species.

The rate of ATRP reaction is affiliated with the rate constant of propagation (k_p) in conjunction with the concentrations of monomer and growing radicals. The value of rate constants such as k_{act} [252], k_{deact} [253] and their ratio K_{ATRP} are strongly influenced by some reaction conditions like temperature, solvent or pressure along with the chemical structure of ligand and type of monomer/dormant species [254, 255]. In order to increase the rate of ATRP, catalyst activity (K_{ATRP}) should be kept high. However, under some conditions such as the realization of radical-radical termination leading low concentration ratio of activator and deactivator due to accumulation of the deactivator concentration, the rate of ATRP may decrease [256]. In conclusion, ATRP is a very powerful and adaptable technique for the synthesis of functional polymers with accurately controlled mechanism and sectional particular functionality [257].

2.6.1.4 Synthesis of poly (methyl methacrylate) (PMMA)

PMMA can be synthesized with different methods such as solution polymerization, bulk polymerization, emulsion polymerization, anionic polymerization and free radical polymerization [258]. ATRP (Atom Transfer Radical Polymerization) is the commonly used technique preferred to polymerize a MMA to obtain living polymer with desired functionality by means of controlled radical polymerization [259].

In the thesis, ATRP was used to prepare PMMA-SNNS nanocomposites in two different ways. The first method is the direct preparation of PMMA-SNNS via surface initiated ATRP (SI-ATRP) method by using bromide functional silicon nitride

nanosheet (SNNS-Br) as an initiator. The second method is the synthesis of alkyne-end functional PMMA (PMMA-Alkyne) by the aid of controlled polymerization technique on the purpose of using in click reaction. However, this section will focus more on the second method, conventional ATRP.

In ATRP method, MMA, which is a colorless liquid and has a chemical formula of $C_5H_8O_2$, is the monomer used for the polymerization of PMMA. The advantageous properties of MMA among the other monomers are its durability, transparency, strength and abrasive resistance alongside having the highest ATRP equilibrium constant ($K_{eq} = k_{act}/k_{deact}$) [260].

Alkyl halides (RX) are generally used as the ATRP initiator in the polymerization of MMA. The rate of polymerization is able to be determined by the dissolved concentration of alkyl halides [261]. The type of halide the initiator has affects the quality of PMMA obtained. Certain overactive initiators can lead side reactions or sudden terminations. The high quality PMMA can be obtainable in the use of alkyl halides bearing bromide and chloride. The selection of an initiator has an important role on ATRP accordingly [262].

Catalysts have an essential role on the kinetic equilibrium of ATRP reactions, such that both the activating and deactivating species of catalytic system must be simultaneously present in the reaction medium. There are some characteristics the catalysts must have such as having at least two accessible oxidation states, having a favorable affinity towards halogens, ability to ensure coordination states to connect the ligands. It means that the type of catalyst proposed for a given reaction affects the kinetics of ATRP and so the controllability of polymerization under the selected combination of reaction conditions. The mostly used catalysts among the other transition metals available for the polymerization of MMA by means of ATRP is the copper based transition metal catalysts when considering the above characteristics [262].

The principal mission of the ligand part of a catalyst complex in the polymerization media in an ATRP is to solubilize the transition metal salts to conform the redox capacity of the metal to contribute the kinetic dynamics of halogen exchange reaction. The electron donating capacity of a ligand directly influences the reactivity of the metal center in halogen abstraction and exchange reactions. Hence, the selection of a

ligand has an essential role in controlling the polymerization dynamics, molecular weight and molecular weight distribution of the polymer to be synthesized. The most commonly used ligands for MMA polymerization through ATRP is the nitrogen based ligands due to their excellent electron donating characteristics [263].

The stage of atom transfer, in other words, exchange reactions and reaction kinetics of polymerizations hinge directly upon the catalyst complex, which is highly affected by the solvent system. Thus, the selection of solvent is quite crucial to reach the efficient polymerization. Several solvents used in ATRP systems for different monomers include toluene, ethyl acetate, benzene, alcohol etc. The solvents accord with the ATRP systems should have a capacity to completely dissolve the catalyst complex and hence polar aprotic solvents are mostly used [261, 262].

Reaction temperature has a direct effect on the rate of polymerization. Rate constants of atom transfer equilibrium, propagation stage and so the rate of polymerization increase proportionally with temperature due to increase in collision frequency of species. Also, high temperatures induce more heat loss causing completion of the reaction in a less time. Most of MMA polymerizations are carried out at a temperature range of around 70-90 °C, otherwise at higher degrees, chain transfer and some side reactions may occur, also at lower degrees, the dissolution capacity of catalyst would be low. The adjustment of polymerization temperatures must be determined mostly according to desired molecular weight, monomer and catalyst system [261, 262].

2.6.2 Step-growth polymerization

In step-growth polymerization, monomers attach to each other in individual respective steps via conventional organic reactions such as urethane, ether, ester and amide formations. Step-growth reactions are divided into polycondensations and polyadditions according to whether the small molecules (byproducts) are eliminated during transitions between the steps (Figure 2.23) [264].

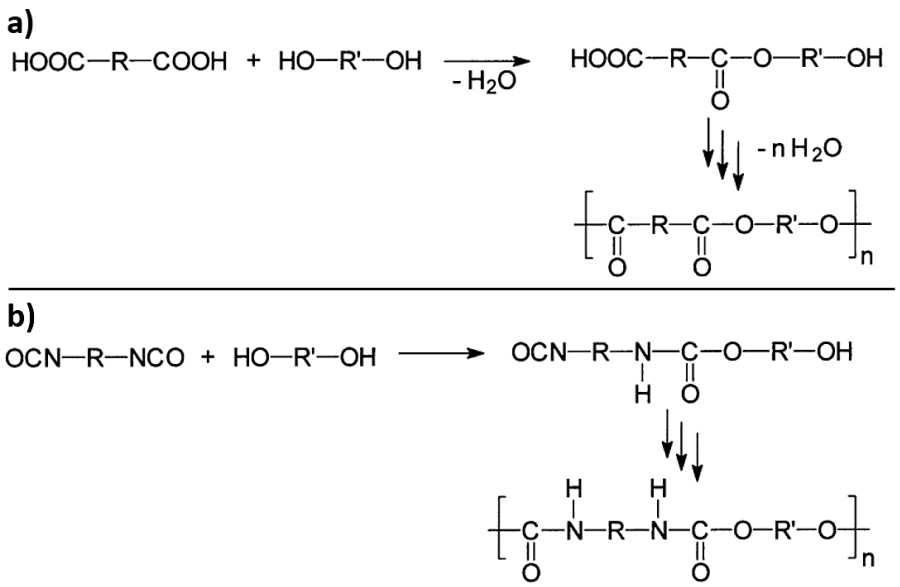

Figure 2.23 : Types of step-growth polymerizations; a)polycondensation and b)polyaddition.

The monomers included in reaction media must have two functional end-groups so that they can form polymer chains via step growth polymerization. Step-growth reactions can end up with cross-linked or branched polymers in the case of monomers more than two functional groups. The chain propagation proceeds generally through the independent sequential reactions of monomers due to the absence of active centers. It progresses via formation of dimers at first step, then short or long oligomers and finally long chain polymers with high conversions called condensation polymers towards the end of the reaction. In order to obtain high molecular weight polymers with high degrees of conversion, the ratio of complementary functional groups monomers bear must be close to 1:1 equivalence [264]. The key differences between chain-growth and step-growth polymerizations are given in Table 2.11 [264].

Table 2.11 : Differences between chain-growth and step-growth reactions.

Chain Growth Polymerization	Step Growth Polymerization
Reaction starts with initiators or catalysts.	No need of catalysts for initiation.
There is need for the active species (e.g. radical or ions) to propagate the polymerization.	Polymerization proceeds through the reactions of end-functional monomers and polymers.
The initiation step requires more activation energy than the propagation step.	Activation energies for each step are almost the same.
The concentration of monomers decrease in the course of time.	More than 99% of monomers react in very beginning of the reaction.
The polymers with high molecular weight can form at the beginning of the reaction.	The polymers with high molecular weight can only form towards the end of the reaction.
The average molecular weight depends less on the reaction time.	The average molecular weight increases steadily with the reaction time.

2.6.2.1 Condensation polymerization

Condensation polymerizations occur through the reactions between two bifunctional monomers by means of releasing a small molecule, generally water. The chain propagation step proceeds in a slow and stepwise fashion. It can be concluded that the average molecular weight of polymer is a function of time and so increases slowly [265]. It is mentioned before that the polymerization proceeds via reaction of monomers bearing functional units with each other by means of elimination of small molecules such as water or methanol, which means polymers produced have fewer atoms than monomers [266]. Due to reversible nature of condensation reactions, the process will halt by reaching the equilibrium at one point unless byproducts are eliminated [267]. Some well-established condensation type polymers are, phenol-formaldehyde resins, polyethers, polyamides, polyphosphates, polyphosphonate esters, polyesters, polycarbonates, polyureas, polyanhydrides, polysiloxanes and polysulfides [267].

2.6.2.2 Synthesis of polysulfone (PSU)

The first synthesis procedure for condensation polymers from p-phenylenedithiols and p, p'- dihalodiphenyl sulfones was proposed by Kreuchunas in 1958 [268, 269]. Polysulfones are obtained by polycondensation reactions which are i) polysulfonylation (a classical electrophilic aromatic substitution) [270, 271] and ii)

polyetherification (a nucleophilic substitution of activated aromatic dihalides) [272]. Polyetherification, which is a kind of condensation polymerization, is more favored route than polysulfonylation and is conducted through the nucleophilic substitution reaction between dihalides and diphenols (Figure 2.24). Hence, polyetherification was applied for the synthesis of polysulfone in this thesis.

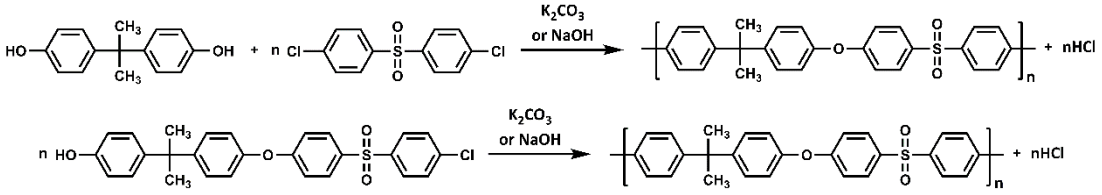

Figure 2.24 : Synthesis of polysulfone via polyetherification route.

In this method, polycondensation is carried out through the reaction between diphenols activated by metal salts and dihalides at elevated temperature in the medium of aprotic dipolar solvents. The aprotic dipolar solvents such as N-methylpyrrolidone (NMP), *N*,*N*-dimethylacetamide (DMAc), cyclohexylpyrrolidone (CHP), dimethylsulfoxide (DMSO) and *N*,*N*-dimethylformamide (DMF) increase the activity of metal salts and contribute to the enhancement of addition steps [273-275]. Figure 2.25 shows the formation of Meisenheimer Complex in consequence of nucleophilic attack of activated diphenol to aromatic carbon of dihalide, then -I effect of sulfone groups (electron withdrawing group) accelerate the aromatic substitution by releasing the leaving group and Meisenheimer complex decomposes in the end.

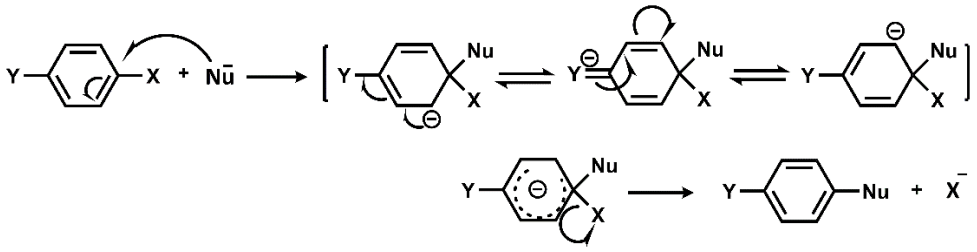

Figure 2.25 : Formation of Meisenheimer Complex in the synthesis of polysulfone via nucleophilic (polyetherification) route.

Poly (ether sulfone)s (PES)s obtained from 4,4′-Dichlorodiphenyl sulfone and Bisphenol-A display high T_g due to the chain rigidity proceeding from the presence of diphenyl and polar sulfone groups. The high polarity of sulfone groups lead the electron withdrawing effect, which causes electron delocalization in aromatic ring, providing the formation double bond with adjacent atoms. Electron delocalization

occured in this way suppresses substantially the chain mobility and so enhances considerably the chain rigidity [276].

The nucleophiles can be ordered considering their basicities as follows; ArS- > RO- > R_2NH > ArO- > OH- > $ArNH_2$ > NH_3 > I- > Br- > Cl- > H2O >ROH. Considering the some typical advantages and disadvantages both strong and weak bases possess, it is seen that the each of diaryl halides are utilized towards different purposes in nucleophilic substitution reactions. For example, potassium or sodium hydroxide are mainly preferred in strong base approach, yet the disadvantage of this method is that it requires stoichiometric control of the base ratio. In other words, in the case of too much or too low proportion of strong base is included in the reaction system, condensation steps will proceeds backward. On the contrary, weak base approach is more attempted route as it does not necessitate the stoichiometric control of the base ratio. Such that, the excess usage of weak base does not affect the course of reaction, but less amount of it can result in low molecular weight polysulfone. Potassium carbonate, compared to sodium carbonate, is the most preferred strong base due to its strong basicity parameters and well solubility in reaction media of polysulfone synthesis. The by-products formed in the condensation reactions used potassium carbonate as a base are water and carbon dioxide, which can be eliminated readily from the media with the help of an azeotropic agent [78].

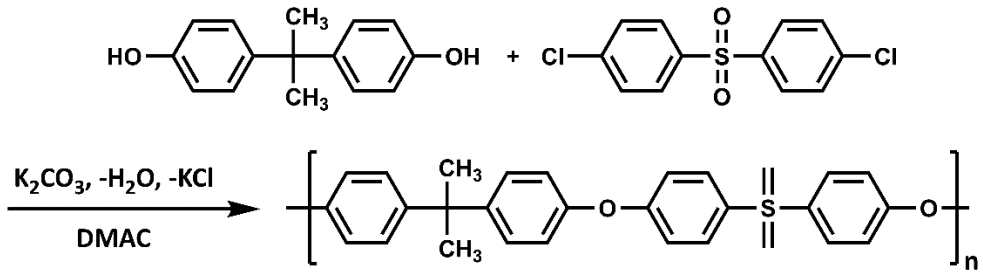

Figure 2.26 : Polysulfone synthesis via K_2CO_3/DMAC system.

Several base/solvent systems have been proposed for the polyetherification reactions [277-279]. Polysulfones can be synthesized by either K_2CO_3/DMAC (N,N'-dimetyhl acetamide) (Figure 2.26) and caustic/DMSO (dimethylsulfoxide) (Figure 2.27) combinations [279-281].

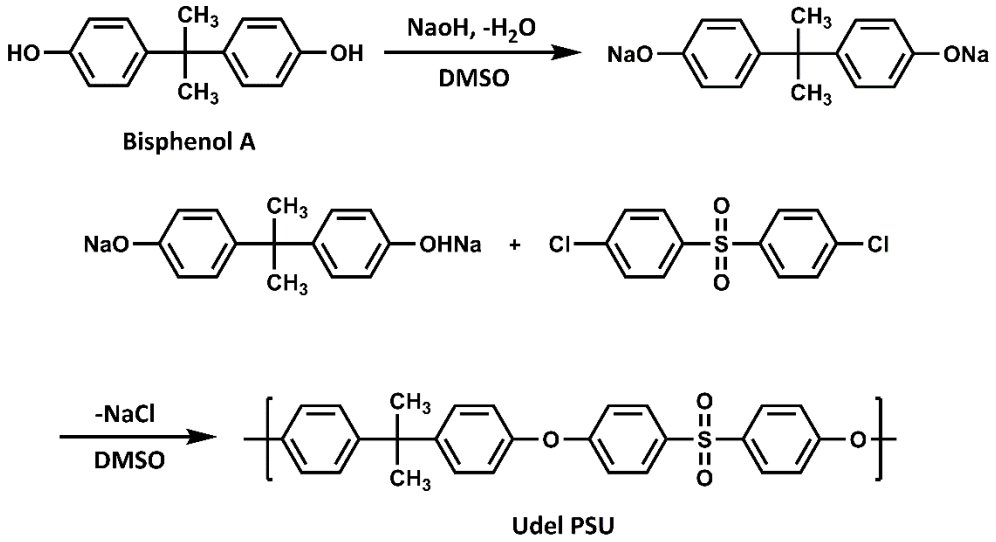

Figure 2.27 : Polysulfone synthesis via caustic/DMSO system.

2.6.2.3 Synthesis of poly (ether ether ketone) (PEEK)

Poly (aryl ether ketone)s (PAEKs) are synthesized by two different routes which are electrophilic aromatic substitution and nucleophilic aromatic substitution. Electrophilic aromatic substitution (EAS) is carried out via Friedel-Crafts acylation reaction, while nucleophilic aromatic substitution (NAS) which is the most preferred way of PAEK synthesis. EAS is accomplished via condensation reaction using aromatic monomer containing halogen units and aromatic diphenols activated by metal salts in the presence of aprotic dipolar solvents such as N-methylpyrrolidone (NMP), N,N-dimethylacetamide (DMAc), dimethylsulfoxide (DMSO), dimethylsulfoxide (DMSO) etc [282-285].

PEEK and other compositions of PAEKs are predominantly synthesized by nucleophilic aromatic substitution (NAS), known also as polyetherification route, of aryl difluorides with aromatic diols catalyzed by inorganic bases, which advances as a consequence of the formation of Meisenheimer complexes activated by carbonyl groups. PEEK is constituted from the reaction occurred between 4,4′-difluorobenzophenone (DFB) and hydroquinone, using AA/BB comonomer system (Figure 2.28). The high temperatures are required to keep the solubility of these semi-crystalline polymers in aprotic dipolar solvents, nevertheless moderate conditions will be sufficient to obtain amorphous compositions [284, 285].

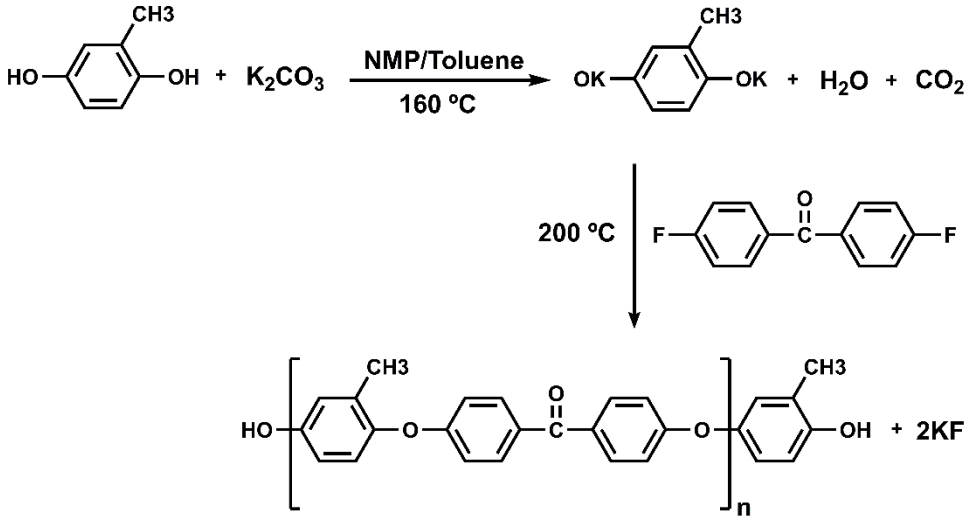

Figure 2.28 : Synthesis of hydroxyl terminated poly (ether ether ketone) via polyetherification route.

NAS mechanism proceeds by first reacting of an aromatic diphenol with a base that ensures its conversion to a phenoxide ion that will act as a nucleophile. Then the nucleophile attacks the other monomer, the aryl halide, activated by strong electron-withdrawing groups such as carbonyl or sulfonyl group in the ortho- or para- positions, to yield anionic aromatic intermediate known as a Meisenhiemer Complex (Figure 2.29) [286, 287]. These ortho- and para- electron withdrawing groups stabilize the Meisenhiemer intermediate by resonance due to their inductive effect and activate the electrophilic site [288]. The aromaticity then is ensured again by means of electron delocalization provided by the carbanion formed in the aryl dihalide after the substitution reaction of the halide groups with the nucleophile [289, 290]. Reduction of halide with the re-aromatization process ends up with the formation of aryl ether bond. The polymer desired is achieved with successive repetitions of this process [287].

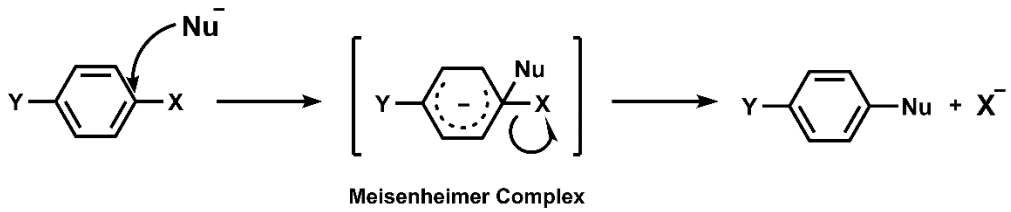

Figure 2.29 : General mechanism of NAS.

The solvent characteristics and the reactivity of dihalide both affect the polymer obtained through polyetherification. The reactivity of dihalide furthermore, depends

on both the kind of halide to be displaced and the activating groups found in compound, and solvent characteristics are also an essential factor for the polymer to be obtained [103, 272]. Such that, aryl difluorides have been proposed as the most effective aromatic electrophiles for the NAS chemistry and they have received attention as promising compounds to yield high molecular weight polymers due to their superior leaving group ability [291, 292]. Potassium carbonate have also been acknowledged as the best metal salt due to its excellent and controllable basic characteristic able to prevent side reactions in a typical NAS reaction [287, 292].

2.6.3 End-functionalization of polymers

Modification strategies that can be carried out without altering the intrinsic properties of poly aryl ethers (PAEs) have been investigated over the years. By introducing various functional groups to the structure and tailoring the existing functionality to another one, the enhanced features can be gained to polymer obtained and predisposed to further reactions. Therefore, the functional groups of many kinds have been studied and combined to the polymers synthesized [293].

The introduction of functionality to polymers is achieved through two pathways as pre-polymerization modification in which functional groups are incorporated to monomers and post-polymerization modification based on the functionalization of polymers produced [103]. The post-polymerization modification approach affords the formation of reactive sites to be exist in particular amount at specific positions for wide variety of synthesis strategies [288]. The chemical post-modification of PAEs able to be achieved either by nucleophilic or electrophilic routes. The substituents on polymer can be converted to another functional group affording to realize desired reactions [78].

2.6.4 Alkynylation Reaction

In this thesis, terminal alkyne functional polymers were prepared by the reaction of terminal hydroxyl groups of PAEs (PSU-OH and PEEK-OH) with 4-pentynoic acid. This reaction is based on condensation reaction, a type of addition reaction, which allows obtaining alkyne-end functionality on polymer matrix to be used in click reaction [294, 295].

The Steglich esterification was first discovered by Wolfgang Steglich in 1978 [296]. This reaction is a kind of esterification procedure of carboxylic acids which proceeds with the use of 4-dimethylaminopyridine (DMAP) as a catalyst and dicyclohexylcarbodiimide (DCC) as a coupling reagent. This reaction is carried out under mild conditions such that at room temperature and in presence of dichloromethane as solvent. Consequently, alkyne-end functional PAEs can be sythesised by means of steglich esterification and then dicyclohexylurea (DCU), the urea compound, forms at the end of the esterification as by-product in concequence of DCC reaction [297]. Figure 2.30 displays the entire reaction steps of steglich esterification.

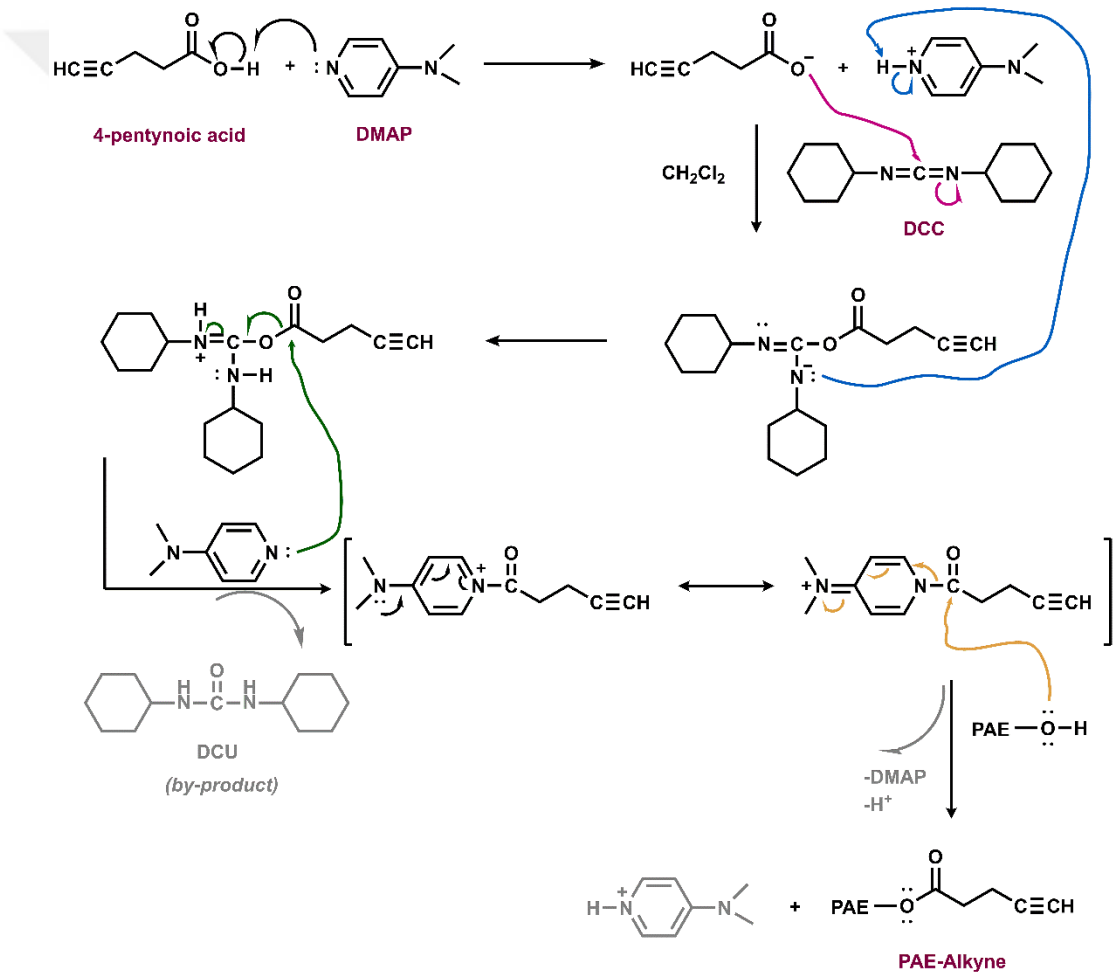

Figure 2.30 : Alkynylation mechanism for post-polymerization modification via steglich esterification.

2.7 Preparation of Thermal Conductive Polymer Nanocomposites via Covalent Functionalization Strategy

In this thesis, two different approaches have been performed in the preparation of nanocomposites. The first is the surface initiated atom transfer radical polymerization (SI-ATRP), based on the PMMA synthesis via propagating of MMA from the SNNS surface by using bromide-functional SNNS (SNNS-Br) as ATRP initiator. This method can be evaluated under *"Grafting from"* approach. The other technique, more extensively performed throughout the thesis, is click reaction, which is examined under *"Grafting to"* approach.

2.7.1 "Grafting From" approach

The *"grafting from"* approach covers in-situ polymerizations of monomers by using surface functionalized nanoparticles as initiators. These initiators are obtained through the sequential chemical modification steps realized on the surface of nanoparticles and functional organic substances are attached covalently to these nanoparticles [298]. The advantage of this technique is that no steric hindrance is encountered during the growth of polymers and it also allows the high grafting density and high molecular weight polymers to be synthesized effectively [299]. Yet, this technique necessitates rigorous control over the reaction conditions required for the polymerization together with the strict adjustment between initiator and substrate [300]. The *"grafting from"* method is applicable especially for the living radical polymerization (LRP) techniques [301, 302] such as addition-fragmentation chain transfer polymerization (RAFT) [303], atom transfer radical polymerization (ATRP) [304] and nitroxide-mediated polymerization (NMP) [305] due to LRP's tolerance to several functional groups.

Surface initiated – atom transfer radical polymerization (SI-ATRP)

The surface modification of nanoparticles performed with the grafting of polymer chains is anticipated to contribute in the design of new generation nanocomposite materials. In this sense, adapting the surface-initiated polymerization (SIP) technique using surface-functional nanoparticles to atom transfer radical polymerization (ATRP) has been attracted great attention in recent years [306]. This method can be applied to a wide variety of monomers under several experimental conditions, and also allows

the fabrication of matrix materials having effective functionalities grafted on the nanoparticle surface to be used in a variety of applications [306, 307].

Surface initiated ATRP (SI-ATRP) has been considered as a versatile tool for modifying especially the nanofiller surfaces and interface characteristics between the materials [308]. The outstanding advantageous properties of SI-ATRP are the controllability over the molecular weight and molecular weight distribution, high grafting density and availability of end-group functionality [309-311]. Also, hydrophobic or hydrophilic groups can be introduced on a nanoparticle surface through SI-ATRP depending on the applications to be performed [312]. This method have become indispensable tool particularly for two reasons; first, the silica surface where initiator groups are located provides a mobility barrier for termination process. Second, since only a limited amount of initiator can be attached to the nanofiller surface, there will be free radical species with restrained amount in reaction media [313]. Moreover, the polymer chains bonded covalently to nanoparticle surface through SIP can manipulate the interfacial properties, grafting density and reaction yield [314]. The preparation of PMMA-SNNS nanocomposite using "Grafting From" approach is given in Figure 2.31 as an example of SI-ATRP technique.

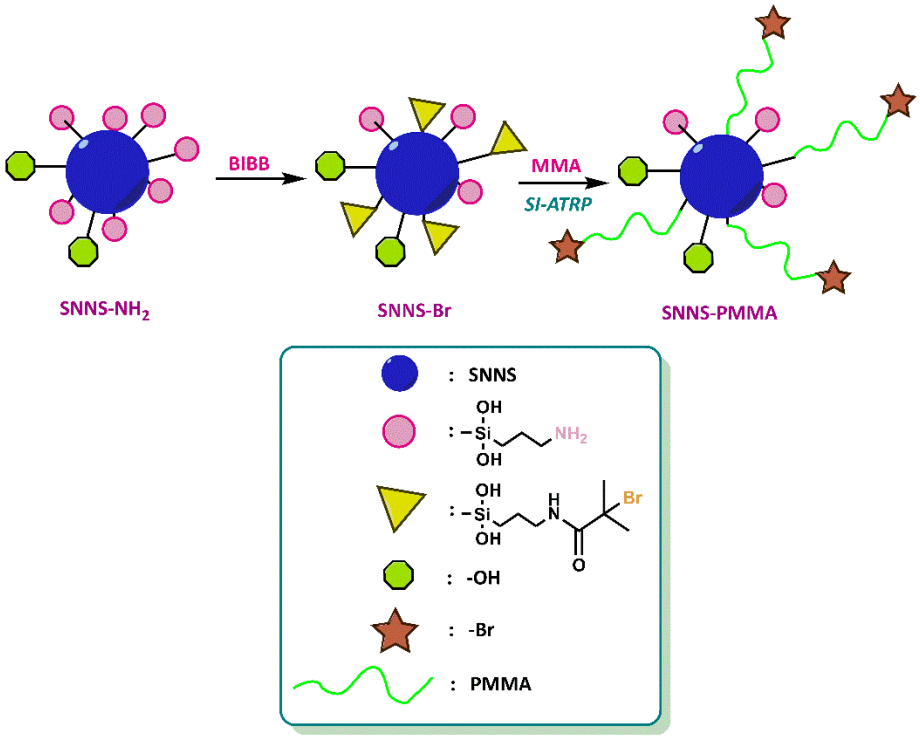

Figure 2.31 : Schematic illustration for "Grafting From" mechanism in the preparation of PMMA-SNNS nanocomposite via SI-ATRP.

2.7.2 “Grafting To” approach

The *“grafting to”* is the most unambiguous method amongst the other polymer grafting routes. In this method, polymers are pre-prepared in the first stage, which then subjected to coupling reaction with complementary chemical groups on the surface of nanoparticles through their functional chain-end groups [315-317]. The main restriction of *“grafting to”* approach is the steric hindrance caused by already available grafted chains on the nanoparticle surface to incoming polymer chains, which may lead to low grafting density for polymers with high molecular weight [318, 319].

However, the surface modification of nanoparticles can end up with the disrupting of NP's colloidal stability in solvent systems, which may restrains the growing capability of polymers from NP's surface [320, 321]. To overwhelm this shortcoming, *“grafting to”* approach which is an efficient tool for direct grafting of end-functional polymers onto modified surface of NP can be proposed [322].

The main advantage of this method over the previous technique (*"grafting from"*) is that the whole characterization processes of polymers can be realized and physical and chemical properties can be defined before the nanocomposite preparation step. Moreover, the nanocomposites prepared with polymers synthesized via controlled polymerization techniques such as ATRP etc. and having narrow molecular weight distribution can be achievable readily by this method. Apart from these, *"grafting to"* approach is less compelling from the chemical perspective than *"grafting from"* approach due to the absence of complex synthetic methodologies [323, 324].

Click chemistry

Lately, click chemistry, particularly the Cu (I)-catalyzed azide-alkyne 1,3-dipolar cycloaddition reaction, has revealed as an attracting and favorable synthetic approach for preparing polymer matrix nanocomposites due to its distinguished virtuousness such as mild reaction conditions, convenience with several solvents, good specificity and high reaction yields [325, 326].

The click reaction can be applied in many fields such as modifications of carbon nanotubes [327], surface modification of nanoparticles [328-330], building of degradable networks [331], macromolecular engineering [332-334], production of nanostructured semiconductors [335] and manufacturing of functional nanocomposites [336]. In particular, the fabrication of nanocomposites using click

chemistry is the novel and feasible technique to accomplish excellent nanofiller dispersion [337, 338]. It has been affirmed that the utilization of click chemistry has been employed prevalently in the manufacturing of polymer matrix nanocomposites having high selectivity (yielding 1,4-regioselective 1,2,3-triazoles), high reactivity (in presence of components with various functional groups) and reliability (not affected by oxidation or moisture) [339-341]. This is because, it can offer reaction products with high yield even at low temperatures, controllability over a wide range of reaction conditions and workability with the wide variety of functional groups [342, 343].

The click chemistry in this thesis is mainly based on the Huisgen cycloaddition between alkyne moiety of end-functional polymer matrix and azide moiety on the surface of modified silicon nitride nanosheets as shown in Figure 2.32.

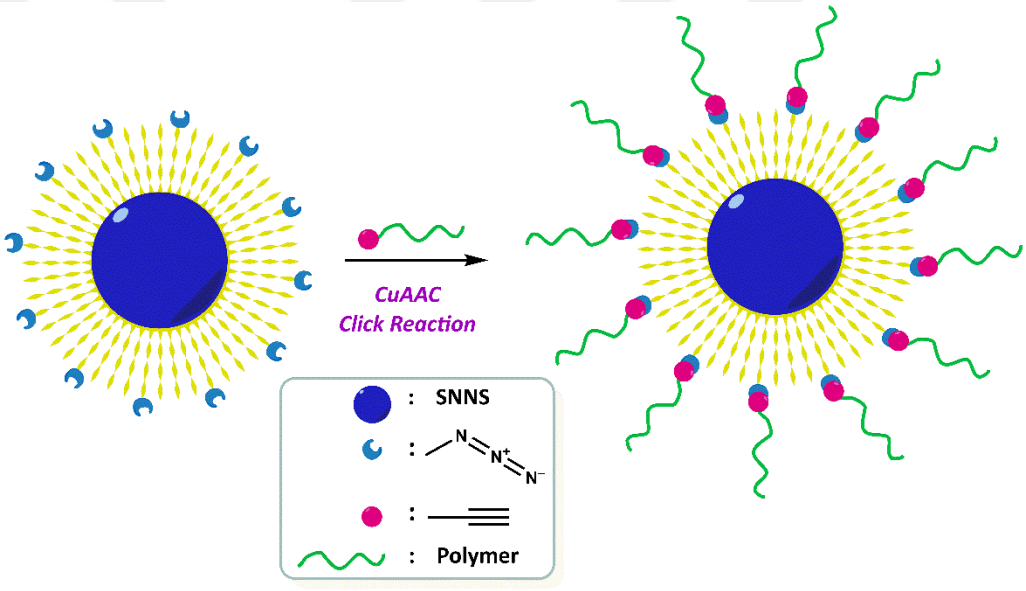

Figure 2.32 : Schematic demonstration of nanocomposite fabrication via CuAAC click reaction.

3. EXPERIMENTAL PART

3.1 Materials

3.1.1 Monomers

Methyl methacrylate (MMA) (Sigma-Aldrich, 99% (GC)),

It was passed through basic alumina column to remove the inhibitor.

Bispehol A (4,4′-Isopropylidenediphenol) (Sigma-Aldrich, ≥ 99 %),

It was used as received.

4,4′-Dichlorodiphenyl sulfone (DCDPS) (Sigma-Aldrich, ≥ 98 %),

It was used as received.

Methylhydroquinone (MeHQ) (Sigma-Aldrich, 99 %),

It was used as received.

4,4’-difluorobenzophenone (DFBP) (Sigma-Aldrich, 99 %),

It was used as received.

3.1.2 Solvents

Dichloromethane (DCM) (Sigma-Aldrich, ≥99.5%),

It was dried by distilling over CaH_2 prior to use. It was stored over molecular sieve (4 Å).

Ethyl acetate (EtOAc) (Sigma-Aldrich, ≥99.5%, GC grade)

It was used as received.

N,*N*-Dimethylformamide (DMF) (Sigma-Aldrich, ≥99%, ReagentPlus®),

It was used as received.

Toluene (Sigma-Aldrich, 99.9 %),

It was refluxed over sodium metal and benzophenone before use. It was stored over molecular sieve (4 Å).

Dimethyl acetamide (DMAc) (VWR, anhydrous ≥ 99.8 %),

It was used as received.

N-Methyl-2-pyrrolidone (NMP) (Sigma-Aldrich, anhydrous 99.5 %),

It was used as received.

3.1.3 Other chemicals

Silicon Nitride nanoparticles (β-Si_3N_4) (Sigma-Aldrich, average particle size of 120 nm, density of 3.44 g/mL, specific surface area of 103-123 m^2/g),

It was used as received. It was used as a thermal conductive nanofiller.

(3-Aminopropyl) triethoxysilane (APTES) (Sigma-Aldrich, ≥98%),

It was used as received. It was used as a coupling agent for the surface of silicon nitride nanoparticle.

2-bromoisobutyryl bromide (BIBB) (Sigma-Aldrich, 98%),

It was used as received. It was used as a bromination agent for the surface of silicon nitride nanoparticle.

Sodium azide (Sigma-Aldrich, ≥ 99.5%, ReagentPlus®),

It was used as received. It was used as an azidation agent for the surface of silicon nitride nanoparticle.

Propargyl alcohol (Sigma-Aldrich, 99%),

It was used as received. It was used for the synthesis of ATRP initiator.

4-(Dimethylamino) pyridine (DMAP) (Sigma-Aldrich, ≥99%, ReagentPlus®),

It was used as received. It was used for the synthesis of ATRP initiator and alkynylation reactions of hydroxyl-end functional polymer matrices.

Trimethylamine (TEA) (Sigma-Aldrich, ≥99.5%),

It was used as received. It was used for the synthesis of ATRP initiator and bromination of the silicon nitride surface.

N, *N*, *N′, N″, N‴*-Pentamethyldiethylenetriamine (PMDETA) (Sigma-Aldrich, %99),

It was distilled over NaOH before use. It was used as a ligand for ATRP and click reactions.

Copper (I) chloride (CuCl) (Sigma-Aldrich, 99.995+ %),

It was used as received. It was used in the synthesis of alkyne-end functional PMMA.

Copper (I) bromide (CuBr) (Sigma-Aldrich, 99.999% metal basis),

It was used as received. It was used in click reactions.

Potassium carbonate (K_2CO_3) (Merck, ≥ 99 %),

It was used as received. It was used as a strong base in the polycondensation reactions.

4-pentynoic acid (Sigma-Aldrich, 95 %),

It was used as received. It was used in the alkynylation reactions of hydroxyl-end functional polymer matrices.

N,N'-Dicyclohexylcarbodiimide (DCC) (Sigma-Aldrich, 99 %),

It was used as received. It was used in the alkynylation reactions of hydroxyl-end functional polymer matrices.

3.2 Characterization

3.2.1 X-ray diffractometer (XRD)

X-ray diffractometry analysis (XRD) were conducted with Rigaku Miniflex-600 desktop X-ray diffractometer using Cu-Kα radiation (1.54 Å) operating at 40 kV and 15 mA. Samples were run at a scanning speed of $1°min^{-1}$ and within the Bragg angle, 2θ range of 3°–60° at ambient temperature. It was utilized to determine the crystallite size of silicon nitride nanoparticles, silicon nitride nanosheets and modified silicon nitride nanosheets and differentiate the structures of nanoparticle and nanocomposite. In order to calculate the distance between the silicate layers, Bragg‟s law was used.

3.2.2 Nuclear magnetic resonance spectroscopy (NMR)

All ^{1}H-NMR spectra were recorded on Agilent NMR System VNMRS 500 spectrometer at room temperature in $CDCl_3$ with $Si(CH_3)_4$ as an internal standard. It

was used for the confirmation of main chain structures and end-functionalities of polymer matrices.

3.2.3 Fourier transform infrared spectrometer (FT-IR)

FT-IR analyzes were recorded on a Perkin–Elmer FT-IR Spectrum One B spectrometer. All FT-IR spectra were collected in the range of 4000 – 450 cm^{-1} with a spectroscopic grade KBr pellets at a room temperature. It was used in structural analysis of all kind of materials.

3.2.4 Gel permeation chromatography (GPC)

The conventional gel permeation chromatography measurements of polymers were obtained using an Agilent instrument (Model 1100) consisting of a pump, a refractive index (RI), and ultraviolet (UV) detectors, and PLgel 5 μm MIXED-D column and guard column. THF was used as an eluent at a flow rate of 0.5 mL/min at 30 °C. Toluene was used as an internal standard. The molecular weight of the polymers was calculated based on linear polystyrene standards (Polymer Laboratories).

3.2.5 Differential scanning calorimeter (DSC)

Differential Scanning Calorimetry (DSC) analysis were performed on Perkin Elmer, Jade DSC from 50 °C to 400 °C with a heating rate of 20 °Cmin^{-1} under nitrogen flow. The glass-transition temperatures (T_g's) of polymers and nanocomposites were collected from second heating cycle.

3.2.6 Thermogravimetric analyzer (TGA)

Thermal stability comparisons and char yield values of nanocomposites and their precursors were performed on Perkin–Elmer Thermogravimetric Analyzer Pyris 1 TGA at a heating rate of 10 °Cmin^{-1} from 20 °C to 900 °C under nitrogen flow.

3.2.7 Scanning electron microscopy (SEM)

Morphological analysis of all samples were performed with TESCAN Vega 3 SBH (Czech Republic) scanning electron microscope. Samples were coated with gold-palladium alloy for 120 minutes prior to analysis.

3.2.8 Thermal conductivity analysis (DTC)

Thermal conductivities ($Wm^{-1}K^{-1}$) of polymer matrices and nanocomposites were inspected using a guarded heater meter DTC 300 (TA Instruments), which was fabricated according to the ASTM D-5470 and operates consistent with ASTM E-1530. The conductivities were measured according to the ASTM D5470 standard, which operates on a guarded heat flow principle. This device has two temperature-controlled surfaces, after a certain pressure and temperature is applied to the material placed between these two metal surfaces, the device starts to collect thermal resistivity data. Thermal conductivity analysis in through-plane direction were carried out at working temperature of 25 °C and under 25 Psi pressure. Cylindirical specimens with 5 cm diameter in pad morphology were used to conduct TC analysis.

3.2.9 Electrical insulation (volume resistivity) analysis

Electrical resistivity (Volume Resistivity) measurements were determined on a 6517B (Keithley, Cleveland, USA) electrometer/high resistance meter operating with 1kV peak source, 200V peak measure and 0.1 A current equipped with Keithley 8009 resistivity test fixture based on ring electrodes. The measurements were done with the pad samples of 50 mm diameter and ~ 1 mm thickness.

3.2.10 Dynamic mechanical analysis (DMA)

Mechanical analysis were carried out by a dynamic mechanic analyzer DMA Q800 (TA Instruments) in a film/tension mode. The tests were performed at 1-Hz frequency from 25 to 150 °C for PMMA samples and from 25 to 150 °C for PEEK samples at a heating rate of 3 °Cmin-1 and an amplitude of 15 μm was applied. Film samples with a dimension of approximately about 15 mm x 8 mm x 2 mm (l,w,t) prepared.

3.2.11 Particle size analysis (Zetasizer)

The particle size distribution of SN and SNNS was investigated by photon correlation spectroscopy (PCS) using a Malvern Zetasizer Nano ZS laser particle size analyzer. The instrument performed at the wevelenght of 632 nm. The dispersion concentration was around 0.001 g/L. The suspension was prepared by dispersing the nanoparticles in 2-propanol and ultrasonicated for 30 minutes to obtain a well-dispersed suspension.

3.3 Synthesis Strategies

3.3.1 Preparation of silicon nitride nanosheets (SNNSs)

10 g of β-Si_3N_4 powder (SN) with average particle size of 120 nm and average crystallite size of 55 nm was mechanically milled with SPEX 8000 D Mixer/Mill® Dual High-Energy ball mill using 50 stainless steel balls with 5 mm in diameter in a stainless steel pot for 8 h at room conditions. A ball to powder ratio of 5:1 was used. The crystallite size change was measured by X-Ray Diffractometry (XRD) in every 2 h [344, 345].

3.3.2 Chemical modifications of silicon nitride nanosheets (SNNSs-R)

Exfoliated silicon nitride nanosheets (SNNSs) were chemically modified to obtain active initiating sites on the filler surface for click reaction. The total modification processes are depicted in Figure 3.1.

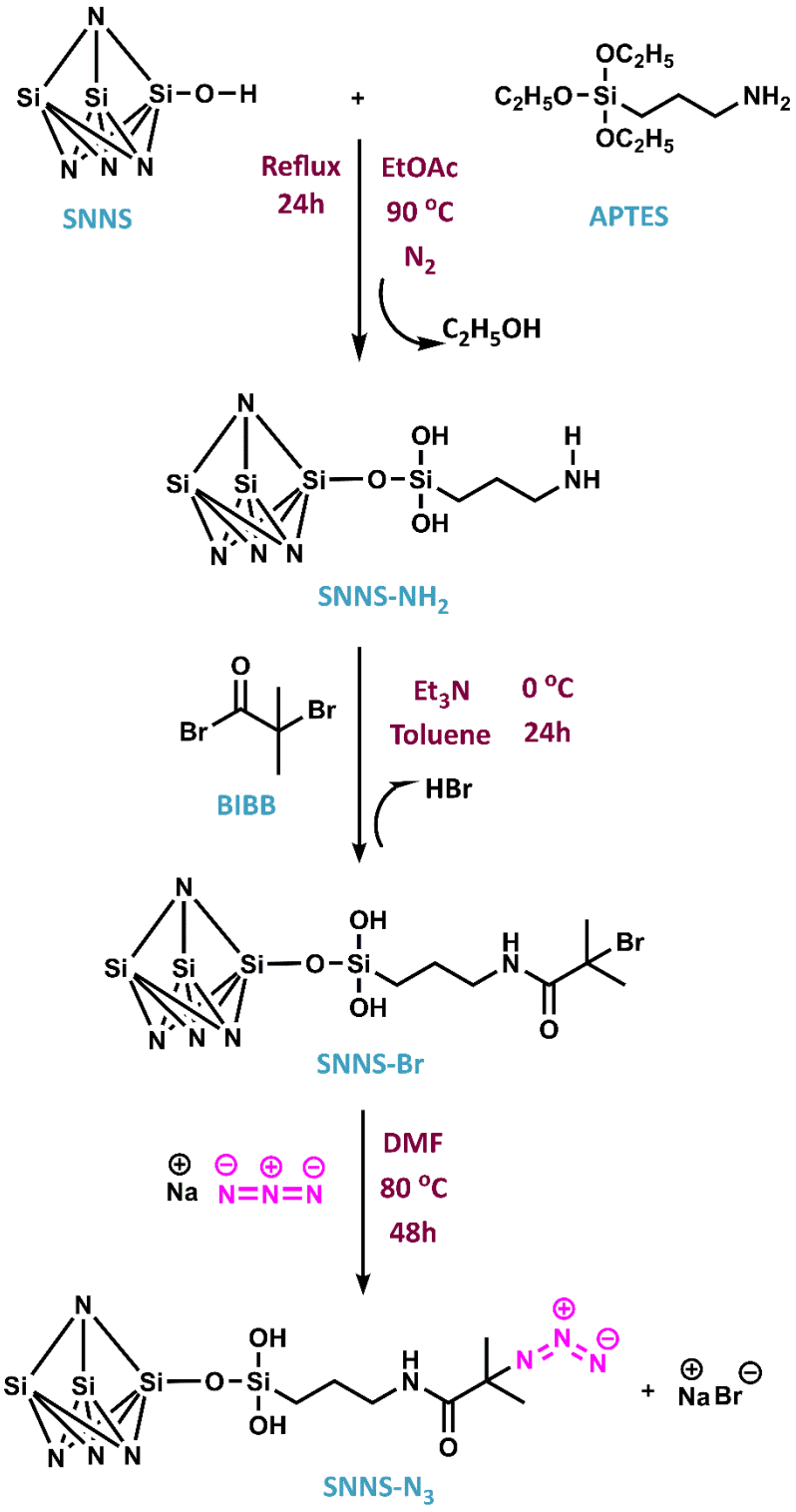

Figure 3.1 : Chemical modification steps of SNNSs.

3.3.2.1 Synthesis of amine modified SNNS (SNNS-NH_2)

SNNS (3.0 g, 0.021 mol) was dispersed in 450 mL ethyl acetate (EtOAc) by ultrasonication for 15 minutes. Mixture was transferred to 1000 mL round-bottomed flask equipped with a magnetic stirring bar. Nitrogen was passed through the stirred solution over 20 minutes. Then, APTES (1.5 g, 0.0069 mol) in 32 mL ethyl acetate was added into flask using a 50 mL syringe while purging with N_2. After addition, the reaction mixture was refluxed at 90 °C for 24 h under a nitrogen atmosphere. After the completion of the reaction, amine-modified SNNS (SNNS-NH_2) were separated by centrifugation at 6300 rpm for 30 min and washed with H_2O and ethanol (EtOH) for once, respectively to eliminate the unreacted APTES. Then, it was dried overnight at 60 °C in a vacuum oven [309, 346]. (Yield: 3.45 g, 77%).

3.3.2.2 Synthesis of bromoamide modified SNNS (SNNS-Br)

SNNS-Br was synthesized in toluene (86 mL) through a reaction of SNNS-NH_2 (2.5 g, 0.0075 mol) with 2-bromoisobutyryl bromide (BIBB) (4,2 mL, 0,036 mL) dissolved in 45 mL of toluene in the presence of triethylamine (TEA) (13 mL, 0.094 mol) in a 250 mL two-necked round-bottom flask at 0 °C. The reaction mixture was stirred at room temperature for 48 h. After reaction, bromoamide modified SNNS (SNNS-Br) was separated via centrifuging at 6300 rpm for 30 min. The precipate was washed with H_2O and EtOH for two times respectively to remove Et_3NHBr salt. Then, SNNS-Br were dried overnight at 45 °C in vacuum oven [347]. (Yield: 2.4 g, 22.4%).

3.3.2.3 Synthesis of azide modified SNNS (SNNS-N_3)

Bromo-terminated nanosheet (SNNS-Br) (0.7 g, 0.0015 mol) and 50 mL DMF were placed in a 250 ml round bottom flask equipped with a magnetic stirrer. The mixture was purged for 30 min with nitrogen. Sodium azide (NaN_3) (0.9 g, 0.015 mol) was added into flask. The reaction mixture was stirred at 80 °C for 48 h under nitrogen atmosphere. After termination of the reaction, azide modified SNNS (SNNS-N_3) were collected by centrifuging at 6300 rpm for 30 min, then washed with H_2O and EtOH for once to eliminate NaBr salt and unreacted NaN_3. Then, SNNS-N_3 were dried overnight at 45°C [348]. (Yield: 0.71 g, 44.4%).

3.3.3 Preparation of thermal conductive PMMA grafted SNNS nanocomposites

Bromide functional silicon nitride nanosheets (SNNS-Br) were used as ATRP initiator to grow PMMA brushes via surface initiated polymerization (SIP) and azide modified silicon nitride nanosheets (SNNS-N_3) were used as CuAAC Click Reaction agent with alkyne-end functional PMMA (PMMA-Alkyne) to yield PMMA-SNNS nanocomposite structure.

3.3.3.1 Preparation of poly(methyl methacrylate)/silicon nitride (PMMA//SNNS) nanocomposite via SI-ATRP

SNNS-Br (0.5 g, 1.04 mmol), MMA (10.37 g, 0.1037 mol) and CuBr (0.148 g, 1.04 mmol) were placed in a 50 mL Schlenk tube equipped with a magnetic stirrer. The mixture was purged with nitrogen for 30 min. PMDETA (0.432 mL, 2.07 mmol) and 8 mL DMF were introduced to the mixture while purging with N_2. After sealing the tube with rubber septa, the reaction mixture was stirred at 80 °C for 6.5 h under a nitrogen atmosphere. At the end of the reaction, the bulk mixture was diluted with THF in order to be able to eliminate readily the catalyst, then centrifugated at 6300 rpm for 30 min to set free polymer aside. This polymer was then precipated in MeOH and filtrated for further analysis. The remained nanocomposite was washed with H_2O and EtOH for two times and dried overnight at 45 °C [347]. (M_n = 104,400 g/mol; Yield: 53%). The preparation of PMMA//SNNS nanocomposite via SI-ATRP method is depicted in Figure 3.2.

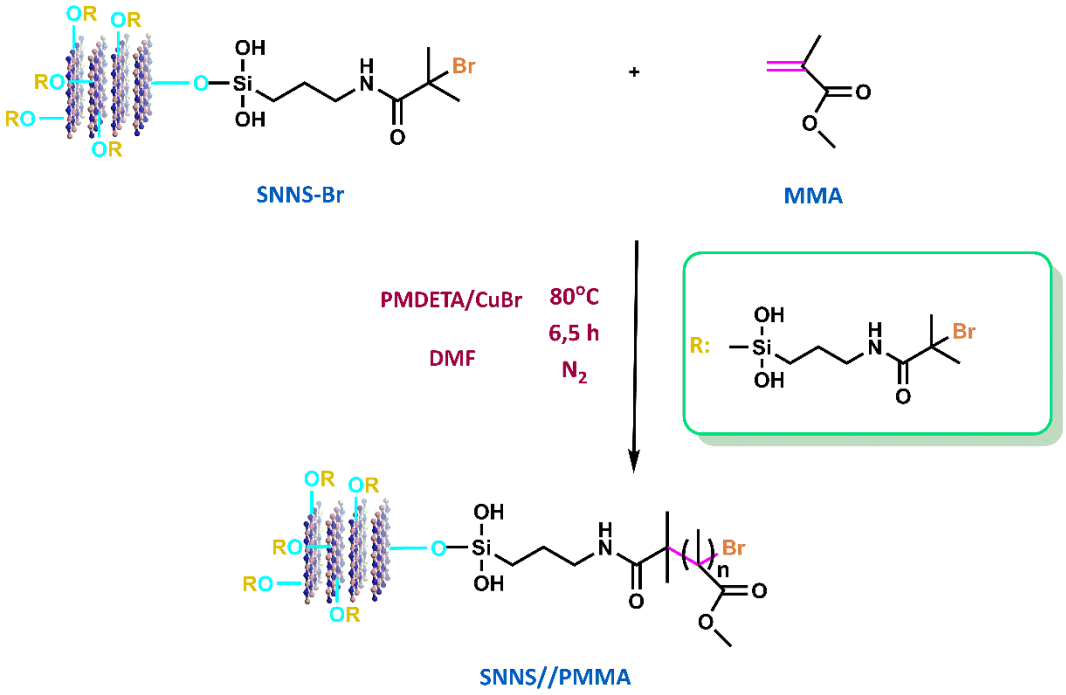

Figure 3.2 : The synthetic representation of PMMA//SNNS via SI-ATRP.

3.3.3.2 Synthesis of prop-2-ynyl-2-bromo-2-methyl propionate

A solution of 2-bromoisobutyryl bromide (1.78 g, 14.4 mmol) in dry dichloromethane (CH_2Cl_2) (20 mL) was added dropwise to a solution of propargyl alcohol (2.28 g, 15.6 mmol), DMAP (953 mg, 7.8 mmol) and triethylamine (3.34 g, 23.4 mmol) in dry CH_2Cl_2 (30 mL) at 0 °C. After complete addition, the reaction mixture was stirred overnight at room temperature. The reaction mixture was extracted 2 times with CH_2Cl_2/H_2O. The organic phase was dried with $MgSO_4$, filtered and the solvent was evaporated. Prop-2-ynyl-2-bromo-2-methylpropanoate was purified by column chromatography using a 1:1 ethyl acetate-Hexane solvent system. ^1H NMR (500 MHz, $CDCl_3$): 4.76 (d, -OCH_2-CH), 2.51 (t, -OCH_2-CH), 1.95 (s, $(CH_3)_2$-C-Br) [334].

3.3.3.3 Synthesis of alkyne-end functional PMMA (PMMA-Alkyne)

In a 50 mL Schlenk tube equipped with a magnetic stirrer, MMA (7.52 g, 75.2 mmol) was dissolved in 8 mL toluene. The mixture was purged with N_2 for 30 min. Then, prop-2-ynyl-2-bromo-2 methyl propionate which was prepared according to literature procedures [349, 350] (10.93 µL, 0.25 mmol) was added into the mixture. Vacuum-nitrogen cycles were performed before the addition of PMDETA (15.67 mL, 0.25 mmol) and CuCl (7.44 mg, 0.25 mmol). The reaction mixture was stirred under nitrogen atmosphere at 90 °C for 21 h. After polymerization, the mixture was diluted

with THF and precipated in MeOH. The precipitate was filtrated and dried overnight at 45°C under vacuum [351]. (M_n=120,600 g/mol; Yield: 54%). The synthesis route of PMMA-Alkyne was demonstrated in Figure 3.3.

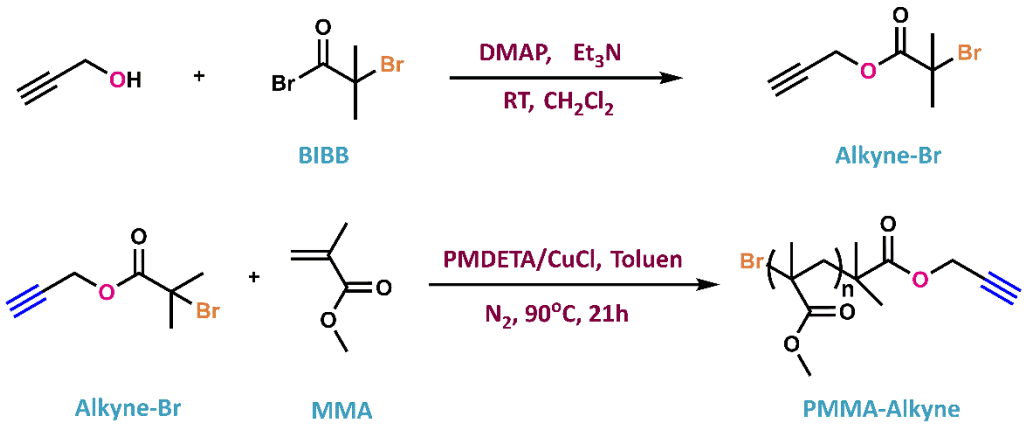

Figure 3.3 : Synthesis procedure of PMMA-Alkyne.

3.3.3.4 Preparation of poly(methyl methacrylate)/silicon nitride nanocomposite via CuAAC click reaction (PMMA-SNNS)

In a 100 mL Schlenck tube, PMMA-Alkyne (2 g, 0.021 mmol) dissolved in 100 mL DMF was purged with nitrogen for 30 min, SNNS-N_3 (3 g, 6.76 mmol) was ultrasonicated in DMF for 30 min, then added into the schlenk tube. Vacuum-nitrogen cycles were performed before the addition of PMDETA (0.14 mL, 0.68 mmol) and CuBr (97 mg, 0.68 mmol). The mixture was stirred at 60 °C for 48 h under N_2 atmosphere. After reaction, the mixture was centrifuged at 6300 rpm for 30 min. While, the supernatant was set aside to be precipated in methanol, the sediment was washed with water and ethanol respectively to remove catalyst, then dried overnight at 45 °C under vacuum (Yield: 4.6 g, 92%) [352]. The preparation of PMMA-SNNS nanocomposite is depicted in Figure 3.4.

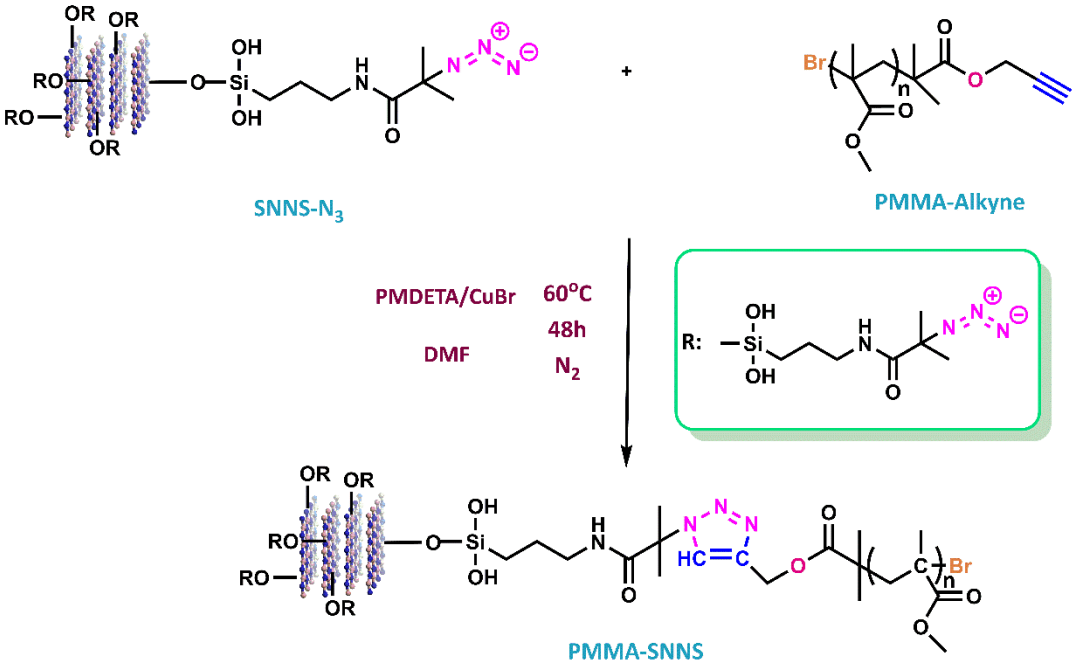

Figure 3.4 : The synthetic representation of PMMA-SNNS via CuAAc Click Reaction.

3.3.3.5 Preparation of poly(methyl methacrylate)/silicon nitride nanocomposite via physical blending (PMMA+SNNS)

SNNS-N_3 and PMMA-Alkyne were blended physically with the same gravimetrical ratio as used in the click reaction.

3.3.4 Preparation of thermal conductive PSU grafted SNNS nanocomposites

3.3.4.1 Synthesis of hydroxyl end-functional PSU (PSU-OH)

Prior to reaction, monomers were dried at 105 °C for 24 h for moisture elimination. In addition, the system was dehumidified under vacuum for 3h and then purged with vacuum-nitrogen cycle for 30 min prior to reaction. To synthesis PSU-OH, Bisphenol A (1.67 g, 7.31 mmol), 4,4'-Dichlorodiphenyl Sulfone (2 g, 6.96 mmol) and dry potassium carbonate (K_2CO_3) (2.12 g, 15.36 mmol) were placed in a 250 mL round bottom flask equipped with a mechanical stirrer, a dean-stark trap and a condenser with nitrogen inlet. 33.38 mL dimethyl acetamide (DMAc) and 4.17 mL dry toluene were added to the flask. The reaciton mixture was heated under reflux at 180 °C for 2 h with water removal, and then the temperature was adjusted to 200 °C for the remaining 4 h. After 6 h, the reaction was stopped. The mixture was diluted with chloroform and filtrated to remove the KCl salt, then, precipated in MeOH. The

precipate was filtrated and dried overnight under vacuum at 50 °C. (Yield 2.9 g, 79 %, M_n = 9,300 g.mol^{-1}) [276, 353, 354]. The synthesis procedure of PSU-OH is drawn as in Figure 3.5. A similar procedure using 2:0 and 1:2 ratios of the monomers (BPA/DCDPS) instead of 1:1.05 resulted PSU-OH-2000($M_{n,GPC}$ = 2050 g/mol) and PSU-OH-4000($M_{n,GPC}$ = 4200 g/mol), respectively.

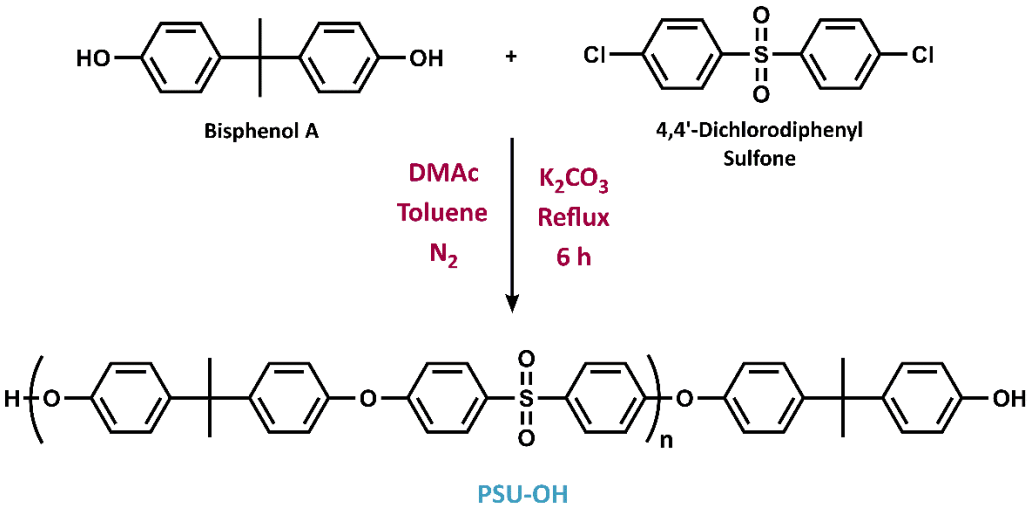

Figure 3.5 : Synthesis of hydroxyl-terminated polysulfones.

3.3.4.2 Synthesis of alkyne-end functional PSU (PSU-Alkyne)

In a 100 mL two necked round bottom flask, PSU-OH (0.50 g, 0.054 mmol) was dissolved in 15 mL dry dichloromethane (DCM) under nitrogen flow. While nitrogen flow continuous, 4-pentynoic acid (0.25 mg, 2.58 mmol) and 4-dimethylaminopyridine (DMAP) (6.57. mg, 0.054 mmol) were introduced the mixture. Then N,N'-Dicyclohexylcarbodiimide (DCC) (0.53 g, 2.58 mmol) dissolved in 20 mL dry DCM was added to the flask in a time period of 30 min in an ice bath. The reaction mixture was stirred at room temperature for 24 h. After reaction, the mixture was filtrated to remove the dicyclohexylurea (DCU) formed as a by-product during the reaction. Then, the filtered mixture was precipated in MeOH. The alkyne-terminated polysulfone (PSU-Alkyne) was dried overnight in a vacuum oven at 50 °C. (Yield: 0.49 g, 66 %, M_n = 9,500 g/mol) [355, 356]. The alkynylation procedure of PSU-OH is drawn as in Figure 3.6.

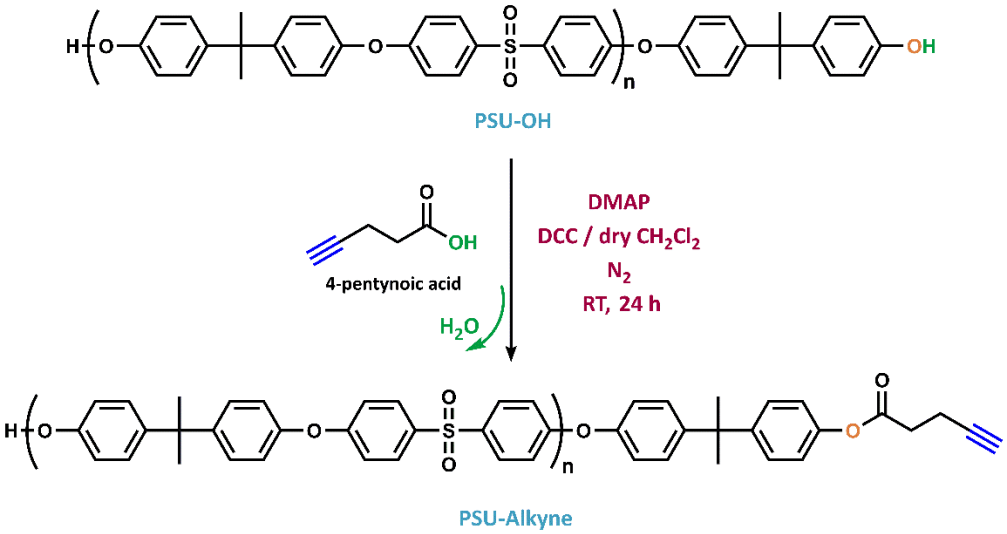

Figure 3.6 : Synthesis of alkyne-end functional polysulfones.

3.3.4.3 Preparation of polysulfone/silicon nitride nanocomposite via CuAAC click reaction (PSU-SNNS)

In a 100 mL Schlenck tube, PSU-Alkyne (0.40 g, 0.042 mmol) dissolved in 20 mL DMF was purged with nitrogen for 30 min, SNNS-N_3 (0.19 g, 0.42 mmol) was ultrasonicated in 20 mL DMF for 30 min, then added into the schlenk tube. Vacuum-nitrogen cycles were performed before the addition of PMDETA (0.088 mL, 0.42 mmol) and CuBr (60 mg, 0.42 mmol). The mixture was stirred at 35 °C for 48 h under N_2 atmosphere. After reaction, the mixture was centrifuged at 6300 rpm for 30 min. While, the supernatant was set aside to precipate in methanol, the sediment was washed with water and ethanol respectively to remove catalyst, then dried overnight at 50 °C under vacuum (Yield: 0.58 g, 99 %) [357-359]. The preparation of PSU-SNNS nanocomposite is pictured as in Figure 3.7.

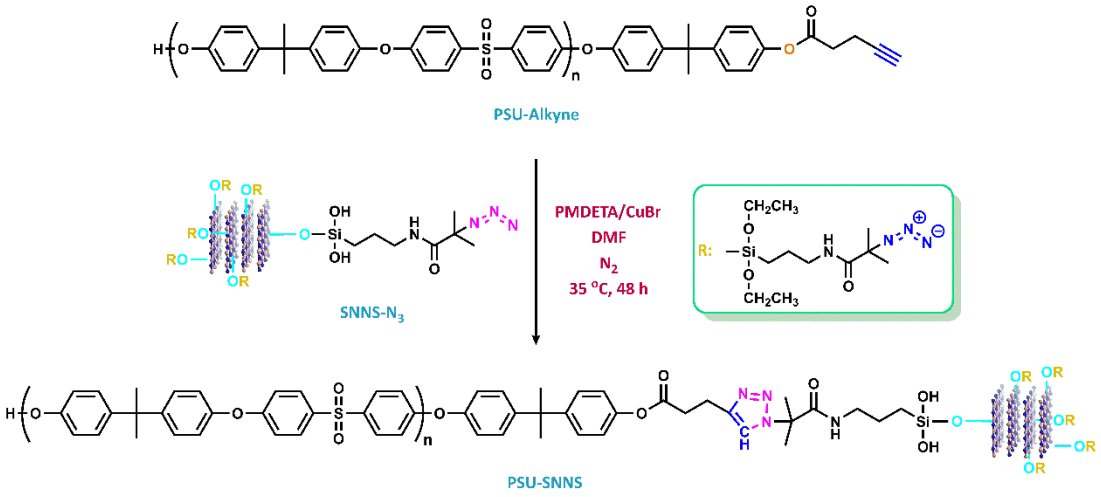

Figure 3.7 : The synthetic representation of PSU-SNNS nanocomposite via CuAAc click reaction.

3.3.4.4 Preparation of polysulfone/silicon nitride nanocomposites via physical blending (PSU+SNNS)

SNNS-N_3 and PSU-Alkyne were mixed physically with the same gravimetrical ratio used in the click reaction.

3.3.5 Preparation of thermal conductive PEEK grafted SNNS nanocomposites

3.3.5.1 Synthesis of hydroxyl end-functional PEEK (PEEK-OH)

Hydroxyl-terminated poly (ether ether ketone) was synthesised via condensation polymerization. Before conducting the reaction, molecular sieves and potassium carbonate (K_2CO_3) were dried at 155 °C and methyl hydroquinone (MeHQ) and 4,4-difluoro benzophenone (DFBP) were vacuum dried at 50 °C for 24 h. In addition, the system was dehumidified under vacuum for 3h and then purged with vacuum-nitrogen cycle prior to reaction for 30 min. Firstly, 6.48 mL N-Methyl-2-pyrrolidone (NMP) and 1.67 mL dry toluene were placed in a 50 mL round bottom flask equipped with a mechanical stirrer, a Dean-Stark trap and a condenser with nitrogen inlet. Then, MeHQ (1.19 g, 9.62 mmol), DFBP (2 g, 9.17 mmol) and dry K_2CO_3 (3.80 g, 27.50 mmol) were introduced the flask. The reaction mixture was heated under reflux at 160 °C along 0.5 h, when toluene azeotrope began to reflux, the temperature adjusted to 180 °C and so the mixture was stirred at this temperature until the reaction termination.The polymerization was terminated by cooling the flask to the room temperature. Then, the mixture was diluted with dimethylformamide (DMF) and sonicated at 90 °C for

couple hours. The diluted mixture filtrated to remove the salt and precipated in a cold mixture of MeOH-H_2O-acetic acid. The precipate was filtrated and dired overnight under vacuum at 50 °C. (Yield: 2.57 g, 80.4 %, M_n = 25,000 g/mol) [360, 361]. The synthesis procedure of PEEK-OH is drawn as in Figure 3.8.

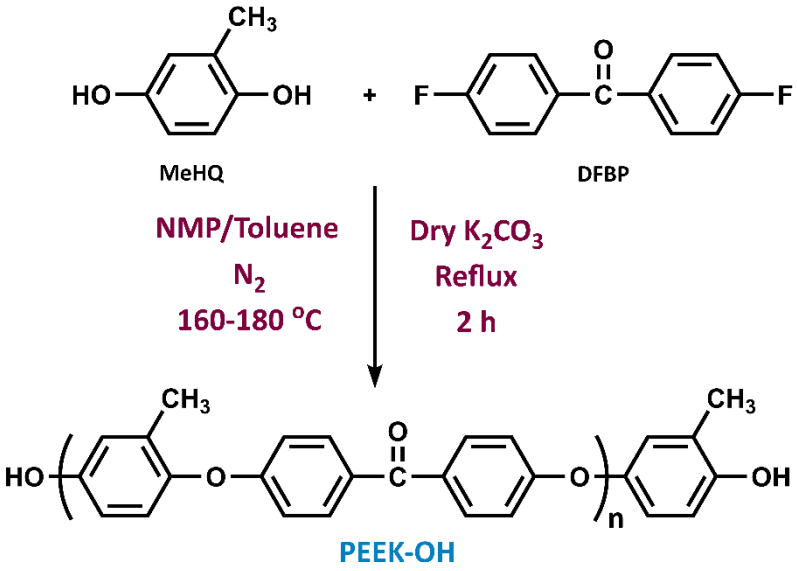

Figure 3.8 : The synthesis procedure of hydroxyl-terminated poly(ether ether ketone).

3.3.5.2 Synthesis of alkyne-end functional PEEK (PEEK-Alkyne)

In a 100 mL two necked round bottom flask, PEEK-OH (M_n = 25,000 g/mol, 2.5 g, 0.1 mmol) was dissolved in 50 mL dimethylformamide (DMF). 4-pentynoic acid (147 mg, 1.5 mmol) and 4-dimethylaminopyridine (DMAP) (36.7 mg, 0.3 mmol) were introduced the mixture. Then N,N'-Dicyclohexylcarbodiimide (DCC) (309.5 mg, 1.5 mmol) dissolved in 20 mL dry DCM was added to the flask in a time period of 30 min in an ice bath. Reaction mixture was stirred at room temperature for 48 h. After reaction, the mixture was filtered to remove the dicyclohexylurea (DCU) formed as a by-product during the reaction and filtered mixture was precipated in methanol. The alkyne terminated poly (ether ether ketone) (PEEK-Alkyne) were dried overnight under vacuum at 50 °C. (0.81 g, Yield: 31 %) [355, 356]. The alkynylation procedure of PEEK-OH is drawn as in Figure 3.9.

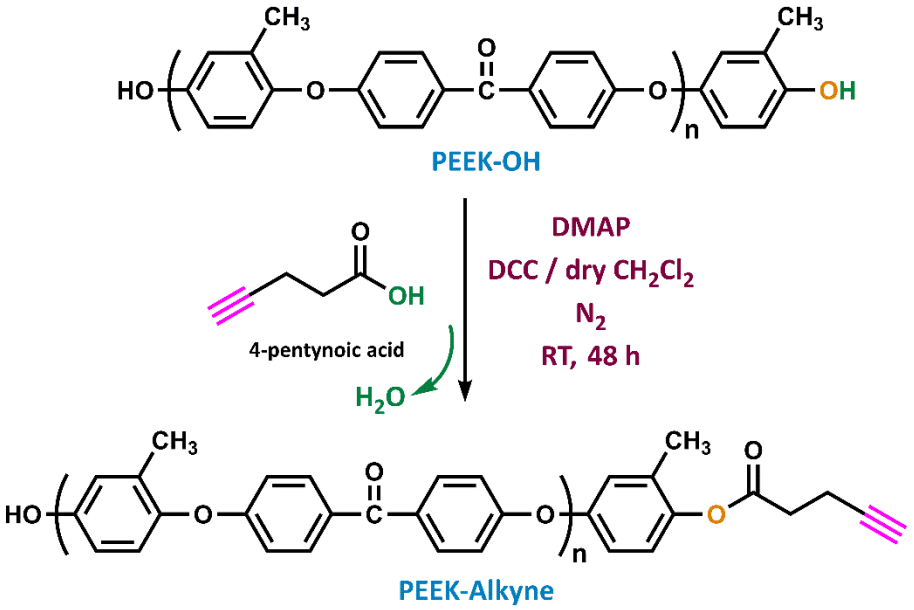

Figure 3.9 : Synthesis of alkyne-terminated poly (ether ether ketone) (PEEK-Alkyne).

3.3.5.3 Preparation of poly(ether ether ketone)/silicon nitride nanocomposites via CuAAC click reaction (PEEK-SNNS)

In a 100 mL Schlenck tube, PEEK-Alkyne (0.80 g, 0.032 mmol) dissolved in 20 mL DMF was purged with nitrogen for 30 min, SNNS-N_3 (0.142 g, 0.32 mmol) was ultrasonicated in 20 mL DMF for 30 min, then added into the schlenk tube. Vacuum-nitrogen cycles were performed before the addition of PMDETA (0.067 mL, 0.32 mmol) and CuBr (46 mg, 0.32 mmol). The mixture was stirred at 40 °C for 48 h under N_2 atmosphere. After reaction, the mixture was precipated in methanol, then dried overnight at 50 °C under vacuum (Yield: 0.72 g, 76.4 %) [357, 359, 362]. The preparation of PEEK-SNNS nanocomposite is pictured as in Figure 3.10.

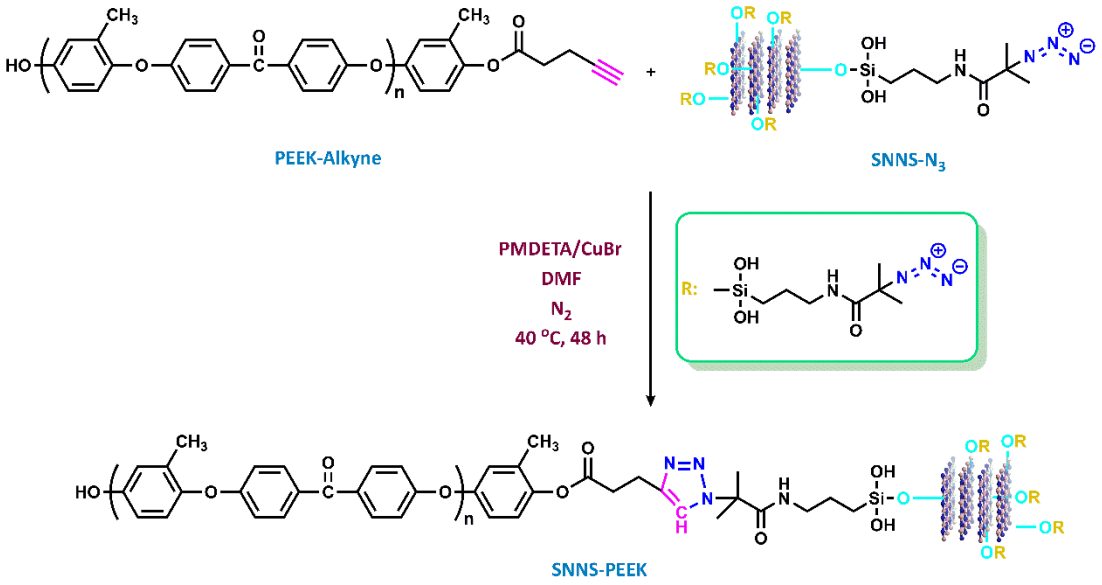

Figure 3.10 : The synthetic representation of PEEK-SNNS nanocomposite via CuAAc click reaction.

3.3.5.4 Preparation of poly(ether ether ketone)/silicon nitride nanocomposites via physical blending (PEEK+SNNS)

SNNS-N_3 and PEEK-Alkyne were mixed physically with the same gravimetical ratio used in the click reaction.

3.3.6 Preparation of test samples as thermal interface materials (TIMs)

3.3.6.1 Preparation of TIMs in film form

DMA test specimens were prepared using a solution casting method.

i. PMMA//SNNS, PMMA-Alkyne, PMMA-SNNS and PMMA+SNNS films

Preparation of PMMA//SNNS film: The PMMA//SNNS film was prepared by dissolving of 1 g PMMA//SNNS nanocomposite in 10 mL dimethyl acetamide (DMAc) with weight ratio of 10 wt% with continuous sonication at 70 °C for 5 h. After the complete dispersion of PMMA//SNNS nanocomposite in DMAc, the solution was poured into a petri dish and dried during the week at 50 °C under vacuum until it was absolutely dried and solidified. After ensuring the complete drying, the solidified PMMA//SNNS film was soaked with distilled water for a while to facilitate removal from the Petri dish.

Preparation of PMMA-Alkyne film: The PMMA-Alkyne solution was prepared by dissolving of 0.8 g PMMA-Alkyne (M_n = 120,600 g/mol) in 8 mL dimethyl acetamide (DMAc) with weight ratio of 10 wt% with continuous sonication at 70 °C for 2 h. After PMMA-Alkyne was completely dissolved, the solution was poured into a Petri dish and dried during the week at 50 °C under vacuum until it was absolutely dried and solidified. After ensuring the complete drying, the solidified PMMA-Alkyne film was soaked with distilled water for a while to facilitate removal from the Petri dish.

Preparation of PMMA-SNNS film: The PMMA-SNNS film was prepared by dissolving of 0.8 g PMMA-SNNS nanocomposite in 8 mL dimethyl acetamide (DMAc) with weight ratio of 10 wt% with continuous sonication at 70 °C for 5 h. After the complete dispersion of PMMA-SNNS nanocomposite in DMAc, the solution was poured into a petri dish and dried during the week at 50 °C under vacuum until it was absolutely dried and solidified. After ensuring the complete drying, the solidified PMMA-SNNS film was soaked with distilled water for a while to facilitate removal from the Petri dish.

Preparation of PMMA+SNNS film: For the preparation of the physically blended nanocomposite film, 0.12 g of PMMA-Alkyne (M_n = 120,600 g/mol) was first dissolved in 8 mL dimethyl acetamide (DMAc) with continuous sonication at 70 °C for 2 h. After the complete dissolution of PMMA-Alkyne, 0.48 g SNNS-N_3 was added to the PMMA solution and sonication was continued for three more hours to ensure a uniform dispersion of SNNS-N_3 nanosheets in the solution. After homogeneity was achieved, the solution was poured into a Petri dish and dried during the week at 50 °C under vacuum until it was absolutely dried and solidified. After ensuring the complete drying, the solidified PMMA+SNNS film was soaked with distilled water for a while to facilitate removal from the Petri dish.

ii. PEEK-Alkyne, PEEK-SNNS and PEEK+SNNS films

Preparation of PEEK-Alkyne film: The PEEK-Alkyne solution was prepared by dissolving of 1.6 g PEEK-Alkyne (M_n = 25,000 g/mol) in 8 mL dimethyl acetamide (DMAc) with weight ratio of 20 wt% with continuous sonication at 70 °C for 3 h. After PEEK-Alkyne was completely dissolved, the solution was poured into a Petri dish, kept in a glove box overnight in first, and then pre-dried under vacuum at room conditions for 48 h to prevent abrupt solvent evaporation prior to heatdry. The

complete drying process was carried out at 35 °C overnight and at 50 °C for 2 days under vacuum, respectively. After ensuring the complete drying, the elastic and saturated form of PEEK-Alkyne film was soaked with distilled water for a while to facilitate removal from the Petri dish.

Preparation of PEEK-SNNS film: The PEEK-SNNS film was prepared by dissolving of 1.3 g PEEK-SNNS nanocomposite in 6.5 mL dimethyl acetamide (DMAc) with weight ratio of 20 wt% with continuous sonication at 90 °C for 3 h. After the complete dispersion of PEEK-SNNS nanocomposite in DMAc, the solution was poured into a petri dish, kept in a glove box overnight in first, and then pre-dried under vacuum at room conditions for 48 h to prevent abrupt solvent evaporation prior to heatdry. The complete drying process was carried out at 35 °C overnight and at 50 °C for 2 days under vacuum, respectively. After ensuring the complete drying, the elastic and tough form of PEEK-SNNS film was soaked with distilled water for a while to facilitate removal from the Petri dish.

Preparation of PEEK+SNNS film: For the preparation of the physically blended PEEK+SNNS nanocomposite film, 1.36 g of PEEK-Alkyne (M_n = 25,000 g/mol) was first dissolved in 8 mL dimethyl acetamide (DMAc) with continuous sonication at 70 °C for 3 h. After the complete dissolution of PEEK-Alkyne, 0.24 g SNNS-N_3 was added to the PEEK solution and sonication was continued for three more hours to ensure a uniform dispersion of SNNS-N_3 nanosheets in the solution. After homogeneity was achieved, the solution was poured into a Petri dish, kept in a glove box overnight in first, and then pre-dried under vacuum at room conditions for 48 h to prevent abrupt solvent evaporation prior to heatdry. The complete drying process was carried out at 35 °C overnight and at 50 °C for 2 days under vacuum, respectively. After ensuring the complete drying, the elastic and tough form of PEEK+SNNS film was soaked with distilled water for a while to facilitate removal from the Petri dish.

3.3.6.2 Preparation of TIMs in pad form

DTC test specimens were prepared from powder products in pad form.

i. PMMA//SNNS, PMMA-Alkyne, PMMA-SNNS and PMMA+SNNS pads

Preparation of PMMA//SNNS pad: The PMMA//SNNS pad was prepared by blending 2.04 g of PMMA//SNNS (60 wt%), 1.29 g of hydroxyl terminated PDMS (M_n = 50,000

g/mol) supplied by Sigma-Aldrich (38 wt%) and 0.07 g of hydrophobic fumed silica known as Aerosil® R805 (2 wt%) homogenously. The nanocomposite pad was obtained in the form of a disc shape (50 mm diameter) for thermal conductivity (TC) measurement. The obtained pad have thicknesses of approximately 0.5-1 mm range.

Preparation of PMMA-Alkyne pad: The PMMA-Alkyne pad was prepared by blending 1.72 g of PMMA-Alkyne (47.5 wt%), 1.5 g of hydroxyl terminated PDMS (M_n = 50,000 g/mol) supplied by Sigma-Aldrich (41.4 wt%) and 0.4 g of hydrophobic fumed silica known as Aerosil® R805 (11 wt%) homogenously. The nanocomposite pad was obtained in the form of a disc shape (50 mm diameter) for thermal conductivity (TC) measurement. The obtained pad has thicknesses of approximately 0.5-1 mm range.

Preparation of PMMA-SNNS pad: The PMMA-SNNS pad was prepared by blending 2 g of PMMA-SNNS (60 wt%), 1.24 g of hydroxyl terminated PDMS (M_n = 50,000 g/mol) supplied by Sigma-Aldrich (37 wt%) and 0.1 g of hydrophobic fumed silica known as Aerosil® R805 (3 wt%) homogenously. The nanocomposite pad was obtained in the form of a disc shape (50 mm diameter) for thermal conductivity (TC) measurement. The obtained pad has thicknesses of approximately 0.5-1 mm range.

Preparation of PMMA+SNNS pad: The PMMA+SNNS pad was prepared by blending 1.3 g SNNS-N_3 (36 wt%) 0.86 g of PMMA-Alkyne (24 wt%), 1.33 g of hydroxyl terminated PDMS (M_n = 50,000 g/mol) supplied by Sigma-Aldrich (37 wt%) and 0.11 g of hydrophobic fumed silica known as Aerosil® R805 (3 wt%) homogenously. The nanocomposite pad was obtained in the form of a disc shape (50 mm diameter) for thermal conductivity (TC) measurement. The thickness of the pad is in the range of 0.5-1 mm.

PSU-Alkyne, PSU-SNNS and PSU+SNNS pads

Preparation of PSU-Alkyne pad: The PSU-Alkyne pad was prepared by blending 2.04 g of PSU-Alkyne (68 wt%), 0.9 g of hydroxyl terminated PDMS (M_n = 50,000 g/mol) supplied by Sigma-Aldrich (30 wt%) and 0.06 g of hydrophobic fumed silica known as Aerosil® R805 (2 wt%) homogenously. The nanocomposite pad was obtained in the form of a disc shape (50 mm diameter) for thermal conductivity (TC) measurement. The thickness of the pad is in the range of 0.5-1 mm.

Preparation of PSU-SNNS pad: The PSU-SNNS pad was prepared by blending 2.3 g of PSU-SNNS (67 wt%), 1.03 g of hydroxyl terminated PDMS (M_n = 50,000 g/mol)

supplied by Sigma-Aldrich (30 wt%) and 0.11 g of hydrophobic fumed silica known as Aerosil® R805 (3 wt%) homogenously. The nanocomposite pad was obtained in the form of a disc shape (50 mm diameter) for thermal conductivity (TC) measurement. The obtained pad has thicknesses of approximately 0.5-1 mm range.

Preparation of PSU+SNNS pad: The PSU+SNNS pad was prepared by blending 2.5 g SNNS-N_3 (60.3 wt%) 0.28 g of PSU-Alkyne (6.7 wt%), 1.26 g of hydroxyl terminated PDMS (M_n = 50,000 g/mol) supplied by Sigma-Aldrich (30 wt%) and 0.13 g of hydrophobic fumed silica known as Aerosil® R805 (3 wt%) homogenously. The nanocomposite pad was obtained in the form of a disc shape (50 mm diameter) for thermal conductivity (TC) measurement. The obtained pad has thicknesses of approximately 0.5-1 mm range.

ii. PEEK-Alkyne, PEEK-SNNS and PEEK+SNNS pads

Preparation of PEEK-Alkyne pad: The PEEK-Alkyne pad was prepared by blending 1.84 g of PEEK-Alkyne (54 wt%), 1.5 g of hydroxyl terminated PDMS (M_n = 50,000 g/mol) supplied by Sigma-Aldrich (44 wt%) and 0.07 g of hydrophobic fumed silica known as Aerosil® R805 (3 wt%) homogenously. The nanocomposite pad was obtained in the form of a disc shape (50 mm diameter) for thermal conductivity (TC) measurement. The obtained pad have thicknesses of approximately 0.5-1 mm range.

Preparation of PEEK-SNNS pad: The PEEK-SNNS pad was prepared by blending 1.84 g of PEEK-SNNS (54 wt%), 1.5 g of hydroxyl terminated PDMS (M_n = 50,000 g/mol) supplied by Sigma-Aldrich (44 wt%) and 0.07 g of hydrophobic fumed silica known as Aerosil® R805 (2 wt%) homogenously. The nanocomposite pad was obtained in the form of a disc shape (50 mm diameter) for thermal conductivity (TC) measurement. The obtained pad have thicknesses of approximately 0.5-1 mm range.

Preparation of PEEK+SNNS pad: The PEEK+SNNS pad was prepared by blending 0.51 g SNNS-N_3 (15 wt%) 1.33 g of PEEK-Alkyne (39 wt%), 1.5 g of hydroxyl terminated PDMS (M_n = 50,000 g/mol) supplied by Sigma-Aldrich (44 wt%) and 0.07 g of hydrophobic fumed silica known as Aerosil® R805 (2 wt%) homogenously. The nanocomposite pad was obtained in the form of a disc shape (50 mm diameter) for thermal conductivity (TC) measurement. The obtained pad have thicknesses of approximately 0.5-1 mm range.

4. RESULTS AND DISCUSSION

This thesis aimed to synthesize a new generation polymer matrix nanocomposites having silicon nitride nanosheets (SNNSs) with thermal conductivity and investigate the experimental parameters. The modification of fillers, crystalline structures of polymers, interaction type between filler and matrix, structural characteristics of nanocomposites were taken into account to obtain optimum thermal conductivity (TC) properties.

4.1 Preparation of Silicon Nitride Nanosheets (SNNSs)

In the design of thermal conductive polymer nanocomposite, in order to increase inter-surface interactions between polymer and nanoparticles, provide a homogeneous distribution of nanopartciles in polymer matrix and facilitate to surface functionalization, silicon nitride nanoparticles were modified in nanosheet morphology. By mechanical exfoliation method, silicon nitride nanosheets (SNNSs) with reduced particle size and layered form was obtained to make the chemical modification process easier. The change in crystallite size of the samples isolated as a result of the exfoliation processes carried out under determined conditions were followed by XRD.

4.1.1 Crystallography investigation (XRD)

The average crystallite sizes of β-Si_3N_4 and SNNS obtained from mechanical exfoliation process were calculated using the XRD analysis results according to the Debye Scherrer equation (4.1) given below [363].

$$D = \frac{K.\lambda}{\beta.\cos(\theta)} \tag{4.1}$$

D = the crystallite size

K = a dimensionless shape factor, has a typical value of about 0.9.

λ = the X-ray wavelength.

β = the line broadening at half the maximum intensity (FWHM)

θ = the Bragg angle.

The distance between layers was calculated according to Bragg Equation (4.2) by using XRD analysis results.

$$n\lambda = 2d.Sin(\theta) \quad (4.2)$$

d = the distance between layers.

λ = the X-ray wavelength.

θ = the Bragg angle.

n = the reflection order, has a typical value of about 1.

Figure 4.1 shows the major (200) diffraction patterns of milled β-Si_3N_4 nanofillers. The Bragg reflections seem broadened as the milling time increases. This change can be associated with the reduction of the crystallite size and the formation of lattice strain [364, 365]. Besides broadened reflections, shifts to lower degrees have also been observed which are explained with changes in the lattice parameters during mechanical treatment which indicate an increase in d-spacing due to the increased distance between the layers [366, 367].

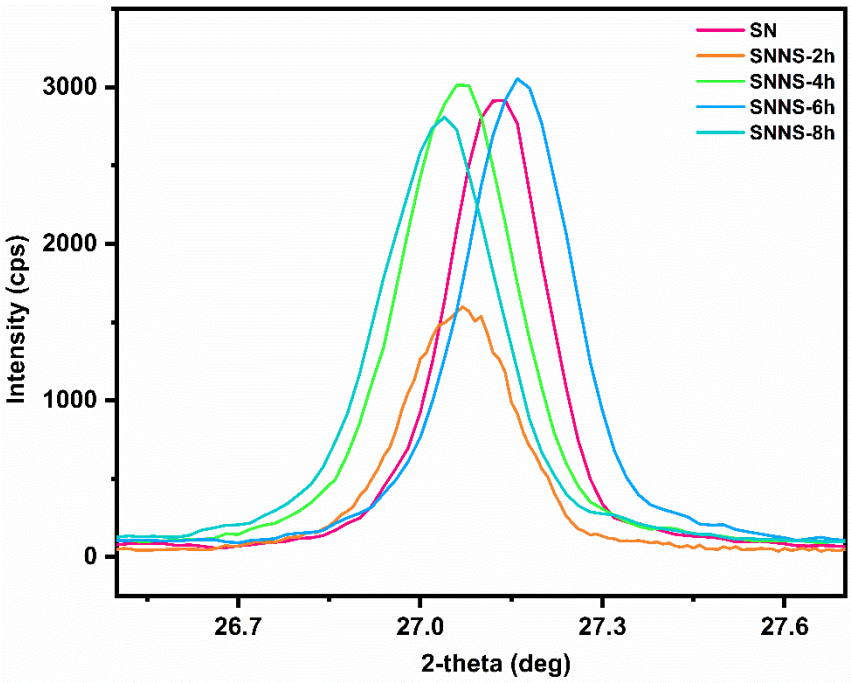

Figure 4.1 : XRD patterns of raw and ball-milled nano silicon nitrides in different time.

It can be seen that the 6-h milled SNNS displayed deviant tendency among the other diffraction patterns. This result may arises from the disorganized stacking due to intensive deformation and the heat generated during the long hour (6 h) milling process [368]. The deformation during the process reachs a saturation point resulted from aggregated strain hardening, while the heat leads to a decrease of lattice strain, so the d-spacing, and increase in the crystallite size. It has been found that the effects of deformation and heat seem disappear as the milling process continues immediately after the cooling process is applied. The increase in lattice strain can be observed from the beginning of the last 2 h milling process and the Bragg reflection behaviors in normal trend can be seen again as the mechanic exfoliation continues as seen in 8-h milled SNNS [365, 369].

Table 4.1 presents the structural parameters of milled powders. It is clearly seen that the change in crystallite size and d-spacing are directly proportional. The full width at half-maximum (FWHM) value is related to the crystallite size, the d-spacing and the strain. As mechanical treatment continuous, the strain increases in the structure, the layers move away from each other and the crystallite size decreases. Thus, the FWHM value appear to be also increases depending on these parameters [370].

Table 4.1 : The effect of milling time on crystal structure of silicon nitride.

Nanofiller	FWHM (deg)	Crystallite Size (nm)	d-spacing (nm)
SN	0.156	54.8	0.3286
SNNS-2h	0.183	46.7	0.3295
SNNS-4h	0.192	44.4	0.3295
SNNS-6h	0.179	47.8	0.3283
SNNS-8h	0.195	43.9	0.3298

The changes in the crystal structure parameters of 8-h milled SNNS such as shifting of diffraction peak to lower degrees, peak broadening, increment in FWHM and diminishment of crystallite size reveal that the layers of the structure diverged from each other. By this treatment, the surface of silicon nitride nanofiller (SNNS) became more suitable for chemical modification process.

4.1.2 Morphological investigation (SEM)

The surface morphologies and crystal structures of pristine SN and ball-milled SN (SNNS) were investigated by Scanning Electron Microscopy (SEM). When the electron microscope images of commercially available SN are examined, it is noticed

that a bulk structure with fractional rod-shape crystal morphlogy with a thickness of 75 nm in average is clumped (Figure 4.2a). A separated layered form known as SNNS was observed in SN that was subjected to mechanical exfoliation for 8 hours. Twisted morphology observed in some layers shows that the layers subjected to torsion with exfoliation after mechanical treatment. The layer thickness of newly formed SNNS was calculated as 41 nm in average (Figure 4.2b). This also confirms the reduction in crystallite size considering the XRD results. The SEM results show that the structure became suitable for easier chemical surface modification.

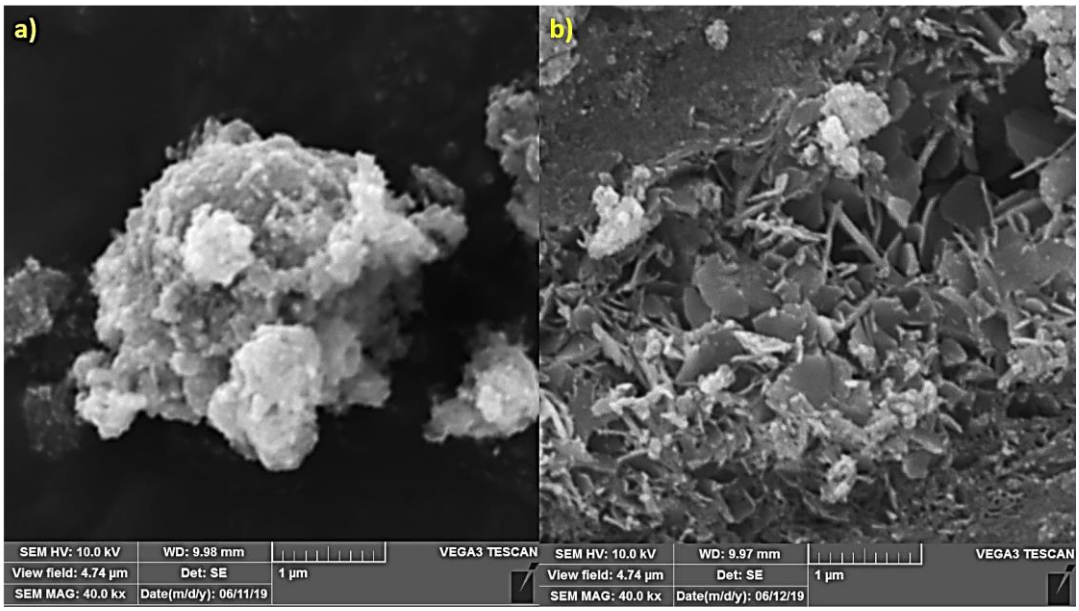

Figure 4.2 : SEM magnification images of a) SN and b) SNNS.

4.1.3 Particle size measurements

Silicon nitride nanosheets (SNNS) were obtained successfully following the mechanical exfoliation process of pristine SN in the range of nano scale. Size, size distribution and layer tickness of silicon nitride (SN) and silicon nitride nanosheet (SNNS) were analyzed through X-Ray Diffractrometry (XRD), Scanning Electron Microscopy (SEM) and ZetaSizer. Dimensional analyses were performed with various particle size characterization tehniques for SN and SNNS. Since each method used to determine the size of the material has a different measuring principle, the results obtained also differ [371]. All techniques have confirmed the particle size reduction of SN through mechanical exfoliation. The measurements with zetasizer showed the highest particle size values (439 nm for SN and 237 nm for SNNS) than those of other methods (i.e. in SEM analysis, 117 nm for SN and 80 nm for SNNS) (Table 4.2). This

discrepancy can be explained by the measurement principle of the zetasizer analysis, which calculates particle size assuming the particles are in spherical morphology [372]. Moreover, the agglomeration in solution is another important factor that can cause this deviation for zetasizer measurement. Apart from this technique, the changes in layer tickness have been monitored also with SEM as discussed in previous part. As in the change of particle size, the thickness of layers also reduced after mechanical treatment.

Table 4.2 : Dimensional analysis of SN and SNNS.

Nanofiller	Crystallite Size (nm) XRD	Particle Size (nm) ZetaSizer	Particle Size (nm) SEM	Layer Tickness (nm) SEM
SN	54.8	439	117	75
SNNS	43.9	237	80	41

The particle size distribution of SN and SNNS was measured by photon correlation spectroscopy (PCS) using a Malvern Zetasizer Nano ZS laser particle size analyzer. The instrument opretated at a wavelength of 632 nm. The suspension was prepared by dispersing the nanoparticles in 2-propanol with the concentration of around 0.001 g/L and ultrasonicated for 30 minutes to obtain a well-dispersed suspension. The green trace represents the SN, while the red trace represents SNNS. It is obviously seen in Figure 4.3, the particle size of SN was reduced via mehanical exfoliation with ball-mill.

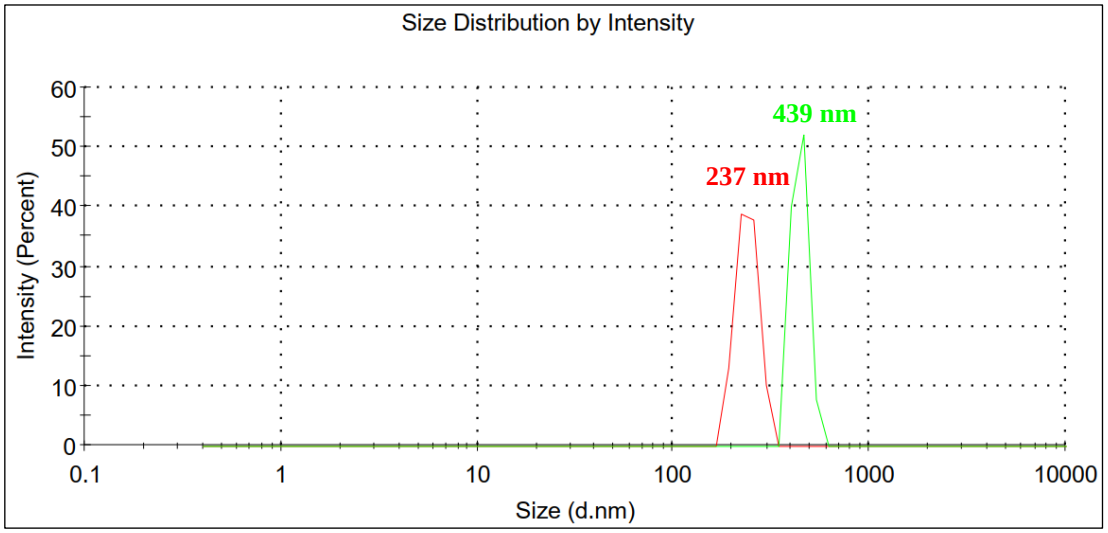

Figure 4.3 : Particle size distributions of SN (green) and SNNS (red).

4.2 Chemical Modifications of Silicon Nitride Nanosheets (SNNSs-R)

Exfoliated silicon nitride nanosheet (SNNS) was chemically modified in order to obtain active initiating sites on filler surface to enhance the interfacial interaction during click reaction. The whole modification processes are depicted in detail in Figure 4.4.

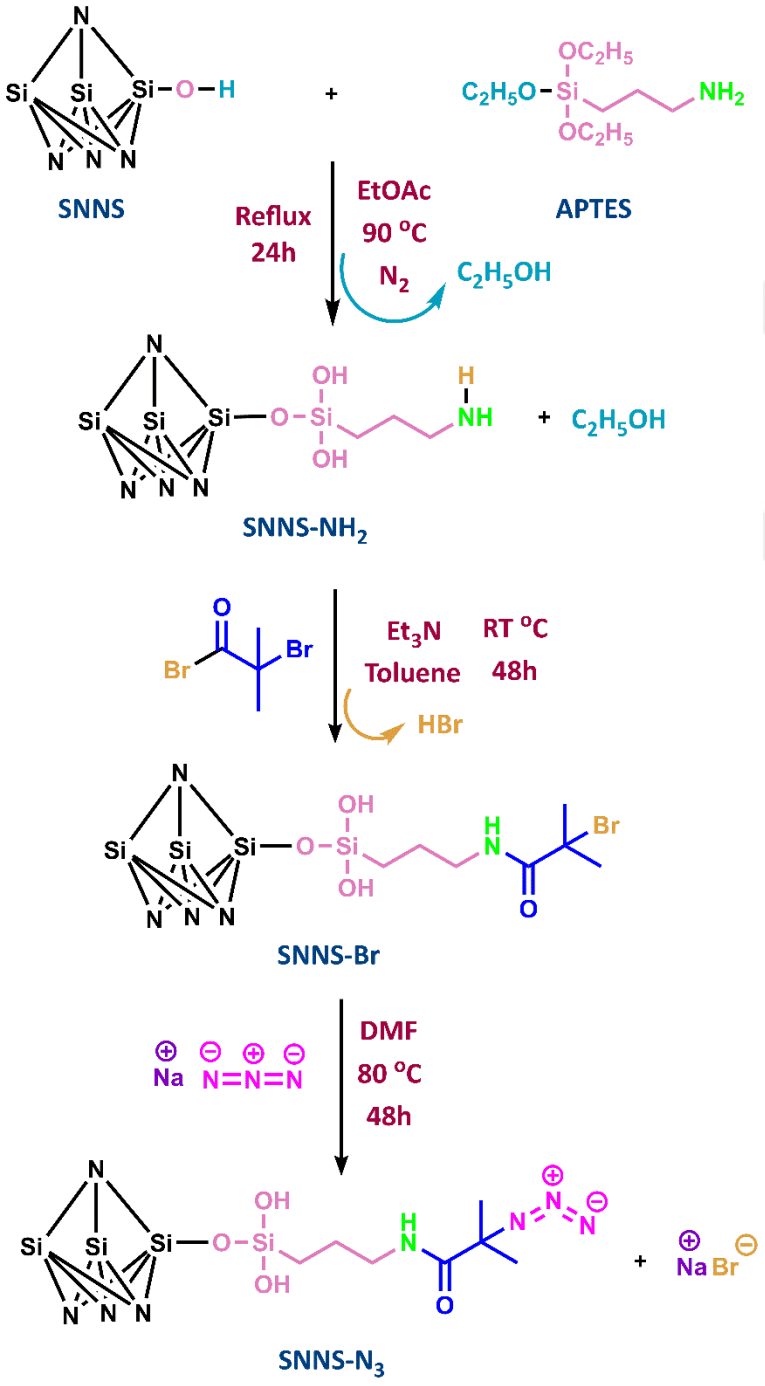

Figure 4.4 : Chemical modifications stages of SNNSs.

A three-step modification process was applied to the mechanically exfoliated silicon nitride nanosheets, these are amination, bromo-amidation and azidation reactions, respectively. Firstly, the existing hydroxyl groups on SNNS surface were converted to bromide groups by introducing APTES as coupling agent via bromoesterification reaction to yield bromo-amide end-functional SNNSs (SNNS-Br). The SNNS-Br were used as an ATRP initiator for the polymerization of MMA by surface initiated atom transfer radical polymerization (SI-ATRP). This process ended up with obtaining of polymer matrix nanocomposites via surface initiation. In *"click chemistry"* approach, the bromide groups were converted to azide groups through the reaction of SNNS-Br with sodium azide without any catalyst to give azide end-functional SNNSs (SNNS-N_3). Finally, SNNS-N_3 were subjected to Copper Catalyzed Azide-Alkyn Click reaction (CuAAc) with alkyn-end functional polymers to yield polymer matrix nanocomposites via click chemistry. The schematic representation of modification process is given in Figure 4.5.

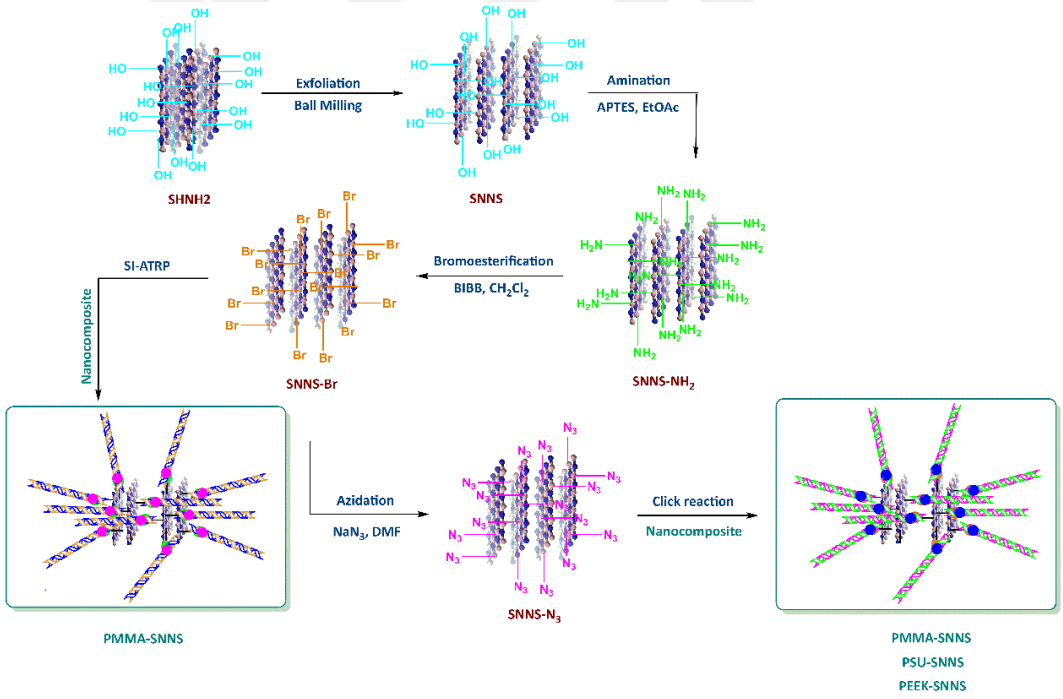

Figure 4.5 : The schematic demonstration of the nanocomposite production process.

Fourier Transform Infrared Spectroscopy was performed for the structral characterization of SNNSs primarily. FTIR spectroscopic analysis afforded proof that the SNNS surface was successfully modified (Figure 4.6).

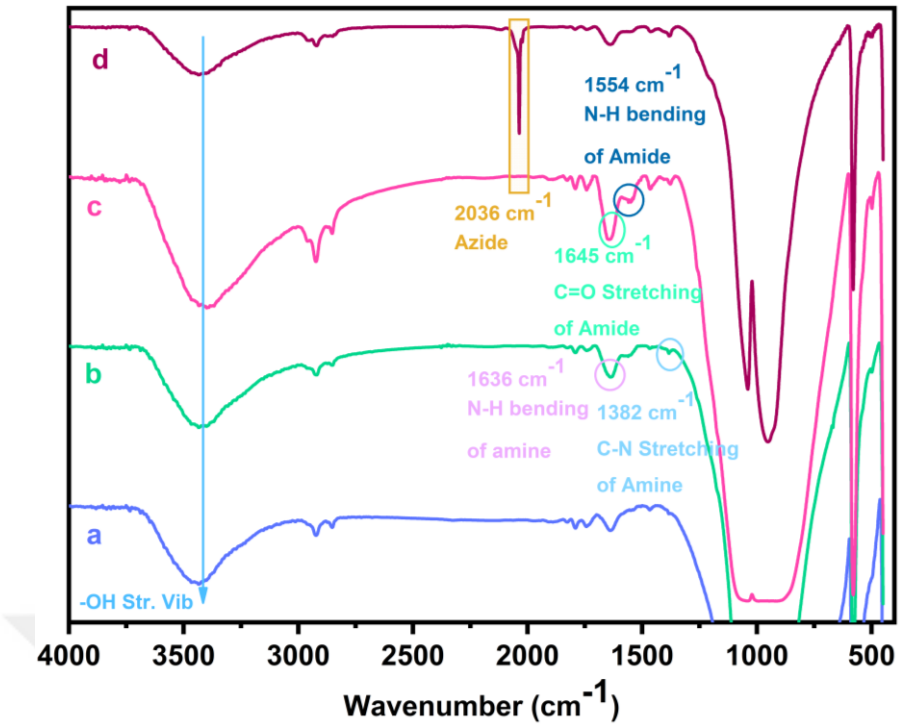

Figure 4.6 : FTIR spectra of modified SNNSs; a) SNNS, b) SNNS-NH_2, c) SNNS-Br, d) SNNS-N_3.

Figure 4.6 shows the FTIR analysis of pristine SN and modified SNNSs. These spectra present clear evidence of modification processes step-by-step. The backbone vibrations of Si-N-Si are noticeable at 950 cm^{-1} in all spectra. Besides, hydroxyl-stretching vibrations are apparent at around 3420 cm^{-1} in all spectras due to -OH groups on the surface of silicon nitride. That can be suggested that not all the hydroxyl groups on SNNS surface have converted to other functional groups by reacting with coupling agent. Therefore, it can be said that there is still substantial aggregate of intact hydroxyl groups on surface of modified SNNSs.

Reactive silane coupling agent of APTES reacted with these hydroxyl groups on SNNS surface to form Si-O-Si bond which appears at 1039 cm^{-1} and the N-H bending vibration at 1636 cm^{-1} indicates that the amine group is successfully attached the nanosheet structure in Figure 4.6b. In addition, absorption peaks at 2925 cm^{-1} and 2850 cm^{-1} are assigned to the C-H stretching vibrations of $-CH_3$ and $–CH_2$ groups respectively in Figure 4.6a, 4.6b and 4.6c. In Figure 4.6c, the peak appeared at 1645 cm^{-1} indicates the carbonyl stretching vibration of amide functional group. The new absorption peak seemed at 1554 cm^{-1} that belongs to N-H bending vibration of amide also proves this phenomenon. After the treatment with sodium azide, distinctive peak

emerged at 2036 cm^{-1} in Figure 4.6d represents that the $–N_3$ group is readily available on the surface of SNNS for the click reaction with polymer matrices.

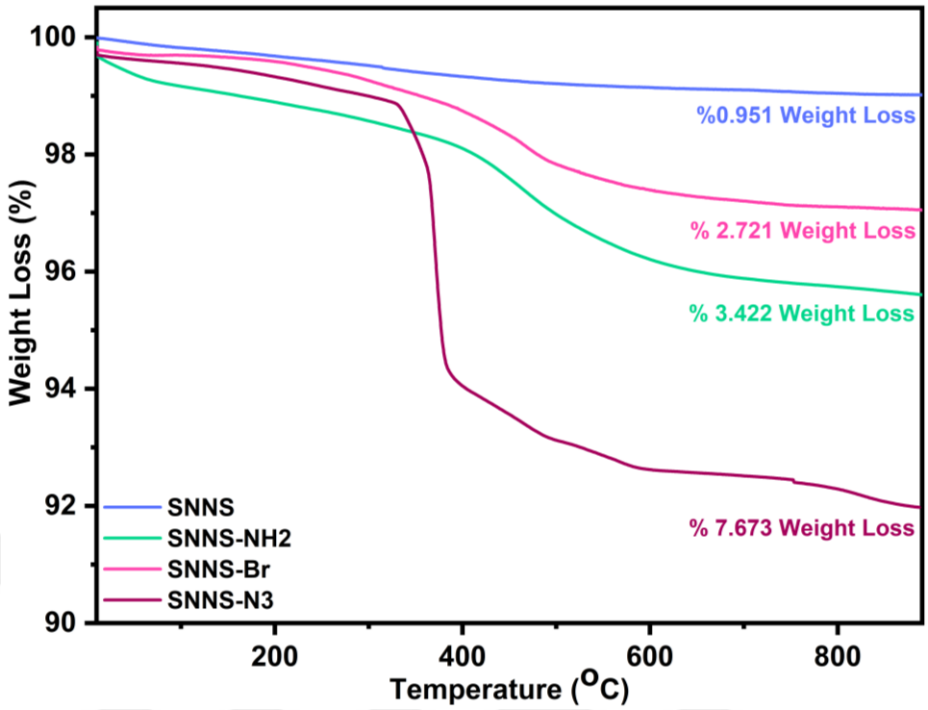

Figure 4.7 : TGA curves of SNNS and modified SNNSs.

The success of modification process was also confirmed by thermal analysis (Figure 4.7). Accordingly, thermal behaviours of SNNS and modified SNNSs were determined by TGA measurements. The weight losses below 200 °C can be attributed to physisorbed water and residual organic solvents. Thermal degradation of pristine SNNS began from 100 °C to 800 °C might be ascribed to hydroxyl groups on SNNS surface and some chemically adsorbed substances. This change corresponds to 0.95 % weight loss. The thermal decomposition of SNNS-NH_2 began at 380 °C and continued to 800 °C. This loss was around 2.5 %. It is observed that weight loss of 2.48 % between 210-800 °C for SNNS-Br and loss of 6.88 % between 330-900 °C for SNNS-N_3 as expected. It is obviously seen that the modified SNNSs showed typical losses after each stage of modification, which can be attributed to successfull attachments of organic functional groups to SNNS surface.

4.3 Preparation of Thermal Conductive Polymer Matrix Nanocomposites

SNNSs used in preparation of polymer matrix nanocomposites are nanosheets obtained by mechanic exfoliation via ball-milling. Based on this method,

nanocomposite fabrication through chemical bonding of three different polymer matrices with SNNS was performed. The polymer nanocomposites containing silicon nitride nanoparticles as thermal conductive filler with polymer phases as poly(methyl methacrylate) (PMMA), polysulfone (PSU) and poly(ether ether ketone) (PEEK) synthesized and functionalized within the scope of the thesis were prepared in different morphologies and their structures were elucidated. Two different nanocomposite preparation methods for each polymer matrices, click chemistry and physical blending, were performed and the structural analysis of the each nanocomposite product was compared. Thus, characterization results of nanocomposites contain the comparisons of these two methods. The differences between these two techniques were reported in detail in each section in order to show the superiority of the fabrication of thermal conductive polymer nanocomposite by chemical interaction approach. Nanocomposite preparation with click chemistry approach is depicted in Figure 4.8.

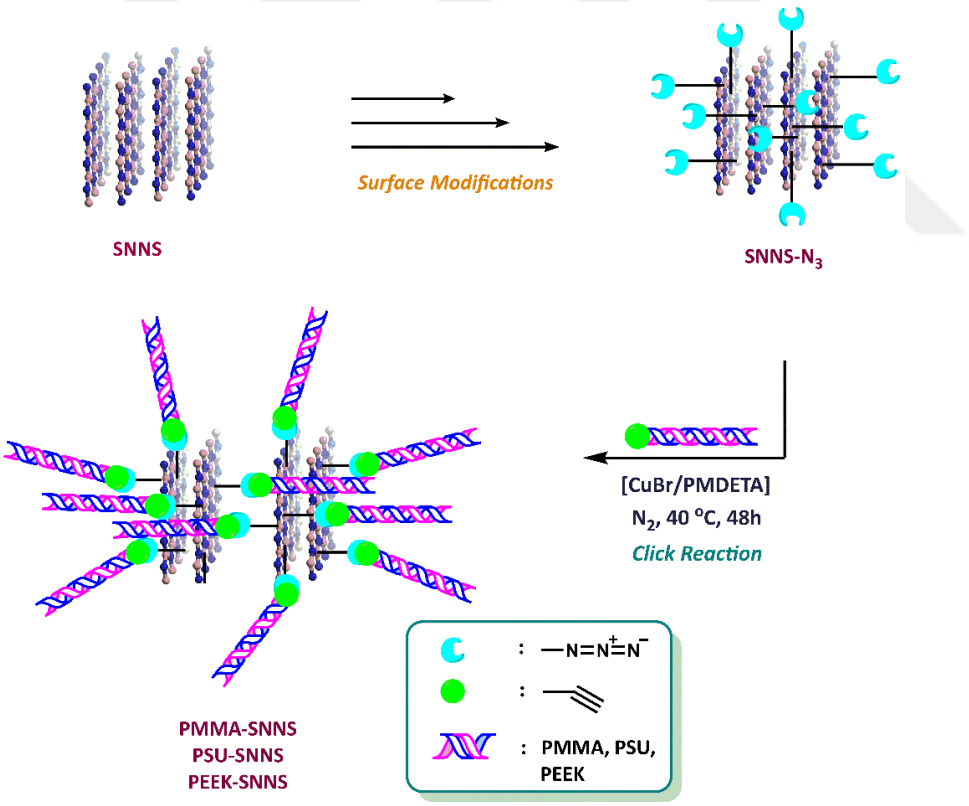

Figure 4.8 : The schematic representation of nanocomposite preparation via click reaction.

4.3.1 Preparation of poly(methyl methacrylate)/silicon nitride nanocomposites via SI-ATRP (PMMA//SNNS)

In the preparation of thermal conductive nanocomposite with PMMA matrices, two synthetic approach have been used: In the first approach, the chemically modifed silicon nitride (SNNS-Br) were used as an ATRP initiator for the controlled polymerization of methyl methacrylate. In the second approach, chemically modified silicon nitride (SNNS-N_3) were used as a "click" agent in the synthesis of nanocomposites via click chemistry by reacting with alkyne end-functional PMMA (PMMA-Alkyne).

For this section, characterization results of PMMA//SNNS nanocomposite synthesized via surface initiated polymerization (SIP) were examined. PMMA//SNNS, was prepared in two stages. For this purpose, in the first stage SNNSs were modified by bromoesterification reaction with modifying agents to yield bromide end-functional nanoparticle (SNNS-Br). Thereafter, bromide groups on SNNS surface were used as an Atom Transfer Radical Polymerization (ATRP) initiator to grow PMMA brushes on SNNS surface. In this reaction, MMA monomer was polimerized with SNNS-Br in the presence of CuBr/PMDETA under nitrogen atmosphere at 80 °C for 6,5 h. Then, PMMA//SNNS nanocomposite particles were collected by centrifugation (Figure 4.9).

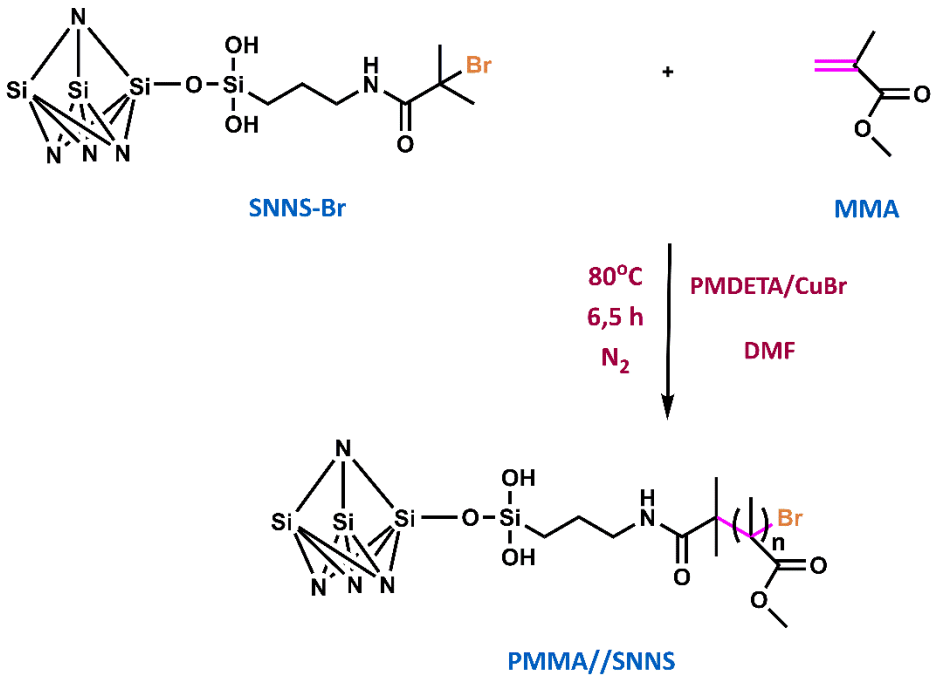

Figure 4.9 : The synthetic route for the preparation of PMMA//SNNS nanocomposite via SI-ATRP.

The experimental conditions and the properties of PMMA obtained by SI-ATRP are given in Table 4.3. It shoulde be noted that the conversion and yield of this reaction are considerably poor due to the low activity of SNNS-Br the ATRP initiator. Thus, the more emphasis has been placed on the preparation of nanocomposites by click reaction instead of by SI-ATRP.

Table 4.3 : Synthesis conditions and molecular weight characterization of PMMA by SI-ATRP.

Sample	DP_n[a]	Conversion[b] (%)	$M_{n,GPC}$[c] (g/mol)	$Đ$[c]	Yield (%)
PMMA//SNNS	100	19.5	104,000	2.97	2.3

[a] In DMF, $[M]_o/[I]_o/[CuBr]_o/[PMDETA]_o$ = 100:1:1:2.
[b] Determined by gravimetry.
[c] Determined by GPC based on linear polystyrene standards.

The successful grafting of PMMA as polymer matrice to the surface of modified SNNSs was confirmed by SEM, FTIR, TGA and DSC analysis.

4.3.1.1 Morphological investigation

Scanning electron microscopy were performed in order to investigate the dispersion of SNNSs within the polymer matrices. The morphologies of SN, SNNS and PMMA//SNNS were investigated using SEM with 25k magnification scales as shown in Figure 4.10.

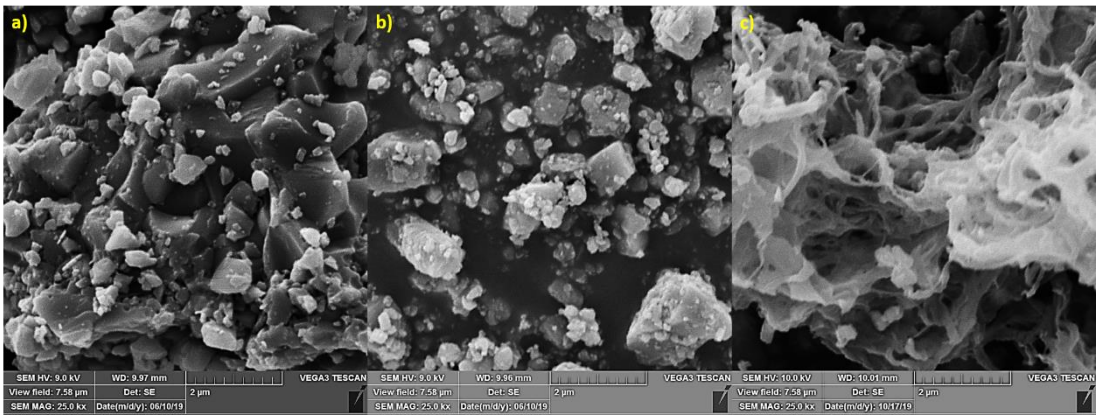

Figure 4.10 : SEM magnification images of a) SN, b) SNNS and c) PMMA//SNNS.

The SEM images for pristine silicon nitride (SN), silicon nitride nanosheets (SNNS), and PMMA grafted silicon nitride nanosheets by SI-ATRP (PMMA//SNNS) with 25k magnification scales were given in Figure 4.10a, 4.10b and 4.10c, respectively. It is clearly seen that the pristine SN particles seem in bulky form consisting dimensionally

uneven rod-shape crystals (Figure 4.10a). After subjecting to mechanic exfoliation with ball mill, the size of the SN particles have been reduced and these particles displayed crumbled and well-dispersed morphology (Figure 4.10b). In addition, the crystal structure of pristine SN have converted into spherical morphology due to shear force effect of the mechanical treatment [373, 374]. This result indicated that the structure became suitable for chemical surface modification more easily. Moreover, the interaction between the nanofiller and polymer matrix is assumed to enhance significantly under the condition of performing modifying agents having fucntional groups to nanofiller. The presence of enhanced interface interaction between the phases leads the formation of thermal pathaway, as confirmed by thermal conductivity analysis. Therefore, the thermal conduction through the thermal pathaway constituted by means of modifiying agent, so as to the formation of carbon-carbon bond between the phases, has high enough probabilty in well-dispersed nanocomposite blends [375]. The confirmation of this phenomenon is clearly seen as well-dispersed morphology in Figure 4.10c.

As grafting densitiy increases, the incompatibility of interface between nanofiller and matrix decreases besides the reduction in interfacial tension, and results in a preferable dispersion of nanofiller in polymer matrix to be yield a more steady morphology [375]. It is also obviously seen that the polymer-grafted nanosheets (nanocomposite) take more space than matrice-free nanoparticles (SNNS) under the same magnification in Figure 4.10c. The absolute surrounding of nanosheets by polymer network verifies that the PMMA have been able to be grafted effectively to the SNNS surface. This consequence points out that the interface compatibility between the surface-modified nanofiller (SNNS-Br) and the polymer matrix (PMMA) due to the covalent bond formation through SI-ATRP [376].

4.3.1.2 Structural investigation

The structural analysis with FTIR spectrospy was performed to investigate the chemical structures of SNNS-Br and PMMA//SNNS and identify their characteristic peaks in Figure 4.11.

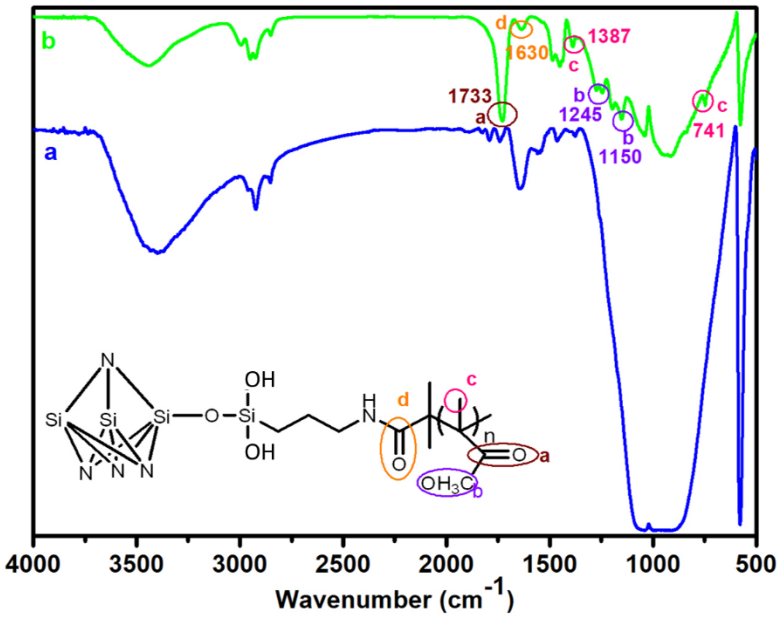

Figure 4.11 : FTIR spectra of a) SNNS-Br and b) SNNS-PMMA.

Bromide modified SNNS (SNNS-Br) used as initiator in polymer grafting process is seen in blue clour and PMMA grafted SNNS (PMMA//SNNS) in green clour in Figure 4.11. In the spectrum of PMMA//SNNS nanocomposite, the absorption at 1733 cm^{-1} indicates the carbonyl streching vibration of ester group on MMA unit. Likewise, the two absorptions at 1245 cm^{-1} and 1150 cm^{-1} designate the C-O-C streching vibrations of ester group. In addition, the absorption peaks at 1387 cm^{-1} and 741 cm^{-1} are corresponds to C-H bending vibrations of α-CH_3 of MMA. The absorption peak seen as low intensity at 1630 cm^{-1} is the carbonyl streching vibration of amide groups comes from SNNS-Br. Characteristic three absorption peaks of PMMA at around 1062 cm^{-1}, 989 cm^{-1} and 841 cm^{-1} could not seen in PMMA//SNNS spectra (Figure 4.11b) due to the overlapping with the characteristic two broad absorption peaks of silicon nitride at 950 cm^{-1} (Si-Ni-Si backbone vibration) and at 1039 cm^{-1} (Si-O-Si). In brief, the absorptions belonging to SNNS-Br and PMMA observed in green spectrum prove that these two structure combined chemically to form nanocomposite.

4.3.1.3 Thermal investigtion

The thermal degredations and thermal stabilities of PMMA//SNNS nanocomposite prepared by SI-ATRP and nanocomposite precursors were investigated by thermogravemetrical analaysis. TGA curves are shown in Figure 4.12.

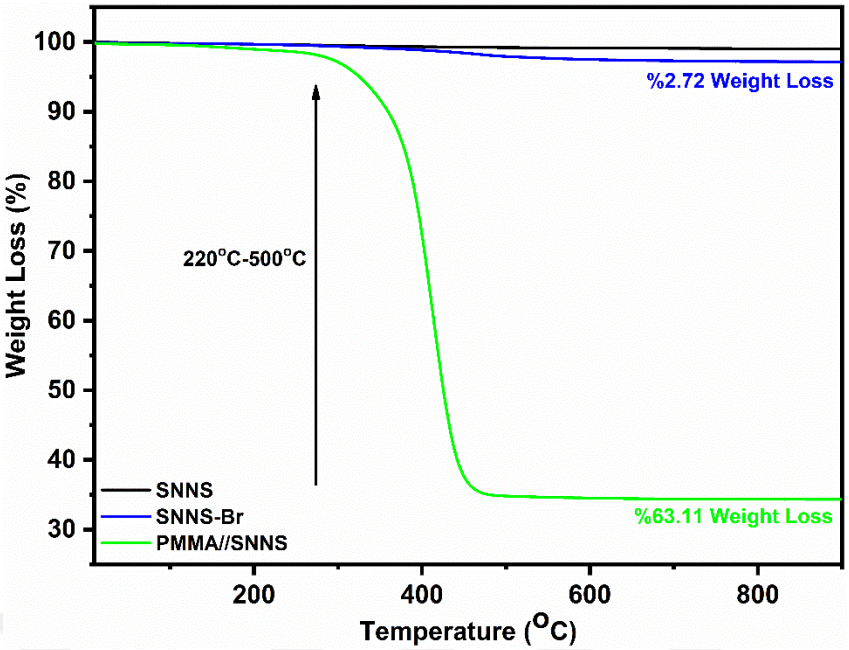

Figure 4.12 : TGA curves of SNNS, SNNS-Br and PMMA//SNNS.

As can be seen, all samples display some but tiny weight losses up to 200 °C. These degradations can be ascribed to physisorbed water and residual organic solvents. The principal degradations of samples started at about 220 °C. PMMA//SNNS shows 63.11% weight loss from 220 °C to 500 °C which is attributed to main-chain pyrolysis with 34.26% char yield, while SNNS-Br gives the weight loss of 2.72%. In literature, PMMA shows weight loss of 75.4% between 300 and 550 °C with about 1.1% char yield [377]. Thus, it can be concluded that about 12% of PMMA were grafted to SNNS-Br via SI-ATRP. Markedly, the char yield of PMMA//SNNS nanocomposite was increased with formation of chemical bond between SNNS-Br and PMMA compared to char yield given in the literature. It is clearly seen that the PMMA at a certain rate introduced to the SNNS structure, which another proof that the surface initiated polymerization of MMA from SNNS-Br surface via ATRP is a successful technique.

Thermal behavior and glass transition temperature of PMMA//SNNS nanocomposite synthesized via SI-ATRP was investigated by differential scanning calorimetry. The DSC trace is shown in Figure 4.13.

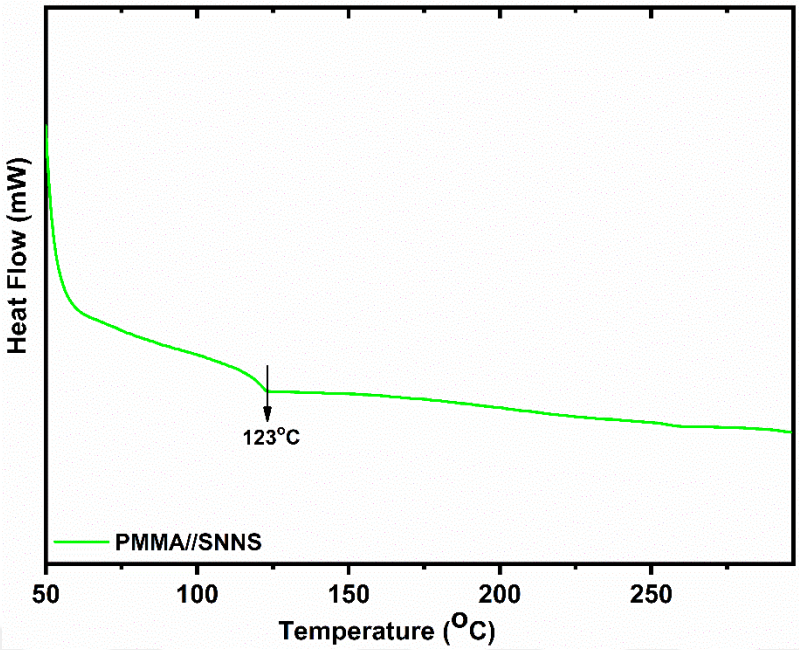

Figure 4.13 : DSC trace of PMMA//SNNS via SI-ATRP.

The T_g of polymers principally based on the trend in chain arrangement f the polymer, which determines the chain stiffness, inter- and intra- molecular interaction, side group effects and cross-link density [378]. It is seen that the T_g of PMMA//SNNS appears at 123 °C. According the literature [379], pristine PMMA has a T_g value at around 103 °C. The PMMA//SNNS nanocomposite having chemical bond between polymer matrix and filler shows approximately 20 °C higher glass transition temperature than pristine PMMA mentinoned in literature. This is the effect of thermally resistant inorganic filler reinforcement. Since, it derives from the reduced chain mobility regarding structural compatibility between the end groups and inner backbone by means of this effect. Apart from the interaction type between the precursors, the chain mobility was reduced leading to increase in T_g due to the restricted segmental motions between the organic-inorganic interfaces resulted from the incorporation of inorganic filler [380-382].

4.3.2 Preparation of poly(methyl methacrylate)/silicon nitride nanocomposites via CuACC click reaction (PMMA-SNNS)

In this section, alkyne-end functional poly(methyl methacrylate) PMMA-Alkyne with narrow molecular weight distribution synthesized via Atom Transfer Radical Polymerization (ATRP) was grafted to the azide modified SNNS (SNNS-N_3) via click chemistry method. This method based on the *"grafting to"* approach in this work,

allowing the scale up process in a quick and easy way as well as providing the end-product flexibility. Copper Catalyzed Azide-Alkyne (CuAAC) click chemistry, a highly adaptable tool, [358, 383] has been successfully utilized for a while in the fabrication of polymeric nanocomposites having high selectivity, reliability and functionality. It proposes high reaction yields at moderate conditions, tolerance to various organic solvents mediums and ease of working with precursors having desired side groups [376].

In the synthetic approach proposed in the work, in order to increase the interphase interactions between the polymer and the nanoparticle and to provide a homogeneous distribution of the nanofiller in the matrix, the grafting to method was implemented. Click chemistry was used as an essential tool to form covalent bond between the filler and matrix [384]. Silicon nitride (SN), which is supplied predominantly in beta phase, was converted into silicon nitride nanosheet (SNNS) morphology using mechanical exfoliation method. The surface of the prepared silicon nitride nanosheets (SNNSs) were modified by successive chemical modifications to obtain azide moiety. In the nanocomposite preparation, the azide functional SNNS (SNNS-N_3) was subjected to Copper Catalyzed Azide-Alkyne Click reaction (CuAAC) with alkyne-end functional poly(methyl methacrylate) (PMMA-Alkyne) in "click chemistry" approach and the nanocomposite was handled in different complex shapes and scaled (Figure 4.14).

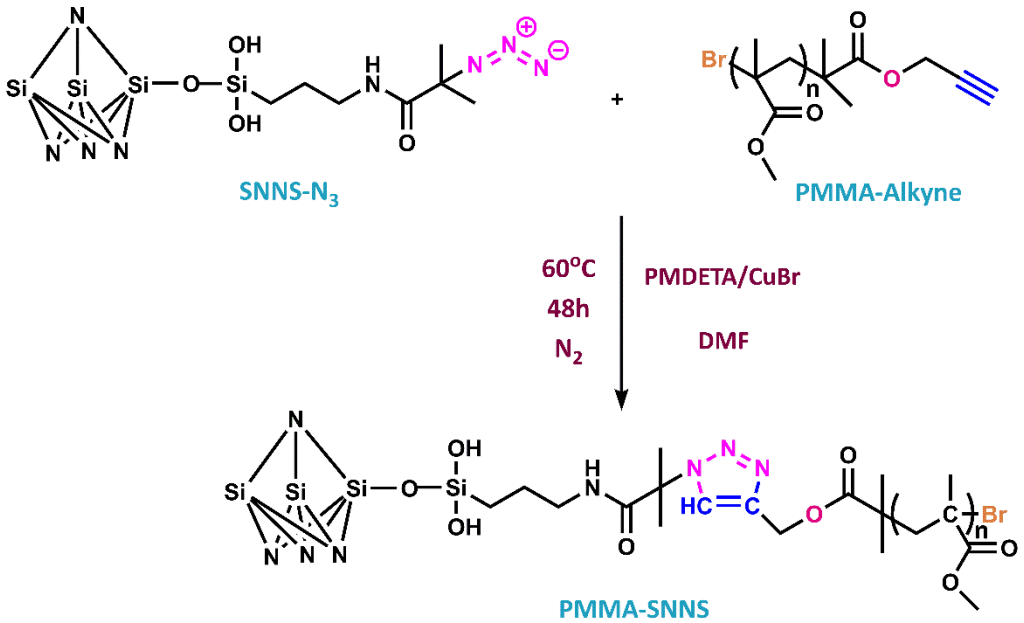

Figure 4.14 : The synthetic representation of PMMA-SNNS via CuAAc Click Reaction.

The experimental conditions and the properties of PMMA-Alkyne obtained by ATRP are given in Table 4.4. It summarizes the ω-end-functional polymerization results. The polymerization produced well-defined end-functional PMMA (PMMA-Alkyne) with targeted molar mass and extremely narrow polydispersity [351]. The PMMA-Alkyne has a molecular weight (M_n) of 120,600 g/mol with 54% yield. Moreover, the polydispersity is typical for controlled polymerization products [249].

Table 4.4 : Synthesis conditions and molecular weight characterization of PMMA-Alkyne.

Sample	DP_n[a]	Conversion[b] (%)	$M_{n,theo}$[c] (g/mol)	$M_{n,GPC}$[d] (g/mol)	$Đ$[d]	Yield (%)
PMMA-Alkyne	1000	65	65,000	120,600	1.17	54

[a] In DMF, $[M]_o/[I]_o/[CuBr]_o/[PMDETA]_o$ = 100:1:1:2.
[b] Determined by gravimetry.
[c] Calculated by using $M_{n,theo}$ = (($[M]_o/[I]_o$) × (%) Conversion × $M_{w,M}$ + $M_{w,I}$).
[d] Determined by GPC based on linear polystyrene standards.

The successful *click reaction* between PMMA-Alkyne as polymer matrix and SNNS-N_3 as thermal conductive nanofiller was confirmed completely by SEM, NMR, FTIR, TGA, DSC, DTC, ER and DMA analyzes.

4.3.2.1 Morphological investigation

The SEM images for pristine silicon nitride (SN), silicon nitride nanosheets (SNNSs), physical blend of SNNS and PMMA (PMMA+SNNS) and PMMA grafted silicon nitride nanosheets by click reaction (PMMA-SNNS) with 25 k magnification scales were given in Figure 4.15a, 4.15b, 4.15c and 4.15d, respectively.

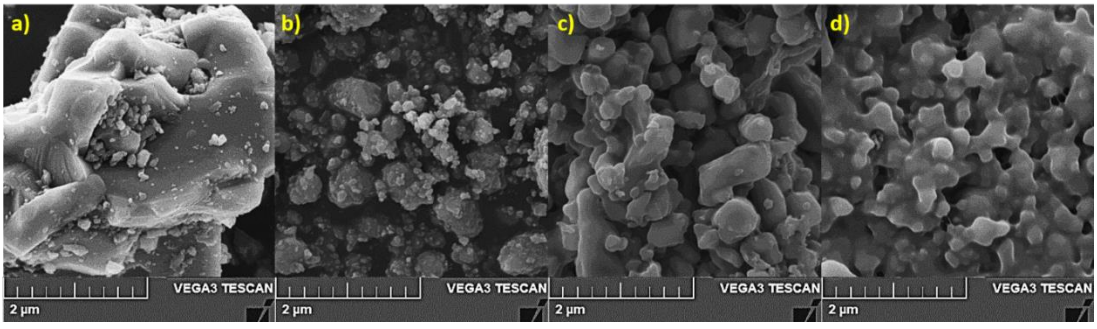

Figure 4.15 : SEM magnification images of a) SN, b) SNNS, c) PMMA+SNNS and d) PMMA-SNNS.

It is clearly seen that the SN appears as rod-shape crystals in bulk (Figure 4.15a). After subjecting to mechanic exfoliation with ball mill, the size of the SN particles reduced and these particles look more separated (Figure 4.15b). In addition, the crystal

structure was converted to spherical morphology due to shear force effect of the process [373, 374]. This result shows that the structure became suitable for facile chemical surface modifications. It is obviously seen that the polymer-introduced nanosheets appear larger than unmodified nanosheets under the same magnification. Figure 4.15c shows irregular and uneven distribution of the particles. SNNS particles are seen dispersed sporadically and agglomerated in the polymer matrix. However, Figure 4.15d displays a more regular and homogeneous distribution of the particles was seen. The complete surrounding of nanosheets by polymer network verifies that the PMMA-Alkyne was effectively grafted to the nanosheet surface and PMMA-SNNS particles emerge more unified and smaller size when compared to unmodified nanosheets due to the good dispersion in polymer matrix. This probably stems from the interface compatibility between nanofiller and polymer matrix due to the covalent bond formation [376].

4.3.2.2 Structural investigation

Alkyne-end functionalized PMMA (PMMA-Alkyne) synthesized by ATRP (Figure 3.3) was characterized by spectral analyzes.

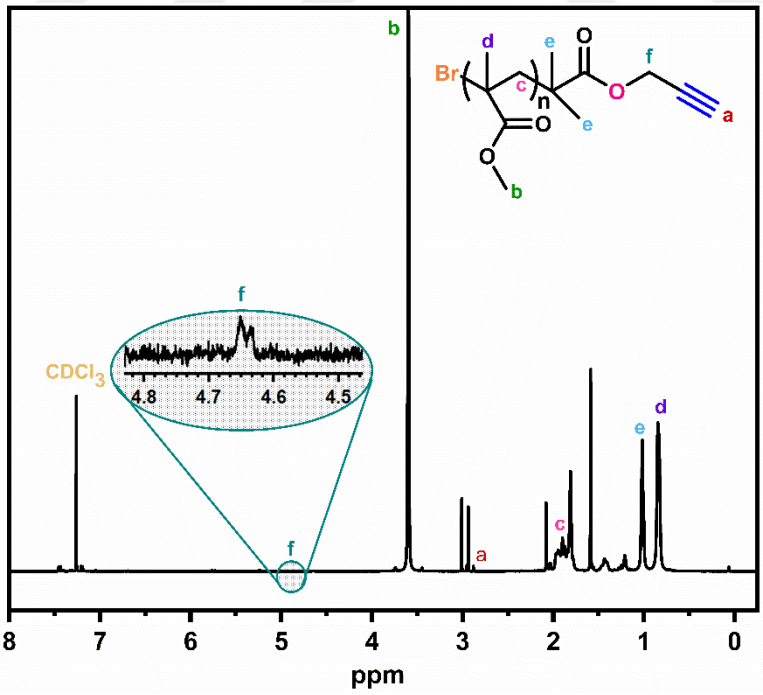

Figure 4.16 : ^{1}H-NMR spectra of PMMA-Alkyne.

Chemical structure of PMMA-Alkyne was confirmed by ^{1}H-NMR (Figure 4.16). The confirmation of alkyne functionality was ensured by the signal appeared at 2.88 ppm

(a, H) indicating the terminal alkyne proton and the signal at 4.66 (f, 2H) [351]. The absorption at 3.59 (b, 3H) is assigned to the α-terminal main-chain methoxy protons [385]. The sharp signal at 0.83 (d, 3H) and the broad signal at 1.90 (c, 3H) can be attributed to methyl protons and methylene protons of repeating unit of MMA, respectively [386].

Incorporation of SNNS to PMMA matrix was confirmed by FT-IR spectral analysis. The chemical structures of PMMA grafted SNNS nanocomposite (PMMA-SNNS) and its precursors, azide modified silicon nitride nanosheet (SNNS-N_3) and alkyne-end functional PMMA (PMMA-Alkyne), were identified by their characteristic vibrations in detail in Figure 4.17.

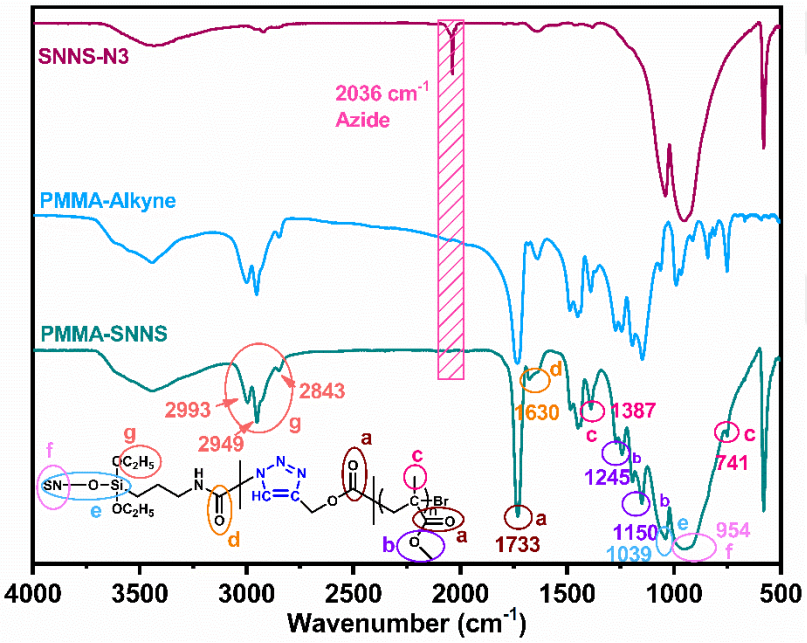

Figure 4.17 : FTIR spectra of SNNS-N_3, PMMA-Alkyne and PMMA-SNNS.

The backbone vibration of Si-N-Si and bending vibration of Si-O-Si are visible at 954 cm^{-1} and 1039 cm^{-1} respectively [207, 387]. Besides, broad absorption peak around 3440 cm^{-1} was assigned to the hydroxyl stretching vibrations due to -OH groups on the surface of SNNS-N_3 and residual solvent in PMMA-Alkyne [309, 388]. Also, the absorption peaks at 2993 cm^{-1}, 2949 cm^{-1} and 2843 cm^{-1} were assigned to symmetric and asymmetric C-H stretching vibrations of the $–CH_3$ group and C-H stretching vibration of the $–CH_2–$ group, respectively coming from SNNS-N_3 and PMMA-Alkyne [389]. In the spectrum of PMMA-SNNS nanocomposite, the absorption at 1733 cm^{-1} indicates the carbonyl stretching vibration of ester group on MMA repeating

unit. Likewise, the two absorptions at 1245 cm^{-1} and 1150 cm^{-1} are C-O-C stretching vibrations of ester group. Moreover, the absorptions at 1387 cm^{-1} and 741 cm^{-1} are corresponds to C-H bending vibrations of α-CH_3 of MMA [390, 391]. The weak band with low intensity at 1630 cm^{-1} is the carbonyl stretching vibration of amide groups which stems from SNNS-N_3 [207, 376]. Furthermore, characteristic three absorption peaks of PMMA at around 1062 cm^{-1}, 989 cm^{-1} and 841 cm^{-1} overlap with the characteristic broad absorption bands of silicon nitride and are therefore not visible. The distinct absorption peak of the azide group at 2036 cm^{-1} disappeared in PMMA-SNNS spectrum and all characteristic vibrations of PMMA appeared, which indicates the click reaction between azide-functional SNNS and alkyne-functional PMMA was successful [392].

4.3.2.3 Thermal investigation

Thermal stability of nanocomposite by physical blend (PMMA+SNNS), nanocomposite by click reaction (PMMA-SNNS) and their precursors (SNNS-N_3 and PMMA-Alkyne) are explored by TGA under N_2 atmosphere. TGA curves are shown in figure 4.18 and results are tabulated in Table 4.5.

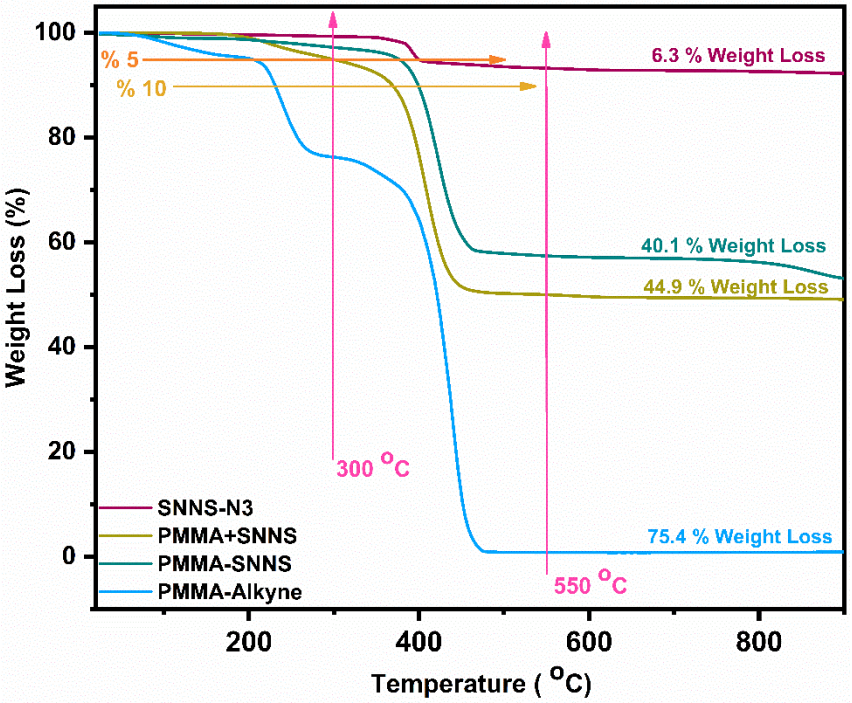

Figure 4.18 : TGA curves of SNNS-N_3, PMMA-Alkyne, PMMA-SNNS and PMMA+SNNS.

The weight losses below 200 °C can be attributed to physisorbed water and residual organic solvent [393]. It is observed that PMMA-Alkyne shows weight loss of 75.4% between 300 and 550 °C which is attributed to main-chain pyrolysis with 1.1% char yield [376, 394, 395]. By the addition of thermally resistant SNNS-N_3, which has a weight loss of 6.3% between 300-550 °C with 92.3% char yield, to the structure, thermal stability and thermal decomposition temperatures of materials increased while its char yield decreased. As expected, the weight losses of nanocomposites are at the intermediate value those of the components forming the composite. Nanocomposite structures demonstrate higher thermal stability than pristine PMMA-Alkyne owing to enhanced inorganic content of the materials. In addition, they do not show significant weight loss before 300 °C according to PMMA-Alkyne. Among silicon nitride added PMMA nanocomposites, PMMA-SNNS nanocomposite by click reaction exhibited the lowest weight loss with 40.1% between 300 and 550 °C and the highest thermal stability and char yield at 900 °C due to the interface compatibility between nanofiller and polymer matrix [396, 397]. This phenomenon might be stem from the formed 3-dimensional crosslink structures between the nanofiller and polymer matrix through click reaction [376].

Table 4.5 : Thermogravimetric properties of PMMA nanocomposites and their precursors.

Samples	T_5% (°C)	T_{10}% (°C)	Y_c (%)
SNNS-N_3	398	-	92
PMMA-Alkyne	202	232	1
PMMA+SNNS	299	370	51
PMMA-SNNS	380	398	53

T_5%: The temperature for which the weight loss is 5%.
T_{10}%: The temperature for which the weight loss is 10%.
Y*c*: Char yields at 900 °C under nitrogen atmosphere.

Thermal behavior and glass transition temperatures of pristine PMMA-Alkyne, PMMA-SNNS and PMMA+SNNS were investigated by differential scanning calorimetry. DSC traces are shown in Figure 4.19.

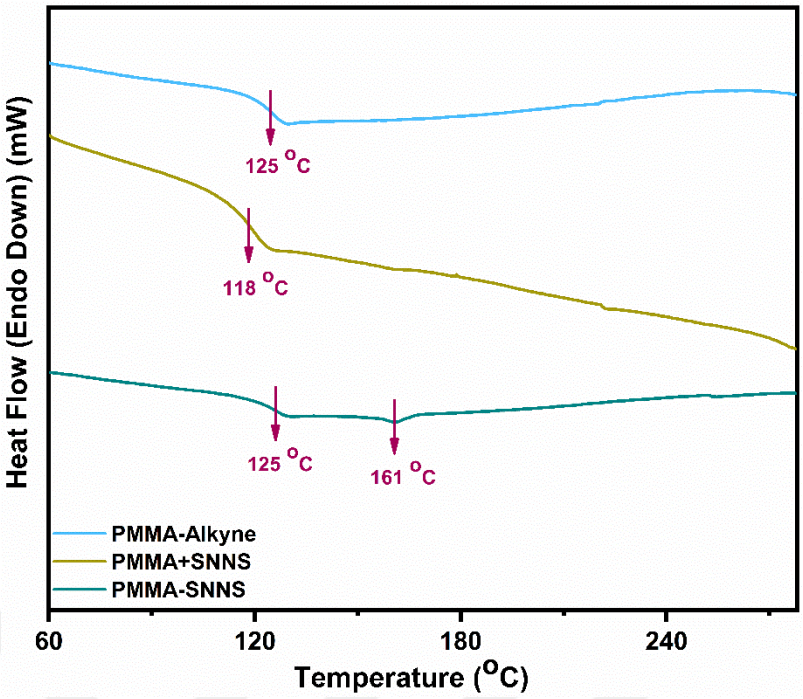

Figure 4.19 : DSC traces of PMMA-Alkyne, PMMA+SNNS and PMMA-SNNS.

It is clearly seen that the glass transition temperature of PMMA-Alkyne appeared at 125 °C. After incorporation of SNNS physically, the glass transition temperature slightly decreased to 118 °C due to the self-aggregation of nanofiler, which causes the polymer chains detract from each other and so leads more vacancies in polymer matrix. Thus, the transition from glassy state to rubbery state occurred at the temperature lower than the pristine PMMA-Alkyne [398, 399]. PMMA-SNNS nanocomposite having chemical bond between polymer and filler shows the highest T_g. In addition, it is seen there are two T_g values in PMMA-SNNS trace [400]. The T_g appeared at 125 °C comes from the pristine PMMA-Alkyne that remained intact during the click reaction. The other T_g of PMMA-SNNS nanocomposite is seen at 161 °C that 26 °C higher than that of its precursor due to the reduced chain mobility regarding structural compatibility between the end groups and the inner backbone [401, 402]. This phenomenon reveals the effect of interaction type of precursors on the thermal behavior of nanocomposite. Apart from the interaction type between the precursors, the chain mobility was reduced leading to increase in T_g due to the restricted polymer network resulted from the incorporation of inorganic filler [380]. However, transition to rubbery state for PMMA-SNNS nanocomposite occurred at higher degrees despite the fact that same amount of nanofiller was used. Consequently, regardless of filler concentration in nanocomposite, filler-matrix interaction would be the case [109, 403].

4.3.2.4 Thermal conductivity and electrical resistance investigation

The thermal resistivity, thermal conductivity and electrical resistivity (Volume Resistivity) analysis of pristine PMMA-Alkyne and nanocomposites by physical blend and click reaction are summarized in Table 4.6, thermal conductivity comparisons of those three samples are demonstrated in Figure 4.20 and thermal and electrical resistivity changes are shown in Figure 4.21.

Table 4.6 : Conductivity and resistivity results of PMMA-Alkyne and nanocomposites.

Samples	Thermal Resistivity (m^2KW^{-1})	Thermal Conductivity ($Wm^{-1}K^{-1}$)	Volume Resistivity (Ω.cm)
	ASTM D5470	ASTM D5470	ASTM D257
PMMA-Alkyne	0.0062	0.072	$6.22e^{12}$
PMMA+SNNS	0.0059	0.103	$3.11e^{13}$
PMMA-SNNS	0.0033	0.255	$2.54e^{14}$

The conductivities were measured according to the ASTM D5470 standard, which operates on a guarded heat flow principle [404]. This device has two temperature-controlled surfaces, after a certain pressure and temperature is applied to the material placed between these two metal surfaces, the device starts to collect thermal resistivity data. Thermal conductivity analysis in through-plane direction were carried out at working temperature of 25 °C and under 25 Psi pressure. The thermal conductivity shows an increase of 43.5% for the nanocomposite derived via physical blending and an increase of 255% for the nanocomposite derived via click reaction when compared to the pristine PMMA-Alkyne. Considering that the filler content in both nanocomposite samples is with 36 wt% the same, the distinct increase of thermal conductivity in the click reaction derived sample is remarkable. These increments can be seen explicitly in Figure 4.20. It can be concluded that the thermal resistance at filler-matrix interface was reduced by means of chemical interaction in PMMA-SNNS nanocomposite [12, 405, 406].

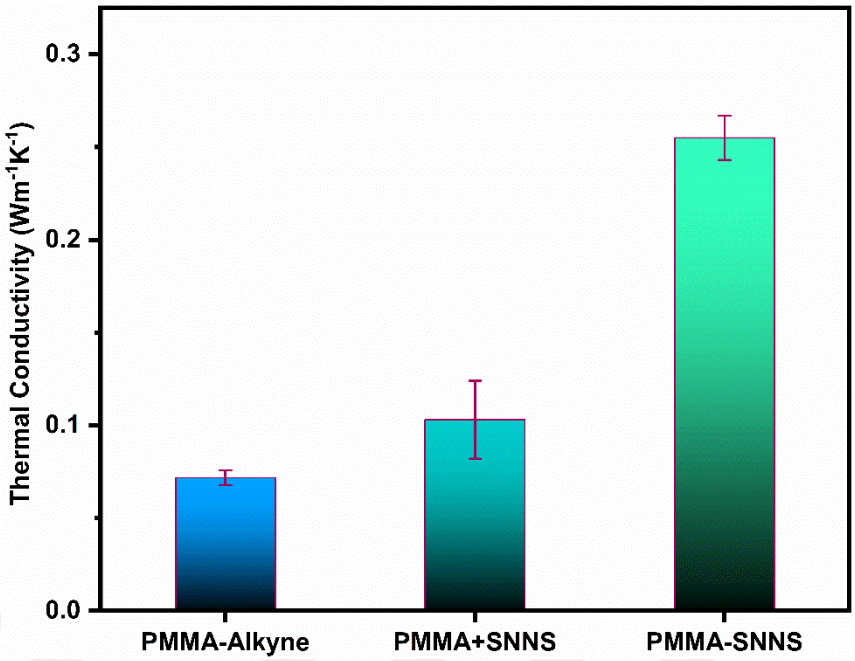

Figure 4.20 : Thermal conductivity comparisons of PMMA-Alkyne, PMMA+SNNS and PMMA-SNNS.

Electrical resistance results are as high as expected. As clearly seen in Figure 4.21, the electrical volume resistance values increased inversely proportional to the decreasing thermal resistance with the incorporation of silicon nitride nanosheets due to their high electrical insulating characteristics. However, the PMMA-SNNS nanocomposite showed the volume resistivity of 2.54 x 10^{14} Ω.cm, which is higher than that of the PMMA+SNNS nanocomposite (3.11 x 10^{13} Ω.cm) with the same SNNS ratio. This difference was probably stems from the chemical interaction in PMMA-SNNS nanocomposite, which leads to homogenous distribution of SNNS in polymer matrix. It can also be said that the lack of strong interaction in the PMMA+SNNS nanocomposite has an effect on this result [407].

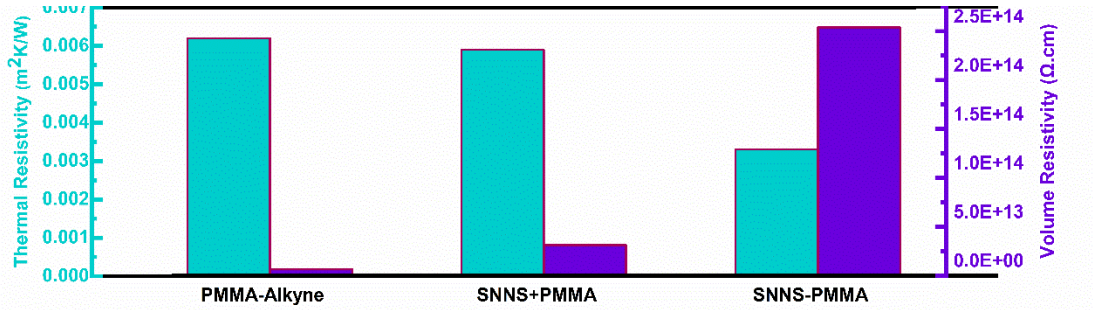

Figure 4.21 : Thermal and electrical resistivity comparisons of PMMA-Alkyne, PMMA+SNNS and PMMA-SNNS.

4.3.2.5 Mechanical investigation

Mechanical behavior of all samples were investigated by dynamic mechanical analysis. DMA curves are shown below.

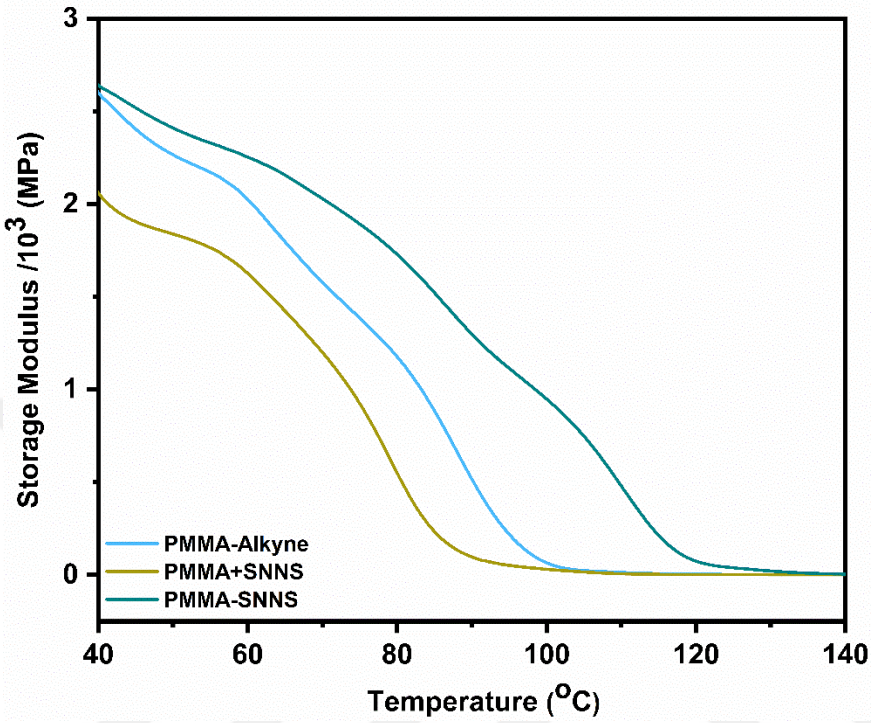

Figure 4.22 : Storage modulus (*E'*) curves of PMMA-Alkyne, PMMA+SNNS and PMMA-SNNS.

The curves of storage modulus (*E'*) versus temperature of PMMA-Alkyne film and nanocomposite films, obtained from DMA at 1 Hz, are demonstrated in Figure 4.22. The dynamic storage modulus is related to elastic modulus evaluated in the concept of load carrying capability or as a stiffness of a material. Furthermore, *E'* depends on the temperature, the filler content and the interaction type between the filler and matrix. In general, the introduction of the filler to polymer matrix increases the stiffness, so the elastic modulus of the material [408]. In the same manner, the storage modulus of nanocomposite enhances with the filler content up to some extent [409]. In the same manner, the storage modulus of nanocomposite enhances with the filler content up to some extent [94]. In this work, the ratio of silicon nitride nanofiller was 60 wt% for both nanocomposite. It is seen that *E'* values for physically blended nanocomposite (PMMA+SNNS) film at any temperature is lesser than that of pristine PMMA-Alkyne film. The reduction of *E'* values in PMMA+SNNS are principally due to the self-aggregation of nanofillers which leads the extra free volumes in polymer chains [410].

Evidently, such a high filler loading results in decreased of the PMMA+SNNS nanocomposite film as shown in Figure 4.23.

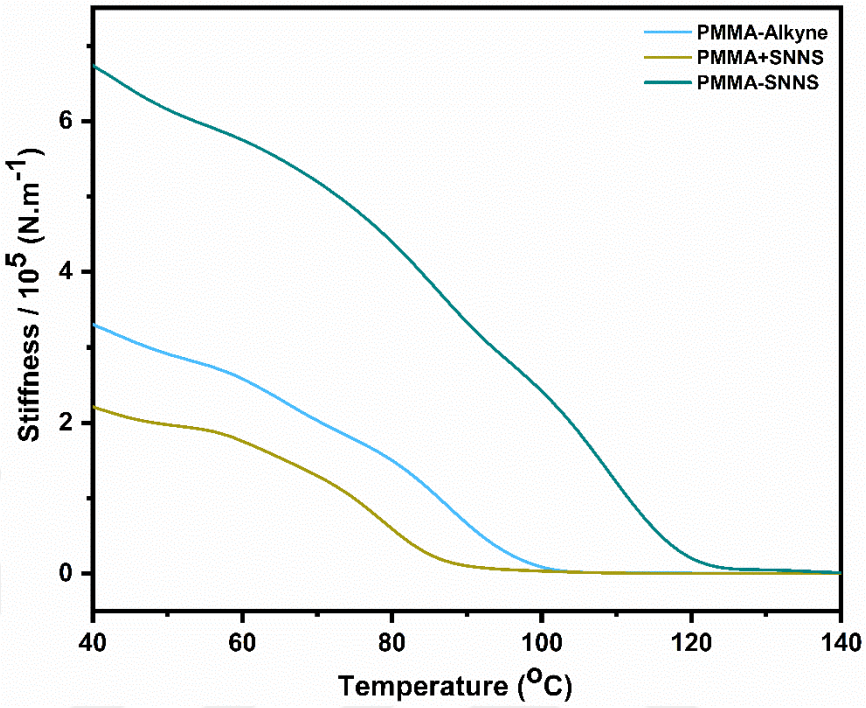

Figure 4.23 : Stiffness curves of PMMA-Alkyne, PMMA+SNNS and PMMA-SNNS.

However, it is obviously seen that the storage modulus values of PMMA-SNNS are much higher than PMMA-Alkyne and PMMA+SNNS as well. The PMMA-SNNS curve displays an enhanced storage modulus values in all region compared to the pristine PMMA-Alkyne. Since, the covalent bond between the modified SNNS and PMMA-Alkyne had an enhancing effect on the stiffness of the material, although as the same nanofiller ratio was used as in the physical blend (Figure 4.23). It is worth to say that the good interfacial compatibility between polymer and nanofiller is responsible for the restriction of the molecular mobility of the polymer matrix, which is featured of this trend [411]. Furthermore, the chemical incorporation of SNNS to PMMA-Alkyne could lead the formation of chemical cross-linking, which increases the stiffness of the material, thus SNNS act as a reinforcing agent for PMMA-SNNS nanocomposite by taking the advantage of chemical interaction [412].

The loss modulus (*E"*) values as a function of temperature of pristine PMMA-Alkyne film and nanocomposite films, obtained from DMA at a frequency of 1 Hz are demonstrated in Figure 4.24.

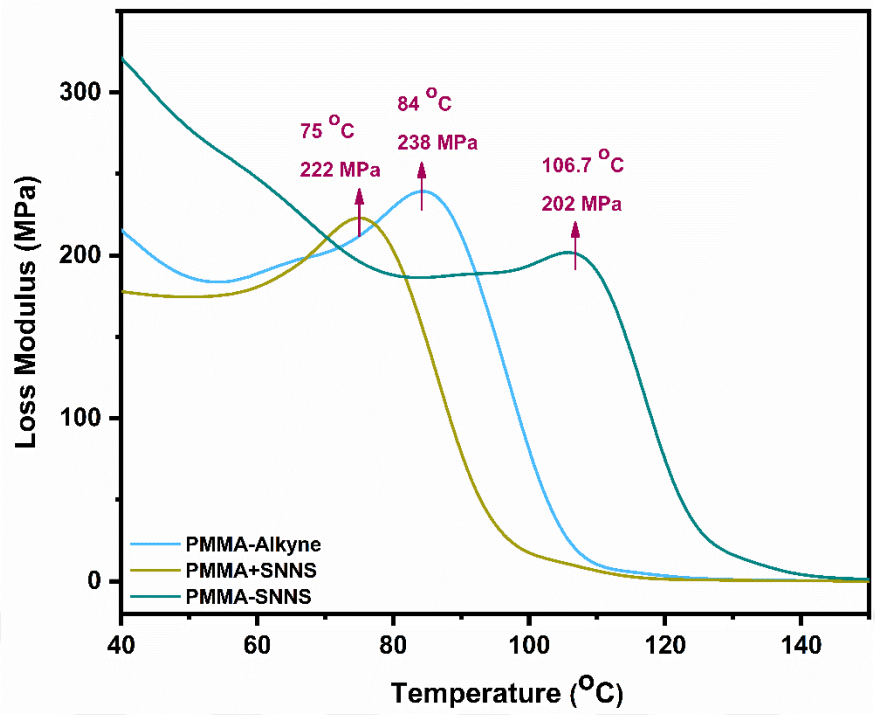

Figure 4.24 : Loss modulus curves of PMMA-Alkyne, PMMA+SNNS and PMMA-SNNS.

E" is related to viscous property of a material, which gives responses as a dissipated energy due to motions of polymer chains. PMMA+SNNS nanocomposite including 60 wt% nanofiller displayed negative shift compared to pristine PMMA-Alkyne. This behavior can be attributed to the incompatible filler-matrix interaction arises from self-agglomeration of the high content SNNSs and lack of chemical interaction [413]. Though, the loss modulus of PMMA-SNNS containing same content of nanofiller as physically blended nanocomposite at any temperature range showed increased values than that of pristine PMMA-Alkyne and PMMA+SNNS nanocomposite due to the compatibility between filler and matrix through covalent bond. Besides interfacial compatibility, chain mobility restriction and 3-dimensional network structure could have been occurred due to the well-dispersion of nanofiller in polymer matrix [409]. This result reveals that the SNNS acts as a reinforcing material for the nanocomposite containing covalent bond.

Tan δ curves of pristine PMMA-Alkyne film and nanocomposite films are presented as a function of temperature in Figure 4.25.

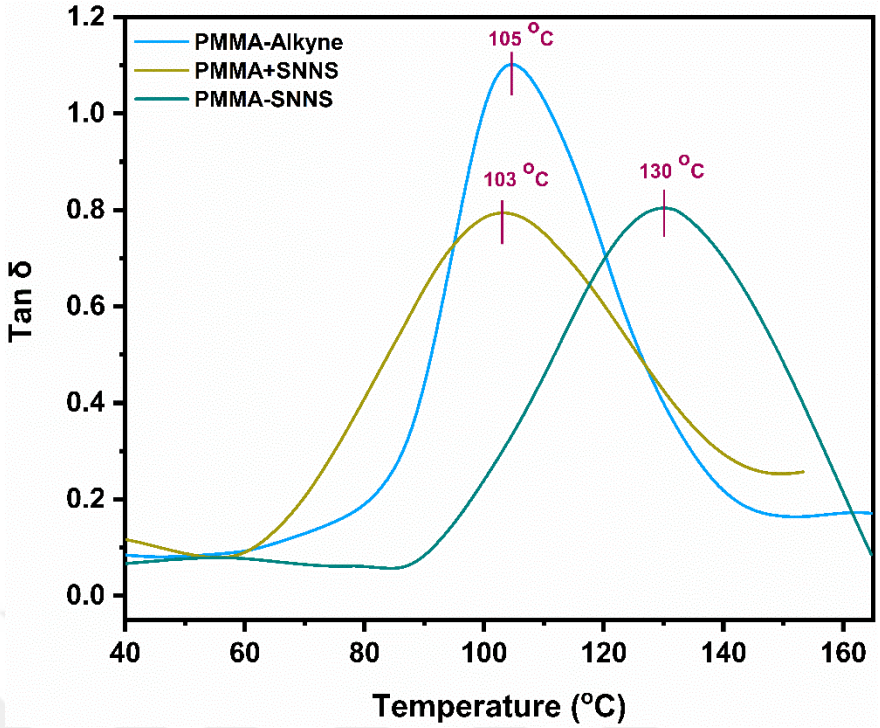

Figure 4.25 : Tan δ curves of PMMA-Alkyne, PMMA+SNNS and PMMA-SNNS.

Tan δ is known as loss factor, damping factor or dissipation factor, defined as the ratio of the loss modulus to storage modulus (*E"/E'*). It provides an information regarding the mechanical behavior whether the material elastic or viscous [414]. The glass transition temperature of a material is associated with the main α-relaxation, corresponding the peak maximum in tan δ curve [413]. It is clearly seen that the tan δ values (peak heights) of nanocomposites diminished, whereas their peak widths enhanced. The decreases in peak heights are directly linked with the elastic character of the film, suggesting the degradation of molecular mobility of PMMA-Alkyne by means of incorporation of SNNS [415]. The broadening of peaks is related to loosening of polymer chains, indicating the segmental constrains of polymer chains to some extent, which are consistent with the loss modulus values (*E"*) [414]. The T_g value of PMMA+SNNS shifted to lower temperature in respect to pristine PMMA-Alkyne. This result can be attributed to nanofiller agglomeration deteriorating the filler-matrix interaction under high filler loading [416]. Contrarily, PMMA-SNNS curve shows the increased T_g at 130 ˚C, implying the better interface compatibility between the nanofiller and polymer matrix due to the formed covalent bond and probable chemical cross-linking, which restrains the chain mobility of the polymer [412, 417]. Consequently, the mechanical transitions of pristine polymer and nanocomposites are consistent with the DSC results as well.

The nanocomposites obtained in two different ways as physical blend and chemical modification and prepared in thermal interface material (TIM) formulation are shown in Figure 4.26.

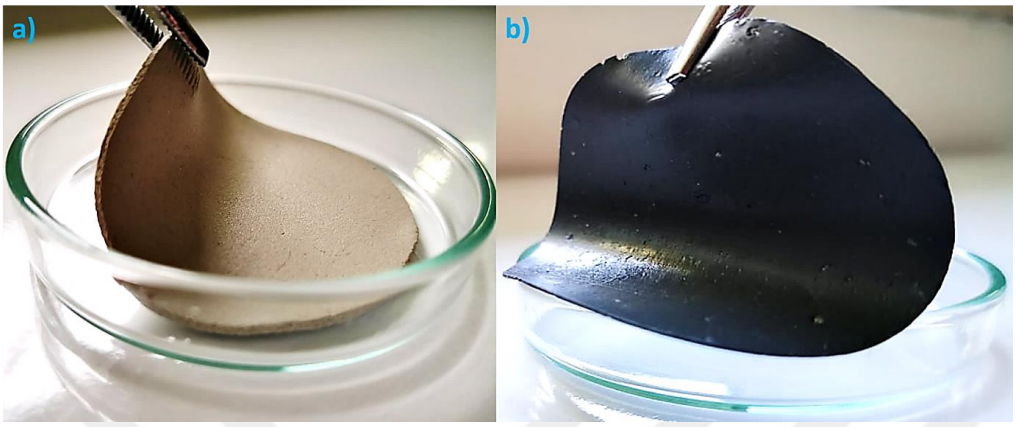

Figure 4.26 : Pad forms of a) PMMA+SNNS and b) PMMA-SNNS.

These nanocomposites in TIM formulation were fabricated in pad form and thermal conductivity and electrical resistance measurements were carried out. To prepare in this form, the finished powder products were blended with hydroxyl-end functional PDMS with 50,000 g/mol supplied by Sigma-Aldrich. PMMA-SNNS seem dark in color due to the various chemicals and catalyst effects used in the chemical processes. Besides, due to the introducing chemical interaction between the nanofiller and the polymer matrix, both the processability with PDMS and the homogeneity of the resulting pad form of PMMA-SNNS was much better than the PMMA+SNNS pad. It was also observed that the PMMA+SNNS nanocomposite has heterogeneous and dispersible structure, while PMMA-SNNS shows more stacked and more flexible structure.

4.3.3 Preparation of polysulfone/silicon nitride nanocomposites via CuAAC click reaction (PSU-SNNS)

In order to prepare the nanocomposite with polysulfone matrix (PSU-SNNS), the two-step synthesis procedure of polysulfone was performed so that give a click reaction with azide functional SNNS (SNNS-N_3) prepared in the chemical modification process. The first stage of the synthesis procedure involves polysulfone synthesis with hydroxyl end-groups with three different molecular weights by condensation polymerization (PSU-OH), followed by conversion of these end-groups to alkyne function (PSU-Alkyne) to be used in Copper Catalyzed Azide-Alkyne Click reaction

(CuAAc). The PSU-OH (PSU-OH-9000) that give the best thermal behavior was used the main PSU matrix in the nanocomposite preparation. The effect of functionalization type and molecular weight of polymer on the thermal behavior of nanocomposite was investigated by characterization studies. Furthermore, the characterization results of the nanocomposite obtained by both physical mixture and click chemistry were examined. The differences between these two methods were reported in detail. The schematic representations of the modification process and the nanocomposite synthesis are shown in Figure 4.27 and Figure 4.28.

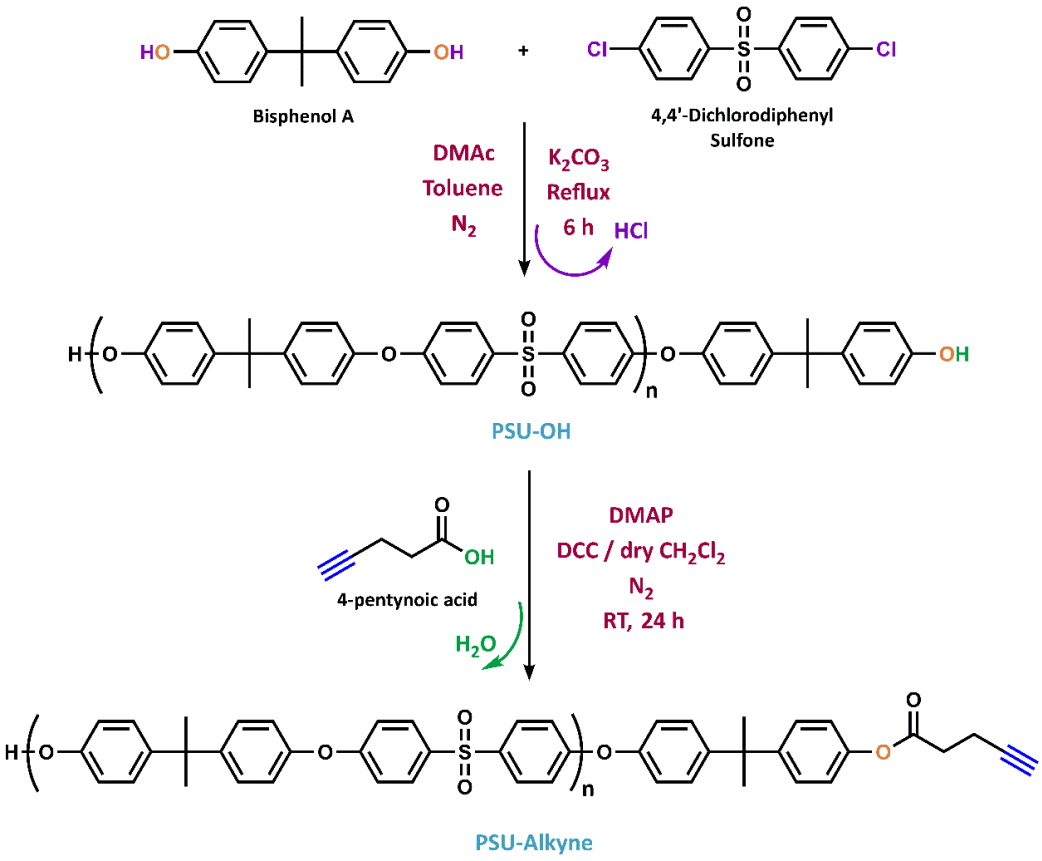

Figure 4.27 : The synthesis route of PSU-Alkyne by polycondensation.

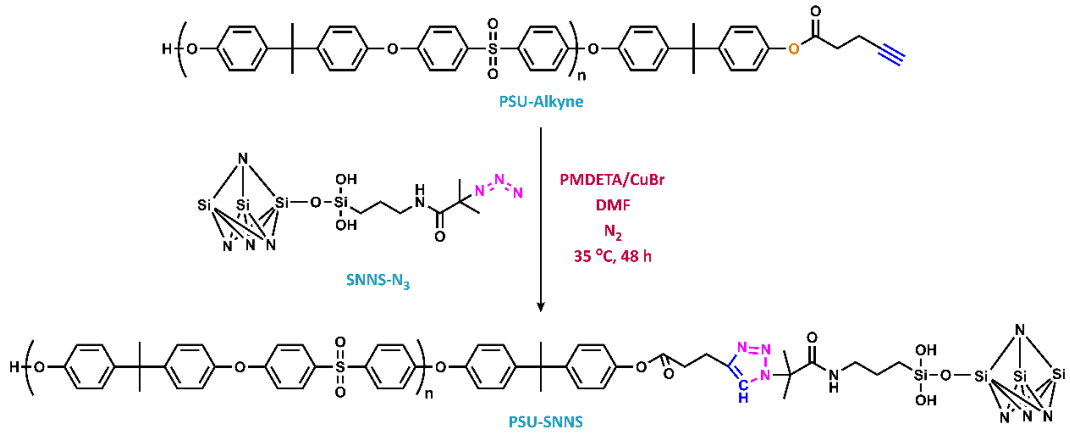

Figure 4.28 : The synthesis of PSU-SNNS nanocomposite via click reaction.

The experimental conditions and the properties of PSU-OH obtained by polycondensation and PSU-Alkyne obtained by end-functionalization reaction are tabulated in Table 4.7 and depicted in Figure 4.29.

Table 4.7 : Synthesis[a] conditions and molecular weight characteristics of hydroxyl and alkyne end-functional polysulfones.

Polymer	[BisphenolA/Chlorosulfone (mol/mol)	Yield[b] (%)	M_n[c] (g/mol)	$Đ$
PSU-OH-2000	2.0	82	2050	1.24
PSU-OH-4000	1.2	66	4200	1.70
PSU-OH-9000	1.05	79	9300	1.60
PSU-Alkyne-2000	-	65	2300	1.21
PSU-Alkyne-4000	-	88	4600	1.64
PSU-Alkyne-9000	-	66	9500	1.60

[a] Reaction temperature: 180 – 200 °C, time: 6 h.
[b] Determined gravimetrically.
[c] Determined from GPC measurements based on polystyrene standards.

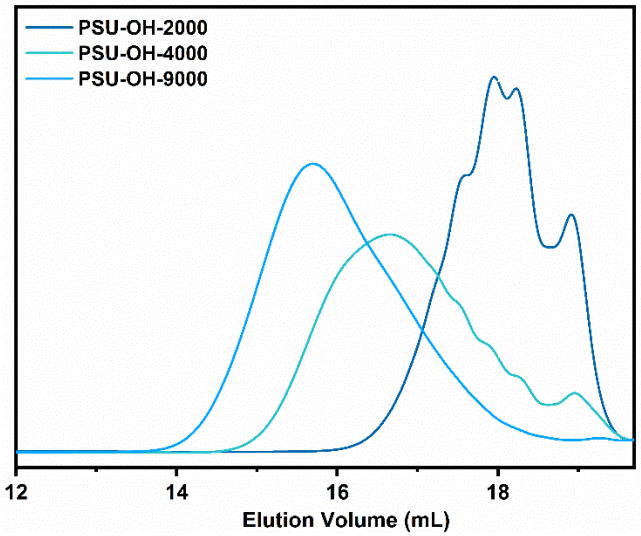

Figure 4.29 : GPC traces of PSU-OH-2000, PSU-OH-4000 and PSU-OH-9000.

Hydroxyl functional polysulfones with three different molecular weights (2000, 4000, 9000 g/mol) were sytnhesized. It is clearly seen that the M_n values of each polysulfones increased slightly after alkynation reaction. Moreover, the polydispersity values and GPC traces of polysulfone are typical for condensation polymerization products.

The differences in thermal stabilities of polysulfones were investigated by thermogravemetrical analysis. The results are shown in Figure 4.30 and details are tabulated in Table 4.8.

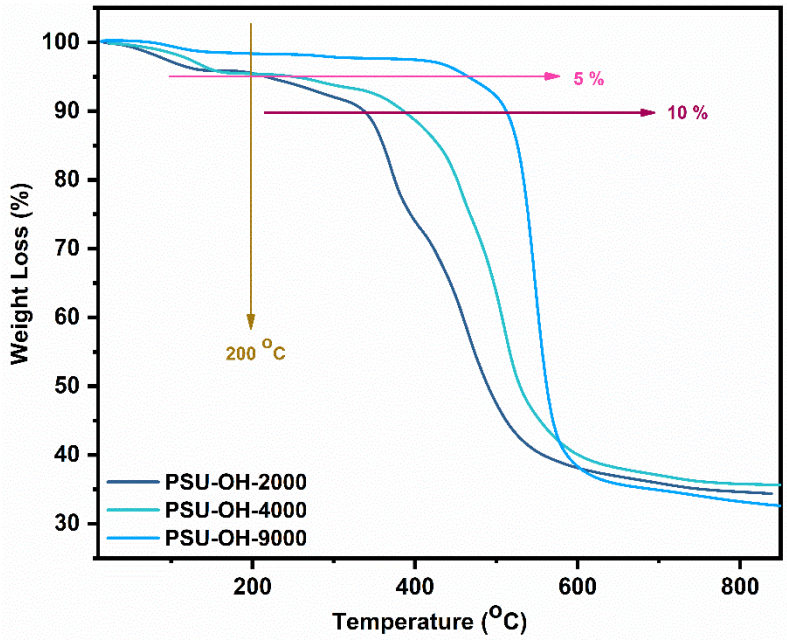

Figure 4.30 : TGA curves of PSU-OH-2000, PSU-OH-4000 and PSU-OH-9000.

The weight losses below 200 °C can be attributed to physisorbed water and residual organic solvent. It is clear that PSU-OH-9000 shows the best thermal stability when compared to polysulfones with lower molecular weight. Also, it has a weight loss of 65.7 % between 200-850 °C that can be attributed to main-chain pyrolysis with 32.5 % char yield. As expected, high molecular weight polysulfones display higher thermal stabilities, while the amount of decomposition is much greater in polysulfones with low molecular weight than high molecular weight. This is owing to chain entanglement observable typically in higher molecular weight oligomers that lead thermal stability enhancement. Among low molecular weight polysulfones, PSU-OH-4000 exhibited the onset of decomposition temperature at 335 °C with the char yield of 35.6 %, while PSU-OH-2000 starts to decompose at 300 °C the lowest temperature among other decompostion temperatures with the char yield of 34.3 %. This phenomenon can be derived from the restriction of chain mobility due to the increased molecular weight. Moreover, PSU-OH-9000 exhibited the highest degradation temperatures of T_5% and T_{10}% at 463 °C and 512 °C, respectively. Conversely, the degradation temperatures of T_5% and T_{10}% for PSU-OH-2000 and PSU-OH-4000, the lower temperatures, such that 217, 252 °C and 338, 384 °C, respectively.

Table 4.8 : Thermogravemetric properties of polysulfones.

Polysulfone	T_5% (°C)	T_{10}% (°C)	$T_{d(\text{onset})}$ (°C)	$T_{d(\text{offset})}$ (°C)	Y_c (%)
PSU-OH-2000	217	338	416	850	34.3
PSU-OH-4000	252	384	335	772	35.6
PSU-OH-9000	464	512	300	770	32.5

The effect of the molecular weight of PSU-OH on glass transition temperatures was investigated by DSC analysis in Figure 4.31.

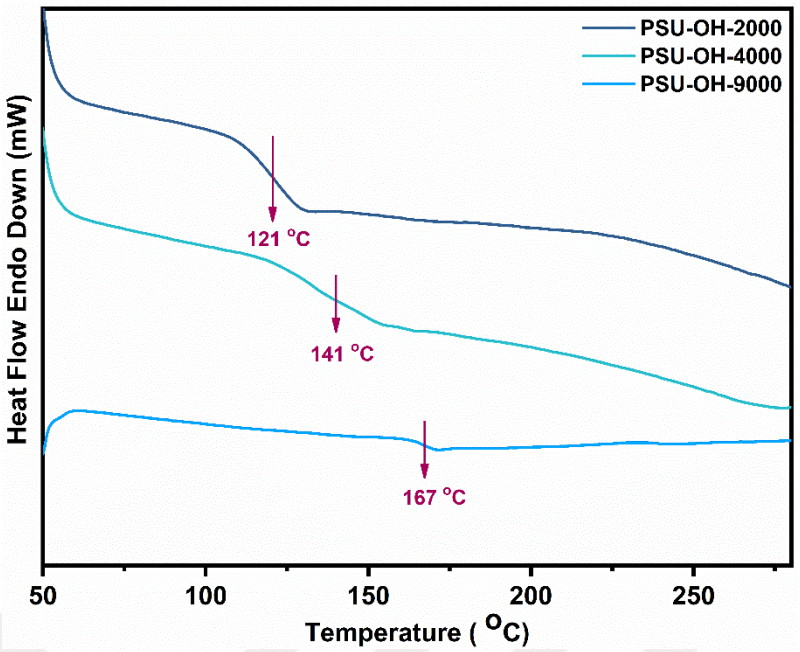

Figure 4.31 : DSC traces of PSU-OH-2000, PSU-OH-4000 and PSU-OH-9000.

While the T_g of PSU-OH-2000 appeared at 121 °C, as molecular wieght increase, the T_g values of polysulfones were detected at higher temperatures, such as 141 °C for PSU-OH-4000 and 167 °C for PSU-OH-9000. This change leads to decrease in chain-end concentration followed by reducing in free volume at end-group site and increment in T_g.

4.3.3.1 Morphological investigation

The SEM images for silicon nitride nanosheets (SNNS), pristine PSU-Alkyne, physical blend of SNNS and PSU (PSU+SNNS) and PSU grafted silicon nitride nanosheets by click reaction (PSU-SNNS) with 15k magnification scales were given in Figure 4.32a, 4.32b, 4.32c and 4.32d, respectively.

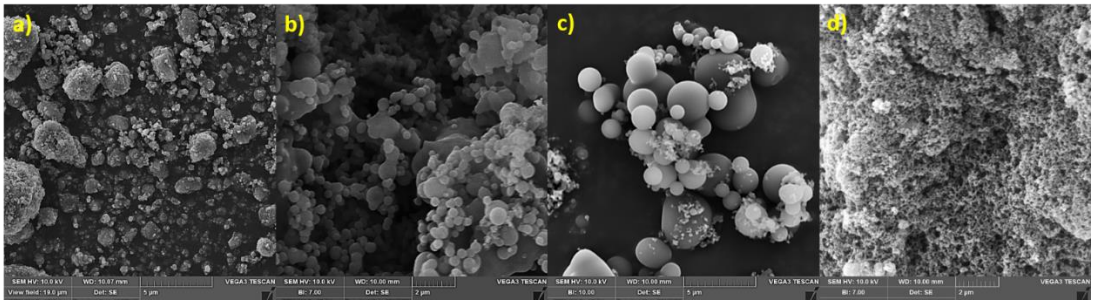

Figure 4.32 : SEM magnification images of a) SNNS, b) PSU-Alkyne, c) SNNS+PSU and d) SNNS-PSU.

Both SNNS (Figure 4.32a) and PSU-Alkyne (Figure 4.32b) seem in granular structure; SNNS particles are more crystal-like and smaller in size, while PSU-Alkyne displays more spherical morphology and larger in size as seen in conventional oligomer structures. It is obviously seen that the polymer-introduced nanosheets appear larger than unmodified nanosheets under the same magnification. Figure 4.32c shows irregular and uneven distribution of the particles. SNNS particles are seen dispersed sporadically and agglomerated in the polymer matrix. However, Figure 4.32d displays a more regular and homogeneous distribution of the particles. The complete surrounding of nanosheets by polymer network verifies that the PSU-Alkyne was effectively grafted to the nanosheet surface and PSU-SNNS particles emerge more unified and smaller size when compared to unmodified nanosheets due to the good dispersion in polymer matrix. It probably stems from the interface compatibility between nanofiller and polymer matrix owing to covalent bond formation [418, 419].

4.3.3.2 Structural investigation

Hydroxyl-terminated PSU (PSU-OH) and alkyne-end functionalized PSU (PSU-Alkyne) were identified by spectral analyzes. Chemical structures of PSU-OH and PSU-Alkyne were investigated by ^{1}H-NMR. The convertion from hydroxyl-end functionality to alkyne-end functionality was also confirmed by ^{1}H-NMR analyzes and presented in Figure 4.33.

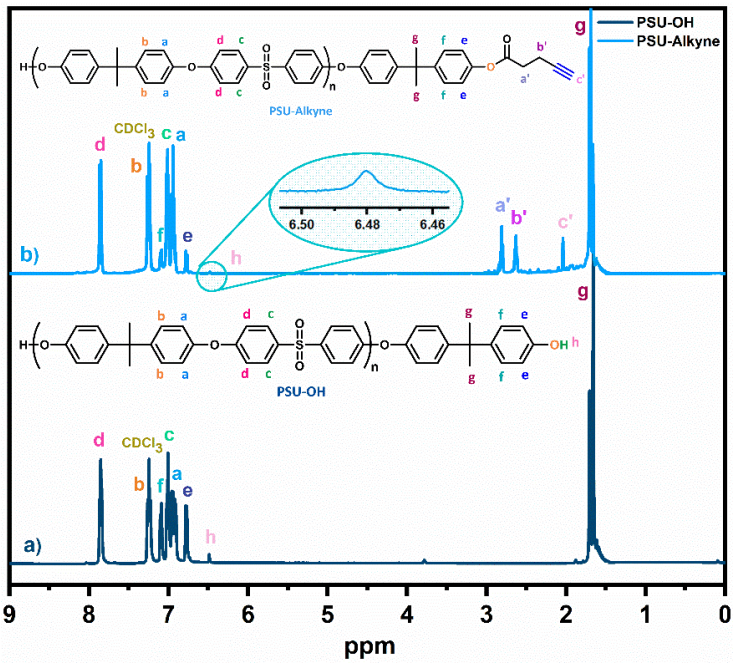

Figure 4.33 : ^{1}H-NMR spectra of a) PSU-OH and b) PSU-Alkyne in $CDCl_3$.

Absorptions corresponding to the methyl protons of BPA and aromatic protons of the PSU main-chain seem in both spectra at 1.65 (g, 6H, *s*) and in the range of 6.78 - 7.85 ppm (d, b, f, c, a, e; 12H; *d*), respectively [353, 420]. The chemical shift of phenolic proton of PSU-OH was spotted as a broad signal at around 6.48 ppm (h, H, *s*) with a rather small intensity in Figure 4.33a. The successful incorporation of alkyne moeity to PSU structure was confirmed through a decrease in intensity of the absorption at 6.48 ppm and appearance of new peaks at around 2 - 3 ppm due to methylene and the terminal alkyne moiety of propargyl group (Figure 4.33b). The two triplets at 2.81 ppm (a', 2H, *t*) and 2.63 ppm (b', 2H, *t*) are assigned to methylene protons of propargyl group. The confirmation of end-functionalization of PSU-Alkyne was ensured mainly by the signal appearance at 2.04 ppm (c', H, *s*) indicating the terminal alkyne proton [377].

Incorporation of SNNS to PSU matrix was confirmed by FT-IR spectral analyzes. The chemical structures of PSU grafted SNNS nanocomposite (PSU-SNNS), its precursors, azide modified silicon nitride nanosheet (SNNS-N_3), alkyne-end functional PSU (PSU-Alkyne), and physical mixture of these precursors (PSU+SNNS) were identified by their characteristic vibrations in detail.

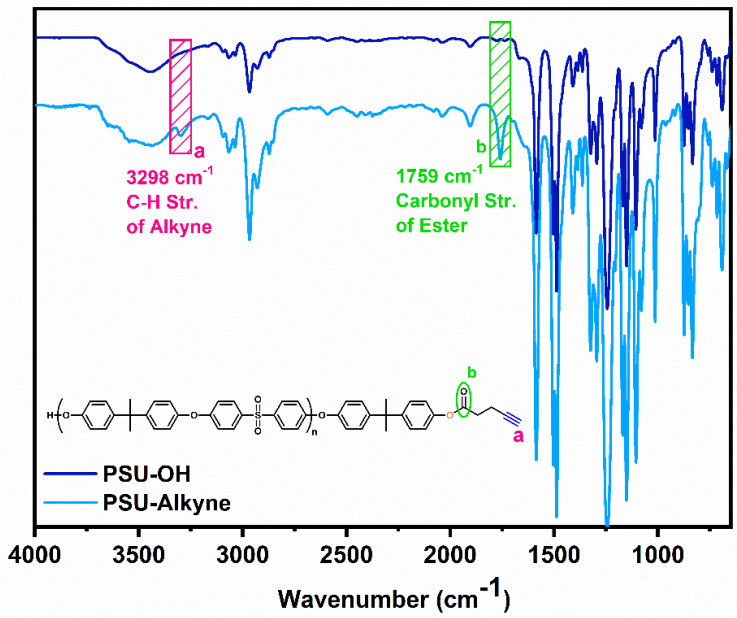

Figure 4.34 : FTIR spectra of PSU-OH and PSU-Alkyne.

Figure 4.34 displays the hydroxyl functional polysulfone (PSU-OH) in dark blue color and alkyne-end functional polysulfone (PSU-Alkyne) in light blue color. FTIR spectroscopy has provided a clear evidence for the conversion of terminal groups of

polysulfone. The successful end-modifiction of polysulfone was confirmed by appearance of the new absorptions at around 3298 cm^{-1} and 2870 cm^{-1} correspond to C-H stretching vibration of terminal alkyne and the strecting vibration of –CH2– groups coming from alkyne moiety, respectively [355, 421]. Moreover, the proof of ester formation stemmed from the alkynylation reaction has been also verified by the existence of an absorption peak at 1759 cm^{-1} corresponding to the carbonyl stretching vibration originated from alkyne moiety [100, 422]. In addition to these distinctive functional group vibrations, the characteristic absorption peaks of polysulfone were listed such as; bands at 3066 and 3044 cm^{-1} indicate the C-H stretching vibrations and while the band at 1294 cm^{-1} designates the C-H bending vibration of aromatic ring [423]. Symmetrical and asymmetrical C-H stretching vibrations of methyl group in PSU backbone appears at 2966 cm^{-1} and 2931 cm^{-1}, respectively, while absorption peaks at 1586, 1504, 1488 and 1409 cm-1 specify the characteristic C=C stretching vibrations of aromatic rings of polysulfone backbone [354, 424]. Besides, asymmetric and symmetric stretching vibrations of sulfone moiety have been observed at 1324 cm^{-1} and 1244 – 1170 - 1151 cm^{-1} (3 peaks), respectively [280] and the asymmetric stretching vibration of ether linkage showed also up at 1012 cm^{-1} [353, 425].

FTIR spectra of azide modified silicon nitride nanosheet (SNNS-N_3), alkyne-end functional PSU (PSU-Alkyne) and PSU grafted SNNS nanocomposite (SNNS-PSU) are shown in Figure 4.35.

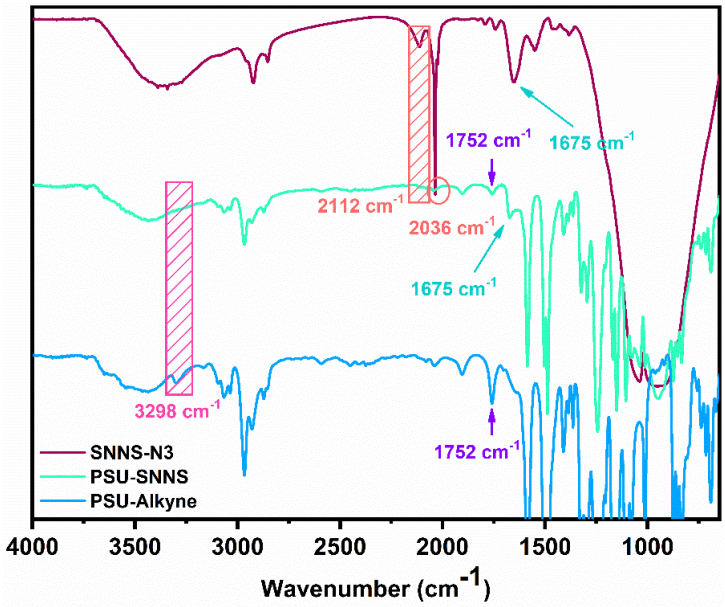

Figure 4.35 : FTIR spectra of SNNS-N_3, PSU-Alkyne and PSU-SNNS by Click Reaction.

The backbone vibration of Si-N-Si and bending vibration of Si-O-Si are visible at 954 cm^{-1} and 1039 cm^{-1}, respectively in the spectra of SNNS-N_3 [207, 387]. Besides, in the spectra of PSU-SNNS, broad absorption peak around 3440 cm^{-1} corresponding to hydroxyl stretching vibrations due to -OH groups on the surface of SNNS-N_3 and residual solvent from PSU-Alkyne have been observed [347, 388]. Moreover, the characteristic stretching and bending vibrations of polysulfone mentioned in Figure 4.34 are apparently seen also in Figure 4.35. It is obviously seen that the absorption peak at 3298 cm^{-1} assigned to the alkyne function of PSU-Alkyne and the absorption peaks at 2036 and 2112 cm^{-1} ascribed to azide moiety of SNNS-N_3 have been disappeared in the spectra of PSU-SNNS. In addition to this, the ester moiety of PSU-Alkyne appearing at 1752 cm^{-1} and the amide moiety of SNNS-N_3 appearing at 1675 cm^{-1} are clearly seen also in the spectrum of PSU-SNNS. These evidences indicate that the click reaction between azide-functional SNNS and alkyne-functional PSU is successful [358, 392].

FTIR spectra of azide modified silicon nitride nanosheet (SNNS-N_3), alkyne-end functional PSU (PSU-Alkyne) and physical blend of PSUAlkyne and SNNS-N_3 (PSU+SNNS) are shown in Figure 4.36.

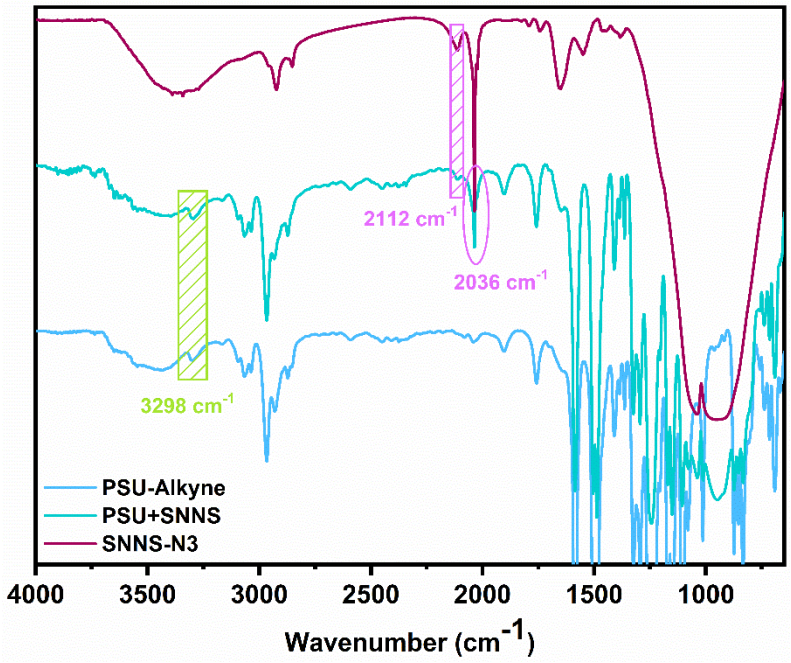

Figure 4.36 : FTIR spectra of SNNS-N_3, PSU-Alkyne and PSU+SNNS by Physical Blend.

Comparing to Figure 4.35, the characteristic bands of alkyne and azide moiety appearing at 3298, 2112 and 2036 cm^{-1}, respectively were obviously seen in the spectra of PSU+SNNS contrary to PSU-SNNS spectra. These vibrations have remained stable due to the absence of chemical interaction. This result reveals that the blending process has based on just physical mixing, not chemical interaction.

4.3.3.3 Thermal investigation

Thermal stability of nanocomposite by physical blend (PSU+SNNS), nanocomposite by click reaction (PSU-SNNS) and their precursors (SNNS-N_3 and PSU-Alkyne) are explored by TGA under N_2 atmosphere. TGA curves are shown in figure 4.37 and results are tabulated in Table 4.9.

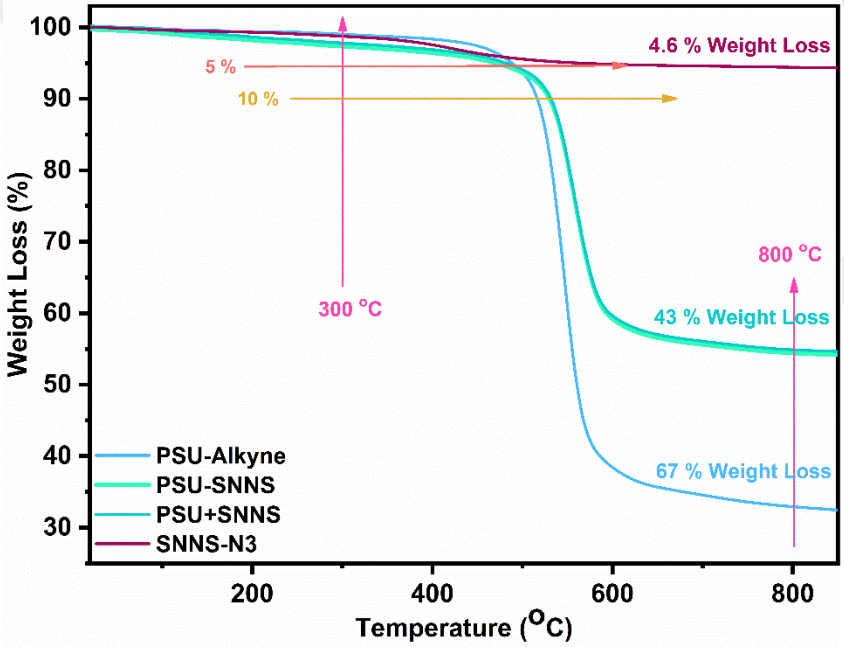

Figure 4.37 : TGA curves of SNNS-N_3, PSU-Alkyne, PSU-SNNS and PSU+SNNS.

The weight losses below 200 °C can be attributed to physisorbed water and residual organic solvents [426, 427]. It is observed that PSU-Alkyne shows greater thermal stability when compared to PMMA-Alkyne and a single-step thermal decomposition with weight loss of 67 % between 300 and 800 °C assigned to main-chain pyrolysis with 33 % char yield [428, 429]. By the addition of thermally resistant SNNS-N_3 having a weight loss of 4.6 % between 300 and 800 °C with 95.4 % char yield to the structure, thermal stability and thermal decomposition temperature of polymer matrix increased while its char yield decreased. As expected, the weight losses of nanocomposites are at the intermediate value those of the components forming the

composite. Nanocomposite structures demonstrate higher thermal stability than pristine PSU-Alkyne owing to enhanced inorganic content of the materials [430]. In addition, they do not show significant weight loss before 300 °C in comparison to PSU-Alkyne. Among silicon nitride added PSU nanocomposites, PSU-SNNS nanocomposite by click reaction exhibited the lowest weight loss with 43 % between 300-800 °C and the highest thermal stability and char yield at 900 °C due to the interface compatibility between nanofiller and polymer matrix [397, 425]. This phenomenon probably stem from the restriction of chain mobility of polymers against SNNS-N_3 surface and also might originated from the the formed 3-dimensional crosslink structures between the nanofiller and polymer matrix through click reaction [376]. Moreover, PSU-SNNS exhibited the highest degradation temperatures of T_5% and T_{10}% at 496 °C and 534 °C, respectively. Conversely, the degradation temperatures of PSU+SNNS displayed lower temperatures at T_5% and T_{10}% regarding lack of chemical interaction between inorganic filler and polymer matrix.

Table 4.9 : Thermogravimetric properties of PSU nanocomposites and their precursors.

Samples	T_5% (°C)	T_{10}% (°C)	Y_c (%)
SNNS-N_3	572	-	95.4
PSU-Alkyne	489	516	33
PSU+SNNS	479	527	57
PSU-SNNS	496	534	57

T_5%: The temperature for which the weight loss is 5%.
T_{10}%: The temperature for which the weight loss is 10%.
Y*c*: Char yields at 900 °C under nitrogen atmosphere.

Thermal behavior and glass transition temperatures of pristine PSU-Alkyne, PSU-SNNS and PSU+SNNS were investigated by differential scanning calorimetry. DSC traces are shown in Figure 4.38.

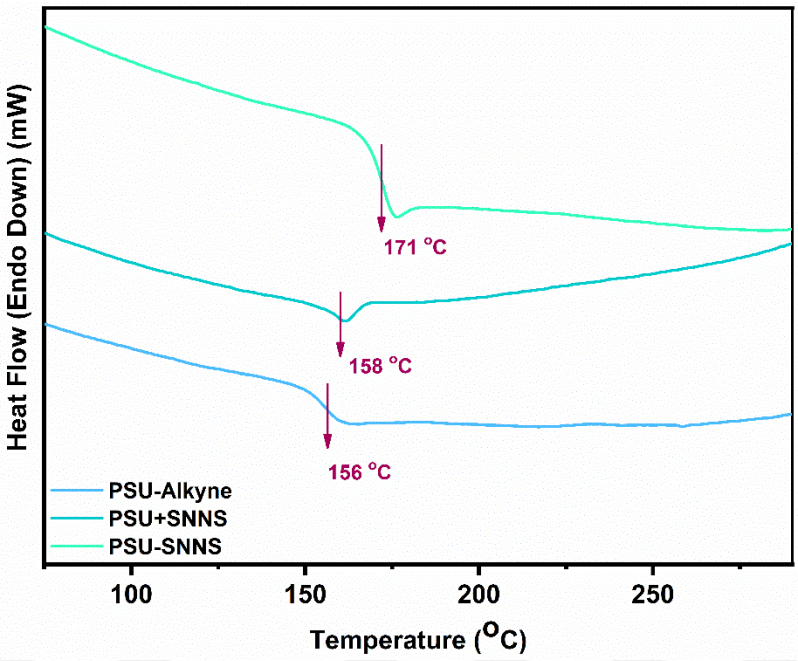

Figure 4.38 : DSC traces of PSU-Alkyne, PSU+SNNS and PSU-SNNS.

It is obviously seen that the glass transition temperature of PSU-Alkyne appeared at 156 °C. After incorporation of SNNS physically, the glass transition temperature has slightly increased to 158 °C due to the partially reduced chain mobility. PSU-SNNS nanocomposite having chemical bond between polymer and filler shows the highest T_g at 171 °C and it is 15 °C higher than that of its precursor due to the reduced chain mobility regarding structural compatibility between the end groups and the inner backbone [401, 402]. This phenomenon reveals the effect of interaction type between filler and matrix on thermal behavior of nanocomposite. Apart from the interaction type between precursors, the chain mobility has reduced leading to increase in T_g due to the restricted polymer network resulted from the incorporation of inorganic filler [380, 431, 432]. However, the transition from glassy state to rubbery state for PSU-SNNS has occured at higher degrees in comparison with PSU+SNNS, considering that the filler content in both nanocomposite samples is with 31 wt% the same. Consequently, regardless of filler concentration in nanocomposite, filler-matrix interaction would be the case [109, 433, 434].

4.3.3.4 Thermal conductivity and electrical resistance investigation

The thermal resistivity, thermal conductivity and electrical resistivity (Volume Resistivity) analysis of pristine PSU-Alkyne and nanocomposites by physical blend and click reaction are summarized in Table 4.10, thermal conductivity comparisons of

those three samples are demonstrated in Figure 4.39 and thermal and electrical resistivity changes are shown in Figure 4.40.

Table 4.10 : Conductivity and resistivity results of PSU-Alkyne and PSU nanocomposites.

Samples	Thermal Resistivity (m^2K/W)	Thermal Conductivity (W/mK)	Volume Resistivity (Ω.cm)
	ASTM D5470	ASTM D5470	ASTM D257
PSU-Alkyne	0.00755	0.083	$1.15e^{14}$
PSU+SNNS	0.00435	0.179	$7.15e^{16}$
PSU-SNNS	0.00278	0.367	$1.58e^{18}$

The conductivities were measured according to the ASTM D5470 standard operating on a guarded heat flow principle [404]. This device has two temperature-controlled surfaces, after a certain pressure and temperature is applied to the material placed between these two metal surfaces, the device starts to collect thermal resistivity data. Thermal conductivity analyses with through-plane direction were carried out at working temperature of 25 °C and under 25 Psi pressure. The thermal conductivities show an increase of 116 % for the nanocomposite derived physical blending (PSU+SNNS) and an increase of 342 % for the nanocomposite derived via click reaction (PSU-SNNS) when compared to PSU-Alkyne. Considering that the filler content in both nanocomposite samples is with 7.5 wt% the same, the distinct increase of thermal conductivity in the click reaction derived sample is remarkable. These increments can be seen explicitly in Figure 4.39. It can be concluded that the thermal resistance at filler-matrix interface in PSU-SNNS nanocomposite has been reduced by means of chemical interaction [12, 405, 406, 435].

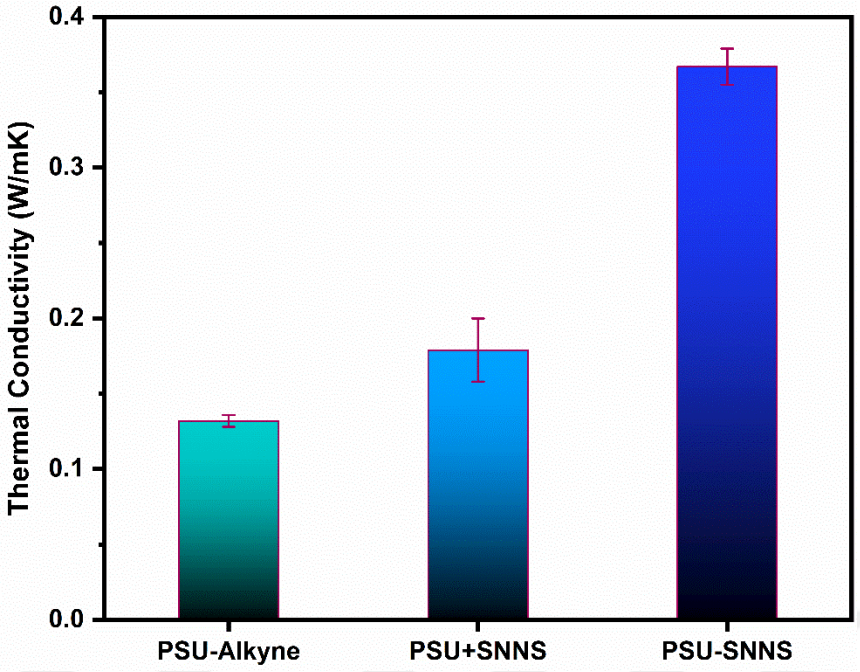

Figure 4.39 : Thermal conductivity comparisons of PSU-Alkyne, PSU+SNNS and PSU-SNNS.

Electrical resistance results are as high as expected. As clearly seen in Figure 4.40, the electrical volume resistance values increased inversely proportional to the decreasing thermal resistance values with the incorporation of silicon nitride nanosheets due to their high electrical insulating characteristics. The most striking evidence of this phenomenon is that the nanocomposites displayed considerable enhancement in volume resistivity ranges compared to PSU-Alkyne ($1.15x10^{14}$ Ω.cm), which is also consistent with the fact that the excellent electrical insulating characteristics of silicon nitride nanofillers. However, the PSU-SNNS nanocomposite showed the volume resistivity of 1.58×10^{18} Ω.cm, which is higher than that of the PSU+SNNS nanocomposite (7.15×10^{16} Ω.cm) with the same SNNS ratio. It is anticipated that this difference is due to the chemical interaction available in PSU-SNNS nanocomposite, which leads to the homogeneous distribution of SNNS in the polymer matrix. It can also said that the lack of strong interaction like chemical bond in the PSU+SNNS nanocomposite has a significiant effect on this result [407, 436, 437].

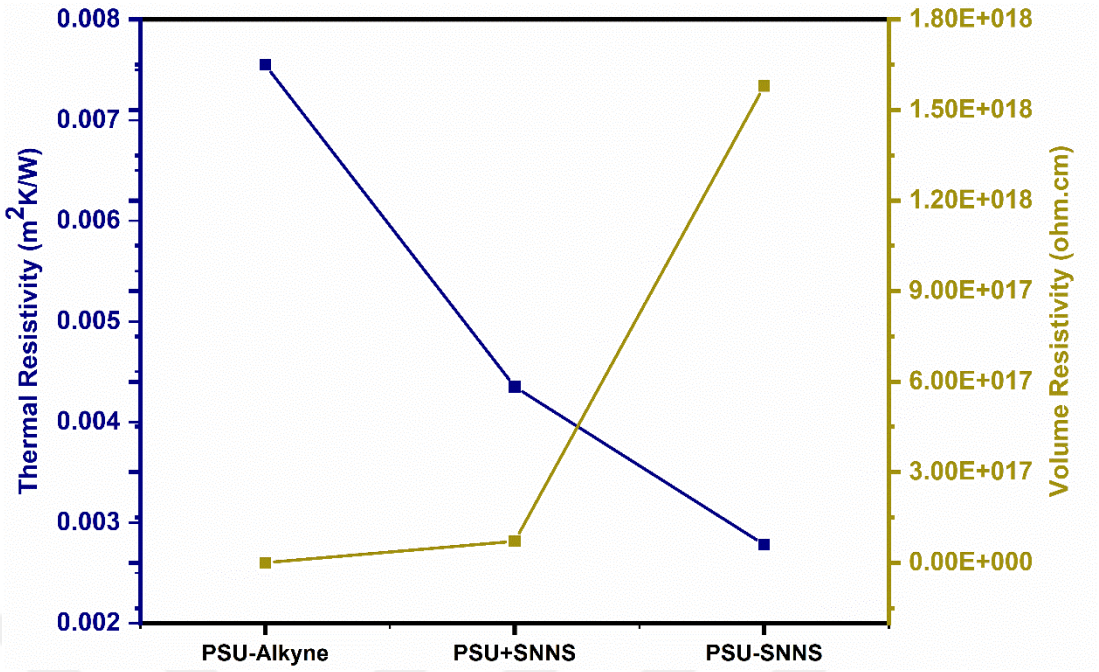

Figure 4.40 : Thermal and electrical resistivity comparisons of PSU-Alkyne and PSU nanocomposites.

4.3.4 Preparation of poly(ether ether ketone)/silicon nitride nanocomposites via CuAAC click reaction (PEEK-SNNS)

In order to prepare the nanocomposite with poly(ether ether ketone) matrix (PEEK-SNNS), the two-step synthesis procedure of PEEK was performed to obtain alkyne functional precursor to enable the click reaction with azide functional SNNS (SNNS-N_3) prepared in the chemical modification process. The first stage of the synthesis procedure involves poly(ether ether ketone) synthesis with hydroxyl end-groups by condensation polymerization (PEEK-OH), followed by conversion of these end-groups to alkyne function (PEEK-Alkyne) to be used in Copper Catalyzed Azide-Alkyne Click reaction (CuAAc). The effect of functionalization on thermal behaviors of nanocomposite was investigated by characterization studies. Furthermore, the characterization results of the nanocomposite obtained by both physical mixture and click chemistry were examined. The differences between these two methods were reported in detail. The schematic representations of the modification process and the nanocomposite synthesis are shown in Figure 4.41 and Figure 4.42.

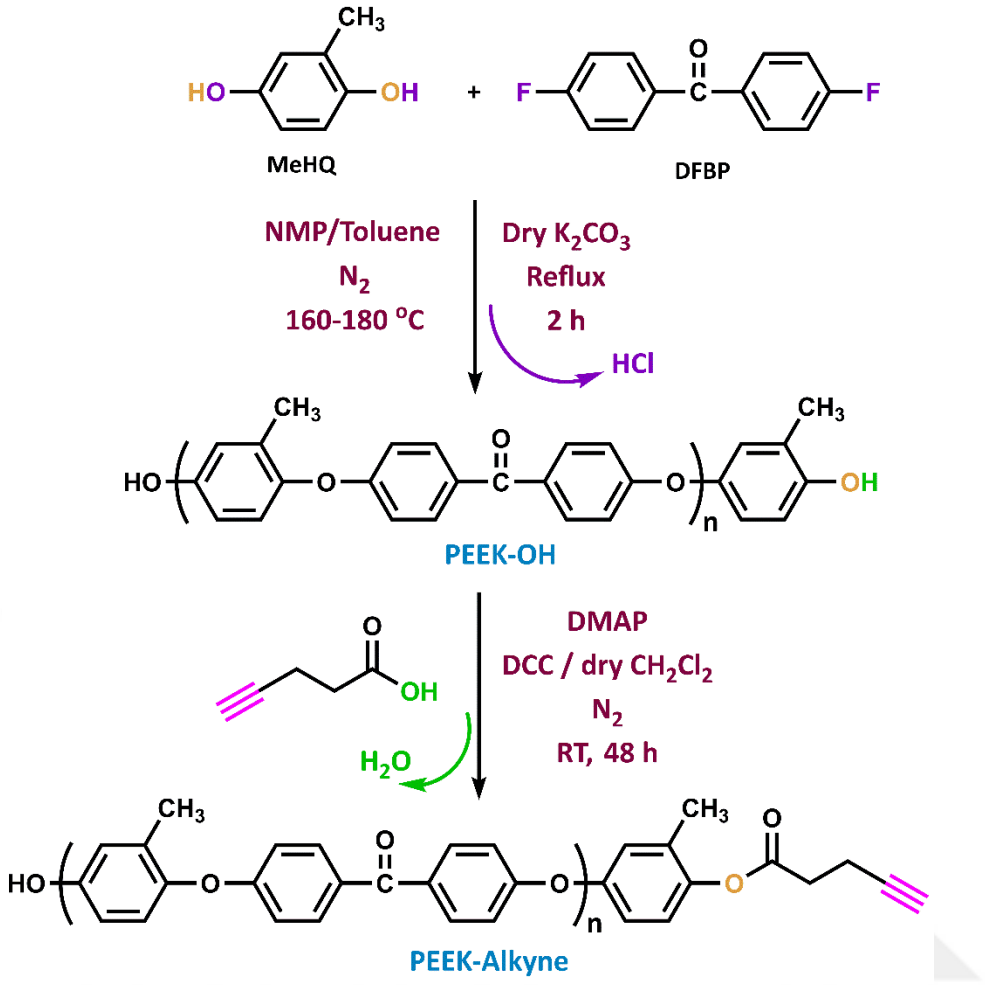

Figure 4.41 : The synthesis route of PEEK-Alkyne by polycondensation.

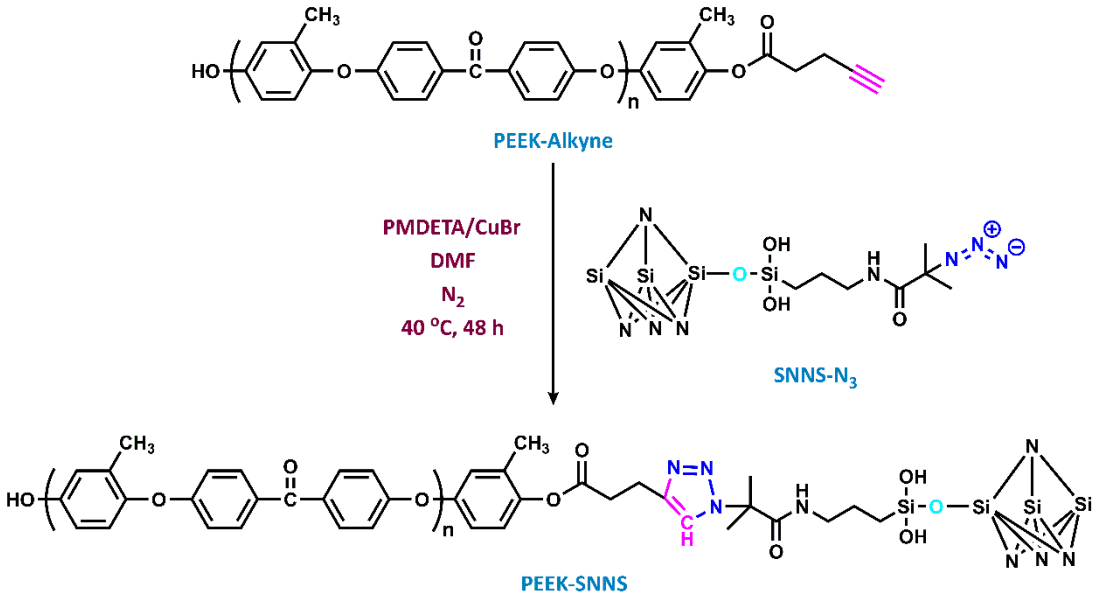

Figure 4.42 : The synthesis of PEEK-SNNS nanocomposite via click reaction.

The experimental conditions and the properties of PEEK-OH obtained by polycondensation and PEEK-Alkyne obtained by end-functionalization reaction are tabulated in Table 4.11. It summarizes the polycondensation and end-functionalization results. The condensation reaction produced high molecular weight PEEK (PEEK-OH) with targeted molar mass and moderate polydispersity. The PEEK-OH has a molecular weight (M_n) of 25,000 g/mol with 80.4% yield, while PEEK-Alkyne has results such as molecular weight (M_n) of 25,500 g/mol with 31% yield. Moreover, the polydispersities are typical for condensation polymerization products [438].

Table 4.11 : Synthesis[a] conditions and molecular weight characteristics of hydroxyl and alkyne end-functional poly(ether ether ketone)s.

Polymer	[MeHQ/DFBP][a] (mol/mol)	Yield[b] (%)	M_n[c] (g/mol)	$Đ$
PEEK-OH	1/1.05	80.4	25,000	1.60
PEEK-Alkyne	-	31.0	25,500	1.62

[a] Reaction temperature: 160 – 180 °C, time: 2 h.
[b] Determined gravimetrically.
[c] Determined from GPC measurements based on polystyrene standards.

The successful click reaction between PEEK-Alkyne as polymer matrix and SNNS-N_3 as thermal conductive nanofiller was confirmed completely by XRD, SEM, NMR, FTIR, TGA, DSC, DTC, ER and DMA analyzes.

4.3.4.1 Crystallography investigation

PEEK-OH is a semi-crystalline engineering polymer apart from other polymers (PMMA and PSU) used as matrix within this thesis study. The aforementioned crystall structure of PEEK-Alkyne has been investigated by X-Ray crystallography (XRD). Crtstal structure comparison of SNNS, PEEK-Alkyne and PEEK-SNNS nanocomposite is demonstrated in Figure 4.43.

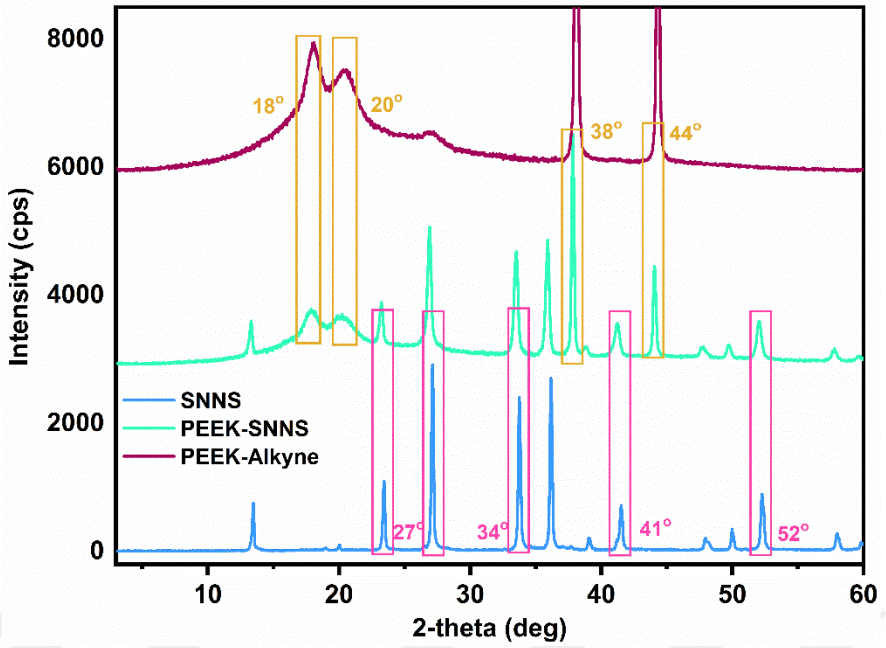

Figure 4.43 : XRD patterns of SNNS, PEEK-Alkyne and PEEK-SNNS.

The characteristic crystal diffraction peaks of β-phase silicon nitride are seen in dark pink spectrum. Poly (ether ether ketone) is a semi-crystalline polymer as it mentioned. Therefore, it has amorphous parts seen at 18° and 20° and crystaline parts seen at 38° and 44°. The green spectrum represents the PEEK-SNNS having both characteristic diffraction peaks of PEEK and SNNS, naturally. Patterns representing the amorphous portions of PEEK-Alkyne exhibited a novel pattern with decreased peak intensities and boradened peak width with the incorporation of crystalline SNNS in PEEK-SNNS pattern (green pattern). This change has confirmed the success of click reaction in PEEK-SNNS nanocomposite and the reduction of crsystall fraction through covalent bond formed [439].

4.3.4.2 Morphological investigation

The SEM images for silicon nitride nanosheets (SNNS), pristine PEEK-Alkyne, physical blend of SNNS and PEEK (PEEK+SNNS) and PEEK grafted silicon nitride nanosheets by click reaction (PEEK-SNNS) with 25k magnification scales were given in Figure 4.44a, 4.44b, 4.44c and 4.44d, respectively.

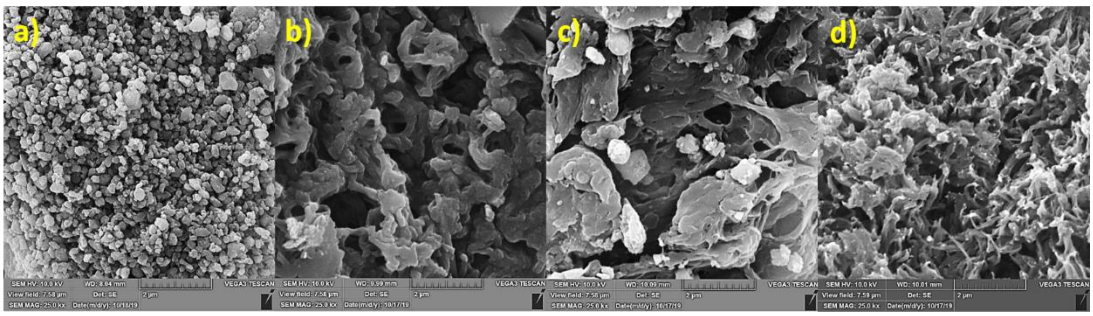

Figure 4.44 : SEM magnification images of a) SNNS, b) PEEK-Alkyne, c) PEEK+SNNS and d) PEEK-SNNS at 25k magnification.

SNNS (Figure 4.44a) seem in granular structure, especially after mechanical treatment, but PEEK-Alkyne (Figure 4.44b) displays network morphology, as is generally seen in conventional polymeric structures. It is obviously seen that the polymer-introduced nanosheets appear larger than unmodified nanosheets under the same magnification. Figure 4.44c shows irregular and uneven distribution of the particles. SNNS particles have arranged sporadically in the polymer matrix and seem agglomerated to each other. However, Figure 4.44d displays a more regular and homogeneous distribution of the particles. The complete surrounding of nanosheets by polymer network verifies that the PEEK-Alkyne was effectively grafted to the nanosheet surface. The another evidence is that the PEEK-SNNS particles emerge more unified and smaller in size when compared to unmodified nanosheets due to the good dispersion in polymer matrix. It probably stems from the interface compatibility between nanofiller and polymer matrix due to the presence of covalent bond [418, 419].

4.3.4.3 Structural investigation

Hydroxyl-terminated PEEK (PEEK-OH) and alkyne-end functionalized PEEK (PEEK-Alkyne) were identified by spectral analyzes. Chemical structures of PEEK-OH and PEEK-Alkyne were investigated by ^{1}H-NMR. The convertion from hydroxyl-end functionality to alkyne-end functionality was also confirmed by ^{1}H-NMR analyzes and presented in Figure 4.45.

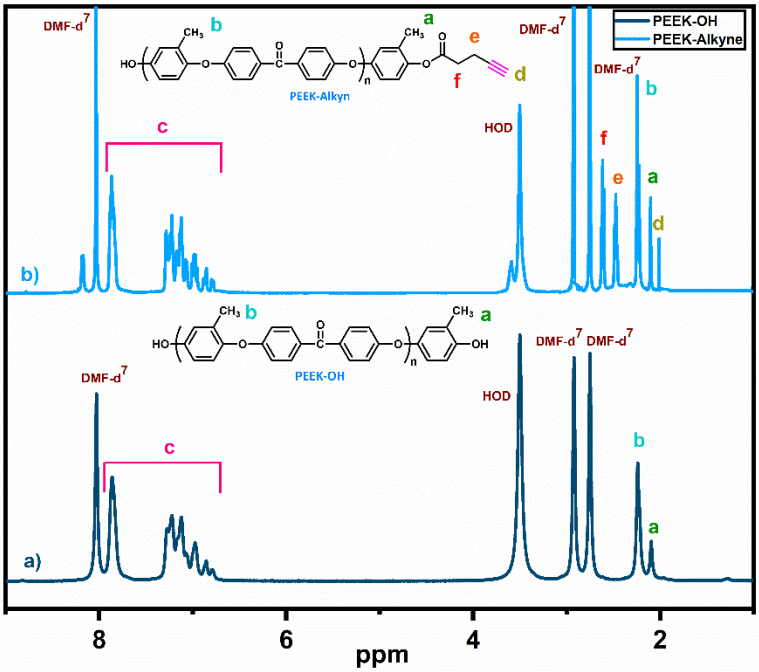

Figure 4.45 : ^{1}H-NMR spectra of a) PEEK-OH and b) PEEK-Alkyne in DMF-d^{7}.

Deuterated solvent peaks (DMF-d^{7}) emerged as three peaks at 8.03, 2.92 and 2.74 ppm and H_2O traces coming from deuterated solvent (HOD) is spotted at 3.50 ppm [440]. Absorptions corresponding to the methyl protons of MeHQ seem at 2.08 (a, 3H, *s*) and 2.74 (b, 3H, *s*) and aromatic protons of PEEK main-chain appear in the range of 6.78 - 7.86 ppm (c, 12H; *d*, *s*) in both spectra [289, 441, 442]. The successful incorporation of alkyne moeity to PEEK structure was confirmed through appearance of new peaks at around 2 - 3 ppm due to methylene and the terminal alkyne moiety of propargyl group (Figure 4.45b). The two triplets at 2.62 ppm (f, 2H, *t*) and 2.46 ppm (e, 2H, *t*) are assigned to methylene protons of propargyl group. The confirmation of end-functionalization of PEEK-Alkyne was ensured mainly by the signal appearance at 2.01 ppm (d, H, *s*) indicating the terminal alkyne proton [377].

Incorporation of SNNS to PEEK matrix was confirmed by FT-IR spectral analyzes. The chemical structures of PEEK grafted SNNS nanocomposite (PEEK-SNNS), its precursors, azide modified silicon nitride nanosheet (SNNS-N_3) and alkyne-end functional PEEK (PEEK-Alkyne), and physical mixture of these precursors (PEEK+SNNS) were identified by their characteristic vibrations in detail.

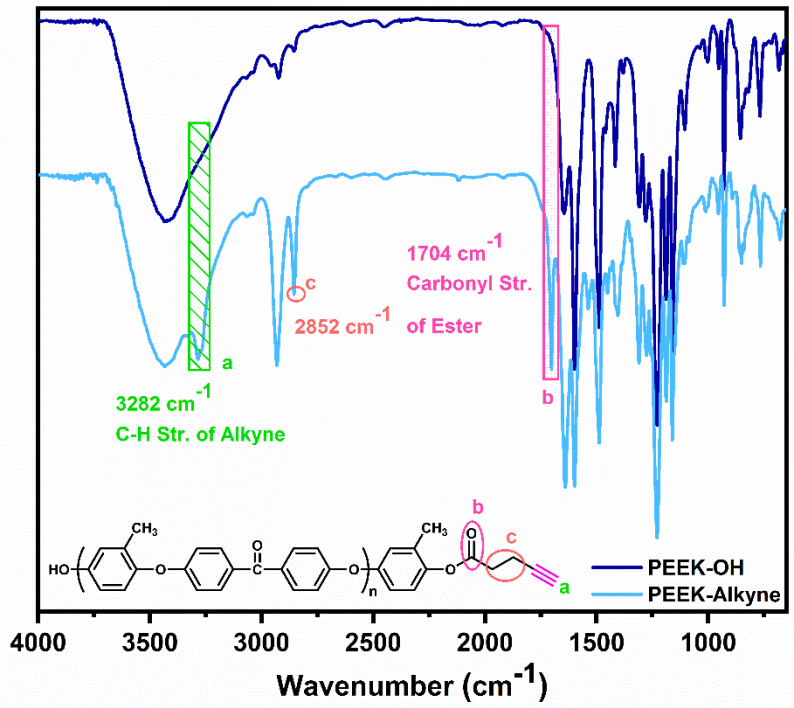

Figure 4.46 : FTIR spectra of PEEK-OH and PEEK-Alkyne.

Figure 4.46 displays the hydroxyl functional poly (ether ether ketone) (PEEK-OH) is seen in dark blue color and alkyne-end functional poly (ether ether ketone) (PEEK-Alkyne) in light blue color. FTIR spectroscopy has provided clear evidence for the conversion of terminal groups of poly (ether ether ketone). It can be clearly seen that hydroxyl end-groups were successfully converted to alkyne groups. Three distinct peaks appeared in the spectra of PEEK-Alkyne are different from spectra of PEEK-OH. The absorption at 3282 cm^{-1} indicates the C-H stretching vibration of terminal alkyne [443]. In addition, the proof of ester formation stemmed from the alkynylation reaction has been also verified by the existence of an absorption peak at 1704 cm^{-1} corresponding to the carbonyl stretching vibration originated from alkyne moiety [422]. Moreover, C-H stretching vibrations of methylene groups came from pentynoic acid is clearly also seen at 2852 cm^{-1} [421]. In addition to these indicative functional group vibrations, the characteristic absorption peaks of poly (ether ether ketone) were listed such as; bands at 3067 and 3035 cm^{-1} refer to the C-H stretching vibrations of aromatic ring and while the band at 1278 cm^{-1} and 1232 cm^{-1} refers to (–C-C=O) the bending and the stretching vibrations of benzophenone, respectively [96, 444]. Symmetrical C-H stretching vibrations of methyl group in PEEK backbone appears at 2929 cm^{-1} [445], while the absorption peaks at 1599, 1539, 1484 and 1406 cm^{-1} specify the characteristic C=C stretching vibrations of aromatic rings of poly (ether ether

ketone) backbone [446]. Furthermore, the strong band at 1640 cm^{-1} represents the C=O stretching vibration of crystalline phase of poly (ether ether ketone) [286, 447]. The absorption band at 1190 cm^{-1} refers to the hydrogen rocking vibration of phenyl groups [447]. Moreover, the asymmetric stretching vibration of ether linkage showed also up at 1227 cm^{-1} [289]. Also, C-H out of plane bending vibrations of phenyl rings appear at 856 cm^{-1} and 769 cm^{-1} [287, 288].

FTIR spectra of azide modified silicon nitride nanosheet (SNNS-N_3), alkyne-end functional PEEK (PEEK-Alkyne) and PEEK grafted SNNS nanocomposite (PEEK-SNNS) are shown in Figure 4.47.

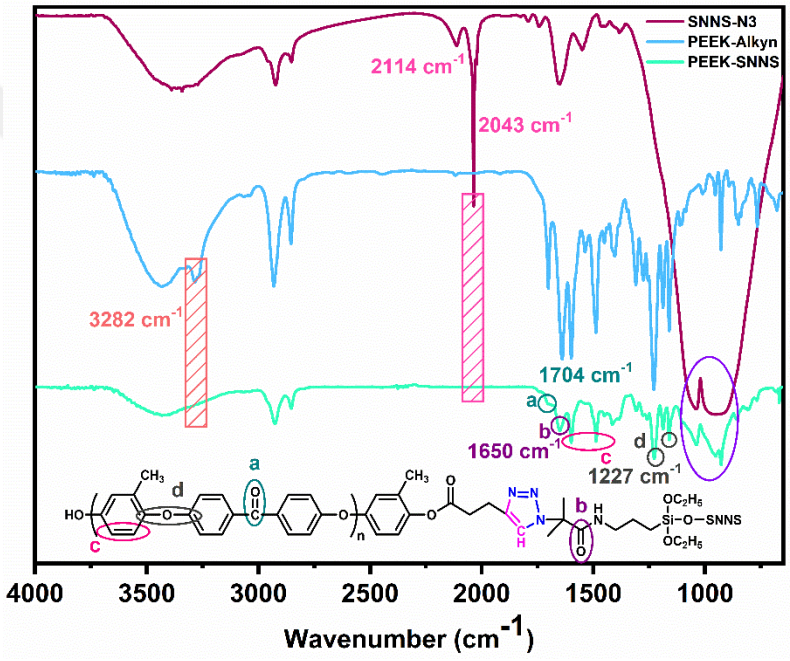

Figure 4.47 : FTIR spectra of SNNS-N_3, PEEK-Alkyne and PEEK-SNNS by Click Reaction.

The backbone vibration of Si-N-Si and bending vibration of Si-O-Si are visible at 954 cm^{-1} and 1039 cm^{-1}, respectively in the spectra of SNNS-N_3 [207, 387]. Besides, in the spectra of PEEK-SNNS, broad absorption peak around 3440 cm^{-1} corresponding to hydroxyl stretching vibrations due to -OH groups on the surface of SNNS-N_3 and residual solvent in PEEK-Alkyne have been observed [347, 388]. Moreover, the characteristic stretching and bending vibrations of poly (ether ether ketone) mentioned in Figure 4.46 are apparently seen also in Figure 4.47. It is obviously seen that the absorption peak at 3282 cm^{-1} assigned to the C-H streching vibration of terminal alkyne of PEEK-Alkyne and the vibrations at 2043 and 2114 cm^{-1} ascribed to azide

moiety of SNNS-N_3 have been disappeared in the spectra of PEEK-SNNS. The appearance of the characteristic peaks of PEEK-Alkyne and SNNS-N_3 that seen in the spectrum of SNNS-PEEK prove that the click reaction between azide-functional SNNS and alkyne functional PEEK was successful. In addition to this, the amide moiety of SNNS-N_3 appearing at 1650 cm^{-1} and the ester moiety of PEEK-Alkyne appearing at 1704 cm^{-1} are clearly seen also in the spectra of PEEK-SNNS. These evidences indicate that the click reaction between azide-functional SNNS and alkyne-functional PEEK is successful [362, 392].

FTIR spectra of azide modified silicon nitride nanosheet (SNNS-N_3), alkyne-end functional PEEK (PEEK-Alkyne) and physical blend of PEEK-Alkyne and SNNS-N_3 (PEEK+SNNS) are shown in Figure 4.48.

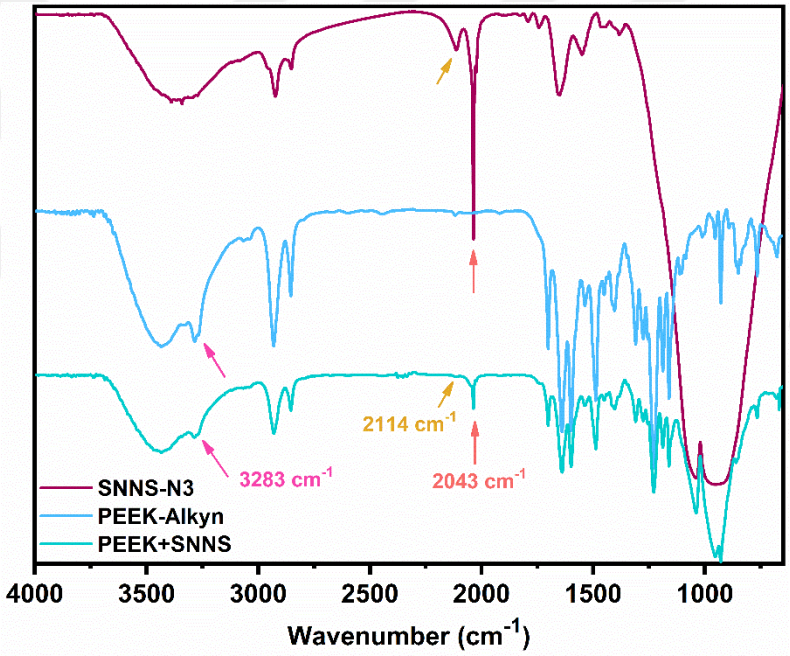

Figure 4.48 : FTIR spectra of SNNS-N_3, PEEK-Alkyne and SNNS+PEEK by Physical Blend.

Comparing to Figure 4.47, the characteristic bands of the alkyne and azide moiety appearing at 3283, 2114 and 2043 cm^{-1}, respectively were obviously seen in the spectra of PEEK+SNNS. These vibrations remained stable due to the absence of chemical interaction. This result reveals that the blending process based on just physical mixing, not chemical interaction.

4.3.4.4 Thermal investigation

Thermal stability of nanocomposite by physical blend (PEEK+SNNS), nanocomposite by click reaction (PEEK-SNNS) and their precursors (SNNS-N_3 and PEEK-Alkyne) are explored by TGA under N_2 atmosphere. TGA curves are shown in Figure 4.49 and results are tabulated in Table 4.12.

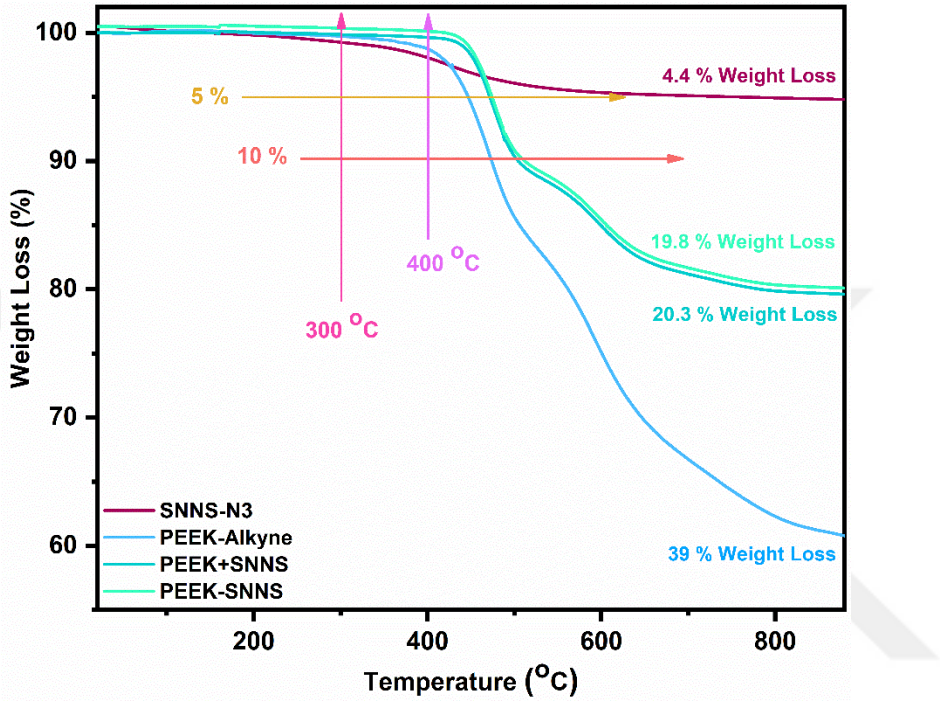

Figure 4.49 : TGA curves of SNNS-N_3, PEEK-Alkyne, PEEK-SNNS and PEEK+SNNS.

The weight losses below 200 °C can be attributed to physisorbed water and residual organic solvents [426, 427]. It is observed that PEEK-Alkyne displays greater thermal stability when compared to PMMA-Alkyne and PSU-Alkyne and besides have a two-step thermal decomposition under nitrogen atmosphere with weight the loss of 39 % between 300-900 °C ascribed to the main-chain pyrolysis with 61 % char yield [448]. While the first degredation step can be attiributed to the indiscriminate chain sicission at the ether and carbonyl linkages in the main chain, the second thermal decomposition has occured mostly due to the disintegration and dehydrogenation of the crosslinked product generated in the first degradation step and crystalline part of the polymer [449-452]. By the addition of thermally resistant SNNS-N_3 having a weight loss of 4.4 % between 300 and 900 °C with 94.9 % char yield to the structure, thermal stability and thermal decomposition temperature of polymer matrix increased while its char yield decreased. As expected, the weight losses of nanocomposites are at the intermediate

value those of the components forming the composite. Nanocomposite structures demonstrate higher thermal stability than pristine PEEK-Alkyne owing to enhanced inorganic content of the materials [453, 454]. In addition, they do not show significant weight loss before 400 °C in comparison to PEEK-Alkyne. Among silicon nitride added PEEK nanocomposites, PEEK-SNNS nanocomposite by click reaction has exhibited the weight loss with 19.8 % between 300-900 °C and the highest thermal stability and char yield at 900 °C due to the interface compatibility between nanofiller and polymer matrix [397, 455, 456]. This phenomenon probably stem from the restriction of chain mobility of polymers against SNNS-N_3 surface and might originated from the formed 3-dimensional crosslink structures between the nanofiller and polymer matrix through click reaction [376, 457]. Moreover, PEEK-SNNS has exhibited the highest degradation temperatures of T_5% and T_{10}% at 475 °C and 508 °C, respectively. Conversely, the degradation temperatures of PEEK+SNNS has displayed slightly lower temperatures at T_5% and T_{10}% regarding lack of chemical interaction between inorganic filler and polymer matrix.

Table 4.12 : Thermogravimetric properties of PSU nanocomposites and their precursors.

Samples	T_5% (°C)	T_{10}% (°C)	Y_c (%)
SNNS-N_3	647	-	94.9
PEEK-Alkyne	447	473	61
PEEK+SNNS	473	500	79.4
PEEK-SNNS	475	508	80

T_5%: The temperature for which the weight loss is 5%.
T_{10}%: The temperature for which the weight loss is 10%.
Y*c*: Char yields at 900 °C under nitrogen atmosphere.

Thermal behavior and glass transition temperatures of pristine PEEK-Alkyne, PEEK-SNNS and PEEK+SNNS were investigated by differential scanning calorimetry. DSC traces are shown in Figure 4.50.

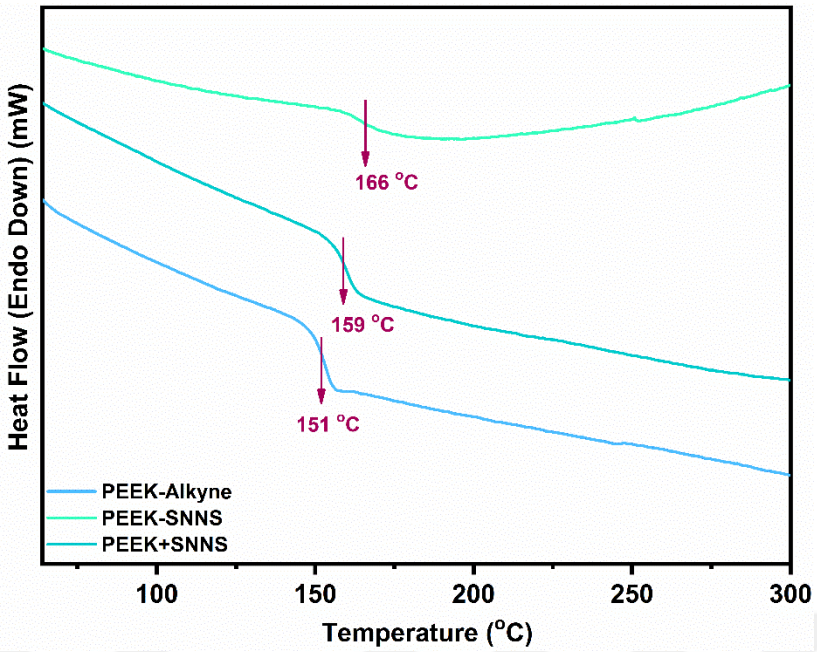

Figure 4.50 : DSC traces of PEEK-Alkyne, PEEK+SNNS and PEEK-SNNS.

The glass transition temperature of PEEK-Alkyne appeared at 151 °C. After incorporation of SNNS physically, the glass transition temperature has slightly increases to 159 °C due to the partially reduced chain mobility. PEEK-SNNS nanocomposite having chemical bond between polymer and filler shows the highest T_g at 166 °C and it is 15 °C higher than that of its precursor due to reduced chain mobility regarding structural compatibility between the end groups and the inner backbone [401, 402]. This phenomenon reveals the effect of interaction type precursors on the thermal behavior of nanocomposite [433]. Apart from the interaction type between precursors, the chain mobility has reduced leading to increase in T_g due to the restricted polymer network resulted from the incorporation of inorganic filler [380, 432, 458-460]. However, transition to rubbery state from glassy state for PEEK-SNNS has occurred at higher degrees in comparison with PEEK+SNNS, considering that the filler content in both nanocomposite samples is with 15 wt% the same. Consequently, regardless of filler concentration in nanocomposite, filler-matrix interaction would be the case [109, 433, 434, 461, 462].

4.3.4.5 Thermal conductivity and electrical resistance investigation

The thermal resistivity, thermal conductivity and electrical resistivity (Volume Resistivity) analysis of pristine PEEK-Alkyne and nanocomposites by physical blend and click reaction are summarized in Table 4.13, thermal conductivity comparisons of

those three samples are demonstrated in Figure 4.51 and thermal and electrical resistivity changes are shown in Figure 4.52.

Table 4.13 : Conductivity and resistivity results of PEEK-Alkyne and PEEK nanocomposites.

	Thermal Resistivity (m^2K/W)	Thermal Conductivity (W/mK)	Volume Resistivity (Ω.cm)
	ASTM D5470	ASTM D5470	ASTM D257
PEEK-Alkyne	0.0239	0.07	8.30 e^{17}
PEEK+SNNS	0.0011	0.34	1.33 e^{18}
PEEK-SNNS	0.00097	0.67	1.41 e^{18}

The conductivities were measured according to the ASTM D5470 standard operating on a guarded heat flow principle [404]. This device has two temperature-controlled surfaces, after a certain pressure and temperature is applied to the material placed between these two metal surfaces, the device starts to collect thermal resistivity data. Thermal conductivity analyses with through-plane direction were carried out at working temperature of 25 °C and under 25 Psi pressure. The thermal conductivities display an increase of 386 % for the nanocomposite derived physical blending (PEEK+SNNS) and an increase of 857 % for the nanocomposite derived via click reaction (PEEK-SNNS) when compared to PEEK-Alkyne. Considering that the filler content in both nanocomposite samples is with 15 % the same, the siginificant enhancement of thermal conductivity in the click reaction derived sampe is remarkable. These increments can seen be explicitly in Figure 4.51. It can be concluded that the thermal resistance at filler-matrix interface in PEEK-SNNS nanocomposite has been reduced by means of chemical interaction [34, 419, 463, 464].

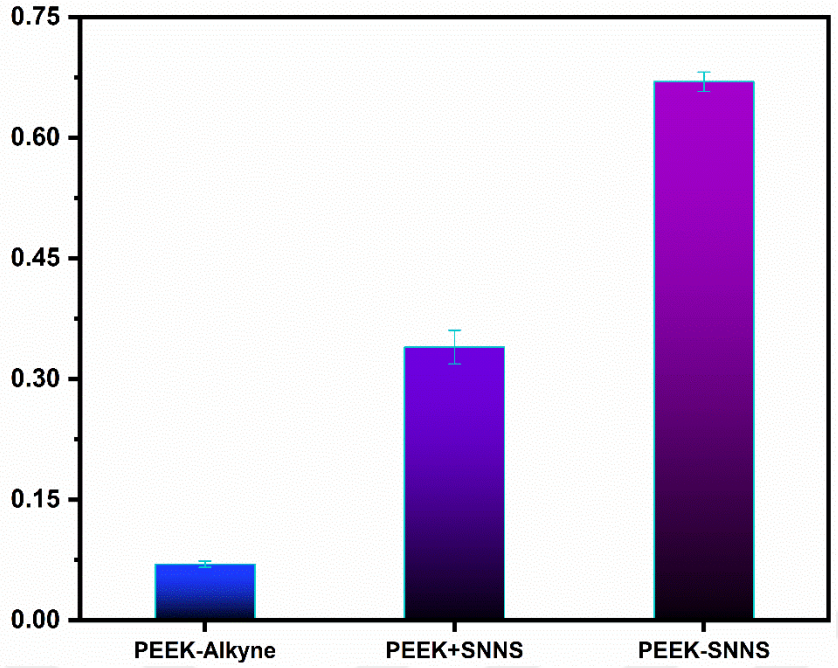

Figure 4.51 : Thermal conductivity comparisons of PEEK-Alkyne, PEEK+SNNS and PEEK-SNNS.

Electrical resistance results are as high as expected. As clearly seen in Figure 4.52, the electrical volume resistance values increased inversely proportional to the decreasing thermal resistance values with the incorporation of silicon nitride nanosheets due to their high electrical insulating characteristics. The most striking evidence of this phenomenon is that the nanocomposites displayed considerable enhancement in volume resistivity ranges compared to PEEK-Alkyne (8.30×10^{17}), which is also consistent with the fact that the excellent electrical insulating characteristics of silicon nitride nanofillers. However, the PEEK-SNNS nanocomposite displayed the volume resistivity of 1.41×10^{18} Ω.cm, which is a bit higher than that of the PEEK+SNNS nanocomposite (1.33×10^{18} Ω.cm) with the same SNNS ratio. It is anticipated that this difference is due to the chemical interaction available in PEEK-SNNS nanocomposite, which leads to the homogeneous distribution of SNNS in the polymer matrix. It can also said that the lack of strong interaction like chemical bond in the PEEK+SNNS nanocomposite has a significiant effect on this result [465, 466].

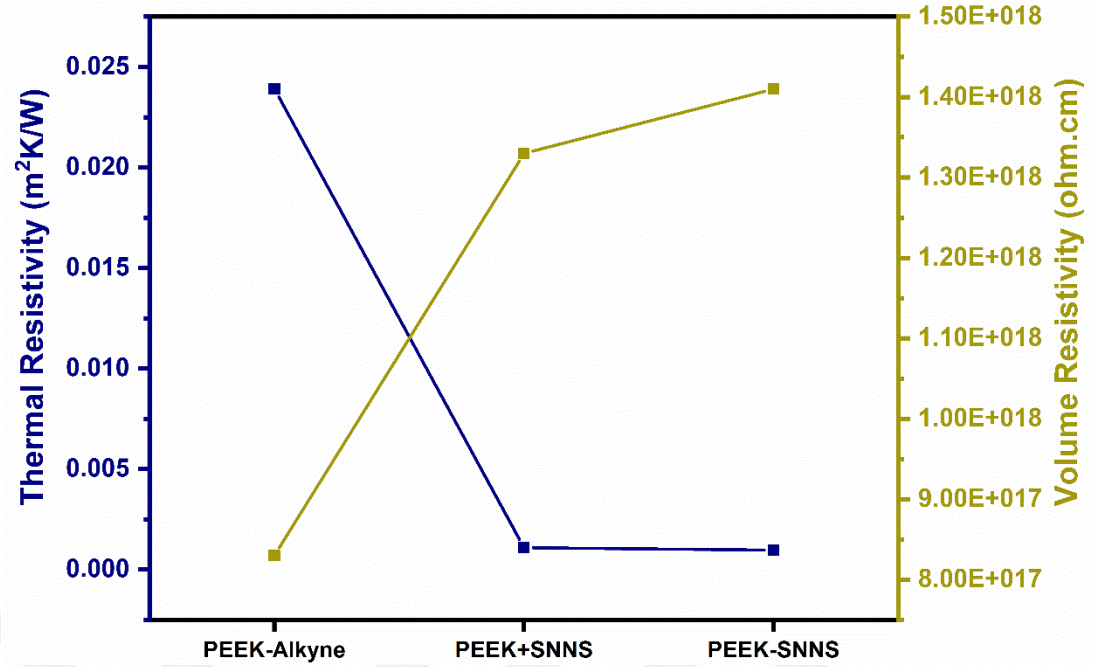

Figure 4.52 : Thermal and electrical resistivity comparisons of PEEK-Alkyne and PEEK nanocomposites.

4.3.4.6 Mechanical investigation

Mechanical behavior of all PEEK samples were investigated by dynamic mechanical analysis. DMA curves are shown below.

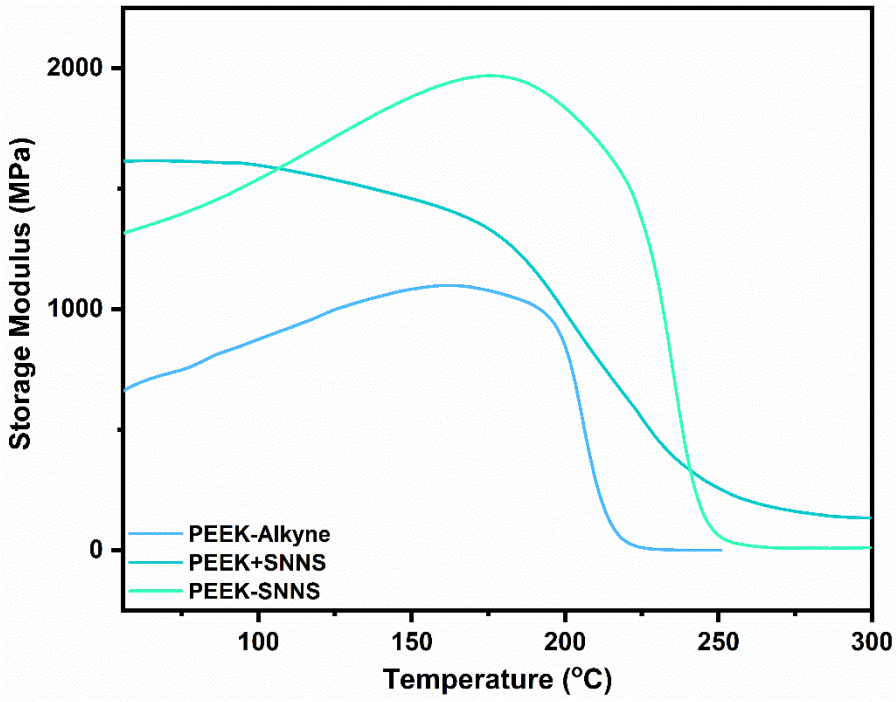

Figure 4.53 : Storage modulus (*E'*) curves of PEEK-Alkyne, PEEK+SNNS and PEEK-SNNS.

The curves of storage modulus (*E'*) versus temperature of PEEK-Alkyne film and nanocomposite films, obtained from DMA at 1 Hz, are demonstrated in Figure 4.53. The dynamic storage modulus is related to elastic modulus evaluated in the concept of load carrying capability or as a stiffness of a material. *E'* depends on the temperature, the filler content and the interaction type between the filler and matrix. In general, the introduction of the filler to polymer matrix increases the stiffness, so the elastic modulus of the material [467-469]. In the same manner, the storage modulus of nanocomposite enhances with the filler content up to some extent [470, 471]. In this work, the ratio of silicon nitride nanofiller was 15 wt% for both nanocomposites. It is seen that *E'* values for covalently bonded nanocomposite (PEEK-SNNS) film at any temperature is much higher than that of pristine PEEK-Alkyne film. The increments of *E'* values are principally owing to diminishment of voids in the PEEK-Alkyne matrix, leading to enhances of stiffness values of the PEEK-SNNS film as shown in Figure 4.54 [472-475].

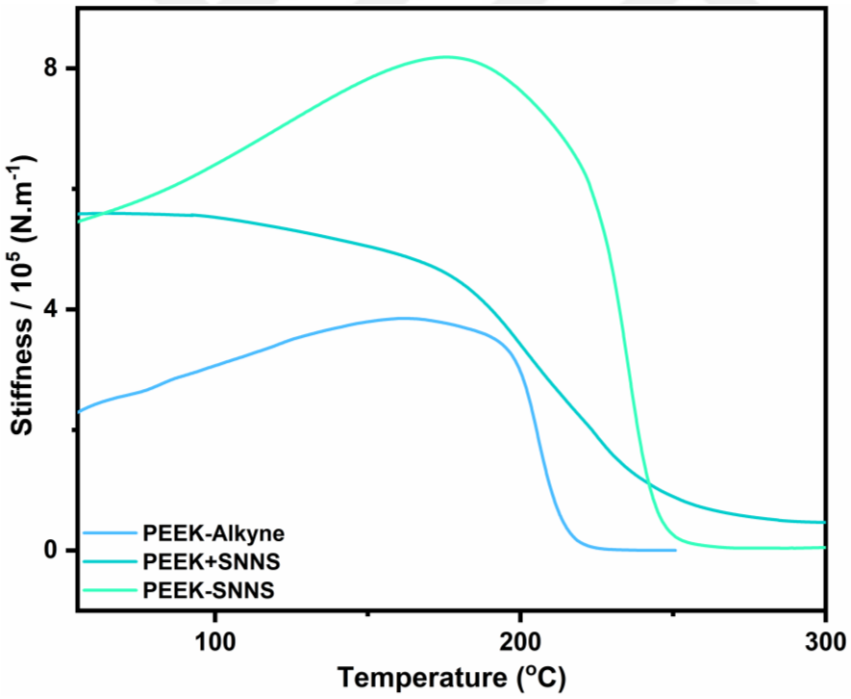

Figure 4.54 : Stiffness curves of PEEK-Alkyne, PEEK+SNNS and PEEK-SNNS.

It can be concluded that the covalent bond between the modified silicon nitride and PEEK-Alkyne has an increasing effect on the stiffness of the material, although as the same nanofiller ratio was used as in the physical blend (PEEK+SNNS) [476]. For PEEK-SNNS nanocomposite, *E'* started to decrease slowly after 178 ˚C, and then a sharp diminishment has seen from the point of 220 ˚C to 260 ˚C. This is the glass

transition region of the film, corresponding the transition from solid-state to rubbery-state. Also, the decrease in *E'* values is ascribe to the energy dissipation due to the motions of the heated polymer chains gained high kinetic energy, stemming from the increase in free volume between the molecular segments [477, 478]. On the other hand, there are some increments in *E'* values of physically blended nanocomposite (PEEK+SNNS) at some point due to decreased chain mobility with respect to incorporation of nanofiller in PEEK matrix, yet the increasing trend of PEEK+SNNS has not appeared as in PEEK-SNNS. This phenomenon can be explained by the filler agglomeration, which takes place in the absence of covalent bonding, which provides the regular distribution of nanofiller in the polymer matrix, as in the PEEK-SNNS film, even though both nanocomposites have the same filling ratio [479, 480]. It is worth to say that the good interfacial compatibility between polymer and nanofiller is responsible for the restriction of the molecular mobility of the polymer matrix, which is featured of this trend [411, 481, 482]. Furthermore, the chemical incorporation of SNNS to PEEK-Alkyne could lead the formation of chemical cross-linking, which increases the stiffness of the material, thus SNNS acted as a reinforcing agent for PEEK-SNNS nanocomposite by taking the advantage of chemical interaction [412, 483].

The loss modulus (*E''*) values as a function of temperature of pristine PEEK-Alkyne film and nanocomposite films, obtained from DMA at a frequency of 1 Hz are demonstrated in Figure 4.55.

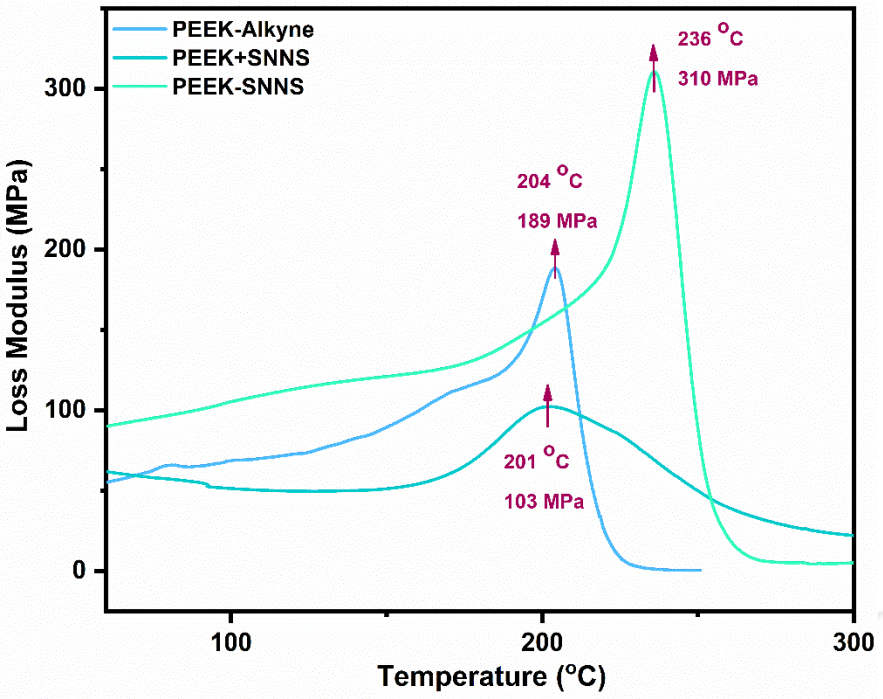

Figure 4.55 : Loss modulus (*E"*) curves of PEEK-Alkyne, PEEK+SNNS and PEEK-SNNS.

E" is related to viscous property of a material, which gives responses as a dissipated energy due to motions of polymer chains. PEEK+SNNS nanocomposite including 15 wt% nanofiller has displayed negative shift and much lower *E"* values compared to pristine PEEK-Alkyne. This behavior can be attributed to the incompatible filler-matrix interaction arises from self-agglomeration of SNNSs and lack of chemical interaction [413]. Though, the loss modulus of PEEK-SNNS containing same content of nanofiller as physically blended nanocomposite at any temperature range has showed increased values than that of pristine PEEK-Alkyne and PEEK+SNNS nanocomposite due to the compatibility between filler and matrix through covalent bond as it is mentioned above. Besides interfacial compatibility, chain mobility restriction and 3-dimensional network structure could have been occurred due to the well dispersion of nanofiller in polymer matrix [484-486]. This result reveals that the SNNS can act as a reinforcing material for the nanocomposite containing covalent bond.

Tan δ curves of pristine PEEK-Alkyne film and nanocomposite films are presented as a function of temperature in Figure 4.56.

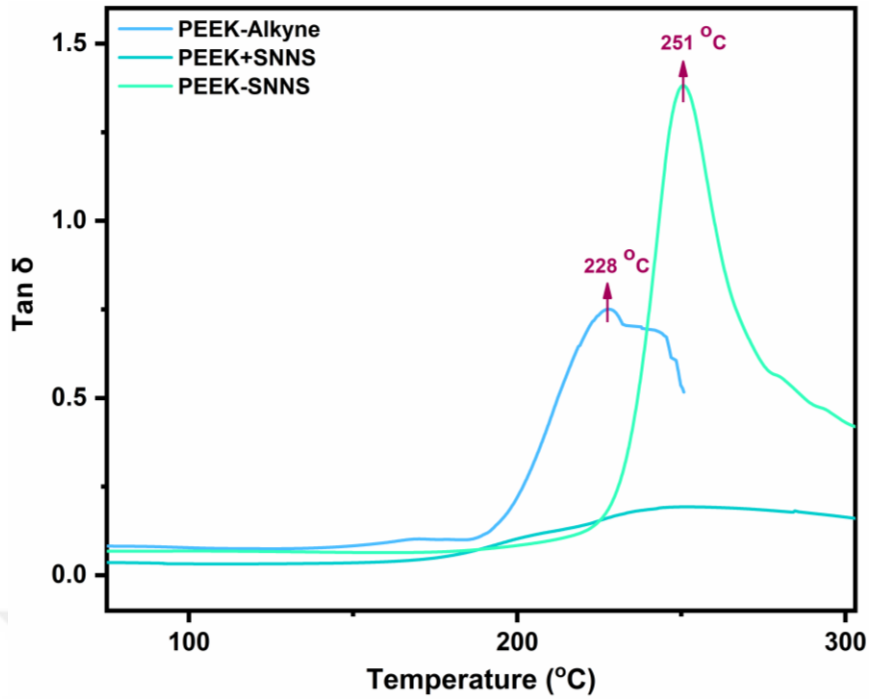

Figure 4.56 : Tan δ curves of PEEK-Alkyne, PEEK+SNNS and PEEK-SNNS.

Tan δ is known as loss factor, damping factor or dissipation factor, defined as the ratio of the loss modulus to storage modulus (*E"/E'*). It provides an information regarding the mechanical behavior whether the material elastic or viscous [414]. The glass transition temperature of a material is associated with the main α-relaxation, corresponding the peak maximum in tan δ curve [413, 487]. It is clearly seen that the tan δ values (peak height) of PEEK-SNNS curve has increased. Since, there is a regular distribution in PEEK-SNNS nanocomposite, the mobility of polymer chains was not restricted, but on the contrary, the peak height has multipliesd due to the dissipated enrgy deriving from enhanced segmental mobility [488]. PEEK-SNNS curve shows the increased T_g at 251 ˚C from 228 ˚C, implying the better interface compatibility between the nanofiller and polymer matrix due to the formed covalent bond and probable chemical cross-linking, which restrain the chain mobility of the polymer [412, 417, 489]. Contrarily, it is clearly seen that the tan δ value (peak heights) of PEEK+SNNS nanocomposite diminished, whereas its peak width enhanced. The decreases in the peak height is directly linked with the elastic character of the film, suggesting the degradation of molecular mobility of PEEK-Alkyne by means of incorporation of SNNS [415]. Due to the incompatible and irregular distribution in the physical blended nanocomposite (PEEK+SNNS), the elasticity of the material has increased while its viscous properties decreased, which reduced also the tan δ values

at any temperature and lowered the peak height [490, 491]. Moreover, the broadening of peaks is related to loosening of polymer chains, indicating the segmental constrains of polymer chains to some extent, which are consistent with the loss modulus values (*E"*) [414, 492, 493]. The irregular distribution and absence of interface compatibility between nanofiller and polymer matrix reduced the mobility of polymer segments, resulting in self-agglomeration of nanofiller [417, 476, 489]. Hence, a large increase in peak width caused by a decrease in free volume has been observed [490]. Consequently, the mechanical transitions of pristine polymer and nanocomposites are consistent with the DSC results as well.

Nanocomposites in film form prepared for mechanical analysis are displayed in Figure 4.57 and the nanocomposite obtained by click reaction in pad form as a thermal interface material (TIM) is shown in Figure 4.58.

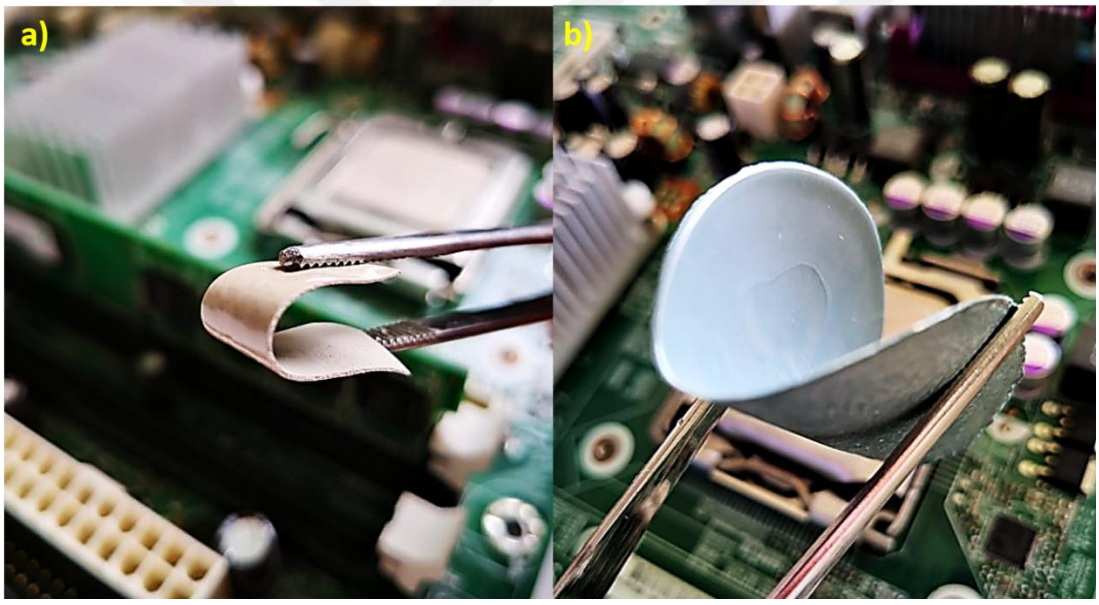

Figure 4.57 : Film forms of a) PEEK+SNNS and b) PEEK-SNNS nanocomposites.

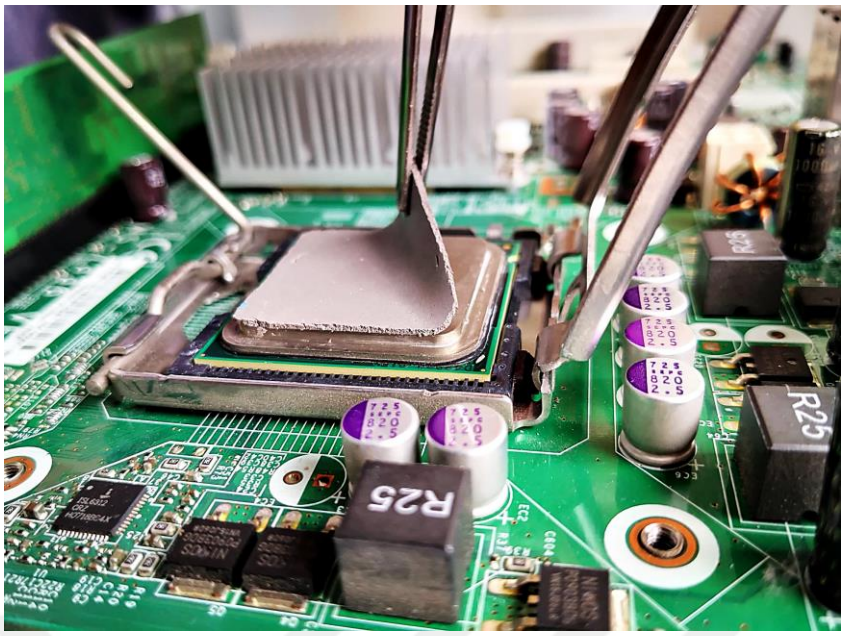

Figure 4.58 : Pad form of PEEK-SNNS Nanocomposite.

5. CONCLUSIONS

In this thesis, silicon nitride (Si_3N_4) containing polymer nanocomposites have been successfully synthesized with three different polymer matrices (PMMA, PSU and PEEK) and formulated as thermal interface material (TIM).

Table 5.1 : End-product characteristics of TIMs produced via click chemistry.

Nanocomposite	TC ($Wm^{-1}.K^{-1}$)	VR (Ω.cm)	T_g (°C)	Decomposition Onset (°C)
PMMA-SNNS	0.255	2.15 e^{14}	161	350
PSU-SNNS	0.367	1.58 e^{18}	171	450
PEEK-SNNS	0.670	1.41 e^{18}	166	450

Until recently, the vast majority of commercial TIMs utilized in the microelectronic industry have been produced by using physical blending technique. The most noteworthy aspect of this thesis study is that the polymer matrix nanocomposites were produced using a click chemistry approach based on the chemical bond formation between the filler and matrix. The advantage of this technique has been evidently demonstrated by each characterization studies. As a result, the presence of chemical connections between inorganic filler and polymer matrices has been proven in all nanocomposites generated via click chemistry, and the superiority of these nanocomposites over their chemical bond-free counterparts has been established.

Thermal resistance is an essential characteristic in TIM applications since it provides information about the material's usability across a wide temperature range. Given the thermal investigation findings of polymer nanocomposites produced with three different matrices in this work, it is evident that materials compatible for utilization even at high temperatures.

The major focus of the thesis is the investigation of thermal conductivity of the polymer nanocomposites. It has been clearly seen that the termal conductivity of nanocomposites bearing the chemical interaction (Polymer-SNNS) increases more

than the thermal conductivity of nanocomposites produced by physical blending (Polymer+SNNS).

PEEK-SNNS has shown the highest thermal conductivity of 0.670 $Wm^{-1}.K^{-1}$ in all nanocomposites synthesized through click chemistry approach, due to its semi-crystalline nature.

Thermal conductivities of nanocomposites developed for the thesis study were found to be lower than those of commercial TIMs. By utilizing a combination of 2D and 3D nanofillers as well as single and hybrid applications of nanofillers with greater thermal conductivity such as BN, Al_2O_3, SiO_2, SiC, etc., nanocomposites with greater thermal conductivities can be produced.

Another critical parameter for TIM applications is having the high electrical resistance. Given that the volume resistance values of the nanocomposites produced in the scope of this study are in the range of 10^{14}-10^{18} Ω.cm, it can be predicted that they would not create any short circuit or other problems in computer circuit components.

This thesis study, which demonstrates the superiority of the chemical technique over the physical method in termal interface material design, ensures that it will meet the demands in various new generation industries with regarding thermal conductive nanocomposite materials by adjusting various matrix-filler combinations.

REFERENCES

[1] **Squitieri, V.** (1989). U.S. Patent No. 4,869,954. Woburn, MA: U.S Patent and Trademark Office.

[2] **Razeeb, K. and Dalton, E.** (2011). Nanowire-Polymer Nanocomposites as Thermal Interface Material, *Advances in Nanocomposites-Synthesis, Characterization and Industrial Applications*, IntechOpen2011.

[3] **Muratov, D. S., Kuznetsov, D. V., Il'inykh, I. A., Burmistrov, I. N. and Mazov, I. N.**. (2015). Thermal conductivity of polypropylene composites filled with silane-modified hexagonal BN, *Composites Science and Technology*, *111*, 40-43.

[4] **Burger, N., Laachachi, A., Ferriol, M., Lutz, M., Toniazzo, V. and Ruch, D.** (2016). Review of thermal conductivity in composites: Mechanisms, parameters and theory, *Progress in Polymer Science*, *61*, 1-28.

[5] **Sato, K., Ijuin, A. and Hotta, Y.** (2015). Thermal conductivity enhancement of alumina/polyamide composites via interfacial modification, *Ceramics International*, *41*(8), 10314-10318.

[6] **Xu, Y., Chung, D. and Mroz, C.** (2001). Thermally Conducting Aluminum Nitride Polymer-Matrix Composites, *Composites Part A: Applied Science and Manufacturing*, *32*(12), 1749-1757.

[7] **Huang, X., Iizuka, T., Jiang, P., Ohki, Y. and Tanaka, T.** (2012). Role of Interface on the Thermal Conductivity of Highly Filled Dielectric Epoxy/AlN Composites, *The Journal of Physical Chemistry C*, *116*(25), 13629-13639.

[8] **Hong, H., Kim, J. and Kim, T.-i.** (2017). Effective Assembly of Nano-Ceramic Materials for High and Anisotropic Thermal Conductivity in a Polymer Composite, *Polymers*, *9*(9), 413.

[9] **Song, N., Hou, X., Chen, L., Cui, S., Shi, L. and Ding, P.** (2017). A Green Plastic Constructed from Cellulose and Functionalized Graphene with High Thermal Conductivity, *ACS Applied Materials & Interfaces*, *9*(21), 17914-17922.

[10] **Cui, S., Song, N., Shi, L. and Ding, P.** (2020). Enhanced Thermal Conductivity of Bioinspired Nanofibrillated Cellulose Hybrid Films Based on Graphene Sheets and Nanodiamonds, *ACS Sustainable Chemistry & Engineering*, *8*(16), 6363-6370.

[11] **Yao, Y., Zeng, X., Guo, K., Sun, R. and Xu, J.-b.** (2015). The effect of interfacial state on the thermal conductivity of functionalized Al2O3 filled glass fibers reinforced polymer composites, *Composites Part A: Applied Science and Manufacturing*, *69*, 49-55.

[12] **Hai, D., Lianhua, F. and Wong, C. P.** (2005). Effect of interface on thermal conductivity of polymer composite, *Proceedings Electronic Components and Technology, 2005. ECTC '05*. IEEE, p. 1451-1454. Lake Buena Vista, FL, USA, 31 May-3 June.

[13] **Ivanoska-Dacikj, A. and Bogoeva-Gaceva, G.** (2019). Chapter Two - Fabrication Methods of Carbon-Based Rubber Nanocomposites. In S. Yaragalla, S. Thomas, H.J. Maria (Eds), *Carbon-Based Nanofillers and Their Rubber Nanocomposites* (pp. 27-47). Elsevier.

[14] **Delogu, F., Gorrasi, G. and Sorrentino, A.** (2017). Fabrication of Polymer Nanocomposites via Ball Milling: Present status and future perspectives, *Progress in Materials Science*, *86*, 75-126.

[15] **Wang, M., Galpaya, D., Lai, Z., Xu, Y. and Yan, C.** (2014). Surface functionalization on the thermal conductivity of graphene–polymer nanocomposites, *International Journal of Smart and Nano Materials*, *5*(2), 123-132.

[16] **Zhou, W.** (2011). Effect of coupling agents on the thermal conductivity of aluminum particle/epoxy resin composites, *Journal of Materials Science*, *46*(11), 3883-3889.

[17] **Song, N., Cao, D., Luo, X., Wang, Q., Ding, P. and Shi**, **L.** (2020). Highly thermally conductive polypropylene/graphene composites for thermal management, *Composites Part A: Applied Science and Manufacturing*, *135*, 105912.

[18] **Zou, H., Wu, S. and Shen, J.** (2008). Polymer/Silica Nanocomposites: Preparation, Characterization, Properties, and Applications, *Chemical Reviews*, *108*(9), 3893-3957.

[19] **He, H., Fu, R., Shen, Y., Han, Y. and Song, X.** (2007). Preparation and properties of Si3N4/PS composites used for electronic packaging, *Composites Science and Technology*, *67*(11), 2493-2499.

[20] **Krishnamoorti, R.** (2001). Polymer Nanocomposites: Synthesis, Characterization, and Modeling. In R.A. Vaia (Ed.), *Journal of the American Chemical Society*, *124*(19), (pp. 5602-5603). Washington, DC.

[21] **Sundaram, A. and Velraj, R.** (2008). Thermal management of electronics: A review of literature, *Thermal Science - THERM SCI*, *12*(2), 5-26.

[22] **Khan, M.** (2012). *Thermally Conductive Polymer Composites for Electronic Packaging Applications.* (Master thesis). UNIVERSITY of Toronto, Mechanical and Industrial Engineering, TORONTO.

[23] **Harper, C. A.** (2000). *Electronic Packaging and Interconnection Handbook*, McGraw-Hill Professional.

[24] **Liu, Y.** (2013). *Power Electronic Packaging: Design, Assembly Process, Reliability and Modeling*. Springer Science & Business Media.

[25] **Zweben, C.** (2001). Advanced composites and other advanced materials for electronic packaging thermal management. *In Proceedings International Symposium on Advanced Packaging Materials Processes, Properties and Interfaces* (IEEE Cat. No. 01TH8562) (pp. 360-365). IEEE.

[26] **Ekpu, M., Bhatti, R., Ekere, N. N. and Mallik, S.** (2011). Advanced thermal management materials for heat sinks used in microelectronics, *Proceedings of 18th European Microelectronics and Packaging Conference.* (pp. 1-8). IEEE.

[27] **Jiang, G., Diao, L. and Kuang, K.** (2013). *Advanced Thermal Management Materials.* Springer Science & Business Media.

[28] **Zweben, C.** (1998). Advances in composite materials for thermal management in electronic packaging, *JOM*, *50*(6), 47-51.

[29] **Garimella, S. V., Fleischer, A. S., Murthy, J. Y., Keshavarzi, A., Prasher, R., Patel, C., ….. Raad, P. E.** (2008). Thermal Challenges in Next-Generation Electronic Systems, *IEEE Transactions on Components and Packaging Technologies*, *31*(4), 801-815.

[30] **Watari, S. L. S. K.** (2001). High Thermal Conductivity Materials, *MRS Bull.*, *26*(6), 440-441.

[31] **Abo Ras, M., Wunderle, B., May, D., Schacht, R., Winkler, T., Rzepka, S. ….. Michel, B.** (2014). Limitations and accuracy of steady state technique for thermal characterization of solid and composite materials. *In 15th International Conference on Thermal, Mechanical and Mulit-Physics Simulation and Experiments in Microelectronics and Microsystems (EuroSimE)* (pp. 1-7). IEEE.

[32] **Tong, X.** (2011). *Advanced Materials for Thermal Management of Electronic Packaging*. Springer Science & Business Media.

[33] **Cui, Y., Li, M. and Hu, Y.** (2020). Emerging interface materials for electronics thermal management: experiments, modeling, and new opportunities, *Journal of Materials Chemistry C*, *8*(31), 10568-10586.

[34] **Idumah, C. and Hassan, A.** (2016). Recently emerging trends in thermal conductivity of polymer nanocomposites, *Reviews in Chemical Engineering*, *32*(4), 413-457.

[35] **Sun Lee, W. and Yu, J.** (2005). Comparative study of thermally conductive fillers in underfill for the electronic components, *Diamond and Related Materials*, *14*(10), 1647-1653.

[36] **Mamunya, Y. P., Valeriy, D., Pissis, P. and Lebedev, E. V.**. (2002). Electrical and thermal conductivity of polymers filled with metal powders, *European Polymer Journal*, *38*(9), 1887-1897.

[37] **Sofian, N., Rusu, M., Neagu, R. and Neagu, E. R.** (2001). Metal Powder-Filled Polyethylene Composites. V. Thermal Properties, *Journal of Thermoplastic Composite Materials*, *14*(1), 20-33.

[38] **Debelak, B. and Lafdi, K.**. (2007). Use of exfoliated graphite filler to enhance polymer physical properties, *Carbon*, *45*(9), 1727-1734.

[39] **Yu, H., Li, L., Kido, T., Xi, G., Guangchen, X. and Guo, F.** (2012). Thermal and insulating properties of epoxy/aluminum nitride composites used for thermal interface material, *Journal of Applied Polymer Science*, *124*(1), 669-677.

[40] **Shen, D., Zhan, Z., Liu, Z., Cao, Y., Zhou, L., Liu, Y., ….. Yu, J.** (2017). Enhanced thermal conductivity of epoxy composites filled with silicon carbide nanowires, *Scientific Reports*, *7*(1), 2606.

[41] **Ren, F., Ren, P.-g., Di, Y.-y., Chen, D.-m. and Liu, G.-g.**. (2011). Thermal, Mechanical and Electrical Properties of Linear Low-Density Polyethylene Composites Filled with Different Dimensional SiC Particles, *Polymer-Plastics Technology and Engineering*, *50*(8), 791-796.

[42] **Kusunose, T., Yagi, T., Firoz, S. and Sekino, T.** (2013). Fabrication of epoxy/silicon nitride nanowire composites and evaluation of their thermal conductivity, *Journal of Materials Chemistry A: Materials for Energy and Sustainability*, *1*(10), 3440-3445.

[43] **Xie, C., Han, Y. and Zhao, R.** (2016). Highly thermal conductivity silicon nitride/carbon fibres/bismaleimide composites, *Polymer Composites*, *37*(2), 468-471.

[44] **Wong, C. P. and Bollampally, R. S.** (1999). Thermal conductivity, elastic modulus, and coefficient of thermal expansion of polymer composites filled with ceramic particles for electronic packaging, *Journal of Applied Polymer Science*, *74*(14), 3396-3403.

[45] **Zeng, J., Fu, R., Shen, Y., He, H. and Song, X.** (2009). High thermal conductive epoxy molding compound with thermal conductive pathway, *Journal of Applied Polymer Science*, *113*(4), 2117-2125.

[46] **Yu, S., Hing, P. and Hu, X.** (2002). Thermal conductivity of polystyrene–aluminum nitride composite, *Composites Part A: Applied Science and Manufacturing*, *33*(2), 289-292.

[47] **Zhou, W., Qi, S., An, Q., Zhao, H. and Liu, N.**. (2007). Thermal conductivity of boron nitride reinforced polyethylene composites, *Materials Research Bulletin*, *42*(10), 1863-1873.

[48] **Lin, Z., McNamara, A., Liu, Y., Moon, K.-s. and Wong, C. P.** (2014). Exfoliated hexagonal boron nitride-based polymer nanocomposite with enhanced thermal conductivity for electronic encapsulation, *Composites Science and Technology*, *90*, 123–128.

[49] **Watari, K.** (2001). High Thermal Conductivity Non-Oxide Ceramics, *Journal of the Ceramic Society of Japan*, *109*(1265), S7-S16.

[50] **Slack, G. A., Tanzilli, R. A., Pohl, R. O. and Vandersande, J. W.** (1987). The intrinsic thermal conductivity of AIN, *Journal of Physics and Chemistry of Solids*, *48*(7), 641-647.

[51] **Zhou, Y., Hyuga, H., Kusano, D., Yoshizawa, Y.-I., Ohji, T. and Hirao, K.** (2015). Development of high-thermal-conductivity silicon nitride ceramics, *Journal of Asian Ceramic Societies*, *3(*3*), 221-229.*

[52] **Hirao, K., Zhou, Y., Hyuga, H., Ohji, T. and Kusano, D.** (2012). High Thermal Conductivity Silicon Nitride Ceramics, *Journal of the Korean Ceramic Society*, *49*(4), 380-384.

[53] **Riley, F. L.** (2000). Silicon nitride and related materials, *Journal of the American Ceramic Society*, *83*(2), 245-265.

[54] **Zhou, Y., Hyuga, H., Kusano, D., Yoshizawa, Y.-I. and Hirao, K.**. (2011). A Tough Silicon Nitride with High Thermal Conductivity, *Advanced materials (Deerfield Beach, Fla.)*, *23*(39), 4563-4567.

[55] **Sarin, V. K.**. (1988). On the α-to-β phase transformation in silicon nitride, *Materials Science and Engineering: A*, *105*, 151-159.

[56] **Meléndez-Martínez, J. J. and Domínguez-Rodríguez, A.** (2004). Creep of silicon nitride, *Progress in Materials Science*, *49*(1), 19-107.

[57] **Hirao, K., Watari, K., Hayashi, H. and Kitayama, M.** (2011). High Thermal Conductivity Silicon Nitride Ceramic, *MRS Bulletin*, *26*(6), 451-455.

[58] **Krstic, Z. and Krstic, V. D.**. (2012). Silicon nitride: the engineering material of the future, *Journal of Materials Science*, *47*(2), 535-552.

[59] **Yoonessi, M. and Gaier, J. R.** (2010). Highly Conductive Multifunctional Graphene Polycarbonate Nanocomposites, *ACS Nano*, *4*(12), 7211-7220.

[60] **Kardos, J. L., Cheng, F. S. and Tolbert, T. L.**. (1973). Tailoring the interface in graphite-reinforced polycarbonate, *Polymer Engineering & Science*, *13*(6), 455-461.

[61] **Ding, P., Su, S., Song, N., Tang, S., Liu, Y. and Shi, L.** (2014). Highly thermal conductive composites with polyamide-6 covalently-grafted graphene by an in situ polymerization and thermal reduction process, *Carbon*, *66*, 576-584.

[62] **Li, X., Shao, L., Song, N., Shi, L. and Ding, P.** (2016). Enhanced thermal-conductive and anti-dripping properties of polyamide composites by 3D graphene structures at low filler content, *Composites Part A: Applied Science and Manufacturing*, *88*, 305-314.

[63] **Mkhabela, V. J., Mishra, A. K. and Mbianda, X. Y.** (2011). Thermal and mechanical properties of phosphorylated multiwalled carbon nanotube/polyvinyl chloride composites, *Carbon*, *49*(2), 610-617.

[64] **Shen, S., Henry, A., Tong, J., Zheng, R. and Chen, G.** (2010). Polyethylene nanofibres with very high thermal conductivities, *Nature Nanotechnology*, *5*(4), 251-255.

[65] **Luo, X. and Chung, D.** (2002). Lithium Doped Polyethylene-Glycol-Based Thermal Interface Pastes for High Thermal Contact Conductance, *Journal of Electronic Packaging*, *124*(3), 188-191.

[66] **Manias, E., Touny, A., Wu, L., Strawhecker, K., Lu, B. and Chung, T. C.** (2001). Polypropylene/Montmorillonite Nanocomposites. Review of the Synthetic Routes and Materials Properties, *Chemistry of Materials*, *13*(10), 3516-3523.

[67] **Miltner, H. E., Grossiord, N., Lu, K., Loos, J., Koning, C. E. and Van Mele, B.** (2008). Isotactic Polypropylene/Carbon Nanotube Composites Prepared by Latex Technology. Thermal Analysis of Carbon Nanotube-Induced Nucleation, *Macromolecules*, *41*(15), 5753-5762.

[68] **And, U. L.** (1998). *Commercial Polymer Blends*, Boston, MA, Springer.

[69] **Göktaş, M.** (2016). *Effects of Boron Compound on Characteristics of Poly(Methyl Methacrylate) and Its Nanocomposites*. (Master thesis). MIDDLE East Technical University, The Graduate School Of Natural And Applied Sciences, ANKARA.

[70] **Ali, U., Abd Karim, K. J. and Buang, N.** (2015). A Review of the Properties and Applications of Poly (Methyl Methacrylate) (PMMA), *Polymer Reviews*, *55*(4), 1-28.

[71] **Wang, J.-S. and Matyjaszewski**, **K.** (1995). Controlled/"living" radical polymerization. atom transfer radical polymerization in the presence of transition-metal complexes, *Journal of the American Chemical Society*, *117*(20), 5614-5615.

[72] **Grimaud, T. and Matyjaszewski, K.** (1997). Controlled/“Living” Radical Polymerization of Methyl Methacrylate by Atom Transfer Radical Polymerization, *Macromolecules*, *30*(7), 2216-2218.

[73] **Mehranpour, S.** (2019). *Comparison of Beta, Neutron and Gamma Attenuation Properties of PMMA/Colemanite Composites*. (Master thesis). Istanbul Technical University, Nuclear Researches Division, ISTANBUL.

[74] **Thomas, P., Ravindran, R. S. E. and Varma, K. B. R.**. (2012). Dielectric properties of Poly(methyl methacrylate) (PMMA)/CaCu3Ti4O12 composites, *In 10th International Conference on the Properties and Applications of Dielectric Materials*, IEEE, Bangalore, India, 24-28 July (pp. 1-4).

[75] **Pullanchiyodan, A., Nair, K. S. and Surendran, K. P.** (2017). Silver-Decorated Boron Nitride Nanosheets as an Effective Hybrid Filler in PMMA for High-Thermal-Conductivity Electronic Substrates, *ACS Omega*, *2*(12), 8825-8835.

[76] **Yilmaz, E.** (2011). *Preparation And Characterization Of Polymer Composites Containing Gold Nanoparticles*, (Doctorate thesis). BILKENT University, The Graduate School of Engineering and Science. ANKARA.

[77] **Harper, E. M. P. C. A.** (2003). *Plastics Materials and Processes: A Concise Encyclopedia*, John Wiley & Sons.

[78] **Dizman, C.** (2013). *Polysulfone Based Oligomers as Precursors for Networks and Block Copolymers*. (Doctorate thesis). ISTANBUL Technical University, Graduate School of Science, Engineering and Tehnology, ISTANBUL.

[79] **DeMeuse, M. T.** (2014). Polysulfones as a reinforcement in high temperature polymer blends. In Mark T. DeMeuse (Ed.) *High Temperature Polymer Blends (*pp. *165-173)*. USA: Woodhead Publishing.

[80] **Alkan, B.** (2014). *Polysulfone-Based Amphiphilic Polymers, Department of Polymer Science and Technology*. (Master thesis). ISTANBUL Technical University, Graduate School of Science, Engineering and Tehnology, ISTANBUL.

[81] **Magurudeniya, H., Huang, P., Gunathilake, S., Rainbolt, E., Biewer, M. and Stefan, M.** (2014). *Encyclopedia of Polymer Science and Technology*. Wiley-Interscience.

[82] **Yilmaz, N.** (2016). *Fabrication, Characterization And Antibacterial Performances Of Composite Polysulfone Membranes Including Graphene Oxide Nanoparticles*, (Master thesis). ISTANBUL Technical University, Graduate School of Science, Engineering and Tehnology, ISTANBUL.

[83] **Sastri, V. R.**. (2010). Chapter 8 - High-Temperature Engineering Thermoplastics: Polysulfones, Polyimides, Polysulfides, Polyketones, Liquid Crystalline Polymers, and Fluoropolymers. In V.R. Sastri (Ed.), *Plastics in Medical Devices. Properties, Requirements and Applications*. (1st ed., pp. 175-215). Boston : William Andrew Publishing.

[84] **Aerts, P., Van Hoof, E., Leysen, R., Vankelecom, I. F. J. and Jacobs, P. A.** (2000). Polysulfone–Aerosil composite membranes: Part 1. The influence of the addition of Aerosil on the formation process and membrane morphology, *Journal of Membrane Science*, *176*(1), 63-73.

[85] **Sánchez, S., Pumera, M., Cabruja, E. and Fàbregas, E.** (2007). Carbon nanotube/polysulfone composite screen-printed electrochemical enzyme biosensors, *Analyst*, *132*(2), 142-147.

[86] **Kuroiwa, T., Miyagishi, T., Ito, A., Matsuguchi, M., Sadaoka, Y. and Sakai, Y.** (1995). A thin-film polysulfone-based capacitive-type relative-humidity sensor, *Sensors and Actuators B: Chemical*, *25*(1), 692-695.

[87] **Karlsson, L. E. and Jannasch, P.** (2004). Polysulfone ionomers for proton-conducting fuel cell membranes: sulfoalkylated polysulfones, *Journal of Membrane Science*, *230*(1), 61-70.

[88] **Lufrano, F., Gatto, I., Staiti, P., Antonucci, V. and Passalacqua, E.** (2001). Sulfonated polysulfone ionomer membranes for fuel cells, *Ž . Solid State Ionics*, *145*(1-4), 47-51.

[89] **Manea, C. and Mulder, M.** (2002). Characterization of polymer blends of polyethersulfone/sulfonated polysulfone and polyethersulfone/sulfonated polyetheretherketone for direct methanol fuel cell applications, *Journal of Membrane Science*, *206*(1), 443-453.

[90] **Sivaraman, K., Kellenberger, C., Pané, S., Ergeneman, O., Lühmann, T., Luechinger, N., ….. Nelson, B.** (2012). Porous polysulfone coatings for enhanced drug delivery, *Biomedical microdevices*, *14*(3), 603-12.

[91] **Tomaszewska, M. and Jarosiewicz, A.** (2004). Polysulfone coating with starch addition in CRF formulation, *Desalination*, *163*(1), 247-252.

[92] **Claes, L.** (1989). Carbon fiber reinforced polysulfone--a new implant material, *Biomed Tech (Berl)*, *34*(12), 315-9.

[93] **Trisca-Rusu, C., Nechifor, A. C., Mihai, S., Parvu, C., Voicu, S. I. and Nechifor, G.** (2009). Polysulfone-functionalized multiwalled carbon nanotubes composite membranes for potential sensing applications, In *2009 International Semiconductor Conference*, Sinaia, Romania, October 12-14, (Vol. 1, pp. 285-288). IEEE.

[94] **Kraemer, S., Puchner, M., Jannasch, P., Lundblad, A. and Lindbergh, G.** (2006). Gas Diffusion Electrodes and Membrane Electrode Assemblies Based on a Sulfonated Polysulfone for High-Temperature PEMFC, *Journal of The Electrochemical Society - J ELECTROCHEM SOC*, *153*(11), A2077.

[95] **Lau, W. W. Y. and Jiang, Y.** (1994). Performance of polysulfone/carboxylated polysulfone membranes, *Polymer International*, *33*(4), 413-417.

[96] **Francis, B., Ramaswamy, R., Lakshmana Rao, V. and Thomas, S.** (2006). Toughening of Diglycidyl Ether of Bisphenol-A Epoxy Resin Using Poly (Ether Ether Ketone) with Pendent Ditert-Butyl Groups, *International Journal of Polymeric Materials and Polymeric Biomaterials*, *55*(9), 681-702.

[97] **Karthikeyan, L., Mathew, D. and Robert, T. M.** (2019). Poly(ether ether ketone)-bischromenes: Synthesis, characterization, and influence on thermal, mechanical, and thermo mechanical properties of epoxy resin, *Polymers for Advanced Technologies*, *30*(4), 1061-1071.

[98] **Zhao, Z., Gu, Y., Chao, D. and Liu, X.** (2019). Synthesis and properties of shape memory poly(aryl ether ketone)s, *European Polymer Journal*, *116*, 336-341.

[99] **Bhattacharyya, S. and Moiz, A.A**. (2018). PEEK: A Unique Choice With A Wide Spectrum Use, *International Journal of Advance Research and Innovative Ideas in Education*, *4*(6), 8-11.

[100] **Collyer, A. A.** (1990). Chapter 4 - High-temperature engineering thermoplastics, *A Practical Guide to the Selection of High-Temperature Engineering Thermoplastics* (pp.53-76). Oxford : Elsevier.

[101] **Rogers, M., Long, T. and Turner, S.** (2003). *Synthetic Methods in Step-Growth Polymers.* John Wiley & Sons.

[102] **Dahl, K. J. J., and In, V.** (1995). *Polymers and Other Advanced Materials,* Boston, MA.: Springer.

[103] **Shukla, D., Negi, Y. S., Uppadhyaya, J. S. and Kumar, V.** (2012). Synthesis and Modification of Poly(ether ether ketone) and their Properties: A Review, *Polymer Reviews*, *52*(2), 189-228.

[104] **Moore, A. L. and Shi, L.** (2014). Emerging challenges and materials for thermal management of electronics, *Materials Today*, *17*(4), 163-174.

[105] **Leung, S. N.** (2018). Thermally conductive polymer composites and nanocomposites: Processing-structure-property relationships, *Composites Part B: Engineering*, *150*,78-92.

[106] **Tritt, T. M.** (2004). *Thermal Conductivity: Theory, Properties, and Applications,* Boston, MA.: Springer.

[107] **iang, G., Diao, Liyong, Kuang, Ken**. (2013). *Advanced Thermal Management Materials*, New York, NY.: Springer-Verlag.

[108] **Acres, R. G., Ellis, A. V., Alvino, J., Lenahan, C. E., Khodakov, D. A., Metha, G. F. ….. Andersson, G. G.** (2012). Molecular Structure of 3-Aminopropyltriethoxysilane Layers Formed on Silanol-Terminated Silicon Surfaces, *The Journal of Physical Chemistry C*, *116*(10), 6289-6297.

[109] **Bansal, A., Yang, H., Li, C., Benicewicz, B. C., Kumar, S. K. and Schadler, L. S.** (2006). Controlling the thermomechanical properties of polymer nanocomposites by tailoring the polymer–particle interface, *Journal of Polymer Science Part B: Polymer Physics*, *44*(20), 2944-2950.

[110] **Akabri, B., Pirhadi Tavandashti, M. and Zandrahimi, M.** (2011). Particle size characterization of nanoparticles - A practical approach, *Iranian Journal of Materials Science and Engineering*, *8*(2), 48-56.

[111] **Alexandre, M. and Dubois, P.** (2000). Polymer-Layered Silicate Nanocomposites: Preparation, Properties and Uses of a New Class of Materials, *Materials Science and Engineering: R: Reports*, *28*(1-2), 1-63.

[112] **Pang, C., Lee, J. W. and Kang, Y. T.** (2015). Review on combined heat and mass transfer characteristics in nanofluids, *International Journal of Thermal Sciences*, *87*, 49-67.

[113] **Kausar, A.** (2020). Thermally conducting polymer/nanocarbon and polymer/inorganic nanoparticle nanocomposite: a review, *Polymer-Plastics Technology and Materials*, *59*(8), 895-909.

[114] **Toberer, E. S., Baranowski, L. L. and Dames, C.** (2012). Advances in Thermal Conductivity, *Annual Review of Materials Research*, *42*(1), 179-209.

[115] **Lim, K., Kim, S.-K. and Chung, M.** (2009). Improvement of the thermal diffusivity measurement of thin samples by the flash method, *Thermochimica Acta*, *494*(1-2), 71–79.

[116] **Ho, R. W. P. C., Liley, P E**. (1974). Thermal Conductivity of the Elements: A Comprehensive Review, *American Institute of Physics*, *3*(1), 1-796.

[117] **Goodson, K. and Flik, M.** (1994). Solid Layer Thermal-Conductivity Measurement Techniques, *Applied Mechanics Reviews - APPL MECH REV*, *47*(3), 101-112.

[118] **Xu, X., Chen, J., Zhou, J. and Li, B.**. (2018). Thermal Conductivity of Polymers and Their Nanocomposites, *Advanced Materials*, *30*(17), 1705544.

[119] **Ebadi-Dehaghani, H. and Nazempour, M.** (2012). Thermal Conductivity of Nanoparticles Filled Polymers, *Smart Nanoparticles Technology*, 519-540.

[120] **Ellis, B., & Smith, R.** (2008). *Polymers: A Property Database*, Boca Raton, CRC Press.

[121] **Anderson, D. R.**. (1966). Thermal Conductivity of Polymers, *Chemical Reviews*, *66*(6), 677-690.

[122] **Erwin Baur, K, O., Brinkmann, S., Osswald, T. A.** (2006). *International Plastics Handbook : The Resource for Plastics Engineers*. Hanser Publications.

[123] **Choy, C. L.** (1977). Thermal conductivity of polymers, *Polymer*, *18*(10), 984-1004.

[124] **Hassanzadeh-Aghdam, M. K., Mahmoodi, M. J. and Jamali, J.** (2018). Effect of CNT coating on the overall thermal conductivity of unidirectional polymer hybrid nanocomposites, *International Journal of Heat and Mass Transfer*, *124*, 190-200.

[125] **Mahmoodi, M. J., Hassanzadeh-Aghdam, M. and Ansari, R.** (2018). Overall thermal conductivity of unidirectional hybrid polymer nanocomposites containing SiO2 nanoparticles, *International Journal of Mechanics and Materials in Design*, *15*(3), 539-554.

[126] **Rethwisch, D. G.** (2016). *Fundamentals of Materials Science and Engineering: An Integrated Approach*, John Wiley High Education.

[127] **Rakesh, E. K., Gupta, K., Kim, K. J.** (2009). *Polymer Nanocomposites Handbook*, CRC Press.

[128] **Yüksel, N.** (2016). The Review of Some Commonly Used Methods and Techniques to Measure the Thermal Conductivity of Insulation Materials, *In Insulation materials in context of sustainability, IntechOpen.*

[129] **Palacios, A., Cong, L., Navarro, M. E., Ding, Y. and Barreneche, C.** (2019). Thermal conductivity measurement techniques for characterizing thermal energy storage materials – A review, *Renewable and Sustainable Energy Reviews*, *108*, 32-52.

[130] **Tzeng, J. J., Weber, T. W. and Krassowski, D. W.**. (2000). Technical review on thermal conductivity measurement techniques for thin thermal interfaces. *In Sixteenth Annual IEEE Semiconductor Thermal Measurement and Management Symposium*, 23 March, San Jose, CA, USA, (pp. 174-181). IEEE.

[131] **ASTM** (2006). Standard Test Method for Evaluating the Resistance of Thermal Transmission of Materials by the Guarded Heat Flow Meter Technique (ASTM E1530-06). Retrieved from

https://www.astm.org/e1530-06.html

[132] **Thomas, S., Stephen, R., Thomas, S. and Bandyopadhyay, S.** (2007). Polymer nanocomposites: Preparation, properties and applications, *Rubber Fibers Plastics International*, *2*, 49-56.

[133] **Gacitua, W., Ballerini, A. and Zhang, J.** (2005). Polymer Nanocomposites: Synthetic and Natural Fillers a Review, *Ciencia y tecnología*, *7*(3), 159-178.

[134] **Hamadneh, N., Khan, W. and Khan, W.** (2016). Polymer nanocomposites – synthesis techniques, classification and properties, *Science and applications of Tailored Nanostructures, 50.*

[135] **Oliveira, M. and Machado, A.** (2013). Preparation of Polymer-Based Nanocomposites by Different Routes. In X. Wang (Ed.), *Nanocomposites: Synthesis, Characterization and Applications. NOVA Publishers.*

[136] **Karak, N.** (2019). Fundamentals of Nanomaterials and Polymer Nanocomposites. In N. Karak (Ed.), *Nanomaterials and polymer nanocomposites* (1st ed., pp. 1-45). Elsevier.

[137] **Fawaz, J. and Mittal, V.** (2014). Synthesis of Polymer Nanocomposites: Review of Various Techniques. In V. Mittal (Ed.), *Synthesis techniques for polymer nanocomposites* (pp. 1-30). Wiley.

[138] **Mosnáčková, K., Kollár, J., Huang, Y.-S., Huang, C.-F. and Mosnáček, J.**. (2019). 1 - Synthesis Routes of Functionalized Nanoparticles, Polymer Composites with Functionalized Nanoparticles. In K. Pielichowski, T. Majka (Eds.), *Polymer Composites with Functionalized Nanoparticles* (1st ed., pp. 1-46). Elsevier.

[139] **Nguyen, T. A., Nguyen-Tri, P., Carriere, P. and Xuan, C.** (2018). Nanocomposite Coatings: Preparation, Characterization, Properties and Applications, *International Journal of Corrosion 2018*, 1-19.

[140] **Tavares, M. I. B., Silva, E. O. d., Silva, P. C. and L. Menezes, R. d.** (2018). Polymer Nanocomposites, *MRS bulletin*, *32*(4), 314-322.

[141] **Göçmen, B. A.**. (2018). *Fabrication And Characterization Of Novel Polymer/Organo-Mmt (Organo-Silica)/ Biopolymer Nanocomposite Blends By Reactive Extrusion*, *Nanotechnology and Nanomedicine*. (Doctorate thesis). HACETTEPE University, Graduate School of Science and Engineering, ANKARA.

[142] **Eken, A. E**. (2008). *Characterization of Magnetite Thin Films Produced By Sol-Gel Processing.* (Master thesis). MIDDLE East Technical University, The Graduate School of Natural and Applied Sciences, ANKARA.

[143] **Zaferani, S. H.** (2018). Introduction of polymer-based nanocomposites. In M. Jawaid, M.M. Khan (Eds.) *Polymer-based Nanocomposites for Energy and Environmental Applications* (1st ed., pp. 1-25). Woodhead Publishing.

[144] **Müller, K., Bugnicourt, E., Latorre, M., Jorda Beneyto, M., Echegoyen, Y., Lagaron, J. M., ….. Schmid, M.**. (2017). Review on the Processing and Properties of Polymer Nanocomposites and Nanocoatings and Their Applications in the Packaging, Automotive and Solar Energy Fields, *Nanomaterials*, *7*(4), 74.

[145] **Neşe, A.** (2006). *Syntheses And Characterization of Polymeric Nanocomposites Preperad By In-Situ Photopolymerization*. (Master thesis). BOĞAZİÇİ University, Institute of Graduate Studies in Science and Engineering, ISTANBUL.

[146] **Hanemann, T. and Szabó, D. V.** (2010). Polymer-Nanoparticle Composites: From Synthesis to Modern Applications, *Materials*, *3*(6), 3468-3517.

[147] **Yu, J., Li, J., Zhang, W. and Chang, H.** (2015). Synthesis of high quality two-dimensional materials via chemical vapor deposition, *Chemical Science*, *6*(12), 6705-6716.

[148] **Pottathara, Y. B., Grohens, Y., Kokol, V., Kalarikkal, N. and Thomas, S.** (2019). Synthesis and Processing of Emerging Two-Dimensional Nanomaterials, *Nanomaterials Synthesis: Design, Fabrication and Applications* (pp. 1-25). Elsevier.

[149] **Rattan, S.** (2015). Polymer nanocomposites using click chemistry: novel materials for hydrogen peroxide vapor sensors, *RSC Advances*, *5*(85), 69573-69582.

[150] **Lee, S. H., Dreyer, D. R., An, J., Velamakanni, A., Piner, R. D., Park, S., ….. Ruoff, R. S.** (2010). Polymer Brushes via Controlled, Surface-Initiated Atom Transfer Radical Polymerization (ATRP) from Graphene Oxide, *Macromolecular Rapid Communications*, *31*(3), 281-288.

[151] **Kolb, H. C., Finn, M. G. and Sharpless, K. B.** (2001). Click Chemistry: Diverse Chemical Function from a Few Good Reactions, *Angewandte Chemie International Edition*, *40*(11), 2004-2021.

[152] **Sume, B. and Vogt, A.** (2009). Macromolecular Engineering through Click Chemistry and Other Efficient Transformations, *Macromolecules*, *43*(1), 1-13.

[153] **Meldal, M. and Tornøe, C. W.** (2008). Cu-Catalyzed Azide−Alkyne Cycloaddition, *Chemical Reviews*, *108*(8), 2952-3015.

[154] **Sanchez-Sanchez, A., Perez Baen, I. and Pomposo, J.** (2013). Advances in Click Chemistry for Single-Chain Nanoparticle Construction, *Molecules (Basel, Switzerland)*, *8*(3), 3339-3355.

[155] **Semerci, E.** (2014). *Modification of Polybenzoxazine Precursors By Thiol-Benzoxazine Chemistry. As a Novel Thiol-X Reaction For Macromolecular Synthesis.* (Master thesis). ISTANBUL Technical University, Graduate School of Science Engineering and Technology, ISTANBUL.

[156] **Lowe, A., Hoyle, C. and Bowman, C.** (2010). Thiol-yne click chemistry: A powerful and versatile methodology for materials synthesis, *Journal of Materials Chemistry*, *20*(23), 4745-4750.

[157] **Tasdelen, M. A.** (2011). Diels-Alder "click" reactions: Recent applications in polymer and material science, *Polym. Chem.*, *2*(10), 2133-2145.

[158] **Šupová, M., Simha Martynková, G. and Cech Barabaszova, K.** (2010). Effect of Nanofillers Dispersion in Polymer Matrices: A Review, *Science of Advanced Materials*, *3*(1), 1-25.

[159] **Tessema, A., Zhao, D., Moll, J., Xu, S., Yang, R., Li, C., ….. Kidane, A.** (2017). Effect of filler loading, geometry, dispersion and temperature on thermal conductivity of polymer nanocomposites, *Polymer Testing*, *57*, 101-106.

[160] **Liu, J., Gao, Y., Cao, D., Zhang, L. and Guo, Z.** (2011). Nanoparticle Dispersion and Aggregation in Polymer Nanocomposites: Insights from Molecular Dynamics Simulation, *Langmuir*, *27*(12), 7926-7933.

[161] **Wu, Y., Ma, J. and Bao, Y.** (2018). Advances in Interfacial Interaction Within Polymer Matrix Nanocomposites, *Cailiao Daobao/Materials Review*, *32*(3), 434-442.

[162] **Fujigaya, T., Fukumaru, T. and Nakashima, N.** (2009). Evaluation of dispersion state and thermal conductivity measurement of carbon nanotubes/UV-curable resin nanocomposites, *Synthetic Metals*, *159*(9-10), 827-830.

[163] **Zhu, B. L., Wang, J., Zheng, H., Ma, J., Wu, J. and Wu, R.** (2015). Investigation of thermal conductivity and dielectric properties of LDPE-matrix composites filled with hybrid filler of hollow glass microspheres and nitride particles, *Composites Part B: Engineering*, *69*, 496-506.

[164] **Chen, J., Yan, L., Song, W. and Xu, D.** (2018). Interfacial characteristics of carbon nanotube-polymer composites: A review, *Composites Part A: Applied Science and Manufacturing*, *114*, 149-169.

[165] **Asakuma, Y. and Yamamoto, T.** (2016). Thermal analysis of resin composites with ellipsoidal filler considering thermal boundary resistance, *Journal of Thermal Science*, *25*(5), 424-430.

[166] **Fu, S., Sun, Z., Huang, P., Li, Y. and Hu, N.** (2019). Some basic aspects of polymer nanocomposites: A critical review, *Nano Materials Science*, *1*(1), 2-30.

[167] **Streletskii, A. N., Permenov, D. G., Bokhonov, B. B., Kolbanev, I. V., Leonov, A. V., Berestetskaya, I. V. and Streletzky, K. A.** (2009). Destruction, amorphization and reactivity of nano-BN under ball milling, *Journal of Alloys and Compounds*, *483*(1), 313-316.

[168] **Ng, H., Lu, X. and Lau, S.** (2005). Thermal conductivity of boron nitride-filled thermoplastics: Effect of filler characteristics and composite processing conditions, *Polymer Composites*, *26*(6), 778-790.

[169] **Huang, X., & Zhi, C.** (2016). *Polymer Nanocomposites*, Springer International Publishing.

[170] **Zhou, W., Wang, C., Ai, T., Wu, K., Zhao, F. and Gu, H.** (2009). A novel fiber-reinforced polyethylene composite with added silicon nitride particles for enhanced thermal conductivity, *Composites Part A: Applied Science and Manufacturing*, *40*(6), 830-836.

[171] **Lu, X. and Xu, G.** (1997). Thermally conductive polymer composites for electronic packaging, *Journal of Applied Polymer Science*, *65*(13), 2733-2738.

[172] **Nicolosi, V., Chhowalla, M., Kanatzidis, M. G., Strano, M. S. and Coleman, J. N.** (2013). Liquid Exfoliation of Layered Materials, *Science*, *340*(6139).

[173] **Coleman, J., Lotya, M., Gallagher, A., Bergin, S., King, P., Khan, U., ….. Nicolosi, V.** (2011). Two-Dimensional Nanosheets Produced by Liquid Exfoliation of Layered Materials, *Science (New York, N.Y.)*, *331*(6017), 568-571.

[174] **Hernandez, Y., Nicolosi, V., Lotya, M., Blighe, F., Sun, Z., De, S., ….. Coleman, J.** (2008). High-yield production of graphene by liquid-phase exfoliation of graphite, *Nature Nanotechnology*, *3*(9), 563-568.

[175] **Backes, C., Higgins, T., Kelly, A., Boland, C., Harvey, A., Hanlon, D. ….. Coleman, J.** (2016). Guidelines for Exfoliation, Characterisation and Processing of Layered Materials Produced by Liquid Exfoliation, *Chemistry of Materials*, *29*(1), 243-255.

[176] **Yao, Y., Lin, Z., Li, Z., Song, X., Moon, K.-s. and Wong, C. P.** (2012). Large-scale production of two-dimensional nanosheets, *J. Mater. Chem.*, *22*(27), 13494-13499.

[177] **Gao, W., Zhao, Y. and Yin, H.** (2018). Lateral size selection of liquid exfoliated hexagonal boron nitride nanosheets, *RSC Advances*, *8*(11), 5976-5983.

[178] **Jan, R., May, P., Bell, A. P., Habib, A., Khan, U. and Coleman, J. N.**. (2014). Enhancing the mechanical properties of BN nanosheet–polymer composites by uniaxial drawing, *Nanoscale*, *6*(9), 4889-4895.

[179] **Kuang, Z., Chen, Y., Lu, Y., Liu, L., Hu, S., Wen, S., ….. Zhang, L.** (2015). Fabrication of Highly Oriented Hexagonal Boron Nitride Nanosheet/Elastomer Nanocomposites with High Thermal Conductivity, *Small*, *11*(14), 1655-1659.

[180] **Khan, U., May, P., O'Neill, A., Bell, A. P., Boussac, E., Martin, A., ….. Coleman, J. N.** (2013). Polymer reinforcement using liquid-exfoliated boron nitride nanosheets, *Nanoscale*, *5*(2), 581-587.

[181] **Gao, E., Lin, S.-Z., Qin, Z., Buehler, M. and Xu, Z.** (2018). Mechanical Exfoliation of Two-Dimensional Materials, *Journal of the Mechanics and Physics of Solids*, *115*, 248-262.

[182] **Yu, Q., Liu, Q., Li, X., Chen, Z., Ren, T., Chen, Z. ….. Huang, Z.** (2020). Research on Preparation Process of Graphene by Modified Ball Milling and Its Thermal Properties, *IOP Conference Series: Materials Science and Engineering*, *735*(1):012011.

[183] **Li, H., Wu, J., Yin, Z. and Zhang, H.** (2014). Preparation and Applications of Mechanically Exfoliated Single-Layer and Multilayer MoS2 and WSe2 Nanosheets, *Accounts of Chemical Research*, *47*(4), 1067-1075.

[184] **Yuan, L., Ge, J., Peng, X., Zhang, Q., Wu, Z., Jian, Y., ….. Han, J.** (2016). A reliable way of mechanical exfoliation of large scale two dimensional materials with high quality, *AIP Advances*, *6*(12), 125201.

[185] **Ye, B., Chongwei, A., Zhang, Y., Song, C., Geng, X. and Wang, J.** (2018). One-Step Ball Milling Preparation of Nanoscale CL-20/Graphene Oxide for Significantly Reduced Particle Size and Sensitivity, *Nanoscale Research Letters*, *13*(1), 1-8.

[186] **Baheti, V., Abbasi, A. M. R. and Militky, J.** (2012). Ball milling of jute fibre wastes to prepare nanocellulose, *World Journal of Engineering*, *9*(1), 45-50.

[187] **Chauruka, S. R., Hassanpour, A., Brydson, R., Roberts, K. J., Ghadiri, M. and Stitt, H.** (2015). Effect of mill type on the size reduction and phase transformation of gamma alumina, *Chemical Engineering Science*, *134*, 774-783.

[188] **Yang, W., Xu, J., Niu, L., Kang, C. and Ma, B.** (2018). Effects of high energy ball milling on mechanical and interfacial properties of PBT/nano-Sb2O3 composites, *Journal of Adhesion Science and Technology*, *32*(3), 291-301.

[189] **Teng, C., Xie, D., Wang, J., Yang, Z., Ren, G. and Zhu, Y.** (2017). Ultrahigh Conductive Graphene Paper Based on Ball-Milling Exfoliated Graphene, *Advanced Functional Materials*, *27*(20), 1700240.

[190] **Yao, Y., Lin, Z., Li, Z., Song, X., Moon, K. S. and Wong, C.P.** (2012). Large-scale production of two-dimensional nanosheets, *Journal of Materials Chemistry*, *22*(27), 13494-13499.

[191] **Deng, S., Qi, X. D., Zhu, Y. I., Zhou, H. J. and Fu, Q.** (2016). A facile way to large-scale production of few-layered graphene via planetary ball mill, *Chinese Journal of Polymer Science*, *34*(10), 1270-1280.

[192] **Chen, Y., Mateti, A., Srikanth, S.** (2017). *European Patent No. EP 3468913 (A1)*. Retrieved from Scopus.

[193] **Yuan, L., Ge, J., Peng, X., Zhang, Q., Wu, Z., Jian, Y., ….. Han, J.** (2016). A reliable way of mechanical exfoliation of large scale two dimensional materials with high quality, *AIP Advances*, *6*(12), 125201.

[194] **Gao, E., Lin, S.-Z., Qin, Z., Buehler, M. J., Feng, X.-Q. and Xu, Z.** (2018). Mechanical exfoliation of two-dimensional materials, *Journal of the Mechanics and Physics of Solids*, *115*, 248-262.

[195] **Nath, A. K., Jiten, C. and Singh, K. C.** (2010). Influence of ball milling parameters on the particle size of barium titanate nanocrystalline powders, *Physica B: Condensed Matter*, *405*(1), 430-434.

[196] **Zemlyanskaya, A., Shishkin, R., Kudiakova, V., Yuferov, Y. and Zykov, F.** (2019). The study of TIM polymer composite materials thermal conductivity. In AIP Conference Proceedings. *Proceedings of the VI International Young Researchers Conference*, Ekaterinburg, Russian Federation, 6 December.

[197] **Vadivelu, M. A., Kumar, C. R. and Joshi, G. M.**. (2016). Polymer composites for thermal management: a review, *Composite Interfaces*, *23*(9), 847-872.

[198] **Vo, V. S., Mahouche-Chergui, S., Nguyen, V. H., Naili, S. and Carbonnier, B.** (2019). Crucial Role of Covalent Surface Functionalization of Clay Nanofillers on Improvement of the Mechanical Properties of Bioepoxy Resin, *ACS Sustainable Chemistry & Engineering*, *7*(18), 15211-15220.

[199] **Rong, M., Zhang, M. and Ruan, W.** (2006). Surface modification of nanoscale fillers for improving properties of polymer nanocomposites: A review, *Materials Science and Technology*, *22*(7), 787-796.

[200] **Bula, K., Jesionowski, T., Krysztafkiewicz, A. and Janik, J.** (2007). The effect of filler surface modification and processing conditions on distribution behaviour of silica nanofillers in polyesters, *Colloid and Polymer Science*, *285*(11), 1267-1273.

[201] **Guo, Z., Pereira, T., Choi, O., Wang, Y. and Hahn, H. T.** (2006). Surface functionalized alumina nanoparticle filled polymeric nanocomposites with enhanced mechanical properties, *Journal of Materials Chemistry*, *16*(27), 2800-2808.

[202] **Hui, C. M., Pietrasik, J., Schmitt, M., Mahoney, C., Choi, J., Bockstaller, M. R. ….. Matyjaszewski, K.** (2014). Surface-Initiated Polymerization as an Enabling Tool for Multifunctional (Nano-)Engineered Hybrid Materials, *Chemistry of Materials*, *26*(1), 745-762.

[203] **Dach, B. I., Rengifo, H. R., Turro, N. J. and Koberstein, J. T.** (2010). Cross-Linked "Matrix-Free" Nanocomposites from Reactive Polymer−Silica Hybrid Nanoparticles, *Macromolecules*, *43*(16), 6549-6552.

[204] **Su, F. and Zhang, S.** (2014). Tribological Properties of Polyimide Coatings Filled with PTFE and Surface-Modified Nano-Si3N4, *Journal of Applied Polymer Science*, *131*(12).

[205] **Cheng, G., Qian, J., Tang, Z., Ding, G. and Zhu, J.** (2015). Dispersion stability of Si3N4 nano-particles modified by γ-methacryloxypropyl trimethoxy silane (MAPTMS) in organic solvent, *Ceramics International*, *41*(1), 1879-1884.

[206] **Tai, Y., Miao, J., Qian, J., Xia, R. and Zhang, Y.** (2008). An effective way to stabilize silicon nitride nanoparticles dispersed in rubber matrix by a one-step process, *Materials Chemistry and Physics*, *112*(2), 659-667.

[207] **Tai, Y.-l., Qian, J.-s., Miao, J.-b., Xia, R., Zhang, Y.-c. and Yang, Z.-G.** (2012). Preparation and characterization of Si3N4/SBR nanocomposites with high performance, *Materials & Design*, *34*, 522-527.

[208] **Luo, Y., Rong, M. Z., Zhang, M. Q. and Friedrich, K.** (2006). Surface functionalization of Si3N4 nanoparticles by graft polymerization of glycidyl methacrylate and styrene, *Journal of Applied Polymer Science*, *102*(2), 992-999.

[209] **Zhang, L.** (2007). Effect of interfacial treatment on the thermal properties of thermal conductive plastics, *Express Polymer Letters*, *1*(9), 608-615.

[210] **Akovali, G. and Dilsiz, N.** (1996). Studies on the modification of interphase/interfaces by use of plasma in certain polymer composite systems, *Polymer Engineering & Science*, *36*(8), 1081-1086.

[211] **Berman, R.**. (1976). Thermal conduction in solids. *Physics Today*, *31*(4), 56.

[212] **Zheng, W.-G., Shen, B. and Zhai, W.** (2013). Surface Functionalization of Graphene with Polymers for Enhanced Properties. *New progress on graphene research.* Retrieved from https://www.intechopen.com/chapters/37771

[213] **To, T., Nguyen, A., Phan, K., Truong, A., Doan, T. and Dang, C.** (2015). Modification of silicon nitride surfaces with GOPES and APTES for antibody immobilization: Computational and experimental studies, *Advances in Natural Sciences: Nanoscience and Nanotechnology*, *6*(4), 045006.

[214] **Klug, J., Pérez, L. A., Coronado, E. A. and Lacconi, G. I.** (2013). Chemical and Electrochemical Oxidation of Silicon Surfaces Functionalized with APTES: The Role of Surface Roughness in the AuNPs Anchoring Kinetics, *The Journal of Physical Chemistry C*, *117*(21), 11317-11327.

[215] **Ebnesajjad, S.** (2014). Surface Treatment and Bonding of Ceramics. *Surface Treatment of Materials for Adhesive Bonding* (2nd ed., pp. 283-299). Oxford : William Andrew Publishing.

[216] **Zakir, M., Ashraf, U., Tian, T., Han, A., Qiao, W., Jin, X., ….. Matinlinna, J.** (2016). The Role of Silane Coupling Agents and Universal Primers in Durable Adhesion to Dental Restorative Materials - a Review, *Current Oral Health Reports*, *3*(3), 244-253.

[217] **Barabanova, A. I., Philippova, O. E., Askadskii, A. A. and Khokhlov, A. R.**. (2012). Transparent Epoxy/Silica Nanocomposites with Increased Glass Transition Temperatures, *Procedia Chemistry*, *4*, 352-359.

[218] **Liu, C.-H. and Pan, C.-Y.** (2007). Grafting polystyrene onto silica nanoparticles via RAFT polymerization, *Polymer*, *48*(13), 3679-3685.

[219] **Bartholome, C., Beyou, E., Bourgeat-Lami, E., Chaumont, P., Lefebvre, F. and Zydowicz, N.** (2005). Nitroxide-Mediated Polymerization of Styrene Initiated from the Surface of Silica Nanoparticles. In Situ Generation and Grafting of Alkoxyamine Initiators, *Macromolecules*, *38*(4), 1099-1106.

[220] **Li, C., Han, J., Ryu, C. Y. and Benicewicz, B. C.** (2006). A Versatile Method To Prepare RAFT Agent Anchored Substrates and the Preparation of PMMA Grafted Nanoparticles, *Macromolecules*, *39*(9), 3175-3183.

[221] **Yang, F. and Nelson, G. L.** (2004). PMMA/silica nanocomposite studies: Synthesis and properties, *Journal of Applied Polymer Science*, *91*(6), 3844-3850.

[222] **Khlifa, M. A. S.** (2013). *Synthesis of Polymer Grafted Silica Nanoparticles: Effect of Grafting on Mechanical Reinforcement*. (Doctorate thesis). HERIOT-Watt University, Institute of Chemical Sciences, EDINBURGH.

[223] **Prado, L. A. S. A., Sriyai, M., Ghislandi, M., Barros-Timmons, A. and Schulte, K.** (2010). Surface modification of alumina nanoparticles with silane coupling agents, *Journal of the Brazilian Chemical Society*, *21*, 2238-2245.

[224] **Lin, J., Siddiqui, J. A. and Ottenbrite, R. M.** (2001). Surface modification of inorganic oxide particles with silane coupling agent and organic dyes, *Polymers for Advanced Technologies*, *12*(5), 285-292.

[225] **González-Guerrero, A. B., Alvarez, M., Castaño, A. G., Domínguez, C. and Lechuga, L. M.** (2013). A comparative study of in-flow and micro-patterning biofunctionalization protocols for nanophotonic silicon-based biosensors, *Journal of Colloid and Interface Science*, *393*, 402-410.

[226] **Cao, P., Xu, K. and Heath, J. R.** (2008). Azidation of Silicon(111) Surfaces, *Journal of the American Chemical Society*, *130*(45), 14910-14911.

[227] **Liebscher, J., Mrówczyński, R., Turcu, R. and Magerusan, L.** (2014). Diazo Transfer at Polydopamine - A New Way to Functionalization, *Polymer Chemistry*, *5*(22), 6593-6599.

[228] **Arslan, M. and Acik, G.** (2019). The Emerging Applications of Click Chemistry Reactions in Modification of Industrial Polymers, *Polymer Chemistry*, *10*(28), 3806-3821.

[229] **Manova, R. K., Pujari, S. P., Weijers, C. A. G. M., Zuilhof, H. and van Beek, T. A.**. (2012). Copper-Free Click Biofunctionalization of Silicon Nitride Surfaces via Strain-Promoted Alkyne–Azide Cycloaddition Reactions, *Langmuir*, *28*(23), 8651-8663.

[230] **Saxon, E., Armstrong, J. I. and Bertozzi, C. R.** (2000). A "Traceless" Staudinger Ligation for the Chemoselective Synthesis of Amide Bonds, *Organic Letters*, *2*(14), 2141-2143.

[231] **Elder, J. A.** (2009). *PMMA Clay Nanocomposites*. (Doctorate thesis). DURHAM University, Faculty of Science, DURHAM.

[232] **Braun, D., Cherdron, H., Rehahn, M., Ritter, H., Voit, B.** (2013). *Polymer Synthesis: Theory and Practice*. Heidelberg, Germany : Springer.

[233] **McKeen, L. W.**. (2016). Introduction to Plastics and Polymers. *Fatigue and Tribological Properties of Plastics and Elastomers* (3rd ed., pp. 45-64). William Andrew Publishing.

[234] **Mita, I., Stepto, R. F. T., & Suter, U. W.** (1994). Basic Classification and Definitions of Polymerization Reactions, *Pure and Applied Chemistry*, *66*(12), 2483-2486.

[235] **Shrivastava, A.** (2018). *Introduction to Plastics Engineering*, William Andrew Publishing.

[236] **Ezeroğlu, F.** (2013). *Synthesis and Characterization of Poly(Ether/Ester) Based Thermoplastic Elastomer Nanocomposites.* (Doctorate thesis). MIDDLE East Technical University, The Graduate School of Natural and Applied Sciences, ANKARA.

[237] **Szwarc, M.** (1956). 'Living' Polymers, *Nature, 178*(4543), 1168-1169.

[238] **Litvinenko, G. and Müller, A. H. E.** (1997). General Kinetic Analysis and Comparison of Molecular Weight Distributions for Various Mechanisms of Activity Exchange in Living Polymerizations, *Macromolecules*, *30*(5), 1253-1266.

[239] **Matyjaszewski, K.** (1995). Introduction to living polymeriz. Living and/or controlled polymerization, *Journal of Physical Organic Chemistry*, *8*(4), 197-207.

[240] **Matyjaszewski, K. and Lin, C.-H.** (1991). Exchange reactions in the living cationic polymerization of alkenes, *Makromolekulare Chemie. Macromolecular Symposia*, *47*(1), 221-237.

[241] **Swift, G., Nuyken, O. and Kricheldorf, H.R.** (2004). *Handbook of Polymer Synthesis*. Boca Raton, FL.: CRC Press.

[242] **Kim, Y. H.** (2000). Comments on "Living Polymerization: Rationale for Uniform Terminology" by Darling et al, *Journal of Polymer Science Part A: Polymer Chemistry*, *38*(10), 1733-1734.

[243] **Ishizone, T. and Goseki, R.** (2014). Living Anionic Addition Polymerization. In S. Kobayashi, K. Müllen (Eds.), *Encyclopedia of Polymeric Nanomaterials* (pp.1-18), Heidelberg, Berlin : Springer.

[244] **Kamigaito, M., Ando, T. and Sawamoto, M.** (2001). Metal-Catalyzed Living Radical Polymerization, *Chemical Reviews*, *101*(12), 3689-3746.

[245] **Matyjaszewski, K., Gaynor, S., Greszta, D., Mardare, D. and Shigemoto, T.** (1995). 'Living' and controlled radical polymerization, *Journal of Physical Organic Chemistry*, *8*(4), 306-315.

[246] **Patten, T. E. and Matyjaszewski, K.** (1999). Copper(I)-Catalyzed Atom Transfer Radical Polymerization, *Accounts of Chemical Research*, *32*(10), 895-903.

[247] **Ribelli, T. G., Lorandi, F., Fantin, M. and Matyjaszewski, K.** (2019). Atom Transfer Radical Polymerization: Billion Times More Active Catalysts and New Initiation Systems, *Macromolecular Rapid Communications*, *40*(1), 1800616.

[248] **Tsarevsky, N. V., Braunecker, W. A., Tang, W. and Matyjaszewski, K.**. (2009). The Atom Transfer Radical Polymerization Equilibrium: Structural and Medium Effects, Controlled/Living Radical Polymerization: Progress in ATRP, *American Chemical Society*, *1023*(6), 85-96.

[249] **Matyjaszewski, K. and Spanswick, J.** (2005). Controlled/living radical polymerization, *Materials Today*, *8*(3), 26-33.

[250] **Wang, J.-L., Grimaud, T. and Matyjaszewski, K.** (1997). Kinetic Study of the Homogeneous Atom Transfer Radical Polymerization of Methyl Methacrylate, *Macromolecules*, *30*(21), 6507-6512.

[251] **Percec, V., Barboiu, B., Neumann, A., Ronda, J. C. and Zhao, M.** (1996). Metal-Catalyzed "Living" Radical Polymerization of Styrene Initiated with Arenesulfonyl Chlorides. From Heterogeneous to Homogeneous Catalysis, *Macromolecules*, *29*(10), 3665-3668.

[252] **Tang, W. and Matyjaszewski, K.** (2007). Effects of Initiator Structure on Activation Rate Constants in ATRP, *Macromolecules*, *40*(6), 1858-1863.

[253] **Tang, W., Kwak, Y., Braunecker, W., Tsarevsky, N. V., Coote, M. L. and Matyjaszewski, K.** (2008). Understanding Atom Transfer Radical Polymerization: Effect of Ligand and Initiator Structures on the Equilibrium Constants, *Journal of the American Chemical Society*, *130*(32), 10702-10713.

[254] **Tang, W., Tsarevsky, N. and Matyjaszewski, K.** (2006). Determination of Equilibrium Constants for Atom Transfer Radical Polymerization, *Journal of the American Chemical Society*, *128*(1598-604.

[255] **Matyjaszewski, K., Paik, H.-j., Zhou, P. and Diamanti, S. J.** (2001). Determination of Activation and Deactivation Rate Constants of Model Compounds in Atom Transfer Radical Polymerization, *Macromolecules*, *34*(15), 5125-5131.

[256] **Fischer, H.** (2001). The Persistent Radical Effect: A Principle for Selective Radical Reactions and Living Radical Polymerizations, *Chemical Reviews*, *101*(12), 3581-3610.

[257] **Murtezi, E.** (2014). *Synthesis of Clickable Hydrogels and Linear Polymers By Type II Photoinitiation*. (Master thesis). ISTANBUL Technical University, Graduate School of Science Engineering and Technology, ISTANBUL.

[258] **Mehranpour, S.** (2019). *Comparison of Beta, Neutron and Gamma Attenuation Properties of PMMA/Colemanite Composites*. (Master thesis). ISTANBUL Technical University, Graduate School of Science Engineering and Technology, ISTANBUL.

[259] **Kumar, K. R., Kizhakkedathu, J. N. and Brooks, D. E.** (2004). Atom Transfer Radical Polymerization Using Multidentate Amine Ligands Supported on Soluble Hyperbranched Polyglycidol, *Macromolecular Chemistry and Physics*, *205*(5), 567-573.

[260] **Wootthikanokkhan, J., Peesan, M. and Phinyocheep, P.** (2001). Atom transfer radical polymerizations of (meth)acrylic monomers and isoprene, *European Polymer Journal*, *37*(10), 2063-2071.

[261] **Matyjaszewski, K. and Xia, J.** (2001). Atom Transfer Radical Polymerization, *Chemical Reviews*, *101*(9), 2921-2990.

[262] **Matyjaszewski, K. and Xia, J.** (2002). Fundamentals of Atom Transfer Radical Polymerization. *Handbook of Radical Polymerization* (pp. 523-628). Retrieved from

https://onlinelibrary.wiley.com/doi/abs/10.1002/0471440264.pst555

[263] **Tian, B. Y., Hu, P. J., Yuan, M., Tang, E. J., Liu, S. J., Zhao, X. Y. ….. Zhao, D. S.** (2012). Effect of different ligands on the controlled polymerization of monodisperse polystyrene nanospheres by atom transfer radical polymerization in an aqueous emulsion, *Express Polymer Letters*, *6*(10), 837-846.

[264] **Braun, C. H. D., Rehahn, M., Ritter, H., Voit, B.** . (2013). *Polymer Synthesis: Theory and Practice*. Heidelberg, Berlin: Springer.

[265] **Jenkins, A. D.** (2004). Contemporary polymer chemistry. *Polymer International*, *53*(9), 1395-1395.

[266] **Rakesh Gupta, A. K. and Kumer, A.** (1998). *Fundamentals of Polymers*. New York, NY.: McGraw-Hill Education.

[267] **Niu, M., Zhao, G.-j. and Mehmet, A.** (2011). Polycondensation reaction and its mechanism during lignocellulosic liquefaction by an acid catalyst: A review, *Forestry Studies in China*, *13*(1), 71-79.

[268] **Mark, H.F.** (2014). *Encyclopedia of Polymer Science and Technology*. Hoboken, New Jersey : John Wiley & Sons Inc.

[269] **Kreuchunas, A.** (1958). *U.S. Patent No. 2,822,351*. Washington, DC: U.S. Patent and Trademark Office.

[270] **Rao, V. L.** (1999). Polyether Sulfones, *Journal of Macromolecular Science, Part C*, *39*(4), 655-711.

[271] **Cohen, S. M. and Young, R. H.**. (1966). A sulfone polymer from diphenyl ether, *Journal of Polymer Science Part A-1: Polymer Chemistry*, *4*(3), 722-727.

[272] **Johnson, R. N., Farnham, A. G., Clendinning, R. A., Hale, W. F. and Merriam, C. N.** (1967). Poly(aryl ethers) by nucleophilic aromatic substitution. I. Synthesis and properties, *Journal of Polymer Science Part A-1: Polymer Chemistry*, *5*(9), 2375-2398.

[273] **Newton, A. B. and Rose, J. B.** (1972). Relative reactivities of the functional groups involved in synthesis of poly(phenylene ether sulphones) from halogenated derivatives of diphenyl sulphone, *Polymer*, *13*(10), 465-474.

[274] **Attwood, T. E., Newton, A. B. and Rose, J. B.** (1972). Kinetic investigation of the synthesis of a polyethersulphone, *British Polymer Journal*, *4*(5), 391-399.

[275] **Kricheldorf, H. R. and Bier, G.** (1983). New polymer synthesis. IX. Synthesis of poly(ether sulfone)s from silylated diphenols or hydroxybenzoic acids, *Journal of Polymer Science: Polymer Chemistry Edition*, *21*(8), 2283-2289.

[276] **Ateş, Ş.** (2012). *Modification of Polysulfones by Ring Opening Polymerization Processes*. (Doctorate thesis). ISTANBUL Technical University, Graduate School of Science Engineering and Technology, ISTANBUL.

[277] **Matsumoto, K., Komuro, H., Kai, T. and Jikei, M.** (2013). Synthesis of poly(ether sulfone)s by self-polycondensation of AB-type monomers, *Polymer Journal*, *45*(9), 909-914.

[278] **Hedrick, J. L., Mohanty, D. K., Johnson, B. C., Viswanathan, R., Hinkley, J. A. and McGrath, J. E.** (1986). Radiation resistant amorphous–all aromatic polyarylene ether sulfones: Synthesis, characterization, and mechanical properties, *Journal of Polymer Science Part A: Polymer Chemistry*, *24*(2), 287-300.

[279] **Hedrick, J. L., Dumais, J. J., Jelinski, L. W., Patsiga, R. A. and McGrath, J. E.** (1987). Synthesis and characterization of deuterated poly(arylene ether sulfones), *Journal of Polymer Science Part A: Polymer Chemistry*, *25*(8), 2289-2300.

[280] **Viswanathan, R., Johnson, B. C. and McGrath, J. E.** (1984). Synthesis, kinetic observations and characteristics of polyarylene ether sulphones prepared via a potassium carbonate DMAC process, *Polymer*, *25*(12), 1827-1836.

[281] **Hale, W. F., Farnham, A. G., Johnson, R. N. and Clendinning, R. A.** (1967). Poly(Aryl ethers) by nucleophilic aromatic substitution. II. Thermal stability, *Journal of Polymer Science Part A-1: Polymer Chemistry*, *5*(9), 2399-2414.

[282] **Covarrubias, G.** (2017). *Toward The Synthesis of Functionalized, Semi-Crystalline Poly (Ether Ether Ketone): Monitoring The Meta-Fluorine Displacement In 3,5,4'-Trifluorobenzophenone*. (Master thesis). WRIGHT State University, Institue of Chemistry, OHIO.

[283] **Hergenrother, P.** (2003). The Use, design, synthesis, and properties of high performance/high temperature polymers: An overview, *High Performance Polymers*, *15*(1), 3-45.

[284] **Teasley, M. F. and Hsiao, B. S.**. (1996). Synthesis and Characterization of Poly(oxy-1,3-phenylenecarbonyl-1,4-phenylene) and Related Polymers, *Macromolecules*, *29*(20), 6432-6441.

[285] **Risse, W. and Sogah, D. Y.** (1990). Synthesis of soluble high molecular weight poly(aryl ether ketones) containing bulky substituents, *Macromolecules*, *23*(18), 4029-4033.

[286] **Covarrubias, G.** (2017). *Toward The Synthesis Of Functionalized, Semi-Crystalline Poly (Ether Ether Ketone): Monitoring The Meta-Fluorine Displacement In 3,5,4'-Trifluorobenzophenone*. (Master thesis). WRIGHT State University, Institue of Chemistry, OHIO.

[287] **Ewing, Z.** (2016). *Synthesis And Characterization Of PEEK Analogues Utilizing 3,5 And 2,4-Difluorobenzophenone*. (Master thesis). WRIGHT State University, Institue of Chemistry, OHIO.

[288] **Stuck, R.** (2017). *Te Synthesis of 3,5-Difluorobenzophenone Derivatives and their Corresponding PEEK Copolymers*. (Master thesis). WRIGHT State University, Institue of Chemistry, OHIO.

[289] **Díez-Pascual, A. M., Martínez, G. and Gómez, M. A.** (2009). Synthesis and Characterization of Poly(ether ether ketone) Derivatives Obtained by Carbonyl Reduction, *Macromolecules*, *42*(18), 6885-6892.

[290] **Smith, J. G.** (2010). *Organic Chemistry*. New York, NY.: McGraw-Hill Education.

[291] **Guirong, Wu. and Jilin, J. Y. X.** (2012). *U.S. Patent No. 8,236,919.* Washington, DC: U.S. Patent and Trademark Office.

[292] **Torrida et. al.** (2004). *European Patent No. EP 1464662 (A1).* Retrieved from Scopus.

[293] **Dizman, C., Tasdelen, M. A. and Yagci, Y.** (2013). Recent advances in the preparation of functionalized polysulfones, *Polymer International*, *62*(7), 991-1007.

[294] **Rengifo, H. R., Chen, L., Grigoras, C., Ju, J. and Koberstein, J. T.** (2008). "Click-Functional" Block Copolymers Provide Precise Surface Functionality via Spin Coating, *Langmuir*, *24*(14), 7450-7456.

[295] **Chen, L., Rengifo, H. R., Grigoras, C., Li, X., Li, Z., Ju, J. ….. Koberstein, J. T.** (2008). Spin-On End-Functional Diblock Copolymers for Quantitative DNA Immobilization, *Biomacromolecules*, *9*(9), 2345-2352.

[296] **Neises, B. and Steglich, W.** (1978). Simple Method for the Esterification of Carboxylic Acids, *Angewandte Chemie International Edition in English*, *17*(7), 522-524.

[297] **Neises, B. and Steglich, W.** (2003). Esterification of Carboxylic Acids with Dicyclohexylcarbodiimide/4-Dimethylaminopyridine: tert-Butyl Ethyl Fumarate, *Organic Syntheses*. *63*, 183-183.

[298] **Morinaga, T., Ohkura, M., Ohno, K., Tsujii, Y. and Fukuda, T.** (2007). Monodisperse Silica Particles Grafted with Concentrated Oxetane-Carrying Polymer Brushes: Their Synthesis by Surface-Initiated Atom Transfer Radical Polymerization and Use for Fabrication of Hollow Spheres, *Macromolecules*, *4*0(4), 1159-1164.

[299] **Parvole, J., Laruelle, G., Guimon, C., Francois, J. and Billon, L.** (2003). Initiator-Grafted Silica Particles for Controlled Free Radical Polymerization: Influence of the Initiator Structure on the Grafting Density, *Macromolecular Rapid Communications*, *24*(18), 1074-1078.

[300] **Li, L., Han, C., Xu, D., Xing, J.-Y., Xue, Y.-H. and Liu, H.** (2018). Polymer-grafted nanoparticles prepared via a grafting-from strategy: a computer simulation study, *Physical Chemistry Chemical Physics*, *20*(27), 18400-18409.

[301] **Homenick, C. M., Lawson, G. and Adronov, A.** (2007). Polymer Grafting of Carbon Nanotubes Using Living Free-Radical Polymerization, *Polymer Reviews*, *47*(2), 265-290.

[302] **Husseman, M., Malmström, E. E., McNamara, M., Mate, M., Mecerreyes, D., Benoit, D. G., ….. Hawker, C. J.** (1999). Controlled Synthesis of Polymer Brushes by "Living" Free Radical Polymerization Techniques, *Macromolecules*, *32*(5), 1424-1431.

[303] **Moad, G., Rizzardo, E. and Thang, S. H.** (2005). Living Radical Polymerization by the RAFT Process, *Australian Journal of Chemistry*, *58*(6), 379-410.

[304] **Jeyaprakash, J. D., Samuel, S., Dhamodharan, R. and Rühe, J.** (2002). Polymer Brushes via ATRP: Role of Activator and Deactivator in the Surface-Initiated ATRP of Styrene on Planar Substrates, *Macromolecular Rapid Communications*, *23*(4), 277-281.

[305] **Hawker, C. J., Bosman, A. W. and Harth, E.** (2001). New Polymer Synthesis by Nitroxide Mediated Living Radical Polymerizations, *Chemical Reviews*, *101*(12), 3661-3688.

[306] **Flejszar, M. and Chmielarz, P.** (2019). Surface-Initiated Atom Transfer Radical Polymerization for the Preparation of Well-Defined Organic-Inorganic Hybrid Nanomaterials, *Materials*, *12*(18), 3030.

[307] **Du, R., Gao, B., Men, J. and An, F.** (2020). Characteristics and advantages of surface-initiated graft-polymerization as a way of "grafting from" method for graft-polymerization of functional monomers on solid particles, *European Polymer Journal*, *127*, 109479.

[308] **Mu, B., Wang, T. and Liu, P.** (2007). Well-Defined Dendritic-Graft Copolymer Grafted Silica Nanoparticle by Consecutive Surface-Initiated Atom Transfer Radical Polymerizations, *Industrial & Engineering Chemistry Research*, *46*(10), 3069-3072.

[309] **Sun, N., Meng, X. and Xiao, Z.** (2015). Functionalized Si3N4 nanoparticles modified with hydrophobic polymer chains by surface-initiated atom transfer radical polymerization (ATRP), *Ceramics International*, *41*(10), 13830-13835.

[310] **Yu, H.-J. and Luo, Z.-H.** (2011). Novel superhydrophobic silica/poly(siloxane-fluoroacrylate) hybrid nanoparticles prepared via surface-initiated ATRP and their surface properties: The effects of polymerization conditions, *Journal of Polymer Science Part A: Polymer Chemistry*, *49*(1), 174-183.

[311] **Haloi, D., Ata, S. and Singha, N.** (2013). Synthesis and Characterization of All Acrylic Block Copolymer/Clay Nanocomposites Prepared via Surface Initiated Atom Transfer Radical Polymerization (SI-ATRP), *Industrial & Engineering Chemistry Research*, *51*(29), 9760-9768.

[312] **Rajender, N. and Suresh, K. I.** (2016). Surface-Initiated Atom Transfer Radical Polymerization (SI-ATRP) From Graphene Oxide: Effect of Functionalized Graphene Sheet (FGS) on the Synthesis and Material Properties of PMMA Nanocomposites, *Macromolecular Materials and Engineering*, *301*(1), 81-92.

[313] **Mohamadi, S., Sharifi-Sanjani, N. and Mahdavi, H.** (2011). Functionalization of Graphene Sheets via Chemically Grafting of PMMA Chains Through in-situ Polymerization, *Journal of Macromolecular Science, Part A*, *48*(8), 577-582.

[314] **Zaman, I., Nor, F. M., Manshoor, B., Khalid; A. and Araby, S.** (2015). Influence of Interface on epoxy/clay Nanocomposites: 1. Morphology Structure, *Procedia Manufacturing*, *2*, 17-22.

[315] **Zheng, Y.** (2017). *Synthesis, Characterization and Application of Polymer-Grafed Nanoparticles.* (Doctorate thesis). UNIVERSITY of South Carolina, College of Arts and Sciences, COLUMBIA.

[316] **Francis, R., Joy, N., Aparna, E. P. and Vijayan, R.** (2014). Polymer Grafted Inorganic Nanoparticles, Preparation, Properties, and Applications: A Review, *Polymer Reviews*, *54*(2), 268-347.

[317] **Hore, M. J. A., Korley, L. T. J. and Kumar, S. K.** (2020). Polymer-Grafted Nanoparticles, *Journal of Applied Physics*, *128*(3), 030401.

[318] **Chancellor, A. J., Seymour, B. T. and Zhao, B.** (2019). Characterizing Polymer-Grafted Nanoparticles: From Basic Defining Parameters to Behavior in Solvents and Self-Assembled Structures, *Analytical Chemistry*, *91*(10), 6391-6402.

[319] **Tunckol, M.** (2012). *Fonctionnalisation de Nanotubes de Carbone Multi-Parois par des Polymères*. (Doctorate thesis). INSTITUT National Polytechnique de Toulouse, Chimie Organométallique et de Coordination, FRANCE.

[320] **Chai, M., Amir, N., Yahya, N. and Saaid, I.** (2018). Characterization and Colloidal Stability of Surface Modified Zinc Oxide Nanoparticle. *Journal of Physics: Conference Series*, *1123*(1), 012007.

[321] **Iijima, M. and Kamiya, H.** (2009). Surface Modification for Improving the Stability of Nanoparticles in Liquid Media, *KONA Powder and Particle Journal*, *27*, 119-129.

[322] **Mazloomi-Rezvani, M., Salami-Kalajahi, M. and Roghani-Mamaqani, H.** (2018). "Grafting to" approach for surface modification of AuNPs with RAFT-mediated synthesized smart polymers: Stimuli-responsive behaviors of hybrid nanoparticles, *Journal of Physics and Chemistry of Solids*, *123*, 183-190.

[323] **Zdyrko, B. and Luzinov, I.** (2011). Polymer Brushes by the "Grafting to" Method, *Macromolecular Rapid Communications*, *32*(12), 859-69.

[324] **Minko, S.** (2008). *Grafting on Solid Surfaces: "Grafting to" and "Grafting from" Methods, Polymer Surfaces and Interfaces*. Heidelberg, Berlin: Springer.

[325] **He, H. and Gao, C.** (2011). Click Chemistry on Nano-Surfaces, *Current Organic Chemistry*, *15*(21), 3667-3691.

[326] **Collman, J. P., Devaraj, N. K. and Chidsey, C. E. D.** (2004). "Clicking" Functionality onto Electrode Surfaces, *Langmuir*, *20*(4), 1051-1053.

[327] **Voggu, R., Suguna, P., Chandrasekaran, S. and Rao, C. N. R.** (2007). Assembling covalently linked nanocrystals and nanotubes through click chemistry, *Chemical Physics Letters*, *443*(1), 118-121.

[328] **Evans, R.** (2007). The Rise of Azide—Alkyne 1,3Dipolar "Click" Cycloaddition and Its Application to Polymer Science and Surface Modification, *Cheminform*, *60*(6), 384-395.

[329] **Fleming, D. A., Thode, C. J. and Williams, M. E.** (2006). Triazole Cycloaddition as a General Route for Functionalization of Au Nanoparticles, *Chemistry of Materials*, *18*(9), 2327-2334.

[330] **Binder, W. H., Sachsenhofer, R., Straif, C. J. and Zirbs, R.** (2007). Surface-modified nanoparticles via thermal and Cu(i)-mediated "click" chemistry: Generation of luminescent CdSe nanoparticles with polar ligands guiding supramolecular recognition, *Journal of Materials Chemistry*, *17*(20), 2125-2132.

[331] **J. A. Johnson, D. R. Lewis, D. D. Díaz, M. G. Finn, J. T. Koberstein and N. J. Turro**. (2006). Synthesis of Degradable Model Networks via ATRP and Click Chemistry, *Journal of the American Chemical Society*, *128*(20), 6564-6565.

[332] **D. Fournier, R. Hoogenboom and U. S. Schubert**. (2007). Clicking polymers: a straightforward approach to novel macromolecular architectures, *Chemical Society Reviews*, *36*(8), 1369-1380.

[333] **Gacal, B., Durmaz, H., Tasdelen, M. A., G. Hizal, Tunca, U., Yagci, Y. ….. Demirel, A. L.** (2006). Anthracene−Maleimide-Based Diels−Alder "Click Chemistry" as a Novel Route to Graft Copolymers, *Macromolecules*, *39*(16), 5330-5336.

[334] **Opsteen, J. and Hest, J.** (2005). Modular synthesis of block copolymers via cycloaddition of terminal azide and alkyne functionalized polymers, *Chemical communications (Cambridge, England)*, *1*, 57-59.

[335] **Bakbak, S., Leech, P. J., Carson, B. E., Saxena, S., King, W. P. and Bunz, U. H. F.** (2006). 1,3-Dipolar Cycloaddition for the Generation of Nanostructured Semiconductors by Heated Probe Tips, *Macromolecules*, *39*(20), 6793-6795.

[336] **Dolci, M., Toulemon, D., Chaffar, Z., Bubendorff, J.-L., Tielens, F., Calatayud, M., ….. Pichon, B. P.** (2019). Nanoparticle Assembling through Click Chemistry Directed by Mixed SAMs for Magnetic Applications, *ACS Applied Nano Materials*, *2*(1), 554-565.

[337] **Thillaiyan, R., Abdala, A., Stankovich, S., Dikin, D., Herrera-Alonso, M., Piner, R., ….. Brinson, L.** (2008). Functionalized graphene sheets for polymer nanocomposites, *Nature Nanotechnology*, *3*(6), 327-31.

[338] **Sanchez-Sanchez, A., Pérez-Baena, I. and Pomposo, J. A.** (2013). Advances in click chemistry for single-chain nanoparticle construction, *Molecules (Basel, Switzerland)*, *18*(3), 3339-3355.

[339] **Feng, X., Zhu, S., Yue, K., Su, H., Guo, K., Wesdemiotis, C., ….. Li, Y.** (2014). T10 Polyhedral Oligomeric Silsesquioxane-Based Shape Amphiphiles with Diverse Head Functionalities via "Click" Chemistry, *ACS Macro Letters*, *3*(9), 900-905.

[340] **Su, H., Zheng, J., Wang, Z., Lin, F., Feng, X., Dong, X.-H., ….. Li, Y.** (2013). Sequential Triple "Click" Approach toward Polyhedral Oligomeric Silsesquioxane-Based Multiheaded and Multitailed Giant Surfactants, *ACS Macro Letters*, *2*(8), 645-650.

[341] **Iha, R. K., Wooley, K. L., Nyström, A. M., Burke, D. J., Kade, M. J. and Hawker, C. J.** (2009). Applications of Orthogonal "Click" Chemistries in the Synthesis of Functional Soft Materials, *Chemical Reviews*, *109*(11), 5620-5686.

[342] **Li, H., Cheng, F., Duft, A. M. and Adronov, A.** (2005). Functionalization of Single-Walled Carbon Nanotubes with Well-Defined Polystyrene by "Click" Coupling, *Journal of the American Chemical Society*, *127*(41), 14518-14524.

[343] **Guo, Z., Liang, L., Liang, J.-J., Ma, Y.-F., Yang, X., Ren, D.-M., ….. Zheng, J.-Y.** (2007). Covalently β-cyclodextrin modified single-walled carbon nanotubes: A novel artificial receptor synthesized by 'click' chemistry, *Journal of Nanoparticle Research*, *10*(6), 1077-1083.

[344] **Xu, X., Nishimura, T., Hirosaki, N., Xie, R.-J. and Tanaka, H.** (2007). Fabrication of a Nano-Si3N4/Nano-C Composite by High-Energy Ball Milling and Spark Plasma Sintering, *Journal of the American Ceramic Society*, *90*(4), 1058-1062.

[345] **Xu, X., Nishimura, T., Hirosaki, N., Xie, R.-J., Zhu, Y., Yamamoto, Y. ….. Tanaka, H.** (2005). New Strategies to Prepare Nano-Sized Silicon Nitride Ceramics, *Journal of the American Ceramic Society*, *88*(4), 934-937.

[346] **Cheng, G., Qian, J., Tang, Z., Ding, G. and Zhu, J.** (2015). Dispersion stability of Si3N4 nano-particles modified by γ-methacryloxypropyl trimethoxy silane (MAPTMS) in organic solvent, *Ceramics International*, *41*(1), 1879-1884.

[347] **Sun, N., Meng, X. and Xiao, Z.** (2015). Functionalized Si3N4 nanoparticles modified with hydrophobic polymer chains by surface-initiated atom transfer radical polymerization (ATRP), *Ceramics International*, *41*(10), 13830-13835.

[348] **Okcu, S. S., Durmaz, Y. Y. and Yagci, Y.** (2010). Synthesis and Characterization of Telechelic Block Co-polymers by Combination of Atom Transfer Radical Polymerization and Click Chemistry Processes, *Designed Monomers and Polymers*, *13*(5), 459-472.

[349] **Bilir, C., Erdogan, T., Odabas, S. and Erdal Unveren, E.** (2016). Novel partially fluorinated graft block copolymer ionomer as potential proton exchange membrane material, *Polymer*, *95*, 91-101.

[350] **Opsteen, J. A. and van Hest, J. C. M.** (2005). Modular synthesis of block copolymers via cycloaddition of terminal azide and alkyne functionalized polymers, *Chemical Communications*, *1*, 57-59.

[351] **Chang, Z., Xu, Y., Zhao, X., Zhang, Q. and Chen, D.** (2009). Grafting Poly(methyl methacrylate) onto Polyimide Nanofibers via "Click" Reaction, *ACS Applied Materials & Interfaces*, *1*(12), 2804-2811.

[352] **Lee, J., Lee, K., Park, J., Kim, J. K. and Chang, T.** (2015). Characterization and fractionation of PS-b-PMMA diblock copolymer synthesized via click chemistry, *Polymer*, *80*, 46-51.

[353] **Dizman, C., Kahveci, M. U. and Yagci, Y.** (2013). Synthesis of polysulfone-b-polystyrene block copolymers by mechanistic transformation from condensation polymerization to free radical polymerization, *Polymer Bulletin*, *70*(7), 2097-2109.

[354] **Sangermano, M., M. Farrukh, M., Tiraferri, A., Dizman, C. and Yagci, Y.** (2015). Synthesis, preparation and characterization of UV-cured methacrylated polysulfone-based membranes, *Materials Today Communications*, *5*, 64-69.

[355] **Durmaz, Y. Y., Sangermano, M. and Yagci, Y.** (2010). Surface modification of UV-cured epoxy resins by click chemistry, *Journal of Polymer Science Part A: Polymer Chemistry*, *48*(13), 2862-2868.

[356] **Yilmaz, G., Toiserkani, H., Odaci Demirkol, D., Sakarya, S., Timur, S., Torun, L. ….. Yagci, Y.** (2011). Polysulfone based amphiphilic graft copolymers by click chemistry as bioinert membranes, *Materials Science and Engineering: C*, *31*(5), 1091-1097.

[357] **Murtezi, E., Ciftci, M. and Yagci, Y.** (2015). Synthesis of clickable hydrogels and linear polymers by type II photoinitiation, *Polymer International*, *64*(5), 588-594.

[358] **Arslan, M.** (2017). Polymer Nanocomposites via Click Chemistry Reactions, *Polymers*, *9*(19), 499.

[359] **Liang, L. and Astruc, D.** (2011). The copper(I)-catalyzed alkyne-azide cycloaddition (CuAAC) "click" reaction and its applications. An overview, *Coordination Chemistry Reviews*, *255*(23), 2933-2945.

[360] **Stuck, R.** (2017). *The Synthesis of 3,5-Difluorobenzophenone Derivatives and their Corresponding PEEK Copolymers. (Master thesis).* WRIGHT State University, Institue of Chemistry, OHIO.

[361] **Jiachun Zhong, M.L., He, P., Nie, X., Fan, Z.** (2011). *Chinese Patent No. CN102492132A.* Retrieved from Espacenet.

[362] **Arslan, M. and Tasdelen, M. A.** (2017). Polymer Nanocomposites via Click Chemistry Reactions, *Polymers*, *9*(10), 499.

[363] **Bourja, L., Bakiz, B., Abdeljalil, B., Ezahri, M., Villain, S. and Gavarri, J.-R.** (2010). Synthesis and characterization of nanosized Ce1−xbixo2−δ solid solutions for catalytic applications, J*ournal of Taibah University for Science*, *4*(1), 1-8.

[364] **Mahmoud, A., Wasly, D.-H. and Doheim, M.** (2014). Studies Of Crystallite Size And Lattice Strain In Al-Al 2 O 3 Powders Produced By High-Energy Mechanical Milling, *JES. Journal of Engineering Sciences*, *42*(6), 1430-1439.

[365] **Daly, R., Khitouni, M., Kolsi, A. and Njah, N.** (2006). The studies of crystallite size and microstrains in aluminum powder prepared by mechanical milling, *physica status solidi (c)*, *3*(9), 3325-3331.

[366] **Lönnberg, B.** (1994). Characterization of milled Si3N4 powder using X-ray peak broadening and surface area analysis, *Journal of Materials Science*, *29*(12), 3224-3230.

[367] **Kanno, Y.** (1985). Properties of SiC, Si3N4 and SiO2 ceramic powders produced by vibration ball milling, *Powder Technology*, *44*(1), 93-97.

[368] **Xi, S. Q., Zhou, J. G. and Wang, X. T.** (2007). Research on temperature rise of powder during high energy ball milling, *Powder Metallurgy*, 50(4), 367-373.

[369] **Mhadhbi, M., Khitouni, M., Azabou, M. and Kolsi, A.** (2008). Characterization of Al and Fe nanosized powders synthesized by high energy mechanical milling, *Materials Characterization*, *59*(7), 944-950.

[370] **Zhang, D. L.** (2004). Processing of advanced materials using high-energy mechanical milling, *Progress in Materials Science*, *49*(3), 537-560.

[371] **Akbari, B., M. Tavandashti, P. and Zandrahimi, M.** (2011). Particle size characterization of nanoparticles–a practicalapproach, *Iranian Journal of Materials Science and Engineering*, *8*(2), 48-56.

[372] **Barhoum, A. and García-Betancourt, M. L.** (2018). Physicochemical characterization of nanomaterials: Size, morphology, optical, magnetic, and electrical properties. In A.S.H. Makhlouf, A. Barhoum (Eds.), *Emerging Applications of Nanoparticles and Architecture Nanostructures* (1st ed., pp. 279-304). Elsevier.

[373] **Zolriasatein, A., Shokuhfar, A., Safari, F. and Abdi, N.** (2018). Comparative study of SPEX and planetary milling methods for the fabrication of complex metallic alloy nanoparticles, *Micro & Nano Letters*, *13*(4), 448-451.

[374] **Malghan, S. G., Minor, D. B. and Lum, L. S. H.** (1991). Silicon nitride powder milling kinetics in a high-energy agitation ball mill, *Powder Technology*, *67*(2), 201-206.

[375] **Abdallah, W.** (2010). *Preparation and Characterization of Thermally Stable Organoclays and Their Use in Polymer Based Nanocomposites.* (Doctorate thesis). MIDDLE East Technical University, The Graduate School of Natural and Applied Sciences, ANKARA.

[376] **Mazumdar, P., Rattan, S. and Mukherjee, M.** (2015). Polymer nanocomposites using click chemistry: novel materials for hydrogen peroxide vapor sensors, *RSC Advances*, *5*(85), 69573-69582.

[377] **Semerci, E., Bedri, T. E. and Kizilcan, N.** (2021). Preparation of thermal conductive Poly(methyl methacrylate)/Silicon nitride nanocomposites via click chemistry, *Polymer*, *212*, 123285.

[378] **Bahadur, P.** (2001). Block copolymers – Their microdomain formation (in solid state) and surfactant behaviour (in solution), *Current Science*, *80*(8), 1002-1007.

[379] **Tsagkalias, S. I., Manios, K. T. and Achilias, S. D.** (2017). Effect of Graphene Oxide on the Reaction Kinetics of Methyl Methacrylate In Situ Radical Polymerization via the Bulk or Solution Technique, *Polymers*, *9*(9), 432.

[380] **Ramdani, N., Wang, J. and Liu, W. B.** (2014). Preparation and Thermal Properties of Polybenzoxazine/TiC Hybrids, Advanced Materials Research, *887*, 49-52.

[381] **Georges, M. K., Veregin, R. P. N., Kazmaier, P. M. and Hamer, G. K.** (1993). Narrow molecular weight resins by a free-radical polymerization process, *Macromolecules*, *26*(11), 2987-2988.

[382] **Benoit, D., Grimaldi, S., Robin, S., Finet, J.-P., Tordo, P. and Gnanou, Y.** (2000). Kinetics and Mechanism of Controlled Free-Radical Polymerization of Styrene and n-Butyl Acrylate in the Presence of an Acyclic β-Phosphonylated Nitroxide, *Journal of the American Chemical Society*, *122*(25), 5929-5939.

[383] **Zhao, B. and Brittain**, **W.** (2000). Polymer Brushes: Surface-Immobilized Macromolecules, *Progress in Polymer Science*, *25*(5), 677-710.

[384] **Mohammadi Ziarani, G., Hassanzadeh, Z., Gholamzadeh, P., Asadi, S. and Badiei, A.** (2016). Advances in click chemistry for silica-based material construction, *RSC Advances*, *6*(26), 21979-22006.

[385] **Sunjuk, M., Abu-Surrah, A. S., Abu Safieh, K. A., Qaroush, A. K. and Al-Qaisi, F. M.** (2017). γ-Diimine palladium(II) based complexes mediated polymerization of methyl methacrylate, *Arabian Journal of Chemistry*, *10*, 1209-1215.

[386] **Anastasaki, A., Willenbacher, J., Fleischmann, C., Gutekunst, W. R. and Hawker, C. J.** (2017). End group modification of poly(acrylates) obtained via ATRP: a user guide, *Polymer Chemistry*, *8*(4), 689-697.

[387] **Xia, R., Zhang, Y., Zhu, Q., Qian, J., Dong, Q. and Li, F.** (2008). Surface modification of nano-sized silicon nitride with BA-MAA-AN tercopolymer, *Journal of Applied Polymer Science*, *107*(1), 562-570.

[388] **Hu, Y., Chen, Z., Zhang, J., Xiao, G., Yi, M., Zhang, W. ….. Xu, C.** (2019). Preparation and mechanical properties of Si3N4 nanocomposites reinforced by Si3N4@rGO particles, *Journal of the American Ceramic Society*, *102*(11), 6991-7002.

[389] **Siddiqui, M. N., Redhwi, H. H., Vakalopoulou, E., Tsagkalias, I., Ioannidou, M. D. and Achilias, D. S.** (2015). Synthesis, characterization and reaction kinetics of PMMA/silver nanocomposites prepared via in situ radical polymerization, *European Polymer Journal*, *72*, 256-269.

[390] **Tsagkalias, I. s., Manios, T. K. and Achilias, D.** (2017). Effect of Graphene Oxide on the Reaction Kinetics of Methyl Methacrylate In Situ Radical Polymerization via the Bulk or Solution Technique, *Polymers*, *9*(9), 432.

[391] **Yang, Y., Ye, X., Luo, J., Song, G., Liu, Y. and Tang, G.** (2015). Polymethyl methacrylate based phase change microencapsulation for solar energy storage with silicon nitride, *Solar Energy*, *115*, 289-296.

[392] **Ergin, M., Kiskan, B., Gacal, B. and Yagci, Y.** (2007). Thermally Curable Polystyrene via Click Chemistry, *Macromolecules*, *40*(13), 4724-4727.

[393] **Wang, Y., Chen, J., Xiang, J., Li, H., Shen, Y., Gao, X. ….. Liang, Y.** (2009). Synthesis and characterization of end-functional polymers on silica nanoparticles via a combination of atom transfer radical polymerization and click chemistry, *Reactive and Functional Polymers*, *69*(6), 393-399.

[394] **Fateh, T., Richard, F., Rogaume, T. and Joseph, P.** (2016). Experimental and modelling studies on the kinetics and mechanisms of thermal degradation of polymethyl methacrylate in nitrogen and air, *Journal of Analytical and Applied Pyrolysis*, *120*, 423-433.

[395] **Hirata, T., Kashiwagi, T. and Brown, J. E.** (1985). Thermal and oxidative degradation of poly(methyl methacrylate): weight loss, *Macromolecules*, *18*(7), 1410-1418.

[396] **Mittal, G., Rhee, K. Y. and Park, S.-J.** (2016). Processing and Characterization of PMMA/PI Composites Reinforced With Surface Functionalized Hexagonal Boron Nitride, *Applied Surface Science*, *415*, 49-54.

[397] **Ramdani, N., Wang, J., Wang, H., Feng, T.-t., Derradji, M. and Liu, W.-b.** (2014). Mechanical and thermal properties of silicon nitride reinforced polybenzoxazine nanocomposites, *Composites Science and Technology*, *105*, 73-79.

[398] **Vaziri, H. S., Omaraei, I. A., Abadyan, M., Mortezaei, M. and Yousefi, N.** (2011). Thermophysical and rheological behavior of polystyrene/silica nanocomposites: Investigation of nanoparticle content, *Materials & Design*, *32*(8), 4537-4542.

[399] **Ash, B. J., Schadler, L. S. and R. Siegel, W.** (2002). Glass transition behavior of alumina/polymethylmethacrylate nanocomposites, *Materials Letters*, *55*(1), 83-87.

[400] **Velmurugan, R. and Mohan, T. P.** (2004). Room temperature processing of epoxy-clay nanocomposites, *Journal of Materials Science*, *39*(24), 7333-7339.

[401] **Dueramae, I., Jubsilp, C., Takeichi, T. and Rimdusit, S.** (2014). High thermal and mechanical properties enhancement obtained in highly filled polybenzoxazine nanocomposites with fumed silica, *Composites Part B: Engineering*, *56*, 197-206.

[402] **Arrighi, V., McEwen, I. J., Qian, H. and Serrano Prieto, M. B.** (2003). The glass transition and interfacial layer in styrene-butadiene rubber containing silica nanofiller, *Polymer*, *44*(20), 6259-6266.

[403] **Selvi, M., Vengatesan, M. R., Devaraju, S., Kumar, M. and Alagar, M.** (2014). In situ sol–gel synthesis of silica reinforced polybenzoxazine hybrid materials with low surface free energy, *RSC Advances*, *4*(17), 8446-8452.

[404] **Bulinski, Z., Pawlak, S., Krysiński, T., Adamczyk, W. and Bialecki, R.** (2019). Application of the ASTM D5470 standard test method for thermal conductivity measurements of high thermal conductive materials, *Journal of Achievements in Materials and Manufacturing Engineering*, *95*(2).

[405] **Kim, K., Ju, H. and Kim, J.** (2016). Surface modification of BN/Fe3O4 hybrid particle to enhance interfacial affinity for high thermal conductive material, *Polymer*, *91*, 74-80.

[406] **Guerra, V., Wan, C. and McNally, T.** (2018). Thermal conductivity of 2D nano-structured boron nitride (BN) and its composites with polymers, *Progress in Materials Science*, *100*, 170-186.

[407] **Morishita, T. and Takahashi, N.** (2017). Highly thermally conductive and electrically insulating polymer nanocomposites with boron nitride nanosheet/ionic liquid complexes, *RSC Advances*, *7*(58), 36450-36459.

[408] **Badawi, A. and Al-Hosiny, N. M.** (2015). Dynamic mechanical analysis of single walled carbon nanotubes/polymethyl methacrylate nanocomposite films, *Chinese Physics B*, *24*(10), 105101.

[409] **Hu, Y.-H., Chen, C.-Y. and Wang, C.-C.** (2004). Viscoelastic properties and thermal degradation kinetics of silica/PMMA nanocomposites, *Polymer Degradation and Stability*, *84*(3), 545-553.

[410] **Sarwar, M. I., Zulfiqar, S. and Ahmad, Z.** (2008). Polyamide–silica nanocomposites: mechanical, morphological and thermomechanical investigations, *Polymer International*, *57*(2), 292-296.

[411] **Zaragoza-Contreras, E. A., Hernández-Escobar, C. A., Mendoza-Duarte, M. E., Flores-Gallardo, S. G., Ibarra-Gómez, R. and Márquez-Lucero, A.** (2009). Thermal and Mechanical Analysis of Silver/Carbon Nanoparticle—PMMA Nanocomposites Obtained by Miniemulsion Polymerization, *Polymer Journal*, *41*(10), 816-821.

[412] **Lai, W.-C. and Tseng, S.-C.** (2009). Novel polymeric nanocomposites and porous materials prepared using organogels, *Nanotechnology*, *20*(47), 475606.

[413] **Zaed, A., Khalifa, M. and Youssef, A.** (2014). Synthesis of Polystyrene Grafting Filler Nanoparticles: Effect of Grafting on Mechanical Reinforcement, *International Journal of Chemical and Molecular Engineering*, *8*(12), 1358-1362.

[414] **Khlifa, M. A. S.** (2013). *Synthesis of Polymer Grafted Silica Nanoparticles: Effect of Grafting on Mechanical Reinforcement*. (Doctorate thesis). HERIOT-Watt University, School of Engineering and Physical Sciences, EDINBURGH.

[415] **Selvin Thomas, P., Thomas, S., Bandyopadhyay, S., Wurm, A. and Schick, C.** (2008). Polystyrene/calcium phosphate nanocomposites: Dynamic mechanical and differential scanning calorimetric studies, *Composites Science and Technology*, *68*(15), 3220-3229.

[416] **Hamming, L., Qiao, R., Messersmith, P. and Brinson, L.** (2009). Effects of dispersion and interfacial modification on the macroscale properties of TiO2 polymer-matrix nanocomposites, *Composites Science and Technology*, *69*(11-12), 1880-1886.

[417] **Akcora, P., Kumar, S. K., García Sakai, V., Li, Y., Benicewicz, B. C. and Schadler, L. S.** (2010). Segmental Dynamics in PMMA-Grafted Nanoparticle Composites, *Macromolecules*, *43*(19), 8275-8281.

[418] **Iwan, M., Andryszewski, T., Wydryszek, M. and Fialkowski, M.** (2015). Fabrication of nanocomposites by covalent bonding between noble metal nanoparticles and polymer matrix, *RSC Adv.*, *5*(86), 70127-70138.

[419] **Bayır, S., Semerci, E. and Erdogan Bedri, T.** (2021). Preparation of novel thermal conductive nanocomposites by covalent bonding between hexagonal boron nitride nanosheet and well-defined polymer matrix, *Composites Part A: Applied Science and Manufacturing*, *146*, 106406.

[420] **Dizman, C., Ates, S., Torun, L. and Yagci, Y.** (2010). Synthesis, characterization and photoinduced curing of polysulfones with (meth)acrylate functionalities, *Beilstein Journal of Organic Chemistry*, *6*(1), 56.

[421] **Zhang, Q., Ren, H. and Baker, G. L.** (2014). An economical and safe procedure to synthesize 2-hydroxy-4-pentynoic acid: A precursor towards 'clickable' biodegradable polylactide, *Beilstein Journal of Organic Chemistry*, *10*(1), 1365-1371.

[422] **Baharuddin, A. A., Ang, B., Abu Hussein, N. A. and Wong, Y. H.** (2017). Mechanisms of highly stabilized ex-situ oleic acid-modified iron oxide nanoparticles functionalized with 4-pentynoic acid, *Materials Chemistry and Physics*, *203*, 212-222.

[423] **Abdul Mannan, H., Mukhtar, H., Shima Shaharun, M., Roslee Othman, M. and Murugesan, T.** (2016). Polysulfone/poly(ether sulfone) blended membranes for CO2 separation, *Journal of Applied Polymer Science*, 133(5).

[424] **Dizman, C., Altinkok, C. and Tasdelen, M. A.** (2017). Synthesis of self-curable polysulfone containing pendant benzoxazine units via CuAAC click chemistry, *Designed Monomers and Polymers*, *20*(1), 293-299.

[425] **Jose, A. J. and Alagar, M.** (2015). Preparation and characterization of polysulfone-based nanocomposites. In V. Mittal (Ed.), *Manufacturing of Nanocomposites with Engineering Plastics* (pp. 31-59). Woodhead Publishing : Elsevier.

[426] **Awang, N., Jaafar, J. and Ismail, A. F.** (2018). Thermal Stability and Water Content Study of Void-Free Electrospun SPEEK/Cloisite Membrane for Direct Methanol Fuel Cell Application, *Polymers*, *10*(2), 194.

[427] **Sibel, E., Bozkurt, P. A. And Çelik, M.** Synthesis and characterization of poly (N-hydroxymethyl acrylamide)/Na-montmorillonite composites, *Journal of the Turkish Chemical Society Section A: Chemistry*, *4*(1), 39-50.

[428] **Li, X.-G. and Huang, M.-R.** (1999). Thermal degradation of bisphenol A polysulfone by high-resolution thermogravimetry, *Reactive and Functional Polymers*, *42*(1), 59-64.

[429] **Perng, L. H.** (2000). Thermal degradation mechanism of poly(arylene sulfone)s by stepwise Py-GC/MS, *Journal of Polymer Science Part A: Polymer Chemistry*, *38*(3), 583-593.

[430] **Muntha, S., Ajmal, M., Kausar, A. and Zia, M.** (2018). Synthesis, Properties, and Applications of Polysulfone/Polyimide Nanocomposite Membrane Reinforced with Silica Nanoparticles, *Polymer Composites*, *40*(5), 1897-1910.

[431] **Olmos, D., Prolongo, S. G. and González-Benito, J.** (2014). Thermo-mechanical properties of polysulfone based nanocomposites with well dispersed silica nanoparticles, *Composites Part B: Engineering*, *61*, 307-314.

[432] **Hu, S.-N., Lin, Y. and Wu, G.-Z.** (2020). Nanoparticle Dispersion and Glass Transition Behavior of Polyimide-grafted Silica Nanocomposites, *Chinese Journal of Polymer Science*, *38*(1), 100-108.

[433] **Natarajan, B., Li, Y., Deng, H., Brinson, L. and Schadler, L.** (2013). Effect of Interfacial Energetics on Dispersion and Glass Transition Temperature in Polymer Nanocomposites, *Macromolecules*, *46*(7), 2833-2841.

[434] **Sottos, N. R.** (1992). The Influence of the Fiber/Matrix Interface on Local Glass Transition Temperature, Studies in Polymer Science, *Elsevier*, *11*(339-358.

[435] **Kochetov, R., Korobko, A., Andritsch, T., Morshuis, P., Picken, S. J. and Smit, J. J.** (2011). Modelling of the thermal conductivity in polymer nanocomposites and the impact of the interface between filler and matrix, *Journal of Physics D: Applied Physics*, *44*(39), 395401.

[436] **Paramane, A. S. and Kumar, K. S.** (2016). A review on nanocomposite based electrical insulations, *Transactions on electrical and electronic materials*, 17(5), 239-251.

[437] **Koo, J.** (2017). Electrical Properties of Polymer Nanocomposites. *Fundamentals, Properties, and Applications of Polymer Nanocomposites* (pp. 521-549). Cambridge : Cambridge University Press.

[438] **Fink, J. K.** (2014). Poly(Arylene Ether Sulfone)s. *High Performance Polymers* (2nd ed., pp. 177-208). Norwich, NY.: William Andrew Publishing.

[439] **Balaji, V., Tiwari, A. N. and Goyal, R. K.** (2011). Study on High-Performance Poly(etheretherketone)/Si3N4 Nanocomposites: New Electronic Substrate Materials, *Polymer Engineering & Science*, *51*(3), 509-517.

[440] **Fulmer, G. R., Miller, A. J. M., Sherden, N. H., Gottlieb, H. E., Nudelman, A., Stoltz, B. M., ….. Goldberg, K. I.** (2010). NMR Chemical Shifts of Trace Impurities: Common Laboratory Solvents, Organics, and Gases in Deuterated Solvents Relevant to the Organometallic Chemist, *Organometallics*, *29*(9), 2176-2179.

[441] **Ye, G., Janzen, N. and Goward, G.** (2006). Solid-State NMR Study of Two Classic Proton Conducting Polymers: Nafion and Sulfonated Poly(ether ether ketone)s, *Macromolecules*, *39*(9), 3283-3290.

[442] **Candia, F. D., Michele, A. and Renzulli, A.** (1994). Molecular motions in polyetheretherketone (peek): NMR analysis of the low-temperature relaxation mechanism, *Journal of Macromolecular Science, Part B*, *33*(3-4), 307-316.

[443] **Baharuddin, A. A., Ang, B. and Wong, Y. H.** (2017). Self-Assembly and Electrical Characteristics of 4-Pentynoic Acid Functionalized Fe 3 O 4 -γ-Fe 2 O 3 Nanoparticles on SiO 2 /n-Si, *Applied Surface Science*, *423*, 236-244.

[444] **Francis, B., Thomas, S., Jose, J., Ramaswamy, R. and Lakshmana Rao, V.** (2005). Hydroxyl terminated poly(ether ether ketone) with pendent methyl group toughened epoxy resin: miscibility, morphology and mechanical properties, *Polymer*, *46*(26), 12372-12385.

[445] **Wang, F., Roovers, J. and Toporowski, P. M.** (1993). Synthesis and molecular characterization of narrow molecular weight distribution fractions of methyl-substituted poly(aryl ether ether ketone), *Macromolecules*, *26*(15), 3826-3832.

[446] **Honkhambe, P. N., Dhamdhere, N. A., Tawade, B. V., Salunkhe, M. M. and Wadgaonkar, P. P.** (2012). Synthesis and characterization of poly(ether ether ketone)s and poly(ether ether ketone ketone)s containing pendant biphenyl and naphthyl groups, *High Performance Polymers*, *25*(3), 260-267.

[447] **Chen, Y.-S., Lin, J.-H. C., Wu, Y.-R., Chang, C.-W., Chang, K.-C., Chen, C.-C., ….. Chen, W.-C.** (2018). Characterizing the differentiation of osteoprogenitor cells on surface modified polyether-ether-ketone, *Surface and Coatings Technology*, *350*, 904-912.

[448] **Vasconcelos, G. d. C., Mazur, R. L., Ribeiro, B., Botelho, E. C. and Costa, M. L.** (2014). Evaluation of decomposition kinetics of poly (ether-ether-ketone) by thermogravimetric analysis, *Materials Research*, *17*, 227-235.

[449] **Patel, P., Hull, R., Lyon, R., Stoliarov, S., Walters, R., Crowley, S. and Safronava, N.** (2011). Investigation of the thermal decomposition and flammability of PEEK and its carbon and glass-fibre composites, *Polymer Degradation and Stability - POLYM DEGRAD STABIL*, *96*(1), 12-22.

[450] **Meenan, B. J., McClorey, C. and Akay, M.** (2000). Thermal analysis studies of poly(etheretherketone)/hydroxyapatite biocomposite mixtures, *Journal of Materials Science: Materials in Medicine*, *11*(8), 481-489.

[451] **Perng, L. H., Tsai, C. J. and Ling, Y. C.** (1999). Mechanism and kinetic modelling of PEEK pyrolysis by TG/MS, *Polymer*, *40*(26), 7321-7329.

[452] **Patel, P., Hull, T. R., McCabe, R. W., Flath, D., Grasmeder, J. and Percy, M.** (2010). Mechanism of thermal decomposition of poly(ether ether ketone) (PEEK) from a review of decomposition studies, *Polymer Degradation and Stability*, *95*(5), 709-718.

[453] **Dandy, L. O., Oliveux, G., Wood, J., Jenkins, M. J. and Leeke, G.** (2014). Accelerated degradation of Polyetheretherketone (PEEK) composite materials for recycling applications, *Polymer Degradation and Stability*, *112*, 52-62.

[454] **Hache, F., Delichatsios, M., Fateh, T. and Zhang, J.** (2015). Comparison of methods for thermal analysis: Application to PEEK and a composite PEEK+CF, *Journal of Fire Sciences*, *33*(3), 232-246.

[455] **Zhang, X.** (2020). Carbon nanotube/polyetheretherketone nanocomposites: mechanical, thermal, and electrical properties, *Journal of Composite Materials*, 55(15), 2115-2132.

[456] **Diez-Pascual, A. M., González-Domínguez, J. M., Martinez Rubi, Y., Naffakh, M., Ansón, A., Martínez, M. T., ….. Gómez, M. A.** (2010). Synthesis and Properties of PEEK/Carbon Nanotube Nanocomposites, *Polymer Nanotube Nanocomposites: Synthesis, Properties, and Applications*, 281-313.

[457] **Wang, N., Yang, Z., Wang, Y., Thummavichai, K., Xia, Y., Ghita, O. ….. Zhu, Y.** (2017). Interface and properties of inorganic fullerene tungsten sulphide nanoparticle reinforced poly (ether ether ketone) nanocomposites, *Results in Physics*, *7*, 2417-2424.

[458] **Mach, P., Geczy, A., Polanský, R. and Bušek, D.** (2019). Glass transition temperature of nanoparticle-enhanced and environmentally stressed conductive adhesive materials for electronics assembly, *Journal of Materials Science: Materials in Electronics*, *30*(5), 4895-4907.

[459] **Mohammadi, M., Davoodi, J., Javanbakht, M. and Rezaei, H.** (2018). Glass transition temperature of PMMA/modified alumina nanocomposite: molecular dynamic study, *Materials Research Express*, *6*(3), 035309.

[460] **Serenko, O. A., Roldughin, V. I., Askadskii, A. A., Serkova, E. S., Strashnov, P. V. and Shifrina, Z. B.** (2017). The effect of size and concentration of nanoparticles on the glass transition temperature of polymer nanocomposites, *RSC Advances*, *7*(79), 50113-50120.

[461] **Hagita, K. and Morita, H.** (2019). Effects of polymer/filler interactions on glass transition temperatures of filler-filled polymer nanocomposites, *Polymer*, *178*, 121615.

[462] **Chen, F., Clough, A., Reinhard, B., Grinstaff, M., Jiang, N., Koga, T. ….. Tsui, O.** (2013). Glass Transition Temperature of Polymer–Nanoparticle Composites: Effect of Polymer–Particle Interfacial Energy, *Macromolecules*, *46*, 4663-4669.

[463] **Chen, H., Ginzburg, V. V., Yang, J., Yang, Y., Liu, W., Huang, Y., ….. Chen, B.** (2016). Thermal conductivity of polymer-based composites: Fundamentals and applications, *Progress in Polymer Science*, *59*, 41-85.

[464] **Li, X., Li, Y., Alam, M. M., Miao, J., Chen, P., Xia, R., ….. Qian, J.** (2020). Enhanced through-plane thermal conductivity in Polymer nanocomposites by constructing graphene-supported BN nanotubes, *Journal of Materials Chemistry C*, *8*(28), 9569-9575.

[465] **Kim, S., Kim, D., Kim, M. and Park, J. M.** (2007). Study on Thermal Conductivity of Polyetheretherketone/Thermally Conductive Filler Composites, *Solid State Phenomena*, *124*, 1079-1082.

[466] **Rivière, L., Caussé, N., Lonjon, A., Dantras, E. and Lacabanne, C.** (2015). Specific heat capacity and thermal conductivity of PEEK / Ag nanoparticles composites determined by Modulated-Temperature Differential Scanning Calorimetry, *Polymer Degradation and Stability*, *127*, 98-104.

[467] **Gacitua, W., Ballerini, A. and Zhang, J.** (2005). Polymer nanocomposites: synthetic and natural fillers a review, *Maderas. Ciencia y tecnología*, *7*(3), 159-178.

[468] **Wu, H.** (2014). *Multifunctional polymer composites containing inorganic nanoparticles and novel low-cost carbonaceous fillers*. (Doctorate thesis). IOWA State University, Materials Science and Engineering, IOWA.

[469] **Panwar, V. and Pal, K.** (2017). Dynamic Mechanical Analysis of Clay–Polymer Nanocomposites. In K. Jlassi, M.M. Chemimi, S. Thomas (Eds.), *Clay-Polymer Nanocomposites* (pp. 413-441). Elsevier.

[470] **Lai, Y., Huang, J. and Chen, M.** (2007). Thermomechanical Properties of Nanosilica Reinforced PEEK Composites, *Key Engineering Materials*, *351*, 15-20.

[471] **Gendre, L., Silva, F., Sachse, S. and Njuguna, J.** (2013). Effect of nano-fillers percentage on mechanical properties and energy absorption of three-phase polymer-nanocomposites. *Proceedings of the 17th International Conference on Composite Structures (ICCS17)*, Porto, Portugal, June.

[472] **Wilberforce, S. I. J., Best, S. M. and Cameron, R. E.** (2010). A dynamic mechanical thermal analysis study of the viscoelastic properties and glass transition temperature behaviour of bioresorbable polymer matrix nanocomposites, *Journal of Materials Science: Materials in Medicine*, *21*(12), 3085-3093.

[473] **Ramachandran, M. G. and Rajeswari, N.** (2021). Influence of Nano Silica on Mechanical and Tribological Properties of Additive Manufactured PLA Bio Nanocomposite, *Silicon*, 1-7.

[474] **Suresha, B., Varun, C. A., Indushekhara, N. M., Vishwanath, H. R. and Venkatesh**. (2019). Effect of Nano Filler Reinforcement on Mechanical Properties of Epoxy Composites, *IOP Conference Series: Materials Science and Engineering*, *574*(1), 012010.

[475] **Budiyantoro, C.** (2018). The Influence of Nano Filler on Thermal and Mechanical Properties of Polypropylene, *Materials Science Forum*, *929*, 78-85.

[476] **Bashir, M. A.** (2021). Use of Dynamic Mechanical Analysis (DMA) for Characterizing Interfacial Interactions in Filled Polymers, *Solids*, *2*(1), 108-120.

[477] **Hou, X., Hu, Y., Hu, X. and Jiang, D.** (2017). Poly (ether ether ketone) composites reinforced by graphene oxide and silicon dioxide nanoparticles: Mechanical properties and sliding wear behavior, *High Performance Polymers*, *30*(4), 406-417.

[478] **Patidar, D., Agarwal, S. and Saxena, N.** (2011). Storage modulus and glass transition behaviour of CdS/PMMA nanocomposites, *Journal of Experimental Nanoscience*, *6*(4), 441-449.

[479] **Gao, N., Hou, G., Liu, J., Shen, J., Gao, Y., Lyulin, A. V. ….. Zhang, L.** (2019). Tailoring the mechanical properties of polymer nanocomposites via interfacial engineering, *Physical Chemistry Chemical Physics*, 21(34), 18714-18726.

[480] **Zhu, B., Wang, Y., Liu, H., Ying, J., Liu, C. and Shen, C.** (2020). Effects of interface interaction and microphase dispersion on the mechanical properties of PCL/PLA/MMT nanocomposites visualized by nanomechanical mapping, *Composites Science and Technology*, *190*, 108048.

[481] **Ciprari, D., Jacob, K. and Tannenbaum, R.** (2006). Characterization of Polymer Nanocomposite Interphase and Its Impact on Mechanical Properties, *Macromolecules*, *39*(19), 6565-6573.

[482] **Ciprari, D. L.** (2004). *Mechanical Characterization of Polymer Nanocomposites and The Role of Interphase*. (Master thesis). GEORGIA Institute of Technology, Materials Science and Engineering, ATLANTA.

[483] **Putz, K. W., Palmeri, M. J., Cohn, R. B., Andrews, R. and Brinson, L. C.** (2008). Effect of Cross-Link Density on Interphase Creation in Polymer Nanocomposites, *Macromolecules*, *41*(18), 6752-6756.

[484] **Kutvonen, A., Rossi, G., Puisto, S., Rostedt, N. and Ala-Nissila, T.** (2012). Influence of nanoparticle size, loading, and shape on the mechanical properties of polymer nanocomposites, *The Journal of chemical physics*, *137*(21), 214901.

[485] **Sapiai, N., Jumahat, A., Manap, N. and Usoff, M.** (2015). Effect of nanofillers dispersion on mechanical properties of clay/epoxy and silica/epoxy nanocomposites, *Jurnal Teknologi*, *76*(9), 107-111.

[486] **Pradhan, S., Lach, R., Le, H. H., Grellmann, W., Radusch, H.-J. and Adhikari, R.** (2013). Effect of Filler Dimensionality on Mechanical Properties of Nanofiller Reinforced Polyolefin Elastomers, *ISRN Polymer Science*, *2013*, 284504.

[487] **Wood, C., Ajdari, A., Burkhart, C., Putz, K. and Brinson, L.** (2016). Understanding Competing Mechanisms for Glass Transition Changes in Filled Elastomers, *Composites Science and Technology*, *127*, 88-94.

[488] **Sun, Y., Zhang, Z., Moon, K.-S. and Wong, C. P.** (2004). Glass transition and relaxation behavior of epoxy nanocomposites, *Journal of Polymer Science Part B: Polymer Physics*, *42*(21), 3849-3858.

[489] **Robertson, C. G., Lin, C. J., Rackaitis, M. and Roland, C. M.** (2008). Influence of Particle Size and Polymer−Filler Coupling on Viscoelastic Glass Transition of Particle-Reinforced Polymers, *Macromolecules*, *41*(7), 2727-2731.

[490] **Qiao, R., Deng, H., Putz, K. W. and Brinson, L. C.** (2011). Effect of particle agglomeration and interphase on the glass transition temperature of polymer nanocomposites, *Journal of Polymer Science Part B: Polymer Physics*, *49*(10), 740-748.

[491] **Hamming, L. M., Qiao, R., Messersmith, P. B. and Brinson, L. C.** (2009). Effects of dispersion and interfacial modification on the macroscale properties of TiO(2) polymer matrix nanocomposites, *Composites Science and Technology*, *69*(11-12), 1880-1886.

[492] **Yousefzade, O. and Garmabi, H.** (2016). Development of a simple model to characterize the complex constrained polymer chains in polymer nanocomposites at the interphase of amorphous/semicrystalline ethylene vinyl acetate and nanosheets, *Journal of Composite Materials*, *51*(2), 179-186.

[493] **Bailey, E. and Winey, K.** (2020). Dynamics of Polymer Segments, Polymer Chains, and Nanoparticles in Polymer Nanocomposite Melts: A Review, *Progress in Polymer Science*, *105*, 101242.

CURRICULUM VITAE

Name Surname **:** Eliften SEMERCİ

EDUCATION **:**

- **Ph.D.** **:** 2021, Istanbul Technical University, Graduate School of Science Engineering and Technology, Department of Chemistry
- **M.Sc.** **:** 2015, Istanbul Technical University, Graduate School of Science Engineering and Technology, Department of Chemistry
- **B.Sc.** **:** 2012, Hacettepe University, Collage of Science, Department of Chemistry

PROFESSIONAL EXPERIENCE AND REWARDS:

- **2018-Current** – Scholarship holder at TUBITAK MAM, Kocaeli, Turkey.
- **2015-2016** – Project Engineer at Leartiker S. Coop., Bizkaia, Spain.
- **2013-2014** – Student Assistantship at ITU, Istanbul, Turkey.
- **2011** – Internship at MN Pharmaceuticals, Kocaeli, Turkey.

PUBLICATIONS AND PRESENTATIONS ON THE THESIS:

- **Semerci, E.**, Bedri, E.T., and Kizilcan, N., (2021). "Preparation of thermal conductive Poly(methyl methacrylate)/Silicon nitride nanocomposites via click chemistry." *Polymer 212*: 123285.
- **Semerci, E.,** Erdogan Bedri, T., Kizilcan, N., "Development of Novel Thermally Conductive Silicon Nitride/Poly (ether ether ketone) Nanocomposites via Click Chemistry", *15th Nonoscience and Nanotechnology Conference (NANOTR'15*), 2019, Antalya, Turkey (Oral Presentation).

- **Semerci**, **E.,** Kizilcan, N., Erdogan Bedri, T., "The Synthesis of Novel Thermal Conductive Si_3N_4-PMMA Nanocomposites via Click Chemistry", *31st National Chemistry Congress*, 2019, Istanbul, Turkey (Poster Presentation).
- **Semerci, E.**, Erdogan Bedri, T., Kizilcan, N., "Preparation of Novel Polymeric Nanocomposite with Thermal Conductivity Containing Modified Silicon Nitride Nanosheets in Polysulfone Matrix", *47th IUPAC World Chemistry Congress*, 2019, Paris, France (Poster Presentation).

OTHER PUBLICATIONS AND PRESENTATIONS:

- Bayır, S., **Semerci, E.,** Bedri, E.T., (2021). "Preparation of novel thermal conductive nanocomposites by covalent bonding between hexagonal boron nitride nanosheet and well-defined polymer matrix." *Composites Part A: Applied Science and Manufacturing 146*: 106406.
- Kiskan, B.; Musa, A.; **Semerci, E.;** Yagci, Y., (2017). Chapter 13 – "Thiol-Benzoxazine Chemistry for Macromolecular Modifications". *Advanced and Emerging Polybenzoxazine Science and Technology*. H. Ishida and P. Froimowicz. Amsterdam, Elsevier: 223-232.
- **Semerci, E.;** Kiskan, B.; Yagci, Y., (2015). "Thiol reactive polybenzoxazine precursors: A novel route to functional polymers by thiol-oxazine chemistry." *European Polymer Journal*, *69*: 636-641.
- Bayir, S., **Semerc**i, **E.**, Erdogan Bedri, T., "The Synthesis of Hexagonal Boron Nitride Additive Thermal Conductive SAN Nanocomposite", *31st National Chemistry Congress*, 2019, Istanbul, Turkey (Poster Presentation).
- **Semerci E.,** Kiskan B., Yagci Y., "Synthesis and Characterization of Benzoxazine and Thiol Functional Poly (ε-caprolactone)", *IUPAC World Polymer Congress – MACRO 2014*, 2014, Chiang Mai, Thailand (Poster Presentation).
- **Semerci E.,** Taskin OS., Yagci Y., "Benzophenone Based Self-Healing Materials", *4th Research and Development Project Market Activity*, 2014, Istanbul, Turkey (Poster Presentation).
- **Semerci E.,** Kiskan B., Yagci Y., "Thiol Reactive Main Chain Benzoxazine Functional Hyper-branched Polymers", *5th EuCheMS Chemistry Congress*, 2014, Istanbul, Turkey (Poster Presentation).